FINITE ELEMENT ACOUSTIC ANALYSIS OF ABSORPTION SILENCERS WITH MEAN FLOW

by

Keshav Lal Rathi (MSc.)

A Doctoral Thesis Submitted in Partial Fulfilment of the Requirements for the Award of Doctor of Philosophy of the Loughborough University of Technology

December 1994

Supervisor: Dr K S Peat (BSc, PhD)
Department of Mathematical Sciences

DEDICATION

To my father, mother, wife , children and foremost , to the glory of God

ACKNOWLEDGEMENTS

I would like to express my deepest gratitude and sincere thanks to my supervisor, Dr K S Peat for his invaluable support, excellent guidance, help and encouragement throughout the research period and for reading and commenting upon the thesis manuscript.

I am grateful to Professor R W Smith, Director of Research, for his advice and encouragement. My thanks go to the staff of the Computer Centre and in particular to the Technical Coordinator of the Department of Mathematical Sciences, Dr K D Watling, for his help.

I would like to thank all my colleagues, friends and all other departmental staff for their co-operation and help.

Many thanks to the Association of Commonwealth Universities and to the British Council for awarding me a scholarship.

Finally I wish to acknowledge the deep understanding and moral support of my wife and children, which greatly helped in completing this work.

ABSTRACT

The acoustic performance of dissipative silencers, including the effects of both a mean flow in the airway and an induced internal steady flow in the absorbent, are analysed. Finite element models, based upon the modified Galerkin method, have been derived for the determination of the noise attenuation of silencers, both by forced response and eigenvalue analysis. The corresponding computer programs, incorporating subroutines from the NAG Finite Element library, have been developed.

The induced steady flow field causes the acoustic field in the absorbent to be inhomogeneous, anisotropic and nonlinear, even if the porous material is isotropic and homogeneous. Material anisotropy and inhomogeneity are also included in the formulations. Comparison of the models with experimental and analytical results is also carried out.

The induced steady flow field in the absorbent is determined by both a simplified linear and a more exact nonlinear model. The benefit of nonlinear modelling is evaluated. The effect of the induced flow field upon the acoustic properties of the "bulk-reacting" absorbent, and hence upon the transmission loss of absorption silencers, is evaluated throughout the frequency range of interest. Results are presented for several different test silencers and they indicate the accuracy of the formulation and the necessity for detailed modelling of the effects of the induced flow. Two different matching schemes, between the acoustic fields of the flow duct and the absorbent region, on their common boundary, are presented and compared.

A detailed study is carried out by changing principal design parameters and a number of practical design guidelines are deduced. Further applications include the modelling of ISO 'anechoic' terminations of flow ducts. The analysis has the potential to explore the benefits of detailed design changes in the most complex of dissipative silencers.

SYMBOLS

A, B, C, D	= Four-pole parameters ~ and ' denotes two different system
A_i	= Attenuation per unit length [dB/m]
$c, c_0, \bar{c}$	= Speed of sound in air subscript 0 and - denotes uniform and steady case
c_i	= Acoustic phase speed
$\underline{\xi}$	= Particle displacement
k	= Wavenumber
[K]	= Global stiffness matrix
$[k_{ij}^e]$	= Element stiffness matrix
ξ, η, ζ	= Local coordinates
x,y,z	= Global coordinates
N	= Number of nodes
f_i^b	= Forcing terms
p^*	= Trial solution
R	= Residual error
J	= Jacobian
$G(\xi, \eta, \zeta)$	= Integral transform function
(ξ_i, η_i, ζ_i)	= Abscissae points
$\psi(\xi, \eta, \zeta)$	= Shape function with local coordinates
M	= Mach number
I	= Local node

m, m_j	= Structure factor subscript j denotes jth direction
P, p	= Pressure, subscript a represent absorbent and - ' notations denote steady and acoustic quantities
ρ	= Fluid density
q	= Velocity subscript a represent absorbent and - ' notations denote steady and acoustic quantities
U, V	= Uniform velocity - denote steady case
ϕ	= Velocity potential -,' and ~ notations denote steady, acoustic and dimensionless quantities
γ	= Ratio of specific heat
χ	= Compressibility
$[\Sigma'],[\bar{\Sigma}],[M_a],[S]$	= Diagonal matrix
z_j	= Characteristic impedance in porous material subscript o and j denotes zero flow and jth direction
Z	= Acoustic impedance Subscript o and e and r denotes zero flow, source and radiation case
γ_j	= Propagation coefficient subscript o and j denotes zero flow and jth direction
∇	= Differential operator
Ω	= Porosity
ρ_a	= Density in porous material

σ_v, σ_i	= Viscous and inertial flow resistivity subscript o and j denotes zero flow and jth direction
ω	= Angular frequency
f	= Frequency
R_1, R_2	= Regions of the silencer
Γ	= Boundary of the duct script I, w, o denotes inlet, wall, outlet boundary
I	= Intensity in Chapter 2
$\psi_l(x,y,z)$	= Weighting function
Φ, Ψ	= Scalar function
s	= Boundary surface
v	= Volume of domain
λ	= Eigen value

CONTENTS

CHAPTER 1

INTRODUCTION

1.1 Problem Definition

Noise pollution has long been recognised as a major problem of the urban environment. However, effort to control noise pollution has gained momentum relatively recently, as people have become more and more conscious of their working and living environment. Two of the main sources of urban noise pollution are noise from internal combustion engines and, within buildings, noise from heating and ventilation systems. Governments of many countries have responded to popular demand with mandatory restrictions on noise emitted by automotive engines and on the maximum allowable noise 'doses' in the industrial work place. These problems have encouraged acousticians and engineers to devote themselves to various research projects on how best to control the noise pollution.

A common approach to the reduction of noise is the use of silencers (also called mufflers). One result of the effort put into noise control is that automobiles and heating and ventilation systems are universally fitted with silencers of various kinds to control the noise. In recent years considerable manpower and resources have been employed to study the behaviour of such silencers. Practical and theoretical research has also been carried out to investigate and/or to quantify the noise reduction which they achieve. In current practice, silencers are still quite often being designed empirically. These empirical methods do not lead to physical understanding of the silencing mechanism

and neither do they account for the complexity of the problem. It is therefore preferable that this area should be further investigated and analysed using modern computational methods, which have the potential to make silencer design more efficient in terms of both effectiveness and cost. The work presented in this thesis was undertaken by the author to improve upon current analysis techniques for the computational prediction of silencer performance. In particular, finite element techniques are developed to analyse the acoustic effectiveness of absorption silencers, with particular attention paid to the effects of steady flow within both the open duct and the dissipative material.

1.2 General description of a silencer

The function of a silencer in a flow duct is to reduce the sound propagation through the system by impedance mismatch, or to dissipate the incoming sound energy into heat, while allowing the mean flow to go through almost unimpeded. Silencers are conventionally classified according to whether the acoustic energy is dissipated into heat or is reflected back by impedance discontinuities. The former type of silencers are called dissipative or absorptive silencers, whilst the others are called reflective, reactive, or nondissipative silencers. However, no silencer is completely reactive or completely dissipative. Every silencer contains some elements with impedance mismatch and some with acoustic dissipation. Typically, "dissipative" silencers contain some acoustically absorptive material, whilst "reactive" silencers do not contain any absorptive material. The latter work on the principle that, where a geometrical discontinuity exists, there will be an impedance mismatch and hence reflection of a substantial part of the incident acoustic energy back towards the source.

1.3 Literature Review

1.3.1 Historical Background

The possible effects of mean flow in dissipative silencers, comprised of a gas flow region surrounded by an absorptive region, do not appear to have received much attention in the literature. However, general developments in the theory of sound propagation and attenuation in acoustically lined ducts have been extensively reported in the literature over the last 50 to 55 years. Much progress was made in this area when large computers appeared and numerical techniques were developed. Excellent reviews of the state of the art of duct acoustics have been published recently by Munjal [1], Cummings [2], Doak [35] and Nayfeh et al [3]. Furthermore, a status report on numerical techniques in linear duct acoustics has been presented by Baumeister [29].

1.3.2 Review of research performed on absorption silencers and lined ducts

The problem of sound propagation in hard-walled rectangular ducts was first studied by Rayleigh [4] in the early nineteenth century. Sivian [5] dealt with the problem of sound propagation in a circular lined duct of a ventilation or exhaust system in which two types of lining were considered: (i) lining in which there is no wave motion propagated in the direction of the duct axis; (ii) lining admitting of such motion. This theory is valid at low frequencies, where the acoustic wavelength is greater than about twice the internal duct diameter and the internal sound pressure is roughly uniform over the cross-section of the duct. Later, Morse [6] published a rigorous description of the propagation of sound in a duct lined with absorbent material, for both rectangular and circular ducts with finite wall impedance. The analysis of Morse is limited to consideration of a "locally-reacting" liner, that is a liner in which there is no axial wave propagation in the liner. This can be achieved, for instance, by the incorporation of regularly spaced solid partitions normal to the wall of the liner. Although this limitation may not be a problem in aircraft silencer design, where solid partitions are used, it is a

problem in general air-conditioning and industrial air-handling systems where the use of solid partitions can often be prohibitively expensive.

Between Rayleigh and Morse, most of the work in duct acoustics was empirical in nature. It involved producing correlations of attenuation rates from experimental work. These correlations satisfied the needs for non-critical applications of absorbers. Sabine [7] describes the experimental study of noise in ventilating ducts and the quieting effects of a sound absorbing duct lining. Tests were made on resistance to airflow of a special baffle structure introduced in the system. The frictional resistance of a duct lined with absorbent was also measured. An expression for the attenuation per unit length was found, namely $\Delta = 12.6\bar{\alpha}^{1.4}P/A$ (dB/ft), where P is the duct perimeter, A its cross-sectional area and $\bar{\alpha}$ the absorption coefficient of the lining material of the reverberation chamber. This formula is certainly useful as a rough guide to expected attenuation in cases where absorption coefficient data are available. Axial wave propagation in the liner was taken into account in an analysis by Scott [8]. This type of liner is referred to as " bulk-reacting", as opposed to "locally-reacting" where no axial wave propagation occurs within the liner. Scott also discussed in detail the limitation of Morse's approach and introduced a more complete theory, by deriving the equation which relates the attenuation and wavelength constants in pipes and channels to the characteristic impedance and propagation constant in the bulk-reacting lining material as well as to the dimensions of the pipes and channels.

The effects of a mean flow in the lined duct were briefly touched on by Meyer et al [74], who carried out an experimental investigation of the effect of turbulent flow on the attenuation in ducts lined with different absorbents. King [80] also measured experimentally the attenuation of sound in a lined air flow duct. Further work was done by Ingard [75], who used wave theory to calculate the attenuation of air-borne sound in absorbing ducts, under the influence of only one-dimensional flow, and made comparison with experimental results. Tack and Lambert [9] formulated the problem of

wave propagation in a two-dimensional lined duct with mean fluid flow in the airway and lined with an isotropic bulk-reacting liner. Both upstream and downstream propagation, with both uniform mean flow and a sheared flow calculated by a 'power -law' boundary layer profile, were examined. No numerical results were presented. Bokor [10,11] performed experimental studies and described a method of measurement of the characteristic impedance and the sound attenuation of bulk-reacting duct liners in rectangular ducts, in order to verify an equation of Scott's [8]. The experimental results were restricted to the first mode of propagation only.

The effect of Mach number on the tuning of an acoustic lining in a flow duct were investigated by Eversman [25]. Tester [23] established a theoretical analysis of the propagation and attenuation of sound in lined ducts containing uniform or "plug" flow and a two-dimensional Green's function was derived. An investigation was made by Ko [81,82,83] of the theoretical prediction of sound attenuation in acoustically lined circular, rectangular and annular cross-sectional ducts in the presence of uniform flow and shear flow. An eigenvalue equation was developed and sound attenuation spectra have been computed. In later work Ko [84] studied the effects of a porous splitter with uniform flow in rectangular, circular and annular cross-sectional ducts, but he did not present any numerical or experimental results from that work. McCormick [38] extended the two-dimensional, lined channel analysis of the previous author to consider rectangular ducts lined on all four sides. Kurze and Vér [13] generalised Scott's model [8] to include the effect of non-isotropy of the lining and compared their prediction with Bokor's measurements on the attenuation constant of a two dimensional duct lined with fiberglass, without mean flow. Experimental data were presented by Wassilieff [12] for anisotropic bulk-reacting duct liners without mean flow and he also explained the reason for the poor agreement demonstrated in earlier work by Bokor and Kurze and Vér. Wassilieff found that, at low frequencies, the least attenuated duct mode was always the lowest order mode (equivalent to a plane wave in a hard-walled non-dissipative duct). This observation remained true at higher frequencies as well, except

for a few cases where the (0,2) mode became the least attenuated. In his analysis he did not consider odd modes. Nayfeh et al [14] examined the effect of a bulk-reacting liner on acoustic wave propagation in two dimensional rectangular and circular ducts carrying sheared flow.

Cummings [15] considered the effects of uniform flow using the bulk-reacting liner model of Scott [8], and also included three-dimensional wave propagation and the effects of a perforated solid facing on the liner. He presented design charts for ducts with various geometric and liner properties. The effect of uniform mean flow along the central passage of an expansion chamber containing a bulk absorber was considered theoretically by Nilsson and Brander [85,86,87,88]. They developed quantitative methods for the calculation of sound attenuation along silencers of both finite and infinite length and uniform cross-section, with a bulk-reacting lining and mean flow in the airway. They also considered the transmission and reflection of sound at a sudden area change in a cylindrical wave guide with two semi-infinite ducts and analysed sound transmission at silencer terminations by the use of the Wiener-Hopf method. They also gave results for bifurcated, axisymetric, semi-infinite ducts, where the bifurcation was of the extended inlet or extended outlet type, including the effects of a perforated tube between the gas flow and absorbent in the wide duct. These methods were also applied to reactive silencers. In parallel with these physical models, the American Society of Heating, Refrigerating and Air-conditioning Engineers (ASHRAE) has published a series of simplified prediction methods in its "Systems Handbooks" (see, for example reference [52]) based on an empirical approach.

Although lined duct acoustics is a part of continuous media mechanics, analytical and empirical methods are not practicable for the solution of problems of acoustic propagation in ducts where the mean flow is non-uniform, or where non-uniform steady flow is induced in the absorbent, or where the liner is non-uniform, or where the ducts have a complicated geometry. Numerical techniques are the natural choice for the

solution of these complex problems. The finite element method (FEM) is one such technique and a brief explanation of this method is given in the next chapter. Another general numerical method, the finite difference technique, has not proved to be a popular choice for the analysis of silencers, partly because the finite element method is better able to model complicated geometry. However, a variety of numerical techniques have been used in linear duct acoustics, see for example the status report by Baumeister [29]. Use of the Galerkin method for acoustic transmission in an attenuating duct was made by Unruh and Eversman [33]. Kapur and Mungur [34] developed an acoustic finite element method for inlet and exhaust jet flow ducts. Use of the variational finite element method in muffler analysis was made for the first time by Young and Crocker [26], for the prediction of transmission loss in mufflers. However, only unmapped rectangular elements were used and the analysis was restricted to consider only single input and output locations for the calculation of transmission loss. Craggs [27,28] considered the application of the finite element method to study the performance of some simple reactive and dissipative muffler elements. He compared the results against some known solutions and added the capability for analysing multiple input and output configurations and locally-reacting boundaries. In his later work, Craggs [40,42] developed a finite element model to represent the effect of a bulk-reacting liner and hence discussed the coupling of the acoustic fields of the dissipative and non-dissipative regions. (The procedure ensures both equality of pressure and compatibility of normal velocity). These applications did not consider steady flow and assumed a rigid porous medium.

Kagawa et al [73,77] developed a finite element formulation for an axisymetric acoustic field problem with a sound absorbing wall, based on the true adjoint system, and verified their analysis with measured results. They used a triangular ring element with a second order polynomial trial function for discretization, and included the effects of temperature gradient. In their numerical examples they considered the transmission characteristics of acoustic filters and the throat impedance of a conical horn. In later

work they extended the finite element approach for acoustic transmission and radiation systems for horn and silencer design, but they did not account for any flow effects.

Young and Crocker [78] expanded the finite element approach to analyse more complicated flow-reversing reactive muffler chambers and chamber-resonator combinations with and without wall vibrations. In their analysis they did not consider steady flow effects and they demonstrated experimentally that steady flow produced negligible effects in the muffler chamber, for the cases considered. Sigman et al [39] described the application of the Galerkin finite element method to determine the acoustic properties of turbofan inlets containing steady flows of high subsonic Mach number, for applications to the inlet ducts of jet engines, but did not include any absorbent effects. Astley and Eversman [24] used the finite element method to formulate the eigenvalue problem for uniform, infinite lined ducts with flow. They considered two-dimensional problems and used Galerkin's method with a point-reacting liner on the boundary. Syed [51] reported a finite difference formulation, together with some analytical results, for the prediction of sound attenuation in acoustically lined ducts with locally-reacting liners and high Mach numbers for applications to aero-engines.

Ross [31] presented an acoustic Langrangian energy expression for a parallel-coupled system (two parallel chambers) using finite element analysis. This analysis broke down the system into two subsystems. The technique has been applied to automotive muffler configurations and has been experimentally verified, but it does not consider steady flow or absorbent effects. Ling et al [41] developed a Galerkin finite element formulation for a semi-infinite acoustic flow duct and proposed an extension to their analysis for high flow cases using a compressible fluid finite element. They allowed for the acoustic impedance of a uniform locally-reacting lining material on the wall of the duct. Peat [32] used a Galerkin finite element formulation to model acoustic wave propagation in reactive silencer elements with nonuniform mean flow. The main goal was the determination of four-pole parameters, since these could be used to connect

muffler components in series. Filippi [30] published a compiled work on theoretical acoustics and numerical techniques, including a comprehensive bibliography.

1.3.3 Recent developments in the analysis of dissipative silencers

There are two main areas of activity reviewed in the above survey. The first is the determination of the acoustic pressure in a duct or cavity which is enclosed by rigid walls lined either with point-reacting or with bulk-reacting absorbent material. The second is the use of finite element methods to predict the propagation of acoustic waves in ducts or silencers, with or without mean flow. Due to the complications created by the presence of a steady flow, most of the studies on sound propagation either ignore flow or assume only one-dimensional uniform mean flow in the duct. In some instances, comparisons with experimental results have shown that the assumption of uniform steady flow in uniform ducts gives good correlation. Further simplifications are necessary for the application of analytical methods, which are generally restricted to ducts of simple shape with uniform material properties.

During the last ten years, some developments in both analytical and numerical techniques have been made. Rienstra [19] examined theoretically the problem of sound propagation in an infinite cylindrical duct with a bulk-reacting liner but no mean flow. He derived the analytical solution for two configurations of liner, firstly for a liner whose properties vary slowly in the axial direction, and secondly for a liner of porous material embedded in a rigid structure of annular partitions with a small pitch. Astley and Cummings [20] presented a general finite element formulation for sound transmission in infinite uniform ducts having bulk-reacting liners and uniform mean airflow. The method was applied to rectangular ducts lined on all four sides, and a series of design charts was also given, but induced flow in the absorbent and its acoustic effects were not taken into account. Later, for the first time, induced flow effects in the absorbent were included in the absorption silencer model by Cummings and Chang [17,18]. They considered both infinite duct and finite expansion chamber

silencers, lined with a bulk-reacting absorbent containing a uniform mean flow, induced by a uniform mean flow in the airway. The mean flow in the absorbent was shown to have a significant influence on the effective flow resistance of the duct liner. Peat [48] obtained a transfer matrix for an absorption silencer element and compared his simple fundamental-mode analysis with the full modal results of Cummings and Chang [17]. Peat [54] also presented a numerical decoupling analysis of an absorption silencer element. Peat's results were reliable at low frequency, but did not indicate such good agreement at high frequencies.

Astley [21] calculated the sound attenuation in ducts with bulk-reacting and locally-reacting liners and then compared both sets of results. Astley et al [63] presented an analysis which considered a general flexible-walled duct with a bulk-reacting liner, using a variational finite element formulation. Computational results of the acoustic propagation were compared with experimental results, but mean flow effects were not considered, either in the airway or in the absorbent. Later, Astley [22] presented a variational formulation for the problem of flexible-walled ducts with bulk-reacting liners, including a uniform flow in the airway, but without any flow effects in the absorbent medium. The effects of flanking transmission on the sound attenuation in lined ducts were studied by Cummings and Astley [76]. Craggs [43] reviewed the performance of acoustic finite elements for sound fields in small enclosures. He considered examples of small lined rooms and compared finite element solutions with those from a simple theory of duct acoustics. Later Craggs [47] used transfer matrix and matrix condensation methods, with finite element analysis, for duct acoustic problems and he proposed models for porous material with damping. However none of his investigations included steady flow effects, either in the duct or in the absorbent.

Christiansen and Krenk [44] used the finite element method to include the simultaneous use of different material models in acoustically lined ducts, and summarised the differential equation for a general porous material medium which was discretized by a

scaled Galerkin procedure. In addition, a hybrid technique was used and compared with experiments in applications to both reflective and absorption silencers , but without any flow. Hobbeling [45] used finite elements for the analysis of typical designs of purely absorption silencers, combined absorption and reflection silencers, and oblique quarter-wavelength Helmholtz resonator silencers, but the interface boundary conditions were inadequate and there was no account of flow in the absorbent. Design curves for rectangular splitter silencers and for circular and annular duct silencers were presented by Ramakrishnan and Watson [68,69]. They used finite element analysis, but flow effects were not considered in their modelling. Easwaran and Munjal [61] carried out a finite element analysis for wedges used in anechoic chambers, hence they did not consider flow effects either. Bies et al [46] gave a generalised theory for sound propagation in a lined flow duct of arbitrary cross-section, where acoustic wave propagation in the lining was also taken into account. The general analysis was applied to ducts of both rectangular and circular cross-section. The applications were restricted to ventilation duct silencers and they did not account for the flow in the absorbent. Rademaker [55] conducted an experimental programme for validation of a theoretical duct acoustic model. This model calculates the sound propagation in a cylindrical flow duct of finite length, which includes an acoustically lined section between two hard-walled sections. Mechel [64] analysed rectangular baffle type silencers of infinite length with locally-reacting absorbers and without any flow, for modal solution charts which are similar with the Morse [6] charts. Frommhold and Mechel [16] discussed simplified methods for calculation of the attenuation of silencers of circular and rectangular cross-section, including mean flow in the airway but not the absorbent, and they compared their results against measurements. Morel et al [65] gave a combined fluid dynamic and acoustic model of a reactive concentric-tube silencer, without any absorbent or flow effects. A time-domain solution for the attenuation of high amplitude sound in perforated tube silencer problems, has been given by Chang and Cummings [72]. Cummings and Sormaz [62] presented a theoretical model describing the sound propagation in infinite, two-dimensional planar silencers incorporating an arbitrary

number of bulk-reacting, anisotropic, sound absorbing splitters with uniform mean flow in the gas flow passage. A numerical computation scheme was also outlined in their analysis, but effects of induced flow in the absorbent were not considered.

Recently Wang et al [79] analysed a three-dimensional muffler with a boundary element method, without any absorbent or mean flow. Zhenlin et al [91] also used the boundary element method for predicting the acoustic performance of an expansion chamber muffler with mean flow. Cummings [70] presented a Rayleigh-Ritz variational formulation for the eigenvalue problem of circular and elliptical shaped silencers, which included the effects of variable density of the porous material. Induced flow effects in the absorbent were not included but the results indicated quite good agreement with experiments.

1.4 Objectives of this Research

The purpose of this thesis is to develop a technique which is suitable for detailed analysis of the most complex of absorption silencer units, for use with internal combustion engines or heating and ventilation systems. As suggested previously, one has to resort to one of the various numerical discretization techniques for the acoustic analysis of general systems of this nature. The finite element method is one such technique and has been used here largely because of the simplicity with which material nonlinearities and complicated geometries can be incorporated. Prior to this work, the finite element method has not been used to analyse dissipative silencers of finite length in the presence either of mean flow in a nonuniform airway, or of any mean flow in the absorbent. Indeed the literature survey above does not indicate any work at all in the former area and very little in the latter, although induced flow effects in the absorbent have been shown to have significant effects (Cummings and Chang [17,18]).

In the application of interest here, the steady flow Mach number of the gas in the flow duct is typically less than 0.3, thus the steady flow may be assumed to be incompressible. Furthermore the Reynolds number of the flow is typically high, such that the steady flow is always turbulent and viscous effects are only important in very thin boundary layers adjacent to the duct walls. Thus shear effects are ignored throughout this work and hence, if the flow duct is uniform in cross-section, then the steady flow will also be uniform in this region. In most silencer applications the flow duct tends to be of uniform-cross-section, but non-uniform geometries, such as conical sections, are sometimes used and flow - splitter silencers also cause an effective non-uniformity of the flow cross-section.

Whenever there is a steady flow present in the flow duct of an absorption silencer, there will be an induced steady flow field in the dissipative region. The numerical techniques presented in this thesis extend previous analytical and experimental work of Cummings and Chang [17,18] to include the non-uniform induced flow effects in the absorbent and to consider nonuniform packing in a silencer of arbitrary shape. Similarly, the finite element analysis of uniform ducts of infinite length by Astley and Cummings [20] is extended to include both induced flow effects in the absorbent and material, and hence flow non-uniformity. The finite element analysis techniques developed here can be used to predict the acoustic effectiveness of a given design of silencer and to explore the potential benefits of structuring the 'lay' of fibrous material or designing the shape of a silencer volume, with respect to the form of the induced flow field.

Three sets of computer codes were developed using the Nag Finite Element Library [53] of subroutines, one for the prediction of the velocity field of the induced flow in a porous material, one for the eigenvalue analysis of an infinite duct of arbitrary cross-section, and the third for the analysis of the acoustic four-pole parameters, and hence transmission loss, of a complete absorption silencer. The accuracy of the results obtained has been checked, wherever possible, against the theoretical and experimental

results of other researchers. Some of the work presented in this thesis has already been published [90] and further items have been submitted for publication, or are in preparation.

A brief summary of the finite element method is given in Chapter 2. The governing equations of acoustic wave propagation in flow ducts and in porous materials are presented in Chapter 3. An eigenvalue analysis of the flow acoustics problem in a uniform dissipative duct of infinite length, using the finite element method, is given in Chapter 4. The results are compared with those from different analysis techniques and with experimental results given by other researchers, for the test case of a section of a Saab silencer. The analysis technique is used to study the effects upon the attenuation of the silencer of nonuniform packing of the absorbent material and of cross-sectional shape of the dissipative duct. In Chapter 5 a comprehensive finite element analysis of a general three-dimensional absorption silencer with a uniform flow duct and induced nonuniform flow in the absorbent material is given. The induced flow in the absorbent is modelled in both a simplistic linear manner and in a more justifiable nonlinear manner and the results are analysed. Iterative algorithms, which have been found to be rapidly convergent, are given for the nonlinear analysis of both the steady induced flow and the acoustic field in the absorbent. Two different schemes for the implementation of the matching conditions on the common boundary of the flow duct and the absorbent region are presented and compared. The general formulation of Chapter 5 is extended to include the case of a non-uniform flow duct in Chapter 6. Results are given for the modelling of ISO anechoic terminations in a flow duct. The last chapter presents the conclusions and a discussion of possible future work.

CHAPTER 2

APPLICATION OF FINITE ELEMENTS TO ACOUSTIC ANALYSIS

2.1 Introduction

The finite element method is a computer-aided mathematical technique for obtaining approximate numerical solutions to the abstract equations of calculus that predict the response of physical systems subjected to external influences. Such problems arise in many areas of science and engineering.

The finite element technique was first introduced in the 1950's and was initially developed for the stress/strain analysis of complex engineering structures. Since then it has been continually developed and improved. Once the method was given a firm mathematical foundation, it was only natural that it should be used for analysing other physical problems which could be represented by partial differential equations. Now, every area of science and engineering makes use of the power of the finite element method of analysis and the field of acoustics has been no exception. Since the original development was made in the area of structural analysis, much of the terminology and many of the current commercial finite element programs are heavily oriented toward the structural analysis discipline.

The extension process of the finite element from structural to non-structural applications, via a variational approach, was documented by Cheung in 1965 [50]. Due

to its diversity and flexibility as an analyst's tool, growth in the use of the method was rapid and it was applied for the first time to the acoustic analysis of silencers during the mid-70's by Young and Crocker [26] .

The focus of this chapter is to introduce the finite element method in the context of the acoustic analysis of silencers and to give a very brief summary of the method, which will highlight the fundamentals of the technique. It is not intended to detail all the historical developments, for there are sufficient reviews and books available concerning this area. Perhaps the most notable is the text by Zienkiewicz [36].

The growth of the finite element technique is attributable directly to the rapid advances in computer technology and computing power, particularly over the last two decades. As the power of the computer has increased, so it has been possible to analyse larger and more complex problems. There now exist a number of so-called general-purpose finite element programs, available commercially. There also exists many smaller, special-purpose programs whose capabilities are more limited. Detailed description of available programs can be obtained from a handbook on finite element systems by Brebbia [89]. A few well-known large, general-purpose finite element packages are discussed later in the chapter.

The major advantage of the finite element method over other numerical methods such as finite difference, lies in the ease with which complicated irregular geometry and local mesh refinement can be incorporated. Each method has its advantages and disadvantages and one cannot say that one method is globally better than any other. Any comparisons that can be made will be in the context of specific problems or in terms of the general theory of each method. The main advantages of the finite element method can be summarised as follows:

- It is well-suited to problems involving complex geometries.

- It can readily handle problems where the physical parameters vary with position within the domain.
- It can be used for non-linear and/or time-varying problems.
- Complex boundary conditions can be readily dealt with.
- Conventional numerical techniques can be used to solve the equations resulting from a finite element analysis.

An important feature of the finite element method which sets it apart from other approximate methods, is the ability to formulate the solution for individual elements, before putting them together to represent the entire problem. This means that a complex problem can be reduced by considering a series of greatly simplified problems.

Another important feature of the finite element method is the variety of ways in which one can formulate the properties of individual elements and even change them within iterations towards the final solution.

2.2 Basic concept of the finite element method

A finite element may be regarded as a piece of a continuum system. Although the method has been developed into a sophisticated and apparently complex technique, underneath, the fundamental concepts and principles are simple. The general procedure for analysis of a system follows a few basic steps. Before outlining the central steps in the procedure, we define the following concepts and related terminology that are germane to every problem that the finite element method can analyse.

- ***System :*** The physical problem to be analysed.
- ***Domain:*** The spatial, and temporal, region occupied by the system.

- ***Governing equations:*** The representation of the response of the system throughout the domain.
- ***Loading conditions:*** The internal, boundary or initial forcing terms on the system.

For example consider the following problem:

System

A sound source of frequency ω and strength f radiating inside a closed room with (ideally) rigid ceiling, walls, and floor.

Domain

The volume occupied by the room. The boundary of domain is comprised of the ceiling, walls, and floor.

Governing equation

$\nabla^2 p + k^2 p = f$ where p is the acoustic pressure and k is the wavenumber

Loading conditions

Interior load f. Boundary conditions $\frac{\partial p}{\partial n} = 0$ on ceiling, walls, and floor (n is the normal to the bounding surface).

2.3 The main steps of the finite element method

Any finite element analysis can be broken down into the following basic steps:

i. Discretization of the problem.

ii. Selection of the approximating function.

iii. Derivation of the element equations.

iv. Assemblage of the element equations to obtain the system equations.

v. Inclusion of the boundary conditions.

vi. Solution of the system of equations.

vii. Post-processing.

Details of these steps are outlined in the following sections.

2.4 Discretization of the problem

2.4.1 Over-view of domain

Consider the system under examination whose domain is given in Figure 2.1. This domain of the problem is divided (partitioned) into smaller regions (subdomains) called "elements", see Figure 2.2 which are considered to be interconnected at joints, known as "nodes". Adjacent elements should touch without overlapping, and there should be no gaps between the elements. The shape of the elements are conventionally made as simple as possible, such as triangles and quadrilaterals in two-dimensional domains and tetrahedra, pentahedra ("wedges" or "pyramids"), and hexahedra ("bricks") in three dimensions, see Figure 2.3. The entire mosaic-like pattern of elements throughout a domain, e.g. Figure 2.2, is called a "mesh". Further details of element choice, their properties and the mesh generation procedure are given in the following sections.

The shape or configuration of the basic element depends upon the number of space co-ordinates necessary to describe the problem and, to some extent, upon the geometry of the domain. The finite element discretization procedure reduces a problem with continuously varying field variables to one of a finite number of unknowns, by dividing the solution region into elements and by expressing the unknown field variables in terms of assumed approximate functions within each element.

2.4.2 Mesh Generation

When the term "mesh generation" is mentioned, the main idea is that the finite element discretization should be performed for the whole region. To minimise the effort and human error in data preparation, an automatic mesh generation routine can be utilised where applicable. A uniform mesh, consisting of elements which are all about the same size and shape and repeated in a fairly regular pattern, needs no special word of advice.

Such meshes provide a more or less uniform distribution of degrees of freedom (number of degrees of freedom per area of domain), and hence they are most appropriate in areas of a domain where the solution varies uniformly smoothly. In those portions of the domain where the solution varies more rapidly (e.g., near concentrated loads and, in some problems, near sharply contoured boundaries), a greater degree of freedom density is necessary in order to maintain a given level of accuracy; that is, the mesh must be locally refined.

2.5 Selection of the approximating function

2.5.1 Interpolation Functions

In the finite element method, the domain is divided into elements within which the field variables are represented by some form of interpolation function. These functions are usually referred to as the element "shape functions" and are generally chosen to be low-order polynomials, although other types of functions may be used for this purpose, e.g. trigonometric functions. The shape functions are defined with respect to specified nodes of the element, most of which are located on element boundaries, though some elements do have interior nodes. Shape functions for the element types used in this thesis are given in Table 2.1 and Figure 2.4.

A key feature of shape functions are that they are local, element-based, functions which have the value one at the node to which they refer and the value zero at all other nodes on the element, see Figure 2.4. Clearly adjacent elements 'share' the same nodes which lie on their common boundary. Thus a node has associated with it shape functions throughout all elements which contain that node. Hence one may consider global, nodal-based interpolation functions, termed "basis functions", which are the sum of all element-based "shape functions" for a single node, see Figure 2.5. It is important to note that a global basis function is zero over all elements which do not contain the node corresponding to the particular basis function.

The complete set of nodal basis functions determine the nature of the allowed form of variation of a field variable throughout the domain. Hence, if the nodal values of a field variable are specified, the full form of the variation of the field variable throughout the domain follows, and is known as the "trial solution".

2.5.2 *Choice of Element Type*

The selection of the mesh of elements, together with the element shape functions, is the most crucial factor in the analysis of the specified problem. The choice of both the finite element mesh and the element shape function determines the potential accuracy of the analysis, the cost of computation and the storage limitations. The dimensions of an element must be chosen to be the same as the problem of interest. The number of nodes assigned to a particular element depends upon the type of shape functions and the degree of element continuity required. To clarify the meaning of the latter term, consider its standard definition. If a field variable is continuous at the element interface, then it is said that the element has C^0 continuity. If, in addition, all first derivatives are continuous across element boundaries, the element has C^1 continuity, and so on.

The main criterion in choosing the mesh and element type for the solution of a given problem is to select a form of trial solution which can reasonably approximate the anticipated variation of the field variable, with a close approximation to the system equations, while using a reasonable amount of computational effort. In addition the entire mesh of elements must adequately approximate the geometric domain of the problem, which can be a particular difficulty if the boundary of the domain is curved. The element shape functions from which the trial solution is generated are defined with respect to a local, element-based, coordinate system defined over a simple geometric domain, see Table 2.1 and Figure 2.4. Thus it is necessary to specify a geometric transformation from local to global coordinate space for each element see, Figure 2.6. A simple method to achieve this is through the use of a set of element shape functions

together with the global coordinates of the nodes to which the shape functions refer, see equation (2.15). The same element shape functions which are used to develop the trial solution can also be used to specify the relationship between the global coordinates and the local element-based coordinate system. If this is so, the element is termed an "isoparametric" element. Isoparametric elements have been used exclusively throughout the work of this thesis. For isoparametric elements with more then two nodes along an edge, the element boundary can be curved in global coordinate space, such that a domain with curved boundaries can be accurately represented. Provided that isoparametric elements have at least C^0 continuity, adjacent elements meet precisely at a common boundary without either gaps or overlaps.

The discretization of a curved domain using small, straight-sided elements is satisfactory provided that the number of elements used to fit the domain, particularly near its boundary, is large enough. An alternative strategy, and one with guaranteed accuracy, is to use curved-sided elements, since then a considerably smaller number of elements is required to achieve a close representation of the domain.

Generally, the larger the number of nodal points the elements have, the more general and hence accurate the trial solution they produce, for a given total number of elements. Thus, for a given number of elements in the mesh, cubic and higher order elements may be used to obtain more accurate results than quadratic or lesser order elements. However, attention should be given to the fact that use of such elements would make it an expensive process in terms of computer storage and computation time, and similar accuracy for less cost might be obtained by using a denser mesh of lower order elements. In addition, cubic and higher order element can suffer from problems of instability. A good compromise is to use quadratic elements, which are relatively simple and yet can model curved boundaries. Eight-noded quadrilateral elements, which are complete to second order, are used in most element discretizations of the

problems involved in this thesis. Where the geometry dictates use of triangular elements, six-noded triangular elements, complete to second order, are used.

2.6 Derivation of the element equations

2.6.1 Element equation

In each element the governing equations, usually in differential or variational (integral) form, are transformed into algebraic equations called the element equations, which are an approximation of the governing equations. The derivation of the element equations follows from the selection of a particular approach of the finite element method and the choice of the element shape functions. The following four basic approaches can be used in the formulation of the finite element method, to obtain the element properties, see Alghatam [50] :

- The direct approach.
- The energy balance approach.
- The variational approach.
- The weighted residual approach.

2.6.2 Direct and energy balance approach

The direct approach may be used for some situations, particularly in structural mechanics, where discrete elements are already present. Also, for problems prescribed by simple geometries and in which direct physical reasoning is used, formulation of the system of equations in terms of the variables of interest can follow from this approach. The energy balance approach relies on the balance of the thermal and mechanical energy of the system. In essence the following two, more general, approaches encompass this approach.

2.6.3 Variational approach

This class of approach can be used when the governing equations of the problem can be written as variational (integral) equations. It requires knowledge of a variational principle (i.e. a functional to be extremized or made stationary) for the given problem. The Rayleigh-Ritz method is one specific, well-defined technique for obtaining approximate numerical solutions to problems in a variational form, and provides an algorithm for minimising a given functional, by choice of a trial function. The variational method is still popular in the field of solid mechanics, but in most practical problems of other disciplines, it is becoming less popular due to restrictions associated with the requirements of a suitable variational principal.

2.6.4 Weighted residuals approach

This approach can be used for any general class of problem and is the most widely applicable technique for finite element analysis. In the method of weighted residuals, the element equations can be derived directly from the governing equations of the problem under consideration, without any need of knowing a functional. The trial solution is substituted directly into the governing equation and the result is termed the error or residual function. The error function is then multiplied by chosen weighting functions and forced to be zero in an integrable sense over the entire domain. In fact, there is a number of methods categorised as weighted residual methods e.g. Galerkin, Collocation, Least Squares and Zero mean error methods, which differ only in the choice of weighting functions used.

The general procedure for all of these methods has been given by Zienkiewicz [36]. The most popular of these, the Galerkin approach, which employs the nodal basis functions as weighting functions, will be adopted in this thesis. In particular the "weak" or "modified" Galerkin formulation is used which reduces the inter-element compatibility requirements. The advantages of the Galerkin technique are that it

produces simple, symmetric element matrices with good convergence properties. Details of the Galerkin approach are given in the following section.

2.6.5 Galerkin Method

By way of example, consider the Galerkin technique for application to the classic Helmholtz equation

$$\nabla^2 p + k^2 p = 0. \tag{2.1}$$

We seek a trial solution p^* formed from the set of global nodal basis function $\psi_J(x,y,z)$, such that

$$p^* = \sum_{J=1}^{N} \psi_J p_J, \tag{2.2}$$

where p_J are the unknown nodal values of p at the N nodes of the entire domain. Then

$$\nabla^2 p^* + k^2 p^* = R \neq 0, \tag{2.3}$$

where R is the residual or error function.

A general weighted residual method would seek to minimise the residual by enforcing

$$\iiint_V W_I(x,y,z) R(x,y,z) dxdydz = 0, \tag{2.4}$$

for a general set of weighting function $W_I(x,y,z)$. Since the Galerkin method is a particular form of weighted residual method for which the weighting functions are taken to be the basis functions $\psi_I(x,y,z)$, then

$$\iiint_v \psi_I(x,y,z)R(x,y,z)dxdydz = 0, \tag{2.5}$$

for $I = 1$ to N. Thus from equation (2.3),

$$\iiint_v \psi_I(\nabla^2 p^* + k^2 p^*)dv = 0\ , \quad I = 1 \text{ to } N \tag{2.6}$$

This set of equations can then be re-written, substituting from equation (2.2), as

$$\sum_{J=1}^{N}\{[\iiint_v \psi_I(\nabla^2\psi_J + k^2\psi_J)dv]p_J\} = 0\ , \quad I = 1 \text{ to } N \tag{2.7}$$

2.6.6 Modified Galerkin Method

The "modified" or "weak" Galerkin formulation is a simple variant of the basic Galerkin method, in which Green's theorem is invoked to reduce the maximum order of derivative terms in the integrals. Green's theorem states that, if Φ and Ψ are two scalar functions with derivatives which are continuous in a domain v, then

$$\iiint_v \Phi\nabla^2\Psi dv = \iint_s \Phi\nabla\Psi \cdot \underline{n}ds - \iiint_v \nabla\Phi \cdot \nabla\Psi dv, \tag{2.8}$$

where s is the surface enclosing the volume v and $\underline{n}$ is the unit outward normal to surface s. Application of Green's theorem to the particular example of the Helmholtz equation (2.6) in the preceding section results in

$$\iiint_v (\nabla\psi_I.\nabla p^* - k^2\psi_I p^*)dv = \iint_s \psi_I \frac{\partial p^*}{\partial n}ds, \quad I = 1 \text{ to } N \tag{2.9}$$

where s is the boundary of the domain v Substitution from equation (2.2) gives

$$\sum_{J=1}^{N}\{\iiint_{v}(\nabla\psi_I\cdot\nabla\psi_J-k^2\psi_I\psi_J)dv\}p_J=\iint_{s}\psi_I\frac{\partial p^*}{\partial n}ds,\qquad I=1\text{ to }N \tag{2.10}$$

2.6.7 Numerical Integration

The integrals in equation (2.10) can be evaluated as the sum of the separate integrals over all volume elements of the domain and surface elements of the boundary, for the left-hand side and right-hand side integrals respectively. Hence equation (2.10) can be written as

$$\sum_{J=1}^{N}\sum_{e=1}^{M}\{\iiint_{v_e}(\nabla\psi_I\cdot\nabla\psi_J-k^2\psi_I\psi_J)dv\}p_J=\sum_{b=1}^{B}\{\iint_{s_b}\psi_I\frac{\partial p}{\partial n}\}ds,\quad I=1\text{ to }N \tag{2.11}$$

for a mesh of M elements with individual volume v_e, and for B surface elements on the boundary with individual area s_b. The basis function ψ_I is zero over all element except those which contain node *I*, for which global node *I* would correspond to a local node number, say i. Hence the non-zero contributions to equation (2.1) are

$$\sum_{j=1}^{n}\sum_{e=1}^{m}\{\iiint_{v_e}(\nabla\psi_i\cdot\nabla\psi_j-k^2\psi_i\psi_j)dv\}p_j=\sum_{b=1}^{B}\iint_{s_b}\psi_i\frac{\partial p}{\partial n}ds,\quad I=1\text{ to }N, \tag{2.12}$$

where ψ_i, ψ_j are the shape functions based on the local element node numbers i, j of a given n -noded element. The contribution of the j^{th} local node of element e to the equation based on the I^{th} weighting function, corresponding to the i^{th} local node of element e, can then be termed the elemental stiffness k_{ij}^e. Similarly the right-hand side gives rise to forcing terms of the form f_i^b. Hence equation (2.12) can be written as

$$\sum_{j=1}^{n}\sum_{e=1}^{m}k_{ij}^e p_j^e=\sum_{b=1}^{B}f_i^b,\qquad I=1\text{ to }N \tag{2.13}$$

where $k_{ij}^e=\iiint_{v_e}(\nabla\psi_i\cdot\nabla\psi_j-k^2\psi_i\psi_j)dv$ and $f_i^b=\iint_{s_b}\psi_i\frac{\partial p}{\partial n}ds$.

The domain integral of equation (2.12), the term k_{ij}^{e}, has a known integrand and, in principle, can therefore be evaluated. In practice, the integral must be evaluated numerically, due to its complexity, for which it is advantageous to conduct a transformation into a simpler space. Since the element shape functions are based on a local coordinate system of $-1 \le \xi, \eta, \zeta \le +1$, the use of isoparametric elements provides an ideal mechanism to accomplish this task. Thus we seek a transformation such that

$$\iiint_{v_e} (\nabla \psi_i \cdot \nabla \psi_j - k^2 \psi_i \psi_j) dv = \int_{-1}^{+1}\int_{-1}^{+1}\int_{-1}^{+1} G(\xi, \eta, \zeta) |J| d\xi d\eta d\zeta \tag{2.14}$$

where $G(\xi, \eta, \zeta)$ is the transform of the integrand and J is Jacobian of the transformation.

Now for isoparametric elements with n nodal shape functions of the form $\psi_i(\xi, \eta, \zeta)$,

$$\begin{aligned} x &= \sum_{i=1}^{n} \psi_i(\xi, \eta, \zeta) x_i \\ y &= \sum_{i=1}^{n} \psi_i(\xi, \eta, y) y_i \\ z &= \sum_{i=1}^{n} \psi_i(\xi, \eta, \zeta) z_i, \end{aligned} \tag{2.15}$$

where (x_i, y_i, z_i) are the global coordinates of local node i i.e. global node I.

The Jacobian matrix $[J]$ is given by

$$[J] = \left[\frac{\partial(x,y,z)}{\partial(\xi,\eta,\zeta)}\right] = \begin{bmatrix} \frac{\partial x}{\partial \xi} & \frac{\partial y}{\partial \xi} & \frac{\partial z}{\partial \xi} \\ \frac{\partial x}{\partial \eta} & \frac{\partial y}{\partial \eta} & \frac{\partial z}{\partial \eta} \\ \frac{\partial x}{\partial \zeta} & \frac{\partial y}{\partial \zeta} & \frac{\partial z}{\partial \zeta} \end{bmatrix} \tag{2.16}$$

and the individual elements follow from equation (2.15), since $\frac{\partial x}{\partial \xi} = \sum_{i=1}^{n} \frac{\partial \psi_i}{\partial \xi} x_i$, etc.

The transformation of the integrand to the form $G(\xi, \eta, \zeta)$ generally involves transformations of the global-coordinate derivatives of the shape function, i.e. $\nabla \psi$ terms. Now

$$\begin{Bmatrix} \frac{\partial \psi}{\partial x} \\ \frac{\partial \psi}{\partial y} \\ \frac{\partial \psi}{\partial z} \end{Bmatrix} = \begin{bmatrix} \frac{\partial \xi}{\partial x} & \frac{\partial \eta}{\partial x} & \frac{\partial \zeta}{\partial x} \\ \frac{\partial \xi}{\partial y} & \frac{\partial \xi}{\partial y} & \frac{\partial \xi}{\partial y} \\ \frac{\partial \xi}{\partial z} & \frac{\partial \xi}{\partial z} & \frac{\partial \xi}{\partial z} \end{bmatrix} \begin{Bmatrix} \frac{\partial \psi}{\partial \xi} \\ \frac{\partial \psi}{\partial \eta} \\ \frac{\partial \psi}{\partial \zeta} \end{Bmatrix} \tag{2.17}$$

where the matrix is simply the inverse of the Jacobian. Higher-order global derivatives can be transformed in a similar manner when this is necessary

Evaluation of the transformed integral of equation (2.14) is performed by the use of a quadrature formula, with given weighting functions w_i and abscissae points (ξ_i, η_i, ζ_i), such that

$$\int_{-1}^{+1}\int_{-1}^{+1}\int_{-1}^{+1} H(\xi, \eta, \zeta) d\xi d\eta d\zeta \approx \sum_{i=1}^{n_q} w_i H(\xi_i, \eta_i, \zeta_i). \tag{2.18}$$

The Gauss quadrature formulae, as used in this work, have quadrature weights and points chosen to exactly integrate polynomial functions. The larger the number of quadrature points, n_q, the higher the order of polynomial which is integrated exactly, but the greater the required computational effort. There are many references which provide tables of general quadrature rules assuming a range of (ξ, η, ζ) values from -1 to $+1$, hence the reason for normalising the element sides in this way. The Gauss quadrature formulae used in this thesis are given in Table 2.2.

2.7 Assemblage of the element equations

2.7.1 General Assembly Rule

The assemblage procedure of the element equations is an important step in the solution of the problem. In this process, the element equations are combined in order to form a set of equations governing the composite set of elements. The assemblage of element equations provides the compensating effect to that of discretizing into subdivisions the region in which the problem of interest is prescribed. Thus, the assemblage of such elements represents the original domain. It includes the assembly of the overall stiffness matrix for the entire region from the individual element stiffness matrices, and the overall right hand side vector from the assembly of individual surface elements on the boundary.

The integration procedure of the previous section is carried out over each element in turn, to give an element stiffness matrix $[k^e]$. This is an $n \times n$ matrix, where n is the number of nodes on the element, with individual components k_{ij}^e, as given in equation (2.13). Each individual component of the element stiffness matrix $[k^e]$ can then assembled into the global stiffness matrix $[K]$, by adding it to the K_{IJ} component of $[K]$, where I is the global node number of local node i on element e, and J is the global node number of local node j on element e. This results in an overall system of equation of the form

$$\begin{bmatrix} K_{11} & K_{12} & . & . & K_{1N} \\ K_{21} & K_{22} & . & . & K_{2N} \\ . & . & . & . & . \\ . & . & . & . & . \\ K_{N1} & K_{N2} & . & . & K_{NN} \end{bmatrix} \begin{Bmatrix} p_1 \\ p_2 \\ . \\ . \\ p_N \end{Bmatrix} = \begin{Bmatrix} f_1 \\ f_2 \\ . \\ . \\ f_n \end{Bmatrix}, \tag{2.19}$$

or $$[K]\{\underline{p}\} = \{\underline{f}\}. \tag{2.20}$$

The right-hand-side vector of forcing terms arises from the boundary integrals of equation (2.12), for elements which have an edge on the boundary of the domain. This step presupposes that the integral contributions from inter-element boundaries cancel, i.e. that there is continuity between elements, see Section 2.2 on element choice.

2.7.2 Bandwidth minimisation

A key feature of equation (2.19) is that most of the terms in the stiffness matrix are zero, since component K_{IJ} will be zero unless nodes I and J lie on the same element. Hence careful global node numbering can give rise to a matrix which is strongly banded, that is all the nonzero terms are clustered within a narrow band about the main diagonal. The bandwidth is the maximum number of terms along a row from one side of the band to the other. The half-bandwidth is the number of terms in a row to one side (or the other) of the main diagonal, plus the main diagonal. Hence designating the half bandwidth by HB the band width is $2(HB)-1$. For a given mesh topology the bandwidth is determined by the global pattern of node-numbering. i.e.

$$HB = (\Delta N)_{\max} + 1 \tag{2.21}$$

for a single degree of freedom problem, where ΔN is the difference between the largest and smallest global node number on a given element. Computer processing and storage costs decrease significantly as the bandwidth of the system stiffness matrix decreases. There always exists at least one global node numbering system for a given mesh for which the bandwidth will be minimum. There are many algorithms that can be used to automatically renumber a mesh to minimise the bandwidth.

2.8 Inclusion of the boundary conditions

Once the main part of the assembly is completed the boundary conditions must be imposed, by modifying both the system matrix and the right-hand side forcing vector.

A boundary value problem of order $2n$ in some function p requires n boundary conditions to be specified at every point on the boundary. A boundary condition is an equation relating the values of p and/or some of its derivatives from order 1 up to order $2n$-1, at points or over regions on the boundary. It is conventional to classify the boundary conditions into three principal types:

2.8.1 Dirichlet or Essential boundary condition

An equation relating the values of any of the derivative of p from order 0 to order n-1. (Note: the 0^{th} order derivative is simply p, the value of the field variable). These conditions may be imposed by two main methods: (i) direct elimination of the freedom from the system; (ii) the Payne-Irons procedure. The method of application for direct elimination is to delete from the system stiffness matrix any entry corresponding to the given boundary freedom. This has the advantages of being exact and of reducing the size of the problem prior to solution of the equations, but it involves a reordering of the full system matrix for each known boundary value. The mechanism involved is best understood by an example. Consider the pressure to be known at node 5, say $p_5 = C$, of the system of equations (2.19), i.e.

$$\begin{bmatrix} K_{11} & K_{12} & . & . & K_{1N} \\ K_{21} & K_{22} & . & . & K_{2N} \\ . & . & . & . & . \\ . & . & . & . & . \\ K_{N1} & K_{N2} & . & . & K_{NN} \end{bmatrix} \begin{Bmatrix} p_1 \\ p_2 \\ . \\ . \\ p_N \end{Bmatrix} = \begin{Bmatrix} f_1 \\ f_2 \\ . \\ . \\ f_n \end{Bmatrix}. \qquad (2.22)$$

For direct elimination one would remove row 5 from the equations and column 5 terms from the system matrix and would replace f_i by $f_i - K_{i5}C$ in all remaining entries on the right-hand side. The Payne-Irons method involves an imposed bias of entries in the system stiffness matrix corresponding to the given boundary freedom values. The leading diagonal of the entry is augmented by some large number (large in comparison with the entries in matrix, say 10^{10}) and the corresponding entry on the

right-hand side is given a similar scaling and a value to enforce the correct condition. For example in equation (2.22), row 5 would be altered to read

$$K_{15}p_1 + K_{25}p_2 + \ldots (K_{55})10^{10}\, p_5 + \cdots K_{N5}p_N = \quad K_{55}C10^{10}, \tag{2.23}$$

thus $p_5 \approx C$. Clearly this approach is approximate and does not reduce the matrix size prior to solution. It is, however, much easier to implement than the direct elimination method and the accuracy can be improved at will by increasing the scaling factor. The Payne-Irons method has been used to implement Dirichlet boundary conditions throughout the work in this thesis

2.8.2 Neumann or Natural boundary condition

An equation relating the values of any of the derivatives of p from order n to order $2n-1$. For a second order problem (n=1), the Neumann condition is a known rate of change of the scalar field p in the direction of the outward normal to the boundary. For example, assuming that $\partial p/\partial n = C$, a known constant, on portion Γ of the boundary S then the right-hand, side of equation (2.10) for this portion of boundary becomes $C\int_{\Gamma} \psi_I ds$ and is zero unless global node I lies on Γ. Let portion Γ of the boundary be represented by N_b elements on the boundary, and let global node I correspond to local node i on a given element, then the non-zero contribution to the right-hand side is $\sum_{b=1}^{N_b} C\int_{\Gamma_b} \psi_i ds$. On occasions when the given derivative is not in the normal direction, then the contribution to the right-hand side must be constructed from the direction cosines of the elements on the boundary.

The form of the elements and hence shape functions on a given boundary depend upon the type of domain elements adjacent to the given boundary, i.e. for a 2-D domain with 8-noded quadrilateral elements adjacent to a boundary, the elements on the boundary will be 1-D, 3-noded line elements. In performing the line or surface integration over

the boundary, numerical quadrature rules, see Table 2.2, can be used accordingly, such that for a 1-D element on the boundary of a 2-D domain

$$C\int_{\Gamma}\psi_i d\Gamma = C\int_{-1}^{1}\psi_i(\xi)|J|d\xi = C\sum_{j=1}^{n_q} w_j\psi_i(\xi_j)|J(\xi_j)| \qquad (2.24)$$

and for a 2-D element on the boundary of a 3-D domain

$$C\int_{-1}^{1}\int_{-1}^{1}\psi_i(\xi,\eta)|J|d\xi d\eta = C\sum_{j=1}^{n_q} w_j\psi_i(\xi_j\eta_j)|J(\xi_j,\eta_j)|. \qquad (2.25)$$

On evaluation, the integral contribution corresponding to ψ_I becomes f_I, the I^{th} element of the right-hand side vector of equation (2.22).

2.8.3 *Cauchy boundary condition*

An equation relating derivative conditions of Dirichlet type to those of Neumann type. e.g. For a second-order problem the normal derivative of the field variable is a known function of the field variable. For example consider $\partial p^*/\partial n = Cp^*$, with known constant C, on some portion of on Γ of the boundary S. Then from the weak Galerkin formulation, equation (2.10), the right-hand side integral over Γ can be written as

$$\int_{\Gamma}\psi_I\frac{\partial p^*}{\partial n}ds = C\int_{\Gamma}\psi_I p^* ds = \sum_{J=1}^{N}\{C\int_{\Gamma}\psi_I\psi_J ds\}p_J. \qquad (2.26)$$

Again, if nodes I and J lie on the same element of the given portion of boundary, the only non-zero contributions of expression (2.26) from a given element on the boundary are $\sum_{j=1}^{n} C\{\int_{\Gamma}\psi_i\psi_j ds\}p_j$ where i and j are the local element numbers corresponding to global nodes I and J. The integrals can be evaluated numerically using the same quadrature rules as given above for the Neumann conditions, to leave contributions of the form $k_{ij}^b p_j^b$ arising from all nodal pairs i, j on a given element b on the boundary. These k_{ij}^b terms are therefore contributions to the global stiffness matrix and since they

arise from right -hand side of equation (2.10) they must be subtracted from the corresponding K_{IJ} terms of equation (2.19).

2.9 Solution of the system of equations

2.9.1 Solution techniques

Once the boundary conditions have been included the resulting system of equations can be solved by one of a range of conventional numerical techniques. Appropriate techniques are chosen to take full advantage of the characteristics of the system matrix i.e. whether it is banded, symmetric, unsymmetric, real or complex. Subroutines from the NAG Library were used throughout the work of this thesis.

2.9.2 Uniqueness and convergence requirements

The nature of the solution and the degree of approximation depend upon the validity and accuracy of the finite element model. Validity means how faithfully the problem is represented by the finite element formulation, while the accuracy depends upon how close the model is to convergence. The actual solution in some domain is approximated by an assembly of simple solutions, each local to some element, and hence the overall accuracy of the entire solution depends mainly on the number of elements used and the order of the shape function within each element. In particular, it is important that the accuracy of an analysis can be increased by using more elements, which in turn implies that elements must satisfy the following convergence requirements:

- ***Completeness***

Completeness is the requirement that, in the limit as the element size decreases indefinitely, the combination of trial functions should exactly reproduce the exact solution. This condition is satisfied if polynomial expressions are used in each element such that the complete m^{th} order polynomial is present, when m^{th} order derivatives exist in the integrals of the finite element matrix equations.

- ***Compatibility***

Compatibility is the requirement that there should be no contribution to the integrals of approximation from the interfaces between the elements. i.e. as the shape functions are constructed in a 'piecewise' manner, the question of inter-element continuity is important. If the integral contains m^{th} order derivatives of the unknown function, then an element is compatible if the shape function and its derivatives up to order $m-1$ are continuous at the boundaries. The element is then said to have $C^{(m-1)}$ continuity.

An element which is not compatible may still be admissible if the inter-element contributions to the integrals which do exist are of a kind which continuously decrease with the fineness of element subdivision. An element which is both complete and compatible is said to be a conforming element, while an element which is complete but non-compatible is termed a non-conforming element. If conforming elements are used, convergence is monotonic, i.e. the accuracy of the solution increases continuously as the number of elements increased. If non-conforming elements are used, convergence to the 'exact' solution may occur in the limit, but in general will not be monotonic. The modified Galerkin method reduces the continuity requirement on the element, by reducing the order of derivatives in the integrand, the 'optimum' condition occurring when the weighting and trial terms are identical in form.

2.10 Post-processing

The final operation, called post-processing, displays the solution to the system equations in tabular, graphical, or pictorial form. Other physically meaningful quantities might be derived from the solution and displayed. For instance, a solution in terms of the acoustic pressure values at all nodes of a mesh can be post-processed to indicate the pressure distribution throughout the domain, or to evaluate four-pole parameters or transmission loss across the domain, etc. Post-processing also includes a

detailed examination of the finite element model to confirm that the whole analysis has been constructed correctly, and some verification of the results to prove that they are reasonable.

2.11 Galerkin formulation of eigenvalue problems

For the finite element solution of an eigenvalue problem, the basic technique is the same as that outlined previously, but a few extra details must be noted. By way of example consider the Helmholtz equation (2.1) for which the weak Galerkin formulation is

$$\sum_{J=1}^{N}\{\iiint_{v}(\nabla\psi_I\cdot\nabla\psi_J-k^2\psi_I\psi_J)dv\}p_J \;=\; \iint_{s}\psi_I\frac{\partial p^*}{\partial n}ds\,, \qquad I=1\text{ to }N \qquad (2.27)$$

see equation (2.10). The natural frequencies of acoustic wave motion inside a rigid-walled enclosure v then follow from the values of the wavenumber k for which non-trivial solutions of the equations

$$\sum_{J=1}^{N}\{\iiint_{v}(\nabla\psi_I\cdot\nabla\psi_J)dv-k^2\iiint_{v}(\psi_I\psi_J)dv\}p_J \;=\; 0, \quad I=1\text{ to }N, \qquad (2.28)$$

exist, since $\partial p^*/\partial n=0$ on a hard wall. The integrals of the left-hand-side follow in the same manner as that outlined previously, namely numerical integration in transformed coordinates over the separate elements, and element assembly is performed as before to give separate global stiffness and mass matrices, $[K]$ and $[M]$ respectively, where

$$\{[K]-k^2[M]\}\{\underline{p}\}=\;\{\underline{0}\}, \qquad (2.29)$$

a generalised eigenvalue problem. Standard equation solvers can then be used to find the eigenvalues k and the corresponding eigenvectors $\{\underline{p}\}_k$. Appropriate NAG routines were used for the solution of eigensystems in this thesis.

2.12 Software for acoustic analysis and their limitations

2.12.1 Commercial finite element packages

There are numerous commercial finite element packages of varying complexity available at present to solve linear acoustic problems involving the two- and three-dimensional Helmholtz equation. Some software systems permit a very compact formulation for the solution and this facilitates programming so that both the inexperienced finite element method user and the expert programmer spend a reduced amount of time and effort in programming and debugging. Detailed description of available programs can be obtained from computer manufacturers, or directly from the code distributor. Large general-purpose finite element programs include NASTRAN, ANSYS, PAFEC and SYSNOISE etc. In particular SYSNOISE, which is dedicated to acoustic problems, can use either the finite element method or the boundary element method. It also deals with the problems of ducts or enclosures with simple liners. PAFEC has the capability to do mixed finite element and boundary element modelling of acoustic problems, but cannot handle dissipative liners or wave propagation in a dissipative material.

To a large degree, the ease and successful application of finite element analysis software depends on the supporting pre- and post-processing programs. The pre-processing programs assist the user in generating the element mesh in the domain of the problem. Since the finite element code requires information about every node and every element, the preparation of required data file can be difficult and tedious. In some software, the pre-processing program reduces this effort by assisting the user in drawing the outline of the problem domain, and then with a simple command it automatically generates the mesh, numbers the elements and nodes, defines coordinates, and places all this

information in a format that the analysis program can read directly. Following the analysis of a fairly large problem, examination of copious amounts of hard-copy output can be a daunting task. The post-processing programs assist in interpretation of results, very often by incorporating graphical displays. However all software has its own limitations. In general these commercial packages have no flexibility with respect to the equation system to be solved, such that one cannot add mean flow effects or general absorbent material types, such as is required in the present work.

2.12.2 NAG FE Library

The NAG Finite Element Library is a library of FORTRAN subroutines [53], each of which performs a single, basic task within the structure of overall finite element programs. For instance there is a subroutine for each geometric element type which will return the shape function and its partial derivatives for each node, evaluated at a specified location within the element. An overall program must be written, which calls the appropriate routine as and when required, and within which the problem to be analysed is completely specified. However the NAG FE Library does not include any pre- and post-processing routines, nor do any of the commercial package available for these tasks include interface routines to the NAG FE Library. Thus mesh generation has been done manually or by in-house routines, and graphical post- processing has been done by UNIRAS software.

Table 2.1

Element Shape Functions

Element	Shape function
Three noded line element (see Figure 2.4(a))	$\psi_1(\xi) = \frac{1}{2}\xi(\xi - 1)$ $\psi_2(\xi) = 1 - \xi^2$ $\psi_3(\xi) = \frac{1}{2}\xi(\xi + 1)$
Six-noded triangular element (see Figure 2.4 (b),(c)) Typical corner node Typical mid-side node	$\psi_1 = (2L_1 - 1)L_1$ $\psi_4 = 4L_2L_3$ where $L_1(\xi,\eta) = \frac{1}{3}(1 + 2\xi)$ $L_2(\xi,\eta) = \frac{1}{3}(1 - \xi - \sqrt{3}\eta)$ $L_3(\xi,\eta) = \frac{1}{3}(1 - \xi + \sqrt{3}\eta)$
Eight-noded quadrilateral element (see Figure 2.4 (d),(e)) Corner nodes Typical midside node,	$\psi_i(\xi,\eta) =$ $\frac{1}{4}(1 + \xi\xi_i)(1 + \eta\eta_i)(\xi\xi_i + \eta\eta_i - 1)$ $\xi_i = 0 \quad \eta_i = \pm 1$ $\psi_i(\xi,\eta) = \frac{1}{2}(1 - \xi^2)(1 + \eta\eta_i)$ where (ξ_i, η_i) are the coordinates of i^{th} node.

Table 2.2

Abscissae points and weighting coefficient of Gaussian quadrature formula

Quadrature Scheme	Abscissae points,	Weighting functions
3 points	ξ_i	w_i
(for line elements)	$\pm\sqrt{3/5}$	40/81
	0.0	64/81
7 points	(ξ,η)	w_i
(for triangular elements)	(0,0)	$(\frac{27}{80}\sqrt{3})$
	(1,0)	$(\frac{3}{80}\sqrt{3})$
	$(-1/2,\pm\sqrt{3}/2)$	$(\frac{3}{80}\sqrt{3})$
	(−1/2,0)	$(\frac{1}{10}\sqrt{3})$
	$(1/4,\pm\sqrt{3}/4)$	$(\frac{1}{10}\sqrt{3})$
9 points	(ξ,η)	w_i
(for quadrilateral elements)	(0,0)	64/81
	$(\pm\sqrt{3/5},\pm\sqrt{3/5})$	25/81
	$(0,\pm\sqrt{3/5})$	40/81
	$(\pm\sqrt{3/5},0)$	40/81

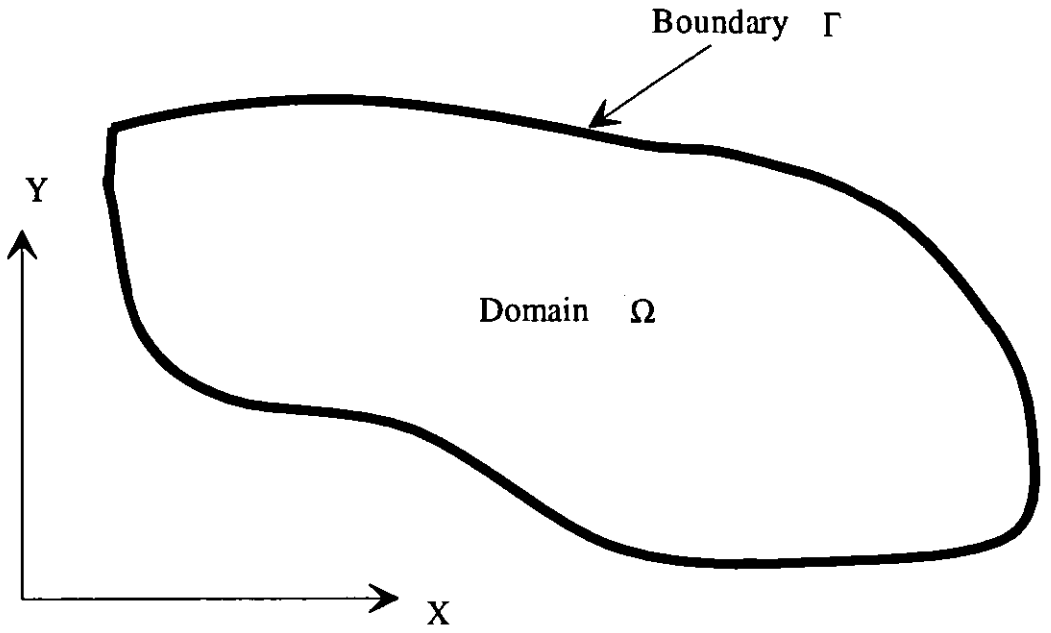

Figure 2.1 Over-view of two dimensional domain

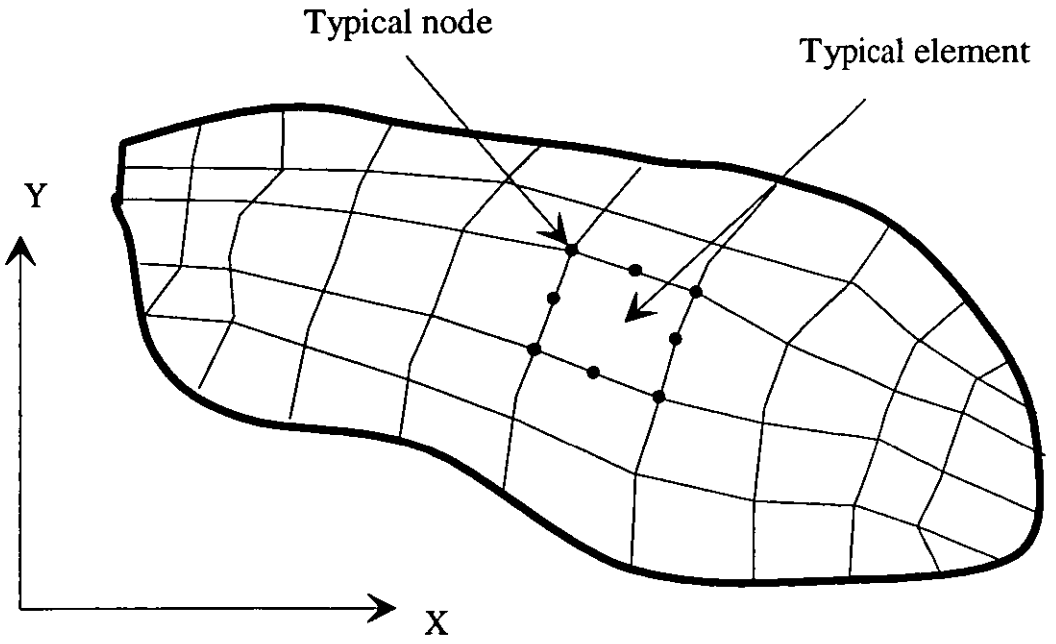

Figure 2.2 Discretization of a domain into a number of finite elements

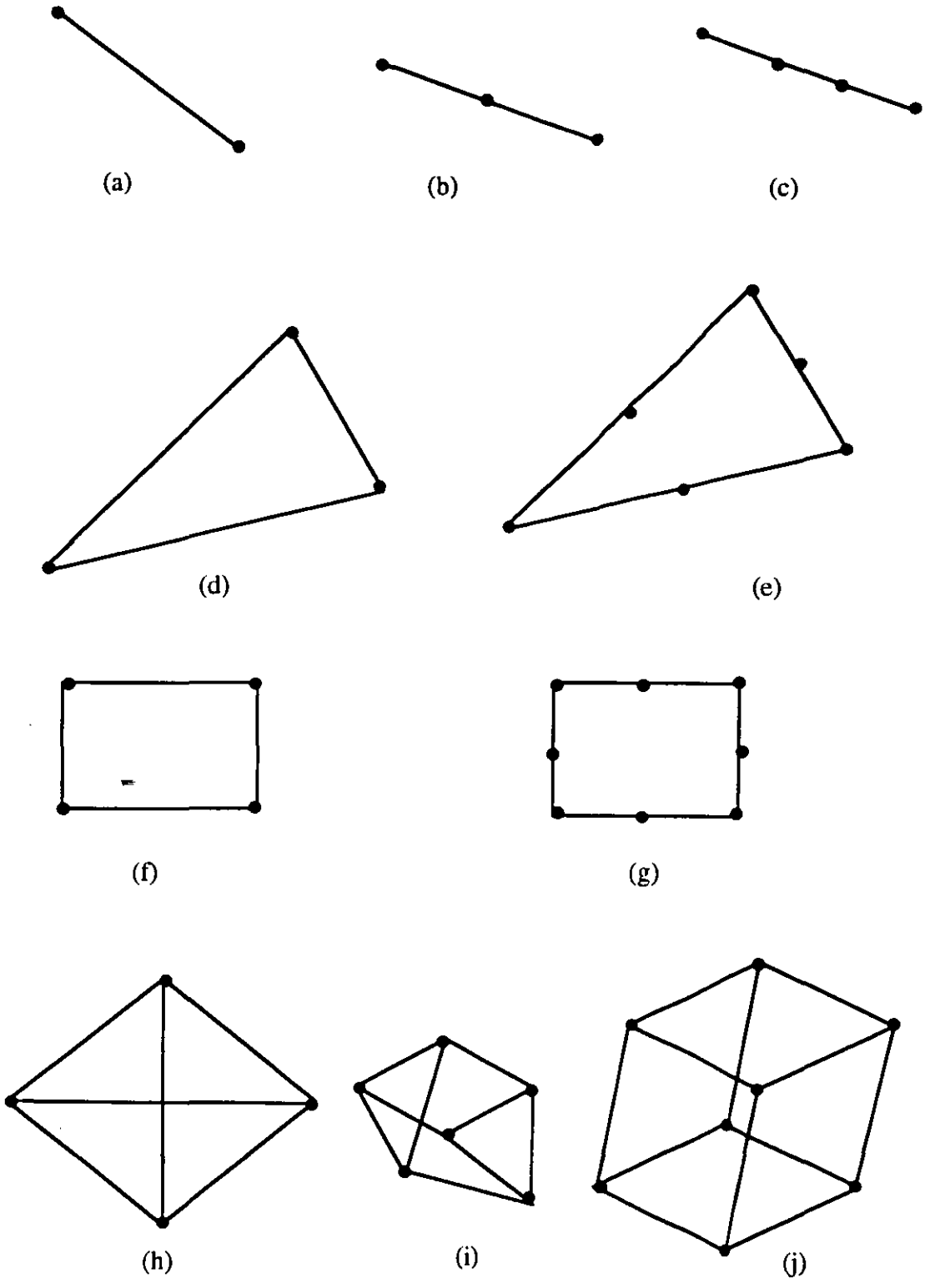

Figure 2. 3 Examples of (a)-(c); 1-D, (d)-(g); 2-D, and (h)-(j); 3-D elements

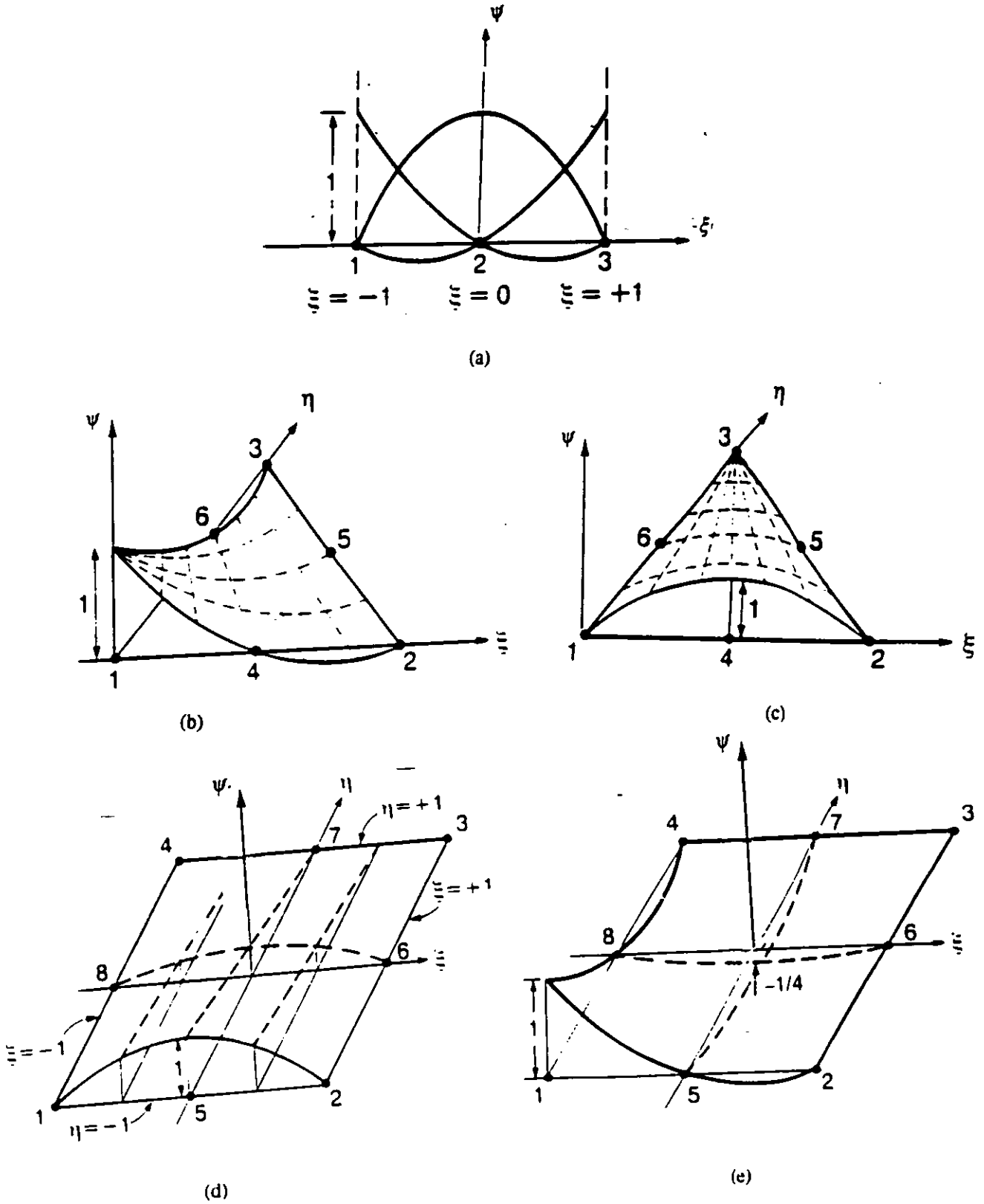

Figure 2.4 (a) Shape functions for a 3-noded, line element. (b),(c) Corner and mid-side shape functions for a 6-noded, triangular element. (d),(e) Midside and corner shape functions for a 8-noded, quadrilateral element.

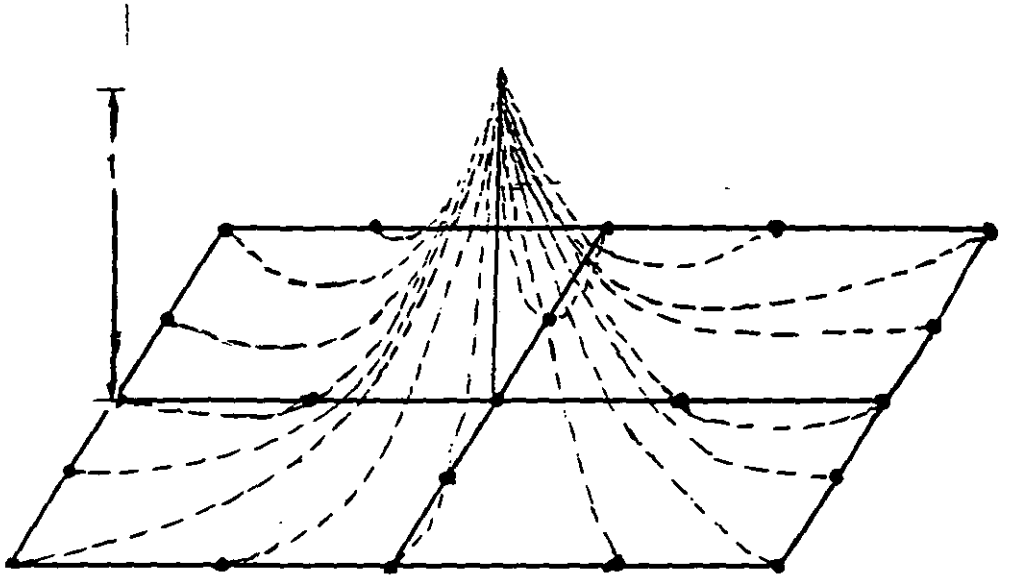

Figure 2.5 Basis function for a single, typical node in a mesh of 8-noded, quadrilateral elements.

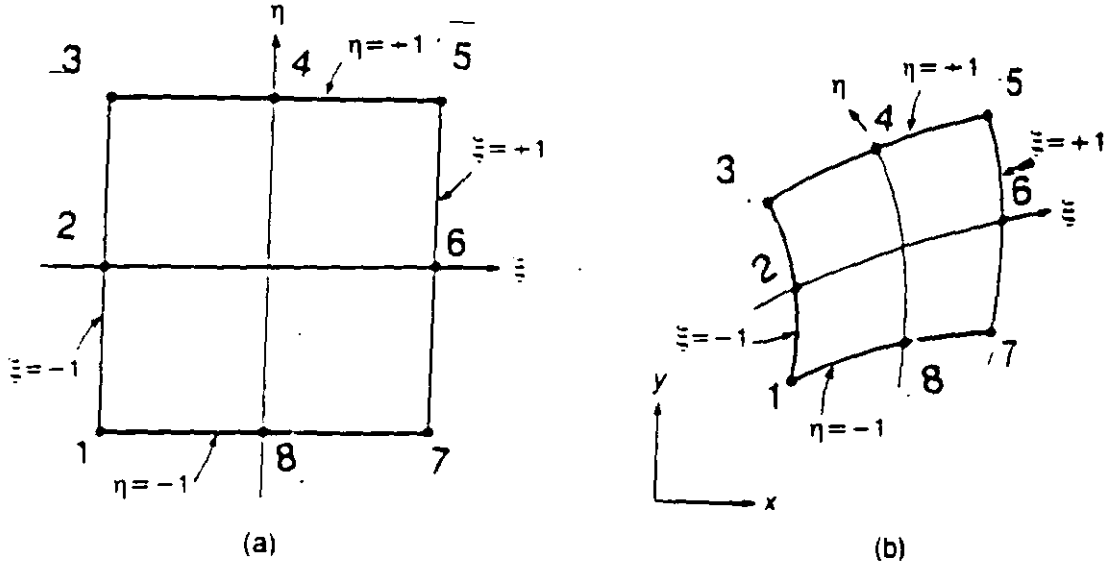

Figure 2.6 (a) 8-noded, isoparametric quadrilateral element in local coordinate space (b) Typical transformation of local element when mapped into global coordinate space.

CHAPTER 3

GOVERNING EQUATIONS

3.1 Introduction

This chapter outlines the fundamental equations for three-dimensional acoustic wave motion through a flow duct and a surrounding silencer volume which is packed with porous material, see Figure 3.1. Both regions of the duct, the gas flow passage and the absorbent, are taken to be of arbitrary shape. In Section 3.2 the general governing equations of the gas flow are developed and their reduced forms, under various simplifications, are given. In section 3.3 the general governing equations in the absorbent region, including steady flow effects through the porous material, are given together with various simplified forms. Properties of bulk-reacting porous materials and their empirical representation, including the effects of steady flow on the porous material properties, are given in Section 3.4. Equations for evaluation of the overall transfer matrix or four-pole parameters of a silencer, and hence the overall performance criteria such as transmission loss, are given in Section 3.5.

3.2 Governing Equations in the Flow Duct

The general equations of conservation of mass and momentum for an inviscid fluid are (e.g. Morse and Ingard [37])

$$\frac{\partial \rho}{\partial t} + \nabla.(\rho \boldsymbol{q}) = 0 \tag{3.1}$$

and

$$\frac{\partial \boldsymbol{q}}{\partial t} + (\boldsymbol{q} \cdot \nabla)\boldsymbol{q} = -\frac{1}{\rho}\nabla p, \tag{3.2}$$

where ρ, p and $\boldsymbol{q}$ are the fluid density, pressure and velocity respectively. Since the fluid is assumed to be inviscid the flow will be irrotational, hence

$$\boldsymbol{q} = \nabla \phi \tag{3.3}$$

where ϕ is the velocity potential. If one assumes that the fluid is non heat-conducting, then the flow will be isentropic and

$$\frac{p}{p_0} = \left(\frac{\rho}{\rho_0}\right)^{\gamma} \tag{3.4}$$

where γ is the ratio of specific heats and subscript $_0$ implies steady-state, stagnation conditions. Small disturbances will propagate through the fluid at the speed of sound c where, from equation (3.4),

$$c^2 = \left(\frac{\partial p}{\partial \rho}\right)_s = \frac{dp}{d\rho} = \gamma \frac{p}{\rho}. \tag{3.5}$$

Expansion of the continuity equation (3.1) gives

$$\frac{\partial \rho}{\partial t} + \boldsymbol{q} \cdot \nabla \rho + \rho \nabla \cdot \boldsymbol{q} = 0 \tag{3.6}$$

and substitution from equation (3.3) into equation (3.6) yields

$$\frac{1}{\rho}\frac{\partial p}{\partial t}+\frac{\nabla\phi\cdot\nabla\rho}{\rho}+\nabla^2\phi \;=\; 0. \tag{3.7}$$

The second term of the momentum equation (3.2) can be expanded by standard vector relations to

$$(\boldsymbol{q}\cdot\nabla)\boldsymbol{q} \;=\; \frac{1}{2}\nabla(\boldsymbol{q}\cdot\boldsymbol{q})-\boldsymbol{q}\times(\nabla\times\boldsymbol{q}) \tag{3.8}$$

or

$$(\boldsymbol{q}\cdot\nabla)\boldsymbol{q} \;=\; \frac{1}{2}\nabla(\boldsymbol{q}\cdot\boldsymbol{q}), \tag{3.9}$$

since the flow is irrotational. Substitution from equations (3.3) and (3.9) into equation (3.2) gives a new form of the momentum equation

$$\frac{\partial}{\partial t}(\nabla\phi)+\frac{1}{2}\nabla(\nabla\phi\cdot\nabla\phi) \;=\; -\frac{1}{\rho}\nabla p, \tag{3.10}$$

or

$$\nabla\left[\frac{\partial\phi}{\partial t}+\frac{1}{2}(\nabla\phi\cdot\nabla\phi)\right] \;=\; -\frac{1}{\rho}\nabla p. \tag{3.11}$$

Spatial integration of equation (3.11) gives

$$\frac{\partial\phi}{\partial t}+\frac{1}{2}(\nabla\phi\cdot\nabla\phi)+\int\frac{dp}{\rho} \;=\; F(t), \tag{3.12}$$

where $F(t)$ is the constant of integration, which could be a function of time. Evaluation of the integral term from equation (3.4) and substitution from equation (3.5) gives

$$\frac{\partial \phi}{\partial t} + \frac{1}{2}(\nabla\phi \cdot \nabla\phi) + \frac{c^2}{\gamma - 1} = \frac{c_0^2}{\gamma - 1}, \tag{3.13}$$

where the integration constant now follows from the stagnation conditions and is found not to be time-dependent. Equation (3.13) can be re-cast to yield the local sound speed as

$$c^2 = c_0^2 - (\gamma - 1)\left[\frac{\partial \phi}{\partial t} + \frac{1}{2}(\nabla\phi \cdot \nabla\phi)\right]. \tag{3.14}$$

Substitution from equation (3.5) into equation (3.11) gives

$$\nabla\left[\frac{\partial \phi}{\partial t} + \frac{1}{2}(\nabla\phi \cdot \nabla\phi)\right] = -\frac{c^2}{\rho}\nabla\rho \tag{3.15}$$

and into the time derivative form of equation (3.12) gives

$$\frac{\partial^2 \phi}{\partial t^2} + \frac{\partial}{\partial t}\left[\frac{1}{2}(\nabla\phi \cdot \nabla\phi)\right] = -\frac{1}{\rho}\frac{\partial p}{\partial t} = -\frac{1}{\rho}\frac{\partial p}{\partial \rho}\frac{\partial \rho}{\partial t} = -\frac{c^2}{\rho}\frac{\partial \rho}{\partial t}. \tag{3.16}$$

Equations (3.15) and (3.16) can now be used to eliminate the density from equation (3.7) to give

$$\nabla^2\phi = \frac{1}{c^2}\left\{\frac{\partial^2 \phi}{\partial t^2} + \frac{1}{2}\frac{\partial}{\partial t}(\nabla\phi \cdot \nabla\phi) + \nabla\phi \cdot \nabla\left[\frac{\partial \phi}{\partial t} + \frac{1}{2}(\nabla\phi \cdot \nabla\phi)\right]\right\} \tag{3.17}$$

or

$$\nabla^2\phi = \frac{1}{c^2}\left\{\frac{\partial^2 \phi}{\partial t^2} + \frac{\partial}{\partial t}(\nabla\phi \cdot \nabla\phi) + \frac{1}{2}\nabla\phi \cdot \nabla(\nabla\phi \cdot \nabla\phi)\right\}. \tag{3.18}$$

Consider the flow to be composed of a steady background flow of potential $\bar{\phi}$ together with a small time-dependent fluctuation of potential ϕ', i.e.

$$\phi = \bar{\phi} + \phi'(t). \tag{3.19}$$

The steady flow forms of equations (3.18) and (3.14) give

$$\nabla^2 \bar{\phi} = \frac{1}{2c^2} \nabla\bar{\phi} \cdot \nabla(\nabla\bar{\phi} \cdot \nabla\bar{\phi}) = \frac{1}{2} \nabla\bar{\phi} \cdot \nabla(M^2) \tag{3.20}$$

and

$$c_0^2 = c^2 + \left(\frac{\gamma - 1}{2}\right) |\nabla\bar{\phi}|^2 = c^2 \left[1 + (\frac{\gamma - 1}{2}) M^2 \right], \tag{3.21}$$

where $M = |\nabla\bar{\phi}|/c$ is the local Mach number of the steady flow. Substitution from equation (3.19) into equation (3.18), followed by subtraction of the steady flow equation (3.20) and linearisation of the small fluctuation terms, leaves the linearised acoustic equation of the form

$$\nabla^2 \phi' = \frac{1}{c^2} \left\{ \frac{\partial^2 \phi'}{\partial t^2} + 2\nabla\bar{\phi} \cdot \nabla(\frac{\partial \phi'}{\partial t}) + \frac{c^2}{2} \nabla\phi' \cdot \nabla(M^2) + (\nabla\bar{\phi} \cdot \nabla)^2 \phi' \right\}. \tag{3.22}$$

The general equations (3.20)-(3.22) simplify considerably under various additional assumptions, as detailed in the following sections.

3.2.1 Zero Steady Flow

For the simplest case of acoustic propagation in a stationary medium, the equations (3.22) and (3.21) reduce to

$$\nabla^2\phi' = \frac{1}{c_0^2}\frac{\partial^2\phi'}{\partial t^2}, \tag{3.23}$$

the standard wave equation with propagation at constant sound speed c_0. The momentum equation (3.11) also simplifies considerably to

$$p' = -\rho_0\frac{\partial\phi'}{\partial t}, \tag{3.24}$$

such that the wave equation (3.23) can be written in terms of the acoustic pressure,

$$\nabla^2 p' = \frac{1}{c_0^2}\frac{\partial^2 p'}{\partial t^2}. \tag{3.25}$$

3.2.2 Uniform Steady Flow

If the steady flow is uniform throughout the flow field, then

$$\nabla\overline{\phi} = \overline{\mathbf{V}}, \text{ a constant}, \tag{3.26}$$

and it follows from equation (3.14) that the speed of sound is constant, say $\overline{c}$, throughout the flow field and hence the Mach number is also constant. Thus equation (3.22) reduces to

$$\nabla^2\phi' = \frac{1}{\overline{c}^2}\left\{\frac{\partial^2\phi'}{\partial t^2} + 2\overline{\mathbf{V}}\cdot\nabla\left(\frac{\partial\phi'}{\partial t}\right) + (\overline{\mathbf{V}}\cdot\nabla)^2\phi'\right\} \tag{3.27}$$

or

$$\nabla^2\phi' = \frac{1}{\overline{c}^2}\left\{\frac{\partial}{\partial t} + (\overline{\mathbf{V}}\cdot\nabla)\right\}^2\phi'. \tag{3.28}$$

The momentum equation (3.11) also simplifies to

$$\rho_0\left(\frac{\partial}{\partial t}+\overline{\mathbf{V}}\cdot\nabla\right)\phi' = -p', \tag{3.29}$$

hence the acoustic equation (3.28) can be written in terms of the acoustic pressure p' as

$$\nabla^2 p' = \frac{1}{\overline{c}^2}\left\{\frac{\partial}{\partial t}+(\overline{\mathbf{V}}\cdot\nabla)\right\}^2 p'. \tag{3.30}$$

3.2.3 Non-Uniform Steady Flow of Low Mach Number

If the local Mach number of the steady flow is small enough everywhere such that terms of $0[M^2]$ can be neglected, then the equation of steady flow (3.20) reduces to

$$\nabla^2\overline{\phi} = 0, \tag{3.31}$$

Laplace's equation of incompressible flow. Furthermore, from equation (3.21),

$$c^2 = c_0^2, \tag{3.32}$$

hence the linearised acoustic equation (3.22) becomes

$$\nabla^2\phi' = \frac{1}{c_0^2}\left\{\frac{\partial^2\phi'}{\partial t^2}+2\nabla\overline{\phi}\cdot\nabla\left(\frac{\partial\phi'}{\partial t}\right)\right\}. \tag{3.33}$$

Once again the momentum equation (3.11) simplifies, giving

$$\rho_0\left(\frac{\partial}{\partial t}+\nabla\overline{\phi}\cdot\nabla\right)\phi' = -p', \tag{3.34}$$

hence the acoustic equation (3.33) can be written in terms of the acoustic pressure as

$$\nabla^2 p' = \frac{1}{c_0^2}\left\{\frac{\partial^2 p'}{\partial t^2} + 2\nabla\bar{\phi}\cdot\nabla\left(\frac{\partial p'}{\partial t}\right)\right\}. \tag{3.35}$$

3.3 Governing Equations in the Absorbent Region

The equation of mass conservation within a porous material is [37]

$$\Omega\frac{\partial \rho_a}{\partial t} + \nabla\cdot(\rho_a \boldsymbol{q}_a) = 0 \tag{3.36}$$

where ρ_a,$\boldsymbol{q}_a$ are the density and the velocity in porous material, and Ω is the porosity, the ratio of the volume of accessible holes to the total volume of the porous medium. Subscript a is used throughout to denote variables within the absorbent region. The momentum equation in the absorbent region must include the change in inertia and the frictional drag suffered by the fluid as it moves through the pores. The inertial term of the momentum equation follows from Smith and Greenkorn [59] and can be written as $\frac{1}{\Omega}\rho_a[M_a]\partial\boldsymbol{q}_a / \partial t$, where $[M_a]$ is a diagonal matrix whose jth term is m_j, the structure factor in direction x_j. Convective acceleration terms, which are of order $|\boldsymbol{q}_a|/c_0$ compared to the local acceleration, have been ignored. The overall resistance to fluid motion in direction j can be expressed as a sum of a viscous resistance $\sigma_{oj}\, q_{aj}$ and an inertial resistance term due to eddy formation $\sigma_{ij}|\boldsymbol{q}_a|q_{aj}$, see Carman [91], where σ_{oj} and σ_{ij} are the complex components of viscous flow resistivity and inertial flow resistivity in the jth direction. Hence the momentum equation for flow in a porous material can be written as

$$\frac{\rho_a}{\Omega}[M_a]\frac{\partial q_a}{\partial t} = -\nabla p_a - [\Sigma]q_a \tag{3.37}$$

where $[\Sigma]$ is a diagonal matrix whose *jth* term is $\sigma_{aj} = \sigma_{oj} + \sigma_{ij}|q_a|$. Let the fluid variables be expanded as the sum of steady-flow and small, time-dependent, perturbation components, such that

$$p_a = \bar{p}_a + p'_a(t), \quad q_a = \bar{q}_a + q'_a(t) \text{ and } \rho_a = \rho_0 + \rho'_a(t). \tag{3.38}$$

Thus equations (3.36) and (3.37) become

$$\Omega\frac{\partial \rho'_a}{\partial t} + (\rho_0 + \rho'_a)\nabla\cdot(\bar{q}_a + q'_a) + (\bar{q}_a + q'_a)\cdot\nabla\rho'_a = 0 \tag{3.39}$$

and

$$\frac{(\rho_0 + \rho'_a)}{\Omega}[M_a]\frac{\partial}{\partial t}(q'_a) = -\nabla(\bar{p}_a + p'_a) - [\Sigma](\bar{q}_a + q'_a). \tag{3.40}$$

For the steady flow case, these equations reduce to

$$\nabla\cdot\bar{q}_a = 0 \tag{3.41}$$

and

$$\nabla\bar{p}_a = -[\bar{\Sigma}]\bar{q}_a \tag{3.42}$$

where $[\bar{\Sigma}]$ is a diagonal matrix whose *jth* term is $\bar{\sigma}_{aj} = (\sigma_{vj} + \sigma_{ij}|\bar{q}_a|)$, and σ_{vj} is the steady viscous flow resistivity.

The first-order perturbation form of equation (3.39) is

$$\Omega \frac{\partial \rho_a'}{\partial t} + \rho_0 \nabla \cdot \boldsymbol{q}_a' + \bar{\boldsymbol{q}}_a \cdot \nabla \rho_a' = 0. \tag{3.43}$$

Once again, the convective acceleration term $\bar{\boldsymbol{q}}_a \cdot \nabla \rho_a'$ is of order $|\bar{\boldsymbol{q}}_a|/c_0$ compared to the local acceleration and will be ignored. Furthermore the equation of state relates the change in density to the excess pressure by the linearised relation [37]

$$\rho_a' = \rho_0 \chi p_a', \tag{3.44}$$

hence equation (3.43) can be written as

$$\chi \Omega \frac{\partial p_a'}{\partial t} + \nabla \cdot \boldsymbol{q}_a' = 0, \tag{3.45}$$

where χ is the effective compressibility of the acoustic medium in the pores.

The first-order perturbation form of the momentum equation (3.40) is

$$\rho_0 \frac{[M_a]}{\Omega} \frac{\partial \boldsymbol{q}_a'}{\partial t} = -\nabla p_a' - [\Sigma'] \boldsymbol{q}_a', \tag{3.46}$$

where $[\Sigma']$ is a diagonal matrix whose *jth* term [18] is

$$\sigma_{aj}' = \sigma_{0j} + \sigma_{ij} \left\{ |\bar{\boldsymbol{q}}_a| + (\bar{\boldsymbol{q}}_a \cdot \boldsymbol{q}_a') \bar{q}_{aj} / |\bar{\boldsymbol{q}}_a| q_{aj}' \right\}, \tag{3.47}$$

where $\sigma_{0j}(\omega)$ is the frequency dependent, complex acoustic flow resistivity in direction j and, as $\omega \to 0$, $\sigma_{0j}(\omega) \to \sigma_{vj}$.

3.3.1 Isotropic and homogeneous porous media, without mean flow

The general wave equation in this case follows by taking the time derivative of equation (3.45) and the divergence of equation (3.46) to give

$$\chi\Omega\frac{\partial^2 p_a'}{\partial t^2}+\frac{\partial}{\partial t}\nabla\cdot q_a' \;=\; 0 \tag{3.48}$$

and

$$\rho_0\frac{m}{\Omega}\frac{\partial}{\partial t}\nabla\cdot q_a' \;=\; -\nabla^2 p_a'-\sigma\nabla\cdot q_a', \tag{3.49}$$

respectively, where $m_j = m$ and $\sigma_{aj}' = \sigma$ are now constant for all j. Hence, from equations (3.45), (3.48) and (3.49)

$$\nabla^2 p_a' \;=\; \rho_0 m\chi\frac{\partial^2 p_a'}{\partial t^2}+\sigma\Omega\chi\frac{\partial p_a'}{\partial t}, \tag{3.50}$$

which is the wave equation for isotropic and homogeneous porous media without mean flow.

3.3.2 Internal steady flow in absorbent

The full equations of the steady flow are the general continuity and momentum equations (3.41) and (3.42). The momentum equation in direction x_j is seen to be nonlinear, of the form

$$\frac{\partial\bar{p}_a}{\partial x_j} = \;-(\sigma_{vj}+\sigma_{ij}|\bar{q}_a|)\bar{q}_{aj}, \tag{3.51}$$

which is termed the Ergun or Forchheimer equation (see book by Carman [93]).

Considerable simplification occurs if the steady flow is uni-directional, in direction x_j say, since it follows from equation (3.51) that

$$\bar{q}_{aj} = [-\sigma_{vj} + (\sigma_{vj}^2 - 4\sigma_{ij}\frac{d\bar{p}_a}{dx_j})^{1/2}]/2\sigma_{ij}. \tag{3.52}$$

The continuity equation (3.41) indicates that $\bar{q}_{aj}$ is invariant with x_j and hence the absorbent properties cannot vary with x_j, but they may still vary over the plane perpendicular to x_j and would then give rise to non-uniform mean flow.

An alternative simplification, applicable to the general flow case, is achieved if the momentum equation (3.51) is approximated as

$$\frac{\partial \bar{p}_a}{\partial x_j} = -(\sigma_{vj} + \sigma_{ij}|\bar{q}_a|_{ave})\bar{q}_{aj} \tag{3.53}$$

where $|\bar{q}_a|_{ave}$ is an estimated constant average value of the real non-uniform flow. The linear momentum equations of this form can then be combined with the continuity equation (3.41) to give

$$\nabla \cdot [S]^{-1} \nabla \bar{p}_a = 0 \tag{3.54}$$

where $[S]$ is a diagonal matrix whose jth term is $\sigma_{vj} + \sigma_{ij}|\bar{q}_a|_{ave}$.

3.3.3 Non-homogeneous and anisotropic porous medium, with flow

If one assumes that the perturbations have harmonic time variation of radian frequency ω, then the continuity and momentum equations (3.45) and (3.46) become

$$\Omega\chi i\omega\, p_a' + \nabla\cdot q_a' = 0 \tag{3.55}$$

and

$$\left(\frac{\rho_0 i\omega}{\Omega}[M_a]+[\Sigma']\right)q_a' = -\nabla p_a' \tag{3.56}$$

respectively. The latter can be simplified to

$$i\omega\rho_0[\Pi]q_a' = -\nabla p_a' \tag{3.57}$$

where matrix $[\Pi]=\left(\frac{[M_a]}{\Omega}+\frac{[\Sigma']}{i\omega\rho_0}\right)$, a diagonal matrix whose *jth* element is $\left(\frac{m_j}{\Omega}-\frac{i\sigma'_{aj}}{\omega\rho_0}\right)$. Let ρ_{aj} be the effective, complex, mean fluid density in the pores of the material for motion in direction j, [17]

$$\rho_{aj} = \frac{\rho_0 m_j}{\Omega}\left(1-\frac{i\Omega\sigma'_{aj}}{\omega\rho_0 m_j}\right) = \rho_0\gamma_j z_j \tag{3.58}$$

where z_j, and γ_j are the characteristic impedance and the propagation coefficient of porous media,[17]

$$z_j = (m_j/\rho_0\chi)^{1/2}(1-\mathrm{i}\Omega\sigma'_{aj}/\rho_0 m_j\omega)^{1/2}/\Omega c_0, \tag{3.59}$$

$$\gamma_j = c_0(\rho_0 m_j\chi)^{1/2}(1-\mathrm{i}\Omega\sigma'_{aj}/\rho_0 m_j\omega)^{1/2}. \tag{3.60}$$

The momentum equation (3.57) can then be written as

$$i\omega\rho_0 q_a' = -[R]\nabla p_a' \tag{3.61}$$

where $[R]=[\Pi]^{-1}$ is a diagonal matrix whose *jth* element is ρ_0/ρ_{aj}. Equations (3.55) and (3.61) can be combined to give

$$\rho_0\omega^2\Omega\chi\, p_a' + \nabla\cdot[R]\nabla p_a' \;=\; 0, \tag{3.62}$$

the wave equation for harmonic waves in a general porous medium.

3.4 Porous Material Properties

It is common practice to use absorption material within at least one volume of an exhaust silencer system or flow-duct system, due to its effectiveness at broad-band sound reduction in the mid- to high-frequency range. Inclusion of absorbent materials increases the complexity of silencer construction and results in cost and weight penalties. It is essential, therefore, that the optimum use of the absorption treatment in a silencer is achieved. In an acoustic absorber, sound energy is absorbed because of frictional dissipation of the energy of motion into heat and irreversible thermal process. The acoustical properties of various porous materials have been examined by numerous authors [56, 57, 67, 92, 93, 94]. These properties are generally determined from five basic parameters (porosity, flow resistivity, tortuosity, steady flow shape factor and dynamic shape factor) and specified in terms of characteristic impedance and propagation constant. This section describes the bulk acoustic properties of absorbent materials and provides the data representation in a mathematical form. It is shown how induced steady flow in the absorbent, forced by the steady flow pressure gradient in the flow duct, affects the representation.

3.4.1 Impedance and propagation coefficient of acoustic absorbers

The acoustic performance of porous material can be predicted using an appropriate prediction model and applicable values of the prediction parameters. A great deal of research has been carried out to obtain correlations between the acoustic impedance of a porous absorber and the various parameters of its construction, and the environment in which it is employed. The zero flow form of the characteristic impedance and propagation coefficient equation follow from equations (3.59) and (3.60), with $\sigma'_{aj} = \sigma_{oj}$ from equation (3.47), and are

$$z_{0j} = (m_j / \rho_0 \chi)^{1/2}(1 - i\Omega\sigma_{oj} / \rho_0 m_j \omega)^{1/2} / \Omega c_0 \tag{3.63}$$

and

$$\gamma_{0j} = c_0(\rho_0 m_j \chi)^{1/2}(1 - i\Omega\sigma_{oj} / \rho_0 m_j \omega)^{1/2} \tag{3.64}$$

respectively.

The acoustical performance of several types of complex fibrous absorbers have been quantified by Delany-Bazley relations [57] with various degree of success by subsequent workers [17,18,20,61,62]. The present analysis also utilises Delany-Bazley relations. The acoustic impedance for fibrous absorbers can be expressed in terms of the thickness and steady flow resistance per unit thickness of the material of the fibrous absorber. Delany and Bazley [57] have deduced an empirical power-law relationship for such absorbers and have shown that, for bulk acoustic properties of porous materials, empirical expressions may be used to represent the zero flow characteristic impedance z_{0j} and propagation coefficient γ_{0j} in direction j as a function of the frequency parameter ϕ_j, where

$$\phi_j = \omega\rho_0 / 2\pi\sigma_{vj}. \tag{3.65}$$

The expressions for z_{0j} and γ_{0j} are of the form

$$z_{0j} = (1 + c_1\phi_j^{c_2}) - \mathrm{i}(c_3\phi_j^{c_4}) \tag{3.66}$$

and

$$\gamma_{0j} = (1 + c_7\phi_j^{c_8}) - \mathrm{i}(c_5\phi_j^{c_6}) \tag{3.67}$$

where the coefficients c_1 to c_8 have to be determined from experimental tests [17,18]. The data obtained from equations (3.66) and (3.67) are not valid at low frequencies, the lower limit of validity of these data accruing when $\phi_j > 0.012$. Below this limit the approximate formulae of Mechel [64] can be used:

$$\gamma_{0j} = (1 - \frac{\mathrm{i}\gamma}{2\pi\varphi_j})^{1/2} \quad \text{and} \quad z_{0j} = \frac{\gamma_{0j}}{\gamma\Omega} \tag{3.68}$$

where γ is the specific heat ratio and Ω is the volume porosity of the absorbent.

3.4.2 Internal mean flow effects

A general expression for the overall resistivity in the presence of non-uniform steady flow within the absorbent was given in equation (3.47). If the internal mean flow is uni-directional in direction l then equation (3.47) simplifies considerably to

$$\sigma'_{al} = \sigma_{al} + 2\sigma_{il}|\overline{q}_a| \quad \text{and} \quad \sigma'_{aj} = \sigma_{aj} + \sigma_{ij}|\overline{q}_a|,\ j \neq l. \tag{3.69}$$

The relations for the characteristic impedance z_j and the propagation constant γ_j in the presence of an internal mean flow, equations (3.59) and (3.60), can be re-written in terms of the zero flow equations (3.63) and (3.64) as

$$z_j^2 = z_{0j}^2 + (-iz_{oj} / \rho_0 \omega \gamma_{oj})(\sigma_j - \sigma_{oj}) \tag{3.70}$$

$$\gamma_j^2 = \gamma_{0j}^2 + (-i\gamma_{oj} / \rho_0 \omega z_{oj})(\sigma_j - \sigma_{oj}). \tag{3.71}$$

3.5 Equations for the Four-Pole Parameters

The overall performance of a silencer can be evaluated in terms of its noise-reducing properties which are usually described by insertion loss, transmission loss or level difference. Insertion loss is defined as the difference in sound pressure level at a specified point exterior to the silencer with and without the silencer present. This value depends upon the properties of the source and termination as well as the silencer. Specifically, the source impedance as well as terminating impedance for the system will affect the amount of insertion loss provided by the silencer. The transmission loss is derived from the ratio of acoustic power incident on the silencer to the power transmitted from the silencer. The level difference is the difference in sound pressure levels at two arbitrary selected points in the upstream exhaust pipe and downstream tail pipe. The transmission loss of a silencer element gives an indication of the independent effectiveness of the element. It is not affected by the terminating impedance or source impedance or other elements of the system. In contrast, insertion loss provides a comparative measure of the effectiveness of a silencer element as installed in a complete silencer system. Level difference does not give a meaningful indication of either element performance or overall system performance and has little value.

The present work is concerned with analysis of the noise-reducing properties of individual absorption silencer elements. Calculated results are generally presented in terms of transmission loss, but the underlying analysis is always in terms of the four-

pole parameters of the elements from which any of the noise measurement criteria can than be evaluated, given the relevant information about the rest of the silencer system.

Four-pole parameters are constituents of the transfer matrix of a given silencer element [1] where, adopting acoustic pressure and velocity as the two state variables, one has

$$\begin{Bmatrix} p_r \\ q_r \end{Bmatrix} = \begin{bmatrix} A_r & B_r \\ C_r & D_r \end{bmatrix} \begin{Bmatrix} p_{r-1} \\ q_{r-1} \end{Bmatrix}. \tag{3.72}$$

where $\{p_r\ q_r\}^T$ is the state vector at some upstream point r, and $\{p_{r-1}\ q_{r-1}\}^T$ is the state vector at some downstream point $r-1$. The transfer matrix for r^{th} element can be denoted by $[T_r] = \begin{bmatrix} A_r & B_r \\ C_r & D_r \end{bmatrix}$ where A_r, B_r, C_r and D_r are known as four-pole parameters. It is implicit in these definitions that plane-wave conditions hold at the upstream and downstream locations r and $r-1$. Analysis is thereby restricted to low frequencies and, for a highly non-uniform silencer element, it may be necessary to consider lengths of uniform duct attached to the inlet and exit plane of the element and to determine the transfer matrix across the combined duct and silencer element, in order to enforce plane-wave conditions on the element boundaries, see Figure 3.1.

Consider a complete system to be composed of a series of n elements, each with a given transfer matrix. The downstream state vector of one element is the upstream state vector of the succeeding element, thus the n equations of the form of (3.72) combine to give

$$\begin{Bmatrix} p_n \\ q_n \end{Bmatrix} = \begin{bmatrix} A_n & B_n \\ C_n & D_n \end{bmatrix} \begin{bmatrix} A_{n-1} & B_{n-1} \\ C_{n-1} & D_{n-1} \end{bmatrix} \cdots \begin{bmatrix} A_r & B_r \\ C_r & D_r \end{bmatrix} \cdots \begin{bmatrix} A_1 & B_1 \\ C_1 & D_1 \end{bmatrix} \begin{Bmatrix} p_0 \\ q_0 \end{Bmatrix}. \tag{3.73}$$

Following matrix multiplication, the above equation can be written as

$$\begin{Bmatrix} p_n \\ q_n \end{Bmatrix} = \begin{bmatrix} A & B \\ C & D \end{bmatrix} \begin{Bmatrix} p_0 \\ q_0 \end{Bmatrix}. \tag{3.74}$$

Hence, for an individual element or an overall system, the state vectors at the inlet and outlet are related by

$$\begin{Bmatrix} p_{in} \\ q_{in} \end{Bmatrix} = \begin{bmatrix} A & B \\ C & D \end{bmatrix} \begin{Bmatrix} p_{out} \\ q_{out} \end{Bmatrix} \tag{3.75}$$

such that individual elements of the transfer matrix, i.e. the four-pole parameters, can be evaluated as

$$A = \left(\frac{p_{in}}{p_{out}} \right)_{q_{out}=0} \quad B = \left(\frac{p_{in}}{q_{out}} \right)_{p_{out}=0} \quad C = \left(\frac{q_{in}}{p_{out}} \right)_{q_{out}=0} \quad D = \left(\frac{q_{in}}{q_{out}} \right)_{p_{out}=0}. \tag{3.76}$$

The transmission loss of an element or system can then be written as [1]

$$TL = 20 \log_{10} \left[\frac{1}{2} \left(A + \frac{B}{\rho_0 c_0} + \rho_0 c_0 C + D \right) \right] \quad [dB] \tag{3.77}$$

and the insertion loss as

$$IL = 20 \log_{10} \left[\frac{\tilde{A} Z_r + \tilde{B} + \tilde{C} Z_e Z_r + \tilde{D} Z_e}{A' Z_r + B' + C' Z_e Z_r + D' Z_e} \right] \quad [dB], \tag{3.78}$$

where Z_e and Z_r are the source and radiation impedance respectively, and four-pole parameters with the tilde ~ and prime ' notations denotes the quantities for two different systems.

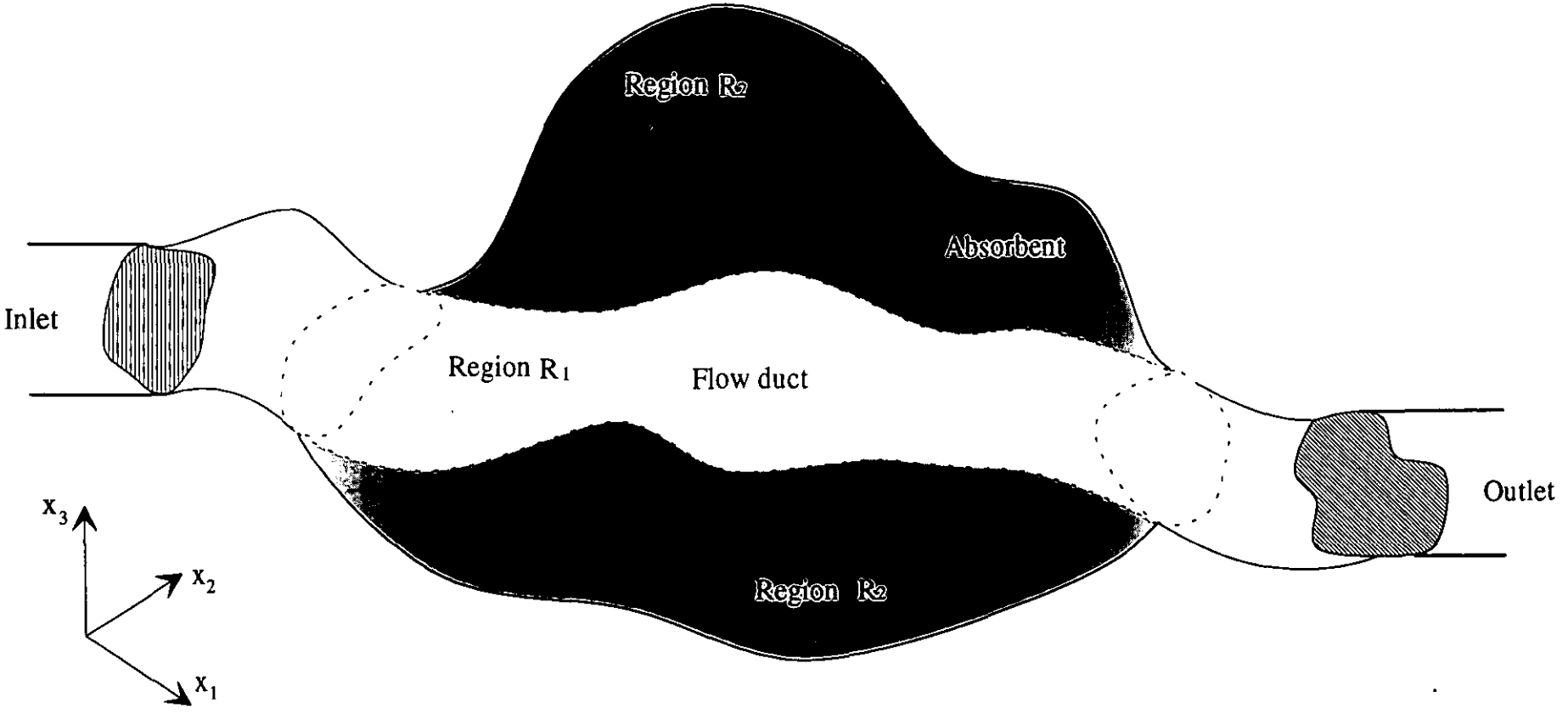
Region R2
Absorbent
Inlet
Region R1
Flow duct
Outlet
Region R2
x3
x2
x1

FIGURE 3.1

CHAPTER 4

EIGENVALUE FORMULATION FOR SILENCERS OF ARBITRARY CROSS-SECTION

4.1 Introduction

Eigenvalue analysis of uniform ducts of circular or rectangular cross-section, with or without mean flow, has been done analytically and numerically. Several researchers have published details of the eigenvalue analysis of silencers of circular-section. For example, Nilsson and Brander [85] have examined sound propagation in an infinite duct with uniform mean flow in the central passage, including the effects of a perforated tube between the gas flow and absorbent, by the use of the Wiener-Hopf method. Cummings and Chang [18] have examined the effects of the induced internal mean flow in the absorbent on sound attenuation in a circular-section silencer. Bies et al [46] presented design charts for infinite circular-section lined ducts with mean flow. Some workers have also made use of the finite element method for eigen analysis of the infinite duct with or without flow consideration in open central passage, but not with flow in the absorbent medium. For example Ramakrishnan and Watson [68,69] used the finite element method and presented design curves for circular and annular section ducts without any flow. Astley and Cummings [20] employed a finite element scheme to analyse a rectangular duct lined on all four sides, with flow in the central airway

passage but not in the absorbent. Cummings [70] used the Rayleigh-Ritz method and compared his results with experimental results for ducts of various cross-section, but again without flow in the absorbent.

In this chapter, a finite element model is presented for analysis of the propagation of acoustic waves in an infinite duct of arbitrary but uniform cross-section, comprised of a central flow passage surrounded by a bulk-reacting lining of sound absorbing material, see Figure 4.1. Computed results of circular and elliptical cross-section absorption silencers are presented and the first few lower-order mode shapes are described. Comparison is made between predicted and experimental results [18,70] of modal axial attenuation rate and phase speed. The model incorporates both uniform flow of gas in the open central passage and non-uniform induced steady flow in the absorbent.

In Section 4.2 the governing equations in both regions of the silencer, together with the respective boundary conditions, are given. Section 4.3 presents the finite element formulation of the problem. In Section 4.4 the construction of the matrix equations for the two cases of with flow and without flow are given. In Section 4.5 results are presented for different test silencers, together with the effects of flow and variation of the absorbent packing. Phase speed, sound attenuation and mode shape are found for the four least attenuated modes. The method can readily cope with a number of physical effects in addition to the general form of cross-section, including inhomogeneity and anisotropy of the absorbent, and induced mean flow through the absorbent.

4.2 Geometry and Governing Equations

The analysis follows closely that of Astley and Cummings [20], who considered the case of isotropic and homogeneous absorbent material and neglected induced flow within the absorbent. The notation used here follows that of [20] as far as possible. The basic geometry and co-ordinate system which are used in the analysis are shown in Figure 4.1. A duct, of arbitrary cross-section in the x–y plane, is lined with porous material of finite thickness. The acoustic properties of the absorbent are assumed to vary in the x–y plane, but not along the z-axis, the axis of the duct. This situation may arise, for example, due to non-uniform packing of a silencer, particularly when the outer shell is not circular in cross-section. The outer shell of the duct, denoted by the contour C_2, is assumed to be rigid and impervious. The common boundary between the open flow passage in the central region of the duct, region R_1 and the outer region which is packed with absorbent material, region R_2, is represented by the contour C_1. A steady, uniform airflow of speed $\overline{U}$ is present in region R_1 and flows along the axis of the duct. An axial pressure gradient is required to drive the steady flow and this pressure gradient induces a small, steady axial flow in the absorbent of speed $U(x, y)$. Coupled acoustical modes, which propagate in both the airway and the absorbent with the same axial wavenumber, are then sought.

4.2.1 Governing equations in the flow passage

The acoustical pressure and particle velocity in the flow passage, region R_1, are denoted by $p_1^*(\boldsymbol{x},t)$ and $\boldsymbol{q}_1^*(\boldsymbol{x},t)$ respectively. The linearised acoustic equation (3.30) can then be written as

$$\nabla^2 p_1^* = \frac{1}{\overline{c}^2}\left\{\frac{\partial}{\partial t}+(\overline{U}\frac{\partial}{\partial z})\right\}^2 p_1^* \tag{4.1}$$

since the steady flow $\overline{U}$ is in the axial z direction. Furthermore, the linearised momentum equation (3.29) for this case is

$$\rho_0(\frac{\partial}{\partial t}+\overline{U}\frac{\partial}{\partial z})\phi' = \quad -p_1^* \tag{4.2}$$

where, from equation (3.3),

$$q_1^* = \quad -\nabla\phi'. \tag{4.3}$$

Hence the momentum equation becomes

$$\rho_0\left(\frac{\partial}{\partial t}+\overline{U}\ \frac{\partial}{\partial z}\right) q_1^* = \quad -\nabla p_1^*. \tag{4.4}$$

The acoustical particle displacement in the flow passage is denoted by $\underline{\xi_1^*}\ (x,t)$. The acoustical velocity is the total derivative of the particle displacement,

$$(\partial / \partial t+\overline{U}\ \partial / \partial z)\ \underline{\xi_1^*} = \quad q_1^*\ , \tag{4.5}$$

hence the momentum equation (4.4) can be written as

$$\rho_0(\partial / \partial t+\overline{U}\ \partial / \partial z)^2\ \underline{\xi_1^*} = -\nabla p_1^*\ . \tag{4.6}$$

A time harmonic solution, of radian frequency ω is then sought for an acoustical wave propagating in the airway with complex wavenumber $k\lambda$ where $k = \omega / \overline{c}$. Thus

$$p_1^*(x,t) = p_1(x,y)e^{i(\omega t - k\lambda z)}, \quad \underline{\xi_1}^* = \underline{\xi_1}(x,y)e^{i(\omega t - k\lambda z)} \tag{4.7,4.8}$$

and the imaginary component of λ determines the degree of attenuation of the wave. Equations (4.1) and (4.6) thus become

$$\nabla^2 p_1 + k^2(1-\lambda M)^2 p_1 - k^2\lambda^2 p_1 = 0 \tag{4.9}$$

and

$$\rho_0\omega^2(1-\lambda M)^2 \underline{\xi_1} = \nabla p_1 \tag{4.10}$$

respectively, where ∇ and $\underline{\xi_1}$ now denote two-dimensional forms – in the x, y plane – of the gradient operator and particle displacement vector, respectively. M is the Mach number of the uniform, steady flow, $\overline{U} / \overline{c}$.

4.2.2 Governing equations in the absorbent

The acoustical pressure and particle velocity in the absorbent material in region R_2 will be denoted by $p_2^*(x)e^{i\omega t}$ and $q_2^*(x)e^{i\omega t}$ respectively, where harmonic time dependence has been assumed. The acoustic wave and momentum equations in the porous region follow from equations (3.62) and (3.61) respectively, thus

$$\rho_0\omega^2\Omega\chi\, p_2^* + \nabla\cdot[R]\nabla p_2^* = \quad 0 \tag{4.11}$$

and

$$i\omega\rho_0 q_2^* = \quad -[R]\nabla p_2^*, \tag{4.12}$$

where $[R]$ is a diagonal matrix whose jth element is ρ_0 / ρ_{aj}, and ρ_{aj} is the effective, complex, mean fluid density in the pores of the material absorbent for motion in direction j, see equation (3.58).

It has been assumed in the derivation of equations (4.11) and (4.12) that the convective fluid acceleration in the absorbent is negligible in comparison to the local acceleration, since the induced steady flow velocities are very small. Hence, to the same approximation,

$$i\omega\underline{\xi_2^*} = \boldsymbol{q}_2^* \ , \tag{4.13}$$

where $\underline{\xi_2^*}(\boldsymbol{x})e^{i\omega t}$ is the particle displacement in region R_2. Once again, solutions for given axial wavenumber are sought, thus

$$p_2^*(\boldsymbol{x}) = p_2(x,y)e^{-ik\lambda z}, \quad \underline{\xi_2^*}(\boldsymbol{x}) = \underline{\xi_2}(x,y)e^{-ik\lambda z}. \tag{4.14,4.15}$$

Equations (4.11) to (4.15) thus combine to yield, for the porous material, the wave equation

$$k^2(\rho_0/\rho_{az})(\gamma_z^2 - \lambda^2)p_2 + \nabla\cdot[R]\,\nabla p_2 = 0 \tag{4.16}$$

and the momentum equation

$$\rho_0\omega^2\underline{\xi_2} = [R]\,\nabla p_2 + ik\lambda(\rho_0/\rho_{az})p_z\boldsymbol{k}\,, \tag{4.17}$$

where the two-dimensional forms of the vector operator ∇ and matrix $[R]$ are now implied, with reference to the x–y plane. $\boldsymbol{k}$ is the unit vector in the axial z direction. Furthermore, following equations (3.58), (3.70) and (3.71),

$$\frac{\rho_0}{\rho_{aj}} = \gamma_j z_j \ , \tag{4.18a}$$

where

$$z_j = \sqrt{z_{0j}^2 + (-\mathrm{i}z_{oj} / \rho_0 \omega \gamma_{oj})(\sigma'_{aj} - \sigma_{oj})} \tag{4.18b}$$

and

$$\gamma_j = \sqrt{\gamma_{0j}^2 + (-\mathrm{i}\gamma_{oj} / \rho_0 \omega z_{oj})(\sigma'_{aj} - \sigma_{oj})} \tag{4.18c}$$

are the non-dimensional characteristic impedance and propagation constant in direction j. It has been assumed that the absorbent material is homogeneous in the axial z direction.

4.2.3 Steady flow equations in the absorbent

The steady flow in the absorbent is assumed to be in the axial z direction with speed U, such that equation (3.51) reduces to

$$dp_0 / dz = -\sigma_{vz} U - \sigma_{iz} U^2 = \text{constant}, \tag{4.19}$$

where p_0 is the static pressure of the mean flow, σ_{vz} is the viscous component of the steady-flow resistivity and σ_{iz} is the inertial component, in the z-direction. If the material is non-homogeneous in the cross-sectional x–y plane, then σ_{vz}, σ_{iz} and hence U are functions of (x, y). It follows from equation (4.19) that

$$U = \left[-\sigma_{vz} + \left(\sigma_{vz}^2 + 4\sigma_{iz} \mid dp_0 / dz \mid \right)^{1/2} \right] / 2\sigma_{iz} \tag{4.20}$$

4.2.4 Acoustic properties of the absorbent

The net components of the acoustic resistivity of an anisotropic porous material in the presence of a steady axial flow of speed U follow from equation (3.69), such that

$$\sigma'_{ax} = \sigma_{ax} + \sigma_{ix} U, \tag{4.21}$$

$$\sigma'_{oy} = \sigma_{oy} + \sigma_{iy} U \tag{4.22}$$

$$\sigma'_{oz} = \sigma_{oz} + 2\sigma_{iz} U \ , \tag{4.23}$$

where σ_{oj} is the frequency-dependent, complex acoustic flow resistivity in direction j. Thus even if the material is isotropic, one effect of steady flow through the absorbent is to introduce anisotropy (see also reference [18]). Delany-Bazley empirical representation of the bulk acoustic properties and coefficient of the porous material used in this model, are given in chapter 3 and Table 4.1

4.2.5 Boundary Conditions

Two conditions must be satisfied by the acoustical fields in regions R_1 and R_2 on their common boundary C_1, namely that the pressure and the component of displacement normal to the boundary must be continuous. Hence

$$p_1 = p_2 \quad \text{and } \boldsymbol{n}_C \cdot \underline{\xi_1} = \boldsymbol{n}_C \cdot \underline{\xi_2} \quad \text{on } C_1 \ , \tag{4.24, 4.25}$$

where $\boldsymbol{n}_C$ is a unit normal to C_1 and hence $\boldsymbol{k}$ The latter condition may be re-written by use of the momentum equations for the two regions, equations (4.10) and (4.17), as

$$\nabla p_1 \cdot \boldsymbol{n}_C = (1 - \lambda M^2)\ [R]\ \nabla p_2 \cdot \boldsymbol{n}_C \ . \tag{4.26}$$

Finally, the assumption of a hard-wall at the outer boundary C_2 implies that the normal component of particle displacement on this boundary is zero, hence from equation (4.17)

$$\nabla p_2 \cdot \boldsymbol{n}_2 = 0 \text{ on } C_2 \ . \tag{4.27}$$

4.3 The Finite Element Formulation

A finite element subdivision of the duct cross-section is performed, where the local variation within each element is expressed as a sum of the product of element-based nodal shape functions and nodal values. The only constraint on the subdivision is that the common boundary C_1 must be formed entirely by element boundaries [20], i.e. that no element can "straddle" C_1. In total, let there be n nodes in the finite element subdivision. The variation of acoustic pressure over the cross-section is approximated by the use of n global trial functions, one for each node, such that the trial function $\psi_J(x,y)$ corresponds to the shape function for elements on which node J lies and is zero over all other elements. Hence the approximation to the acoustic pressure can be represented as

$$p = \sum_{J=1}^{N} \psi_J(x,y) p_J \tag{4.28}$$

where p_J is the value of p at the Jth node.

The Galerkin formulation is used, thus the weighting function $\psi_I(x,y)$ yields a weighted residual statement of equation (4.9)

$$\iint_{R_1} \psi_I \left[\nabla^2 p_1 + k^2(1-\lambda M)^2 p_1 - k^2\lambda^2 p_1\right] dxdy = 0 \tag{4.29}$$

for each node I within R_1. Use of Green's theorem then gives the 'weak' form of equation (4.29), namely

$$\left\{\iint_{R_1}\left(\nabla\psi_I\cdot\nabla\psi_J+k^2\left[\lambda^2-(1-\lambda M)^2\right]\psi_I\psi_J\right)dxdy\right\}\{p\}$$
$$=\oint_{\Gamma_1}\psi_I\nabla p_1\cdot\boldsymbol{n}_1\,d\Gamma \tag{4.30}$$

where Γ_1 is the boundary of R_1, $\boldsymbol{n}_1$ is the unit outward normal to Γ_1 and $\boldsymbol{p}$ is the vector of p_J values. Similarly, a weighted residual statement of equation (4.16) can be written for each node I within R_2 as

$$\iint_{R_2}\psi_I\left[\nabla\cdot[R]\nabla p_2+k^2\left(\rho_0/\rho_{az}\right)\left(\gamma_z^2-\lambda^2\right)p_2\right]dx\,dy=0. \tag{4.31}$$

Green's theorem then gives the 'weak' Galerkin expression

$$\left\{\iint_{R_2}\left[\nabla\psi_I\cdot[R]\nabla\psi_J-k^2(\rho_0/\rho_{az})(\gamma_z^2-\lambda^2)\psi_I\psi_J\right]dx\,dy\right\}\{p\}$$
$$=\oint_{\Gamma_2}\psi_I[R]\nabla p_2\cdot\boldsymbol{n}_2 d\Gamma \tag{4.32}$$

where Γ_2 is the boundary of R_2 and $\boldsymbol{n}_2$ is the unit outward normal to Γ_2.

The continuity of pressure boundary condition, equation (4.24), is satisfied implicitly by use of the trial functions of equation (4.28). The boundary Γ_1 corresponds exactly to C_1, see Figure 4.1, and the hard-wall boundary condition of equation (4.27) on C_2 implies that the integral contribution from equation (4.32) over Γ_2 is only non-zero over C_1, as $\Gamma_2 = C_1 + C_2$. Furthermore since $\boldsymbol{n}_2 = -\boldsymbol{n}_1$ on C_1, the boundary integrals can be eliminated between equations (4.30) and (4.32) by use of the constant displacement boundary condition, equation (4.26), to yield

$$\left\{\iint_{R_1}\left(\nabla\psi_I\cdot\nabla\psi_J+k^2\left[\lambda^2-(1-\lambda M)^2\right]\psi_I\psi_J\right)dx\,dy\right.$$

$$\left.+(1-\lambda M)^2\iint_{R_2}\left[\nabla\psi_I\cdot[R]\nabla\psi_J-k^2(\rho_0/\rho_{az})(\gamma_z^2-\lambda^2)\psi_I\psi_J\right]dx\,dy\right\}\{p\}=0 \tag{4.33}$$

Equation (4.33), for all nodes I, can be written in matrix form as

$$\left\{[K_1]+k^2\lambda^2[M_1]-k^2(1-\lambda M)^2[M_1]+(1-\lambda M)^2([K_2]\right.$$
$$\left.-k^2[M_2']+k^2\lambda^2[M_2])\right\}\{p\}=\{0\} \tag{4.34}$$

where the (I, J)th elements of the matrices are

$$[K_1]_{I,J}=\iint_{R_1}\nabla\psi_I\cdot\nabla\psi_J\;dx\,dy, \tag{4.35a}$$

$$[M_1]_{I,J}=\iint_{R_1}\psi_I\psi_J\;dx\,dy, \tag{4.35b}$$

$$[K_2]_{I,J}=\iint_{R_2}\nabla\psi_I\cdot[R]\,\nabla\psi_J\;dx\,dy, \tag{4.35c}$$

$$[M_2]_{I,J}=\iint_{R_2}(\rho_0/\rho_{az})\;\psi_I\psi_J\;dx\,dy, \tag{4.35d}$$

$$[M_2']_{I,J}=\iint_{R_2}(\rho_0/\rho_{az})\gamma_z^2\psi_I\psi_J\;dxdy. \tag{4.35e}$$

Equation (4.34) is a fourth order-eigenvalue problem in λ namely

$$\left\{[A]+\lambda[B]+\lambda^2[C]+\lambda^3(2/M-\lambda)[D]\right\}\{p\}=\{0\}\;, \tag{4.36}$$

where

$$[A] = [K_1] - k^2[M_1] + [K_2] - k^2[M_2'], \tag{4.37}$$

$$[B] = 2Mk^2[M_1] - 2M[K_2] + 2Mk^2[M_2'], \tag{4.38}$$

$$[C] = k^2(1 - M^2)[M_1] + M^2[K_2] - M^2k^2[M_2'] + k^2[M_2], \tag{4.39}$$

$$[D] = -M^2k^2[M_2]. \tag{4.40}$$

Equation (4.36) is of the same form as that obtained by Astley and Cummings [20], who outlined the scheme for matrix partitioning and the technique for solution of the eigenvalues which is given in the following section.

4.4 Construction of Matrix Eigen-Equation and Mode Shape

The complex matrices of equations (4.37-4.40) are constructed by assembling the element matrices from the appropriate element contributions, as discussed in chapter 2. The assembled version of these matrices is then used to construct the overall system eigenmatrix as shown in the following sections. The solution of the eigensystem produces a complete set of eigenvalues λ_i and corresponding acoustical eigenmodes, for a given frequency of interest. The attenuation per unit length, A_i of the i^{th} mode then follows from equation (4.7) as

$$A_i = 20\log_{10}(e^{-1})^{\mathrm{Im}(k\lambda_i)} = -8.6858\,\mathrm{Im}(k\lambda_i) \quad [dB/m] \tag{4.41}$$

and the axial acoustic phase speed, c_i is given by

$$c_i = \frac{c_0}{\mathrm{Re}(\lambda_i)} \quad [\mathrm{m/s}]. \tag{4.42}$$

4.4.1 Linear eigenvalue matrix

For the case of no flow in the airway, $M = 0$, the matrices [B] and [C] are identically zero. Equation (4.36) then reduces to

$$\{[A] + \lambda^2[C]\}\{p\} = \{0\}, \tag{4.43}$$

giving a linear eigenvalue problem of order n. The eigenvalues λ_i, and corresponding eigenvectors $\{p_i\}$, of equation (4.43) can be found by using a generalised complex eigenvalue NAG routine.

4.4.2 Non zero mean flow

Equation (4.36) does not simplify when mean flow in the airway is present. The system of equations (4.37-4.40) can be reduced to a standard eigenvalue problem by partitioning of the matrices. Matrices $[A]$ and $[B]$ are partitioned into upper and lower submatrices $[A_1], [A_2], [B_1]$ and $[B_2]$ respectively, that is

$$[A] = \left[\frac{A_1}{A_2}\right] \text{and } [B] = \left[\frac{B_1}{B_2}\right] \tag{4.44}$$

where $[A_1]$ and $[B_1]$ are of order $r \times n$ and $[A_2]$ and $[B_2]$ of order $(n-r) \times n$, where r is the number of nodal points interior to region R_1 (not including nodes on the common boundary C_1). It has been assumed that the global node numbering pattern is such that the nodes internal to region R_1 are numbered as nodes 1 to r, whilst nodes on

the boundary C_1 and the region R_2 are numbered as $r+1$ to n. The matrices $[C]$ and $[D]$ are also partitioned into submatrices such that

$$[C]=\left[\begin{array}{c|c} C_{11} & C_{12} \\ \hline C_{21} & C_{22} \end{array}\right] \text{ and } [D]=\left[\begin{array}{c|c} D_{11} & D_{12} \\ \hline D_{21} & D_{22} \end{array}\right] \tag{4.45}$$

where $[C_{11}]$ and $[D_{11}]$ are of order $r\times r$, $[C_{12}]$ and $[D_{12}]$ of order $r\times(n-r)$, $[C_{21}]$ and $[D_{21}]$ of order $(n-r)\times r$ and $[C_{22}]$ and $[D_{22}]$ are of order $(n-r)\times(n-r)$. It follows from equations (4.35) and (4.40) that the matrix $[D]$ has only one non-zero subcomponent, namely $[D_{22}]$. This is the case since the integral required to evaluate the component of $[D]$ (see equation 4.40) involves only an integration over the absorbent region R_2, within which the shape functions $\psi_1,\psi_2,\cdots\psi_r$ are identically zero, since they are associated with nodes $1,2,\cdots r$ which are interior to region R_1. The original nonlinear eigenvalue problem of equation (4.36) may therefore be written in partitioned form as

$$\left[\begin{array}{c} A_1 \\ \hline A_2 \end{array}\right]\{p\}+\lambda\left[\begin{array}{c} B_1 \\ \hline B_2 \end{array}\right]\{p\}+\lambda^2\left[\begin{array}{c|c} C_{11} & C_{12} \\ \hline C_{21} & C_{22} \end{array}\right]\left\{\begin{array}{c} p_1 \\ \hline p_2 \end{array}\right\}+ \lambda^3\left(\frac{2}{M}-\lambda\right)\left[\begin{array}{c|c} 0 & 0 \\ \hline 0 & D_{22} \end{array}\right]\left\{\begin{array}{c} p_1 \\ \hline p_2 \end{array}\right\}=\{0\}, \tag{4.46}$$

or by rearrangement as

$$[A_1]\{p\}+[B_1]\{\lambda p\}+[C_{11}]\{\lambda^2 p_1\}+[C_{12}]\{\lambda^2 p_2\}=\{0\} \tag{4.47a}$$

$$[A_2]\{p\}+[B_2]\{\lambda p\}+[C_{21}]\{\lambda^2 p_1\}+[C_{22}]\{\lambda^2 p_2\}+ [D_{22}]\left(\frac{2}{M}-\lambda\right)\{\lambda^3 p_2\}=\{0\}, \tag{4.47b}$$

where $\{p_1\}$ is the vector of nodal pressure at nodes internal to R_1, namely $\{p_1, p_2, \cdots p_r\}$, and $\{p_2\}$ is the vector of pressure values $\{p_{r+1}, p_{r+2}, \cdots p_n\}$, such that $\{p\} = \{p_1\} + \{p_2\}$.

These equations can now be written in the form of a standard linear eigenvalue problem, but with an increase of order of the system to a size of (*4n-2r*), as

$$\begin{bmatrix} 0 & I & 0 & 0 \\ -C_{11}^{-1}A_1 & -C_{11}^{-1}B_1 & -C_{11}^{-1}C_{12} & 0 \\ 0 & 0 & I & 0 \\ 0 & 0 & 0 & I \\ D_{22}^{-1}\left[A_2 - C_{21}C_{11}^{-1}A_1\right] & D_{22}^{-1}\left[B_2 - C_{21}C_{11}^{-1}B_1\right] & D_{22}^{-1}\left[C_{22} - C_{21}C_{11}^{-1}C_{12}\right] & \left(\frac{2}{M}\right)I \end{bmatrix}$$

$$\begin{Bmatrix} p \\ \lambda p \\ \lambda^2 p_2 \\ \lambda^3 p_2 \end{Bmatrix} = \lambda \begin{Bmatrix} p \\ \lambda p_1 \\ \lambda p_2 \\ \lambda^2 p_2 \\ \lambda^3 p_2 \end{Bmatrix} \qquad (4.48)$$

The presence of flow introduces "hydrodynamic" modes whose eigenvalues are effectively real and whose eigenvectors contain small pressure components similar to those in [24]. These are neutrally stable hydrodynamic disturbances which are convected with the mean flow, i.e. with phase velocity $\overline{U}$. Table 4.2 shows a list of the eigenvalues computed from equation (4.48) for a particular silencer cross-section at a frequency of 500 Hz, with $M = 0.13$ and c_0 =340 [m/s]. The hydrodynamic modes are identifiable in Table 4.2 as modes whose eigenvalues are, to within computational error, (7.69,0). This implies, from equation (4.41) and (4.42), that they have zero attenuation and a phase speed of $\overline{U} = Mc_0 = 44.2\,[m/s]$ (=340/7.69= $c_0 / \mathrm{Re}(\lambda)$). They may be neglected when considering acoustical propagation in the silencer.

4.5 Discussion of results

Acoustical design information for two test silencers (of circular and approximately elliptical cross-section) in terms of the attenuation, phase speed and mode shapes corresponding to the four least attenuated acoustical modes have been obtained by using the finite element method outlined above. At each frequency of evaluation for each silencer tested, the solution of equation (4.48) gave a list of eigenvalues of the form shown in Table 4.2 and a corresponding set of eigenvectors. Software was written to post-process the results and reject the hydrodynamic modes, prior to searching for the least attenuated acoustical modes. In cases where modes have the same eigenvalues, to within computational accuracy, a check was made on the eigenvectors to see whether the modes were repeated or distinct.

Results are given for attenuation and phase speed as a function of frequency, but only samples of the mode shapes at selected frequencies are presented. The density of packing of the absorbent material and its variation with respect to both the radial and peripheral directions, as well as flow effects in the absorbent material, have been investigated and found to be important parameters for design information.

Taking advantage of the two axes of symmetry of the test silencers, see Figure 4.2, only one quarter of the cross-section was taken into account for the initial finite element representation, see Figure 4.3 and Figure 4.14. Boundary conditions of zero normal pressure gradient were imposed on the axes of symmetry. However it was found that a few higher order modes with some circumferential variation were missed by this approach and that it was essential to model the full cross-section in order to identify all possible modes. Discretization of the circular and elliptical cross-section silencers into

quarter models with 75 nodes and full models with 177 nodes are illustrated in Figures 4.3 and 4.14. Finite element discretization for both silencers was originally done by writing a routine to generate the meshes of 6-noded triangular and 8-noded quadrilateral elements and was later performed on FEMGEN software, when this became available. Results were compared by using 35 nodes, 75 nodes and 142 nodes in the quarter section mesh of each silencer and with 105 nodes and 177 nodes in the full cross-section. For further design information, an "equivalent area" circular cross-section silencer was also tested and compared with the elliptical cross-section silencer. Comparisons have been made for both test silencers with available experimental and analytical test data to validate the finite element model.

4.5.1 Circular silencer

The circular test silencer shown in Figure 4.2(a) is the same as that used in reference [18], with dimensions of outer diameter 76 mm and inner diameter 39.6 mm. Similarly the absorbent material (Polyether foam) and properties given in [18], and shown in Table 4.1, are utilised for estimation of the results and comparison purposes.

Results in terms of the axial sound attenuation A_i and phase speed c_i of the least attenuated mode as the function of frequency are shown in Figures 4.4 and 4.5. Results for zero mean flow in Region R_1 are shown in both Figures, in comparison to the results for mean flow of Mach numbers $M = \pm.197$ and $M = \pm.149$ in Figures 4.4 and 4.5 respectively. In each Figure, for each non-zero mean flow case, results are shown on the assumption of zero flow in the absorbent and with induced flow in the absorbent calculated on the basis of the measured pressure gradient for each case [18].

In each figure, the upper graph compares the finite element results with experimental results [18] which are denoted by symbols. The lower graph in each case compares the

finite element results with results from a mode-matching analysis [18], and this time the finite element results are denoted by symbols. The continuous curves of finite element results shown in the upper plots are simply interpolations through the set of finite element data given in the lower plots. The results obtained from the finite element method agree well with the experimental and analytical data of [18]. This suggests that the finite element formulation and implementation are fundamentally correct and use of the various mesh densities indicated that numerical convergence has been obtained in these results. Further information from the same silencer was obtained in terms of the mode shapes at select frequencies. Figures 4.6 and 4.7 present the predicted distribution of the relative sound pressure amplitude in terms of contours for the least attenuated mode at frequencies of 500 Hz and 2000 Hz respectively. In each figure, mode shapes for the case of zero mean flow and mean flow Mach number $M = 0.197$, with and without induced flow in the absorbent are given. Upper plot contours are without mean flow, the middle plots are with mean flow of Mach number $M = 0.197$, and the lower plots also include internal flow in the absorbent. These contours show little variation between each case of without flow, with flow and with induced flow. The variation in sound pressure with induced flow at frequency 500 Hz is very small and the erratic form of some contours is almost certainly due to computational inaccuracy. This computational error might be reduced by use of a different interpolation scheme or be made less apparent by plotting the normalise mode shapes on a scale of -1 to +1.

It became apparent that the quarter cross-section model was not sufficient for inclusion of all low-order modes, hence a full circular cross-section model with the same dimensions was discretized for a finite element solution and the results in terms of the sound attenuation and phase speed for the first four lower-order eigenvalues, without mean flow, are given in Figures 4.8 and 4.9. It is seen that, at low frequencies, the

attenuation rate of the 2nd, 3rd and 4th modes is much higher than that of the least attenuated mode. It is seen from Figure 4.9 that the phase speed of the higher-order modes drops as the modes become effectively cut-on, from extreme values towards the order of the speed of sound. The high-order modes are not cut-off in the absolute sense of modes in open, rigid ducts, but in practical terms it is seen in Figure 4.8 that the higher-order modes become cut-on at high frequencies, above 1 kHz in this case. In the effectively cut-off low frequency region, the phase speed of these modes increases with frequency. At low frequencies it is clear that the behaviour of the least attenuated mode is the dominant factor in the overall effectiveness of a silencer.

The mode shapes of the four least-attenuated modes, in terms of three-dimensional contours of their real and imaginary parts, have been obtained at frequencies of 500 Hz and 2000 Hz and are shown in Figures 4.10 to 4.13. Figures 4.10 (a-d) and 4.11 (a-d) show mode shapes for the four modes in the case of zero mean flow (i.e. $M = 0$), for frequencies of 500 Hz and 2000 Hz respectively. Figures 4.12 (a-d) and 4.13 (a-d) are similar mode shapes corresponding to a flow Mach number M =0.197. In Figures 4.10-13 one can observe that the first mode at both frequencies is virtually plane, i.e. at frequency 500 Hz there is no variation in pressure value and at frequency 2000 Hz there is only a small variation. The presence of mean flow is seen to cause the mode to become increasingly non-planar. Once again the erratic form of the contours at frequency 500 Hz for M=0.197 is presumably due to numerical error in an almost planar contour plot. It is observed, though, that flow causes an inversion of the mode shape at 500, Hz, but no change at 2000 Hz.

The next least-attenuated mode shows rather more interesting characteristics. At 500 Hz, M=0.0, Figure 4.10 (b), the mode is radial and the inverse of the shape of the least attenuated mode. In all other cases, the mode is a circumferential mode, and would

have been missed on a quarter wave model. It is also true, of course, that this mode would not be excited in a totally axisymmetric system.

The third least-attenuated mode shows even more variation. At 500 Hz, M=0, it is found to be a circumferential mode, see Figure 4.10(c). In the presence of flow of M=0.197, Figure 4.12(c), it is like a second radial mode, although still nearly planar. At 2000 Hz, with and without flow, the third least-attenuated mode is like a second circumferential mode, Figures 4.11(c) and 4.13(c).

The fourth least-attenuated mode shows similar varied behaviour. At 500 Hz, M=0, it is very complicated and yet with flow of M=0.197, see Figure 4.12(d), it is like a first circumferential mode. At 2000 Hz, with and without mean flow, the mode is radial and show elements of first and second mode behaviour in the real and imaginary parts, but switches with flow.

4.5.2 SAAB Silencer

The second test silencer has an approximately elliptical outer duct cross-section, with a circular-section central gas flow region, as shown in Figure 4.2(b). In particular, this test silencer is the case of a SAAB automobile silencer and has inhomogeneous absorbent material of variable density. The same silencer was also investigated by Cummings [70], both experimentally and analytically using the R-R (Rayleigh-Ritz) method, but without mean flow in the absorbent. Here, the same silencer has been analysed by the finite element method and results have been compared with the experimental and R-R results of Cummings [70]. In addition the effects of induced mean flow in the absorbent have been included. The bulk acoustic properties of the porous material (Basalt wool) given by Cummings [70] have been used here and the coefficients of viscous flow resistivity, σ_v and the inertial flow resistivity, σ_i as given in [70], are shown in Table 4.1. The density of packing of the absorbent material

varies circumferentially from the major axis to minor axis and the corresponding flow resistivity coefficient varies from 8000 SI rayl/m to 24000 rayl /m for the viscous coefficient σ_v and from 3755 to 9177 Ns^2 / m^2 for the inertial coefficient σ_i.

In the first instance, analysis was restricted to a quarter model of the silencer cross-section, as shown in the Figure 4.14. Figures 4.15 and 4.16 show the attenuation rate A_i and the axial phase speed c_i for the fundamental mode in the SAAB silencer, plotted as a function of frequency, for no flow ($M = 0$) and with mean flow Mach number M =0.067 and 0.13 respectively, both with and without induced flow in the absorbent. These results are compared with the experimental and R-R method results given in [70]. Upper plots show the comparison of experimental results with finite element results, the symbols corresponding to the experimental data and the curves to the finite element results. Similarly the lower plots compare finite element results with those from the R-R method, but here the symbols represent the finite element predictions and the curves are the R-R results without induced flow. The axial mean flow pressure gradient which was used to calculate the internal flow in the absorbent region was that given by Cummings [70], who measured the pressure drop between a series of pressure tappings. For a mean flow Mach number of 0.067, the axial mean pressure gradient was -3.12 kPa/m, and for a Mach number of 0.13, the pressure gradient was -10.02 kPa/m.

The finite element results and R-R results are seen to be virtually identical at low frequencies, which indicates that the finite element formulation and code is fundamentally correct in this more general case. The two sets of results diverge at high frequencies as one would expect, since R-R results have been obtained using a much simpler form of trial solution than the finite element results. The finite element results suggest that at some frequencies the internal flow in the absorbent can make a

difference of the order of 10 dB/m in the attenuation rate and clearly must be taken into account. Similarly internal flow in the absorbent has a noticeable effect upon the phase speed. Inclusion of internal flow in the finite element results gives better correlation with experimental results for phase speed and also with attenuation at the higher flow Mach number of M=0.13, but not obviously so at the lower flow rate.

Contours of relative sound pressure amplitude for the least attenuated mode over a quarter cross-section are presented in Figures 4.17 and 4.18 at frequencies of 500 and 2000 Hz respectively. The upper graph is without mean flow, the middle one is with mean flow of Mach number 0.13 and the lower one also includes induced flow in the absorbent. At frequency 500 Hz there is little change in the mode shape for each case, although the case with internal flow in absorbent shows greater variation in sound pressure over the quarter duct area than the other two. At high frequency the presence of mean flow creates a substantial change in mode shape which is further modified by induced flow. For computation of the four least-attenuated acoustic modes the full elliptical cross section has been discretized and the results in terms of sound attenuation and phase speed for these modes without flow are presented in Figures 4.19 and 4.20. This time the modal attenuation of modes two to four is much closer to that of the first mode and they are all of similar magnitude at high frequencies. Similarly the phase speed of all modes are of comparable order, except that the fourth mode does not become effectively cut-on until the frequency is about 500 Hz. This indicates that in order to calculate the overall transmission loss at high frequencies many modes must be included. The practical application of a mode-matching scheme would seem to be in doubt at very high frequencies. The corresponding mode shapes in terms of three-dimensional contours have been obtained at frequencies 500 Hz (Figures 4.21 and 4.23) and 2000 Hz (Figures 4.22 and 4.24) for the two cases of zero mean flow (Figures 4.21 and 4.22) and with mean flow of Mach number M=0.13 (Figure 4.23

and 4.24). In all cases the least-attenuated mode is basically a radial mode. The second mode at 500 Hz and the third mode at 2000 Hz are like first circumferential modes and would have been missed on a quarter-duct model. The same is true for the fourth least-attenuated mode in all cases, the only difference being that the position of the maxima and minima now lie on the minor axis, instead of the major axis as occurred in lower modes.

4.5.3 Effects of non-homogeneous absorbent material

As mentioned above, the density of packing of the absorbent material in the SAAB silencer varies with respect to the circumferential direction. It would appear that the reason for this was the manufacturing process rather than intentional design, with the highest density of material occurring along the minor axis of the "ellipse", where it was compressed during manufacture. It was decided to use the finite element model to investigate the effect of non-uniform packing, using the same basic shape and the same extremes of material variation as for the SAAB silencer. The results, in terms of attenuation and phase speed, were repeated for the same geometry of model but with differing geometric variation of the material properties. Figures 4.25 and 4.26 present results for attenuation and phase speed of the least attenuated mode respectively, showing the comparison between five different cases namely: (i) no material variation (i.e. with averaged flow resistivity); (ii) circumferential variation only, from highest density on the minor axis to least density on the major axis; (iii) circumferential variation only, from highest density on the major axis to lowest density on the minor axis; (iv) radial variation only , from highest density at the outer radius to lowest density at the inner radius; (v) radial variation only, from highest density at the inner radius to lowest density at the outer radius. In both figures, separate plots are shown for the cases of zero mean flow and mean flow of Mach number M=0.067 and 0.13, both with and without induced flow in the absorbent. The results for attenuation,

Figure 4.25, show that variation of material density can be beneficial in comparison to uniform packing, but equally the wrong choice of variation can be detrimental. In the zero flow case, Figure 4.25(a), it is seen that radial variation from least dense at the inner radius to most dense at the outer gives better low frequency performance than uniform packing. For a limited range of higher frequencies, the opposite radial variation is more beneficial than uniform packing. In all other cases, material variation results in performance which is worse, or no better, than that achieved by uniform packing.

At a flow Mach number of 0.067, Figure 4.25(b), similar features are observed, except that circumferential variation of packing, from least dense at the minor axis to most dense at the major axis, is the only form to clearly dominate over uniform packing at high frequencies. The presence of induced flow, Figure 4.25 (c), exaggerates this effect, but also makes the radial variation, least dense at the inner boundary, superior to uniform packing at all frequencies. The same features are observed at the higher flow speed of M=0.13, see Figure 4.25(d), without induced flow. Addition of induced flow, Figure 4.25(e), now causes the radial variation, least dense at the inner boundary, and the tangential variation, least dense at the minor axis, to be superior to uniform packing throughout the frequency range. It should be noted that the form of material variation used causes the total mass of absorbent material present in the silencer to be greatest for these two cases and least for the other two variational forms. It is possible that this is the major reason for differences in performance and this should be investigated in the future.

Variation in material density causes slight changes to the phase speed of the waves, as seen in Figure 4.26. In all flow cases, there is a tendency in the mid-frequency range for the cases of circumferential variation, highest density on the major axis, and radial

variation, highest density at the outer radius, to have greater phase speed than the uniform packing case. The other two forms of variation have lower phase speed. At frequencies below 300 Hz and above 1700 Hz there are some local variations to this pattern. The effect of mean flow, and further of induced flow, appears to be to reduce any differences in phase speed brought about by variation of material density.

4.5.4 Comparison between elliptical and equal area circular silencer

For further design guidelines an "equivalent area" circular silencer was discretized and results from this were compared with those for the SAAB silencer for the cases of zero mean flow and flow of Mach number 0.13, with and without induced flow. Once again, results are obtained in terms of attenuation and phase speed for the least attenuated mode and are shown in Figures 4.27 and 4.28. These results were computed by taking the same set of variations of absorbent material as were used in Section 4.5.3. Separate plots are shown for the cases of zero material variation (i.e. with averaged flow resistivity), variation circumferentially from maximum density at the minor axis to minimum density at the major axis, and for both sets of radial variation. For the case of homogeneous material it is seen in Figure 4.27(a) that the attenuation at high frequencies is greater for the circular-section silencer than for the SAAB silencer. It is seen from the figure that the presence of mean flow and then internal flow in the absorbent serves to accentuate the differences and reduce the frequency at which the effects are observed. However, rather surprisingly, the figure also indicates that the SAAB silencer has marginally better attenuation at low frequencies than the circular-section silencer.

In Figure 4.27(b) the effect of variation along the circumferential direction, from least dense at the major axis of the SAAB silencer, is included. In the absence of flow there is no observable difference between the circular and oval silencers at low frequencies,

but the circular silencer is clearly better at high frequencies. Similar comments hold in the presence of mean flow of Mach number 0.13, but the addition of induced flow does make oval silencer clearly beneficial at low frequencies.

For radial variation of material density, from least dense at the inner boundary, Figure 4.27(c), the oval section is clearly better than the circular section at low frequencies, for all flow situations. For the opposite radial variation, Figure 4.27(d), the circular silencer is to be preferred for all frequencies and for all flow cases. Once again it should be noted that the total mass of absorbent material is greatest for the circular silencer in this case, but was greatest for the oval silencer in the previous case.

It is seen from Figure 4.28 that in all flow cases and for all forms of material variation, there is a tendency for the phase speed of the waves in the oval silencer to be slightly higher than the phase speed of the waves in the circular silencer. This is always true in the mid-frequency range, but there are some localised exceptions at low and high frequencies. It is seen form Figures 4.25-4.28 that use of simplified modelling, either representing a given cross-sectional shape by an equivalent area circular silencer, or representing a silencer with non-uniform packing by an equivalent uniformly packed silencer, will give results which correctly predict general trends but which are inaccurate in actual level throughout the frequency spectrum.

4.6 Conclusion

The results obtained by use of the finite element formulation described in this Chapter, in terms of both attenuation and phase speed, were compared against some established results for two test cases. The first was a circular cross-section test silencer, the same

as that which was analysed by Cummings and Chang [18]. The second test case was that of a SAAB automobile silencer, which was also investigated by Cummings [70]. Finite element results were compared with analytical and experimental results [18,70] to validate the current finite element modelling for eigenvalue analysis. Detailed investigations were carried out to obtain design information regarding the effect upon performance of silencer shape, density variation of the absorbent material and inclusion of induced mean flow in the absorbent.

In both test silencers, the attenuation and phase speed as computed from the finite element results were shown to have good agreement with the available experimental and analytical results [18,70]. Additional computations for both test silencers were obtained, to include induced mean flow in the absorbent and determine its effects on the overall sound attenuation and phase speed. Results were also obtained for the "lowest four acoustic modes" of propagation in terms of attenuation and phase speed versus frequency. The corresponding mode shapes were plotted in terms of three dimensional contours at selected frequencies. Further design information was obtained by comparison of the acoustic performance for different variations of packing density of the absorbent material throughout the cross-section of the second test silencer. Comparison was also made between the performance of an oval cross-section silencer and an "equivalent area" circular cross-section silencer, for different variations of packing density. It was found that the circular cross-section, uniform packing silencer was not always the best. Careful choice of shape and variation of packing density could produce slight benefits, but generally over a restricted frequency range. Conversely, the wrong combination of shape and variation of packing density could make matters significantly worse. The method used to specify variation of material density caused some differences in the overall mass of the absorbent between different test cases and this rather warrants further investigation.

Table 4.1

Delany-Bazley coefficients for absorbent materials

Delany-Bazley coefficient	Porous material	
	Polyether foam	*Basalt wool*
c_1	0.196	0.0414
c_2	-0.399	-0.774
c_3	0.112	0.124
c_4	-0.55	-0.645
c_5	0.157	0.196
c_6	-0.58	-0.639
c_7	0.185	0.0971
c_8	-0.475	-0.749

Flow resistivity coefficients

Porous material	Flow resistivity σ_v, σ_i
Polyether Foam	5430,3070
Basalt wool	max 24000,9000 min 8000,3755

Table 4.2

Computed eigenvalues at frequency 500 Hz, Mach number M=0.13, for the SAAB silencer (quarter cross-section model)

No	Eigen value
1	(-.438917607069016,-57.5583534240723)
2	(.4547904431819915,57.16033554077148)
3	(-.132483303546906,50.94334030151367)
4	(-.132030710577965,-50.9431800842285)
5	(-.250597655773163,46.19968032836914)
6	(-1.205345056951045E-02,-46.1097030639648)
7	(-.204949215054512,44.48196029663085)
8	(-6.184955313801765E-02,-44.4252471923828)
9	(.2560570240020751,40.74885559082031)
10	(-.239587068557739,-41.1795692443848)
11	(-.500091731548309,38.83007049560546)
12	(.442850142717361 4,-38.4723167419434)
13	(-.382357597351074,36.66651535034179)
14	(.1695096343755722,34.91752624511718)
15	(-.282103091478348,33.991943359375)
16	(.248755007982254,-36.4216651916504)
17	(-.438133865594864,-35.5338935852051)
18	(19.76343154907226,16.13166809082031)
19	(-.471595764160156,31.31706428527832)
20	(-.222312495112419,29.94469451904296)
21	(1.47109460830688,29.61311149597167)
22	(4.161543026566505E-02,-33.8487586975098)
23	(-2.08591365814209,-32.1414833068848)
24	(-.619812846183777,28.16487121582031)
25	(17.67169952392578,13.92497730255126)
26	(16.03779602050781,14.47114467620849)
27	(.627413272857666,25.63568878173828)
28	(-.266403913497925,25.75009536743164)
29	(-.467945069074631,25.14741706848144)
30	(14.75516128540039,10.30178165435791)
31	(13.13383293151855,12.01153945922851)
32	(.5204967260360717,23.25580215454101)
33	(.2420987039804458,23.00268936157226)

34	(1.08799159526825,22.56097030639648)
35	(-.350765705108643,21.58371353149414)
36	(.3667117059230804,-30.8501129150391)
37	(-.138078421354294,19.71438598632812)
38	(-4.000199586153030E-02,-29.6382274627686)
39	(-.531609058380127,18.22828865051269)
40	(-.45193949341774,17.00961875915527)
41	(-.206515178084373,16.45929718017578)
42	(-6.219318136572837E-02,14.62305831909179)
43	(.3607182204723358,13.89950847625732)
44	(-.2243712246418,13.26188659667968)
45	(-.986545085906982,-27.92893409729)
46	(1.39414000511169,-27.4869403839111)
47	(-.291223704814911,10.98579978942871)
48	(5.559276416897773E-02,10.73978042602539)
49	(-.161222815513611,9.8976993560791)
50	(-2.62904262542725,-24.7477512359619)
51	(1.24738311767578,-24.6647529602051)
52	(.2038390934467315,-24.9701881408691)
53	(-.170571729540825,-23.92431640625)
54	(-.961073279380798,-23.6531200408936)
55	(-.409695655107498,7.77131271362305)
56	(-.475720554590225,6.44649362564087)
57	(-.503364741802216,5.37132596969604)
58	(-.850029468536377,2.65186786651611)
59	(-1.88065612316132,.8875285387039184)
60	(1.16250193119049,-20.9446811676025)
61	(.448605865240097,-20.1648139953613)
62	(-5.98281383514404,-14.9376449584961)
63	(-4.10381555557251,-15.6994581222534)
64	(-2.92940497398376,-15.9656972885132)
65	(2.36957120895386,-17.8907585144043)
66	(2.44754648208618,-17.187385559082)
67	(.5969531536102294,-16.7269420623779)
68	(1.58494651317596,-.477984249591827)
69	(1.25474810600281,-2.44407033920288)
70	(.1160146817564964,-14.6734018325806)
71	(.8339191675186157,-5.08532619476318)
72	(-1.34251773357391,-6.28385162353516)
73	(-1.68729913234711,-10.792929649353)

74	(2.21084117889404,-8.05904006958008)
75	(.4210554659366607,-8.13520622253418)
76	(1.52967441082001,-12.573956489563)
77	(1.4107049703598,-11.3189554214478)
78	(1.73119854927063,-9.70550918579102)
79	(-1.01791477203369,-10.5234880447388)
80	(.146771028637886,-10.6156949996948)
81	(7.69813013076782,-2.613438409753143E-04)
82	(7.69219923019409,-5.492344498634338E-03)
83	(7.68648195266724,2.621556923259049E-04)
84	(7.69241380691528,5.492270458489656E-03)
85	(7.69669485092163,-1.606825971975922E-04)
86	(7.68791770935059,1.611126353964209E-04)
87	(7.69227027893066,-3.294871188700199E-03)
88	(7.69234466552734,3.294832538813352E-03)
89	(7.692298412323,-2.844636095687747E-03)
90	(7.69231605529785,2.844625385478138E-03)
91	(7.69228649139404,-2.267907606437802E-03)
92	(7.69227981567383,-2.184925600886344E-03)
93	(7.6937050819397,-1.054535154253244E-03)
94	(7.69372749328613,1.013369532302021E-03)
95	(7.69376373291016,-2.252467857033479E-05)
96	(7.69232606887817,-1.729338429868221E-03)
97	(7.69232797622681,2.267994219437241E-03)
98	(7.69233465194702,2.184842946007847E-03)
99	(7.69088745117188,-1.013122382573783E-03)
100	(7.6923189163208,-1.347989542409777E-03)
101	(7.69237852096558,-1.000421936623752E-03)
102	(7.69222784042358,-9.356471127830445E-04)
103	(7.69090938568115,1.054344116710126E-03)
104	(7.69085264205933,2.251038495160173E-05)
105	(7.6912784576416,8.736064046388491E-06)
106	(7.69173240661621,-6.621706415899097E-05)
107	(7.69333648681641,-8.732807145861443E-06)
108	(7.69288349151611,6.616813334403559E-05)
109	(7.69228839874268,1.729381619952619E-03)
110	(7.69229555130005,1.348047284409403E-03)
111	(7.69223642349243,1.000540098175406E-03)
112	(7.69238710403442,9.355011861771345E-04)

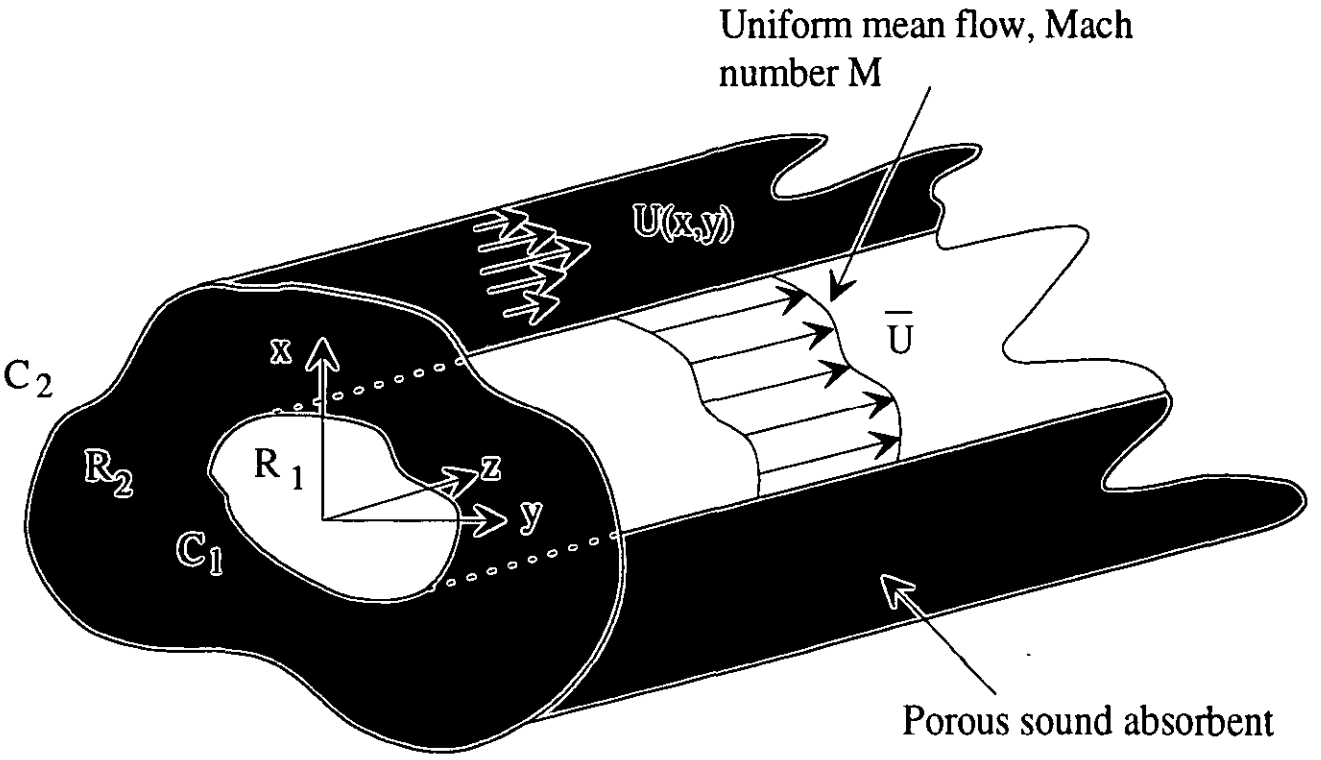

Figure 4.1 Geometry of the system.

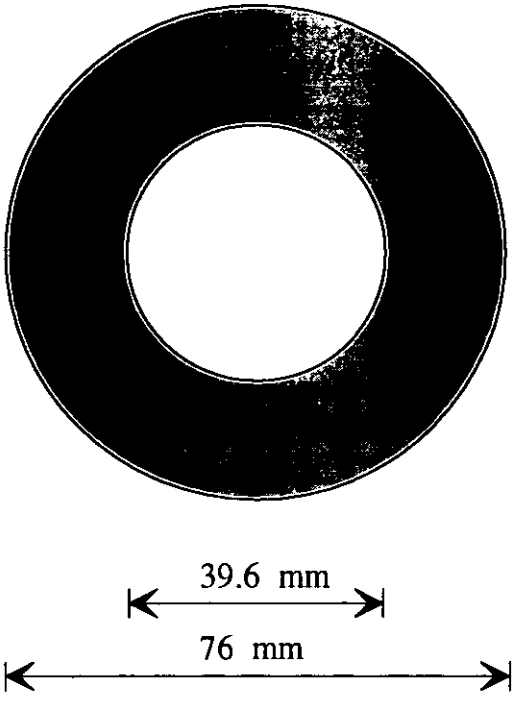

(a) Cross-Sectional Geometry of Circular Silencer

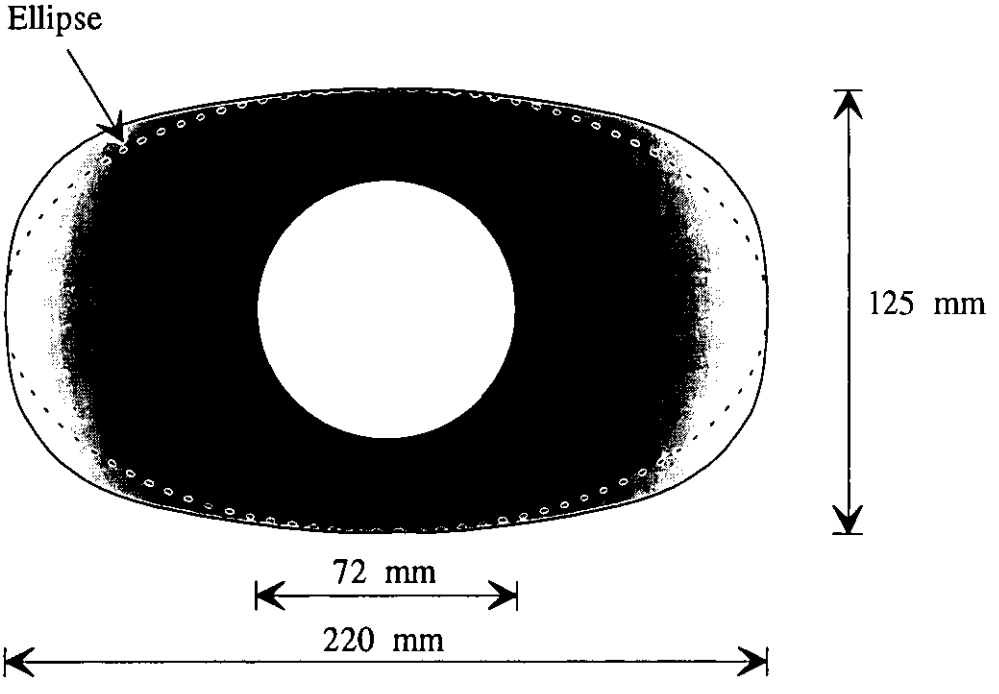

(b) Cross-Sectional Geometry of Saab Silencer

Figure 4.2

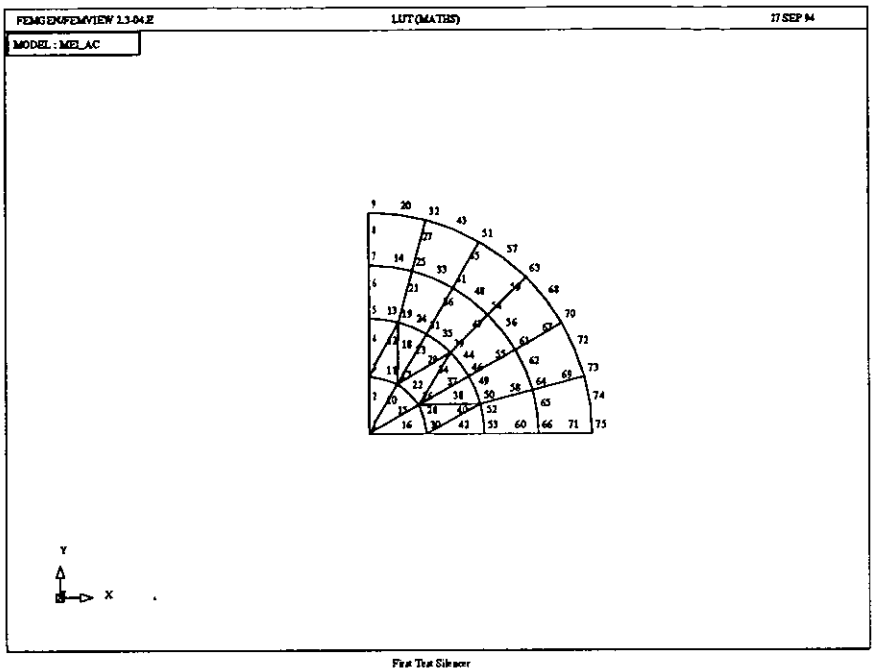

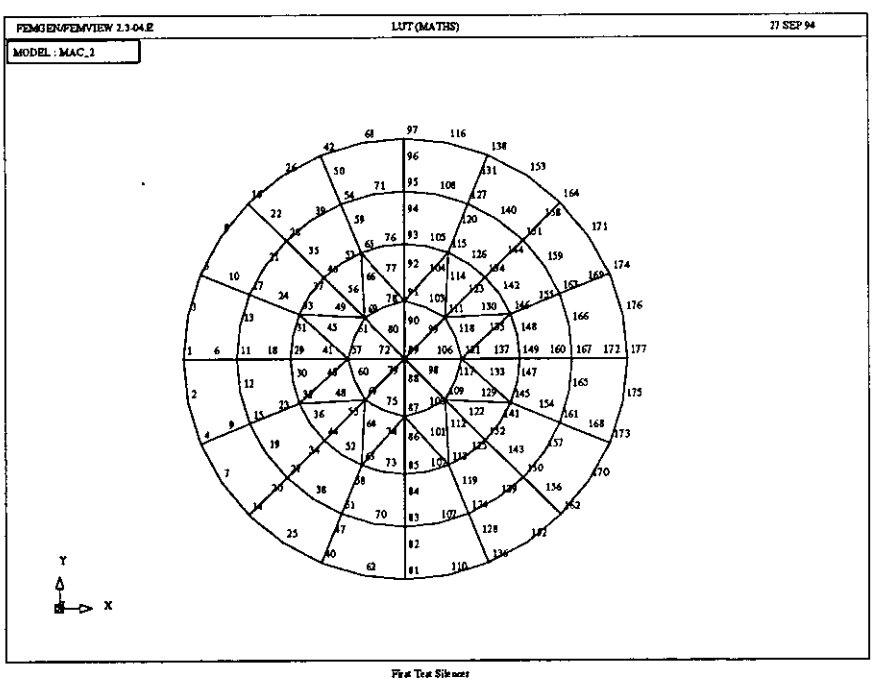

Figure 4.3 Quarter and full mesh model of the circular cross-section silencer

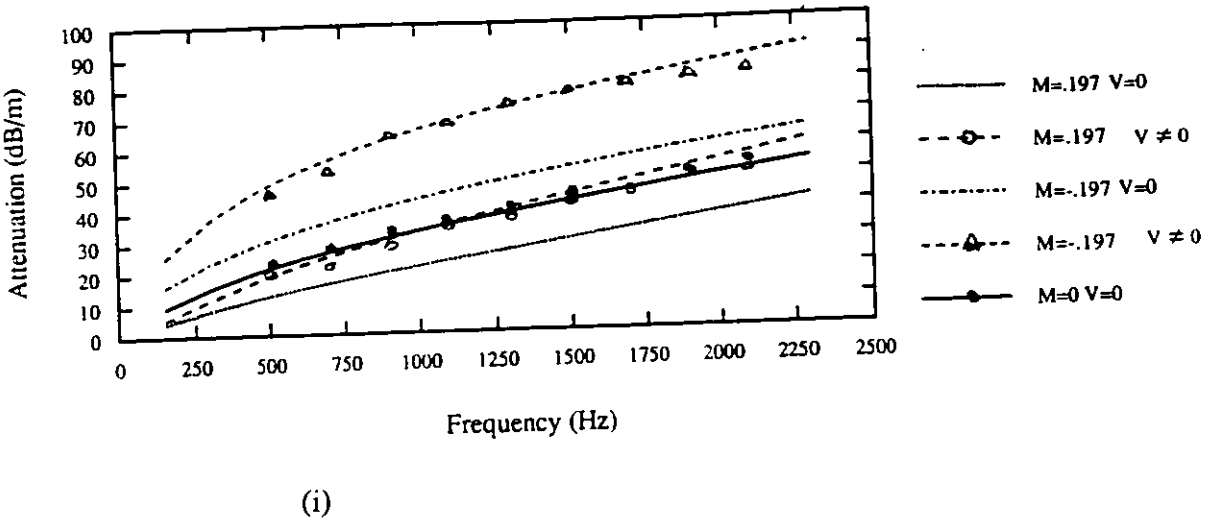

(i)

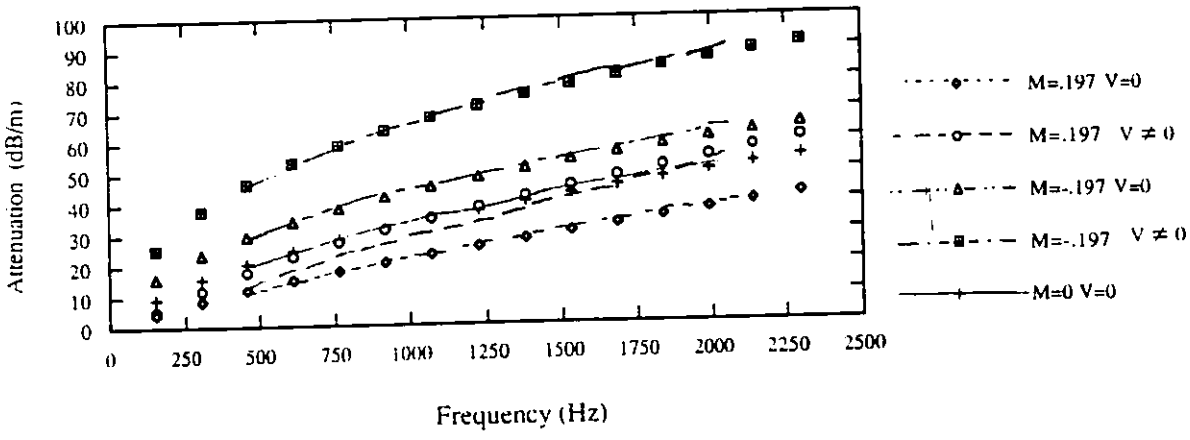

(ii)

Figure 4.4(a) Circular cross-section silencer axial attenuation rate (i) Comparison of FE solution (curves) with experimental results (symbols) of Cummings and Chang [18] (ii) Comparison of FE results (symbols) with analytical solution (curves) of Cummings and Chang [18]

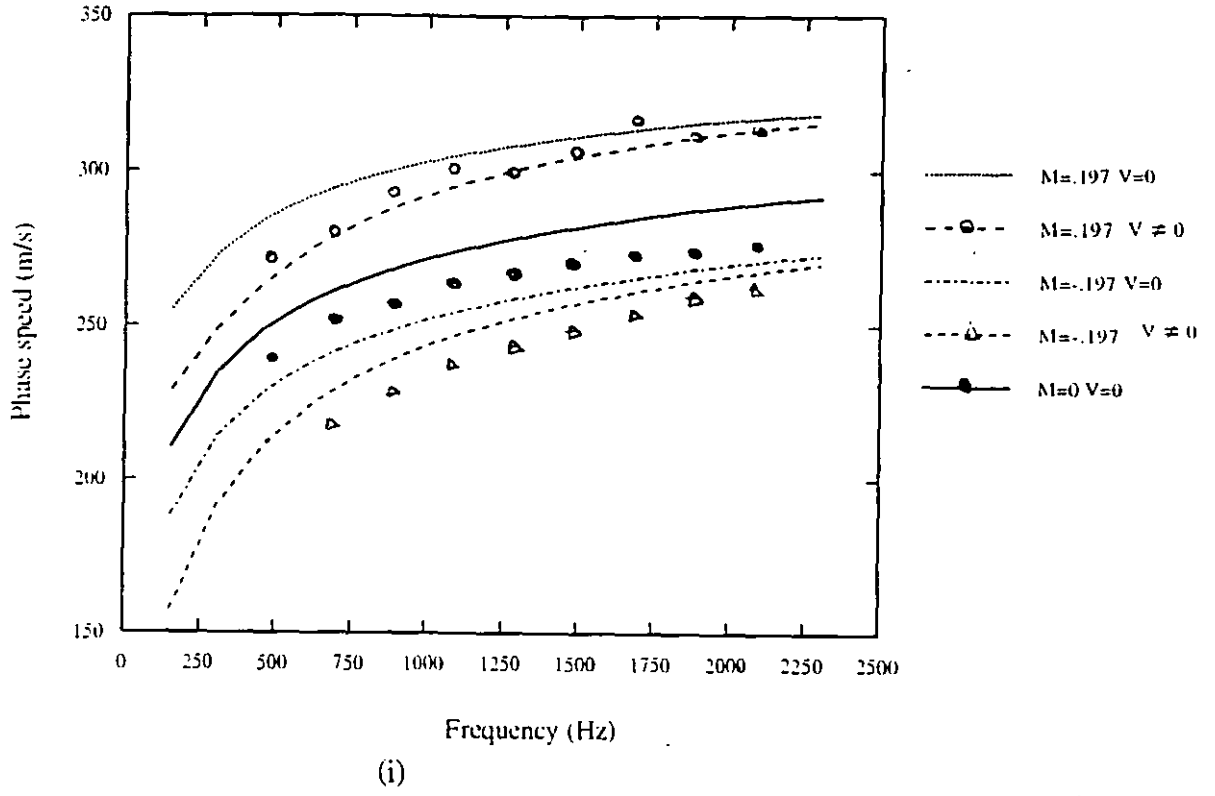

(i)

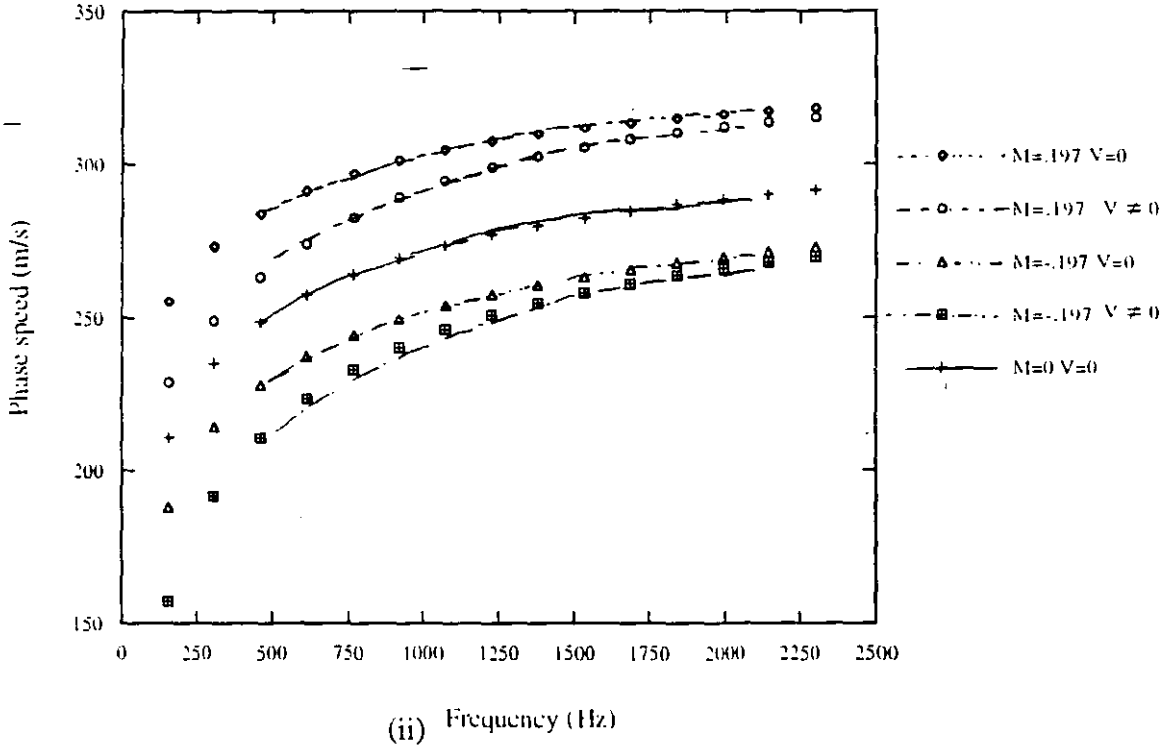

(ii) Frequency (Hz)

Figure 4.4(b) Circular cross-section silencer phase speed (i) Comparison of FE solution (curves) with experimental results (symbols) of Cummings and Chang [18] (ii) Comparison of FE results (symbols) with analytical solution (curves) of Cummings and Chang [18]

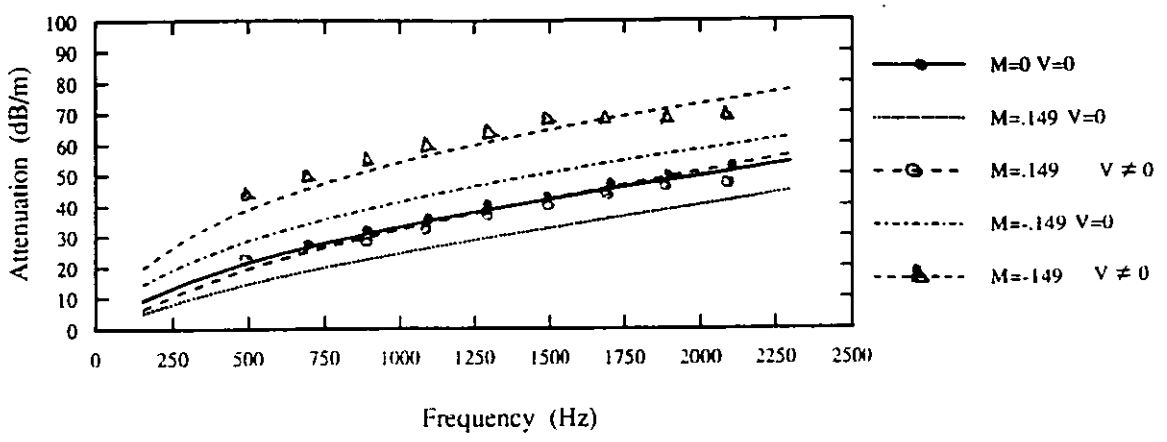

(i)

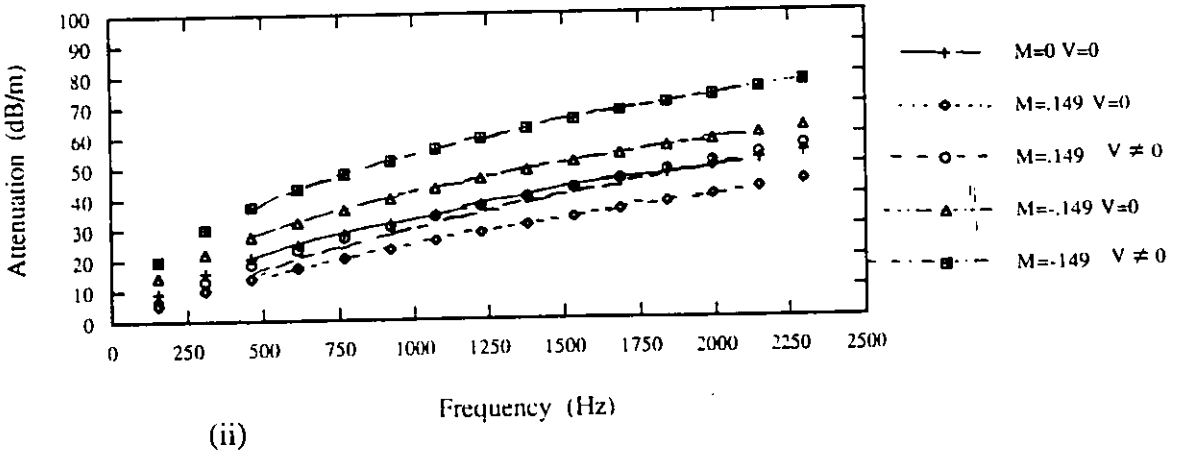

(ii)

Figure 4.5(a) Circular cross-section silencer axial attenuation rate (i) Comparison of FE solution (curves) with experimental results (symbols) of Cummings and Chang [18] (ii) Comparison of FE results (symbols) with analytical solution (curves) of Cummings and Chang [18]

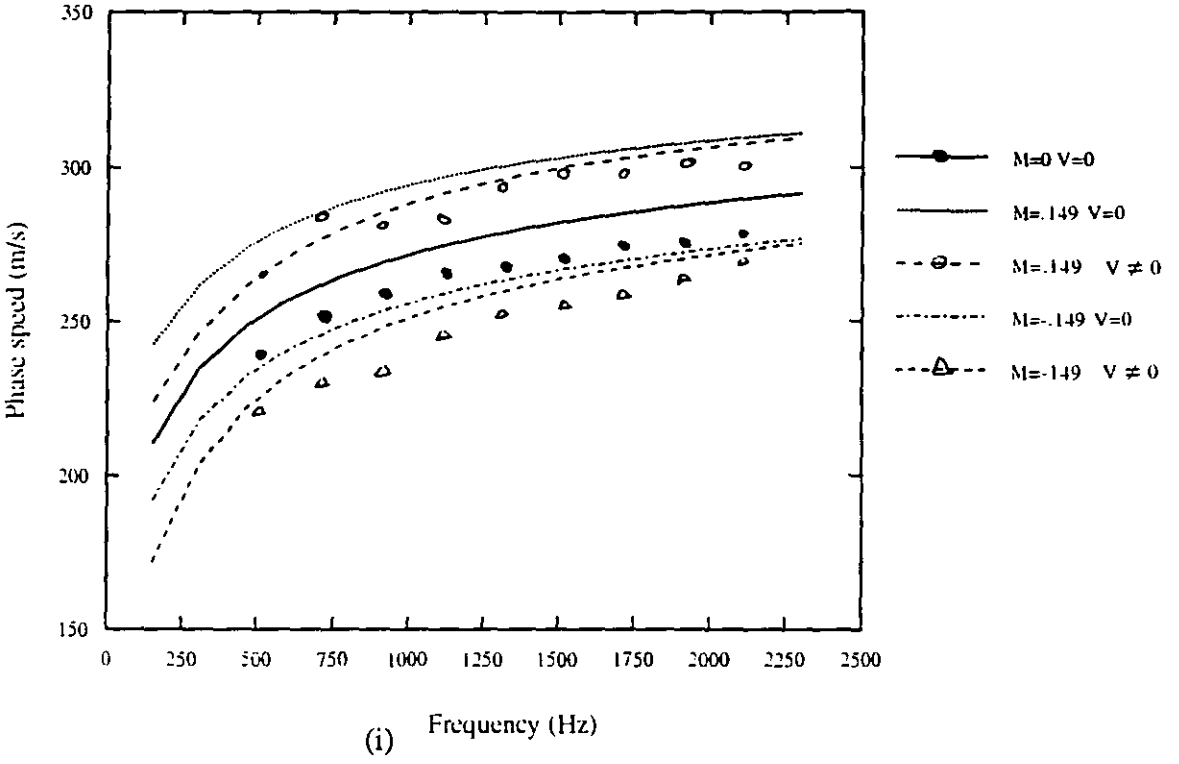

(i)

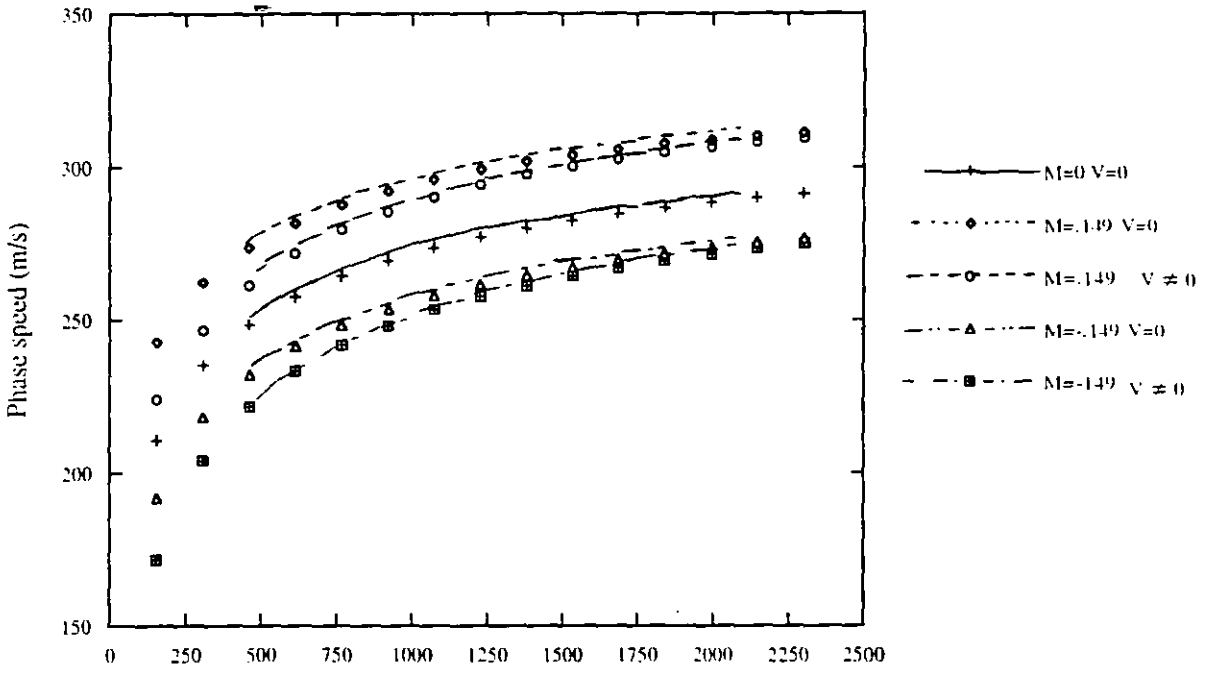

(ii) Frequency (Hz)

Figure 4.5(b) Circular cross-section silencer phase speed (i) Comparison of FE solution (curves) with experimental results (symbols) of Cummings and Chang [18] (ii) Comparison of FE results (symbols) with analytical solution (curves) of Cummings and Chang [18]

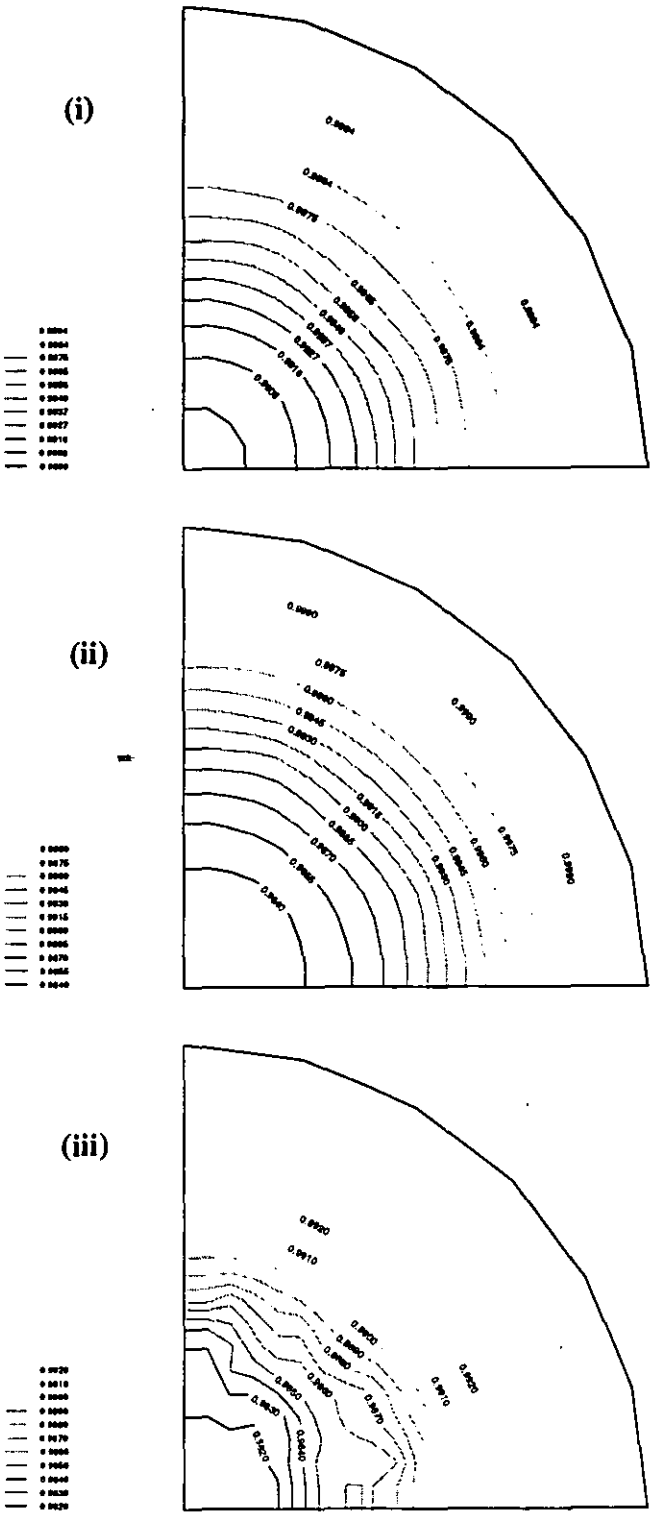

Figure 4.6. Sound pressure amplitude for the circular silencer, least-attenuated mode, frequency =500 Hz (i) M=0.0 (ii) M=0.197 without induced flow (iii) M= 0.197 with induced flow

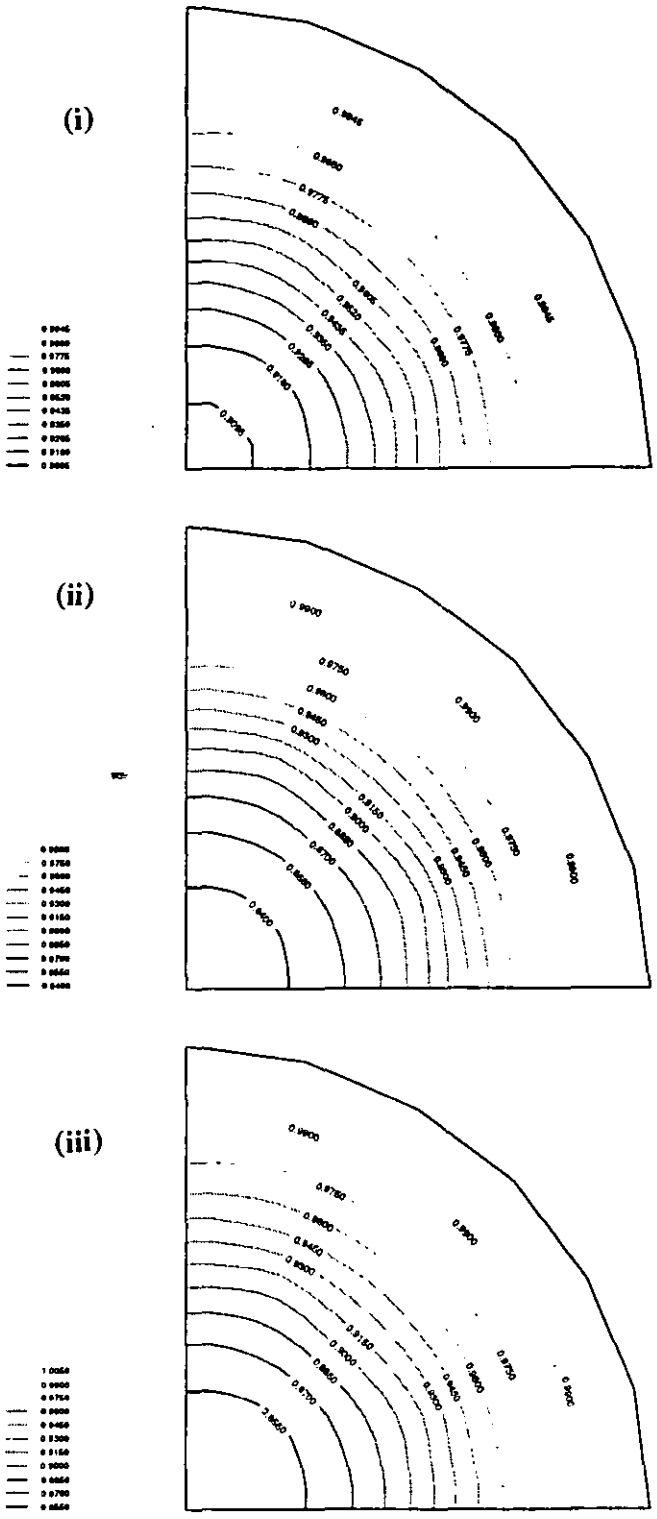

Figure 4.7. Sound pressure amplitude for the circular silencer, least-attenuated mode, frequency =2000 Hz (i) M=0.0 (ii) M=0.197 without induced flow (iii) M= 0.197 with induced flow

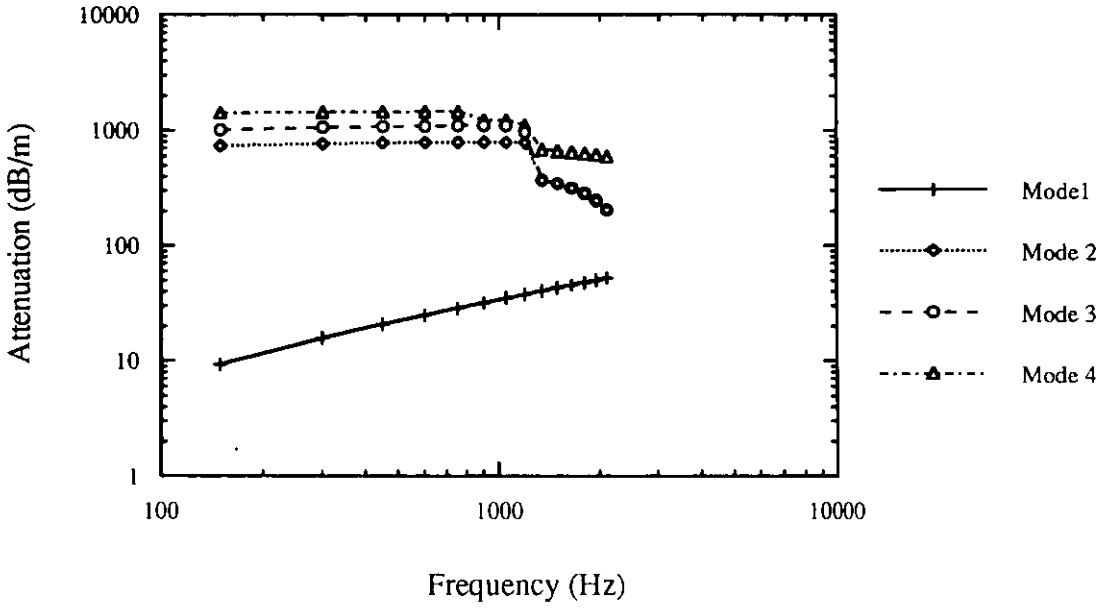

Figure 4.8. Axial attenuation rate for the circular test silencer for the four least-attenuated modes.

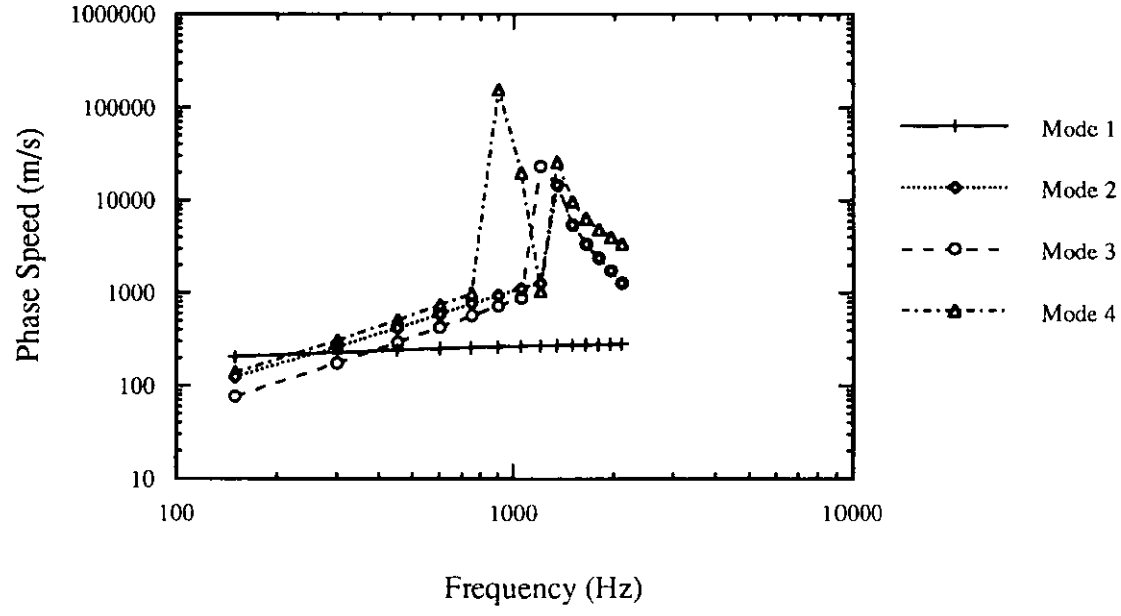

Figure 4.9. Phase speed for the circular test silencer for the four least-attenuated modes.

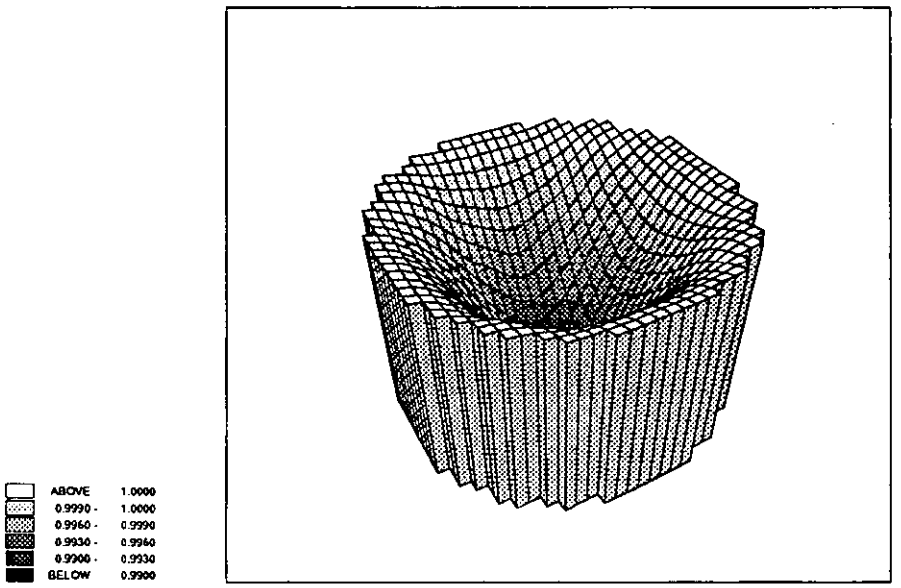

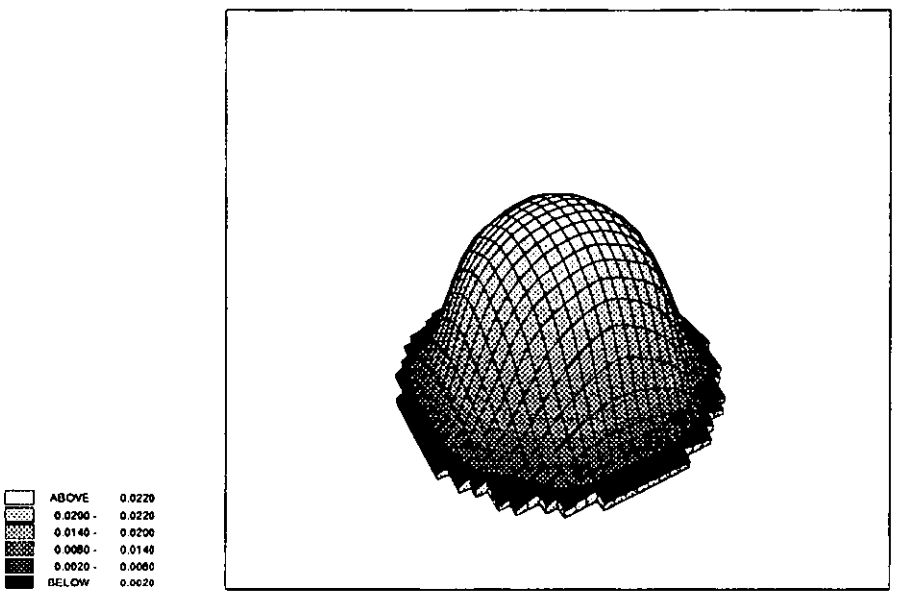

Figure 4.10(a) Mode shape for circular silencer. Mode 1, M=0.0, frequency=500 Hz (upper plot:real part, lower plot:imaginary part)

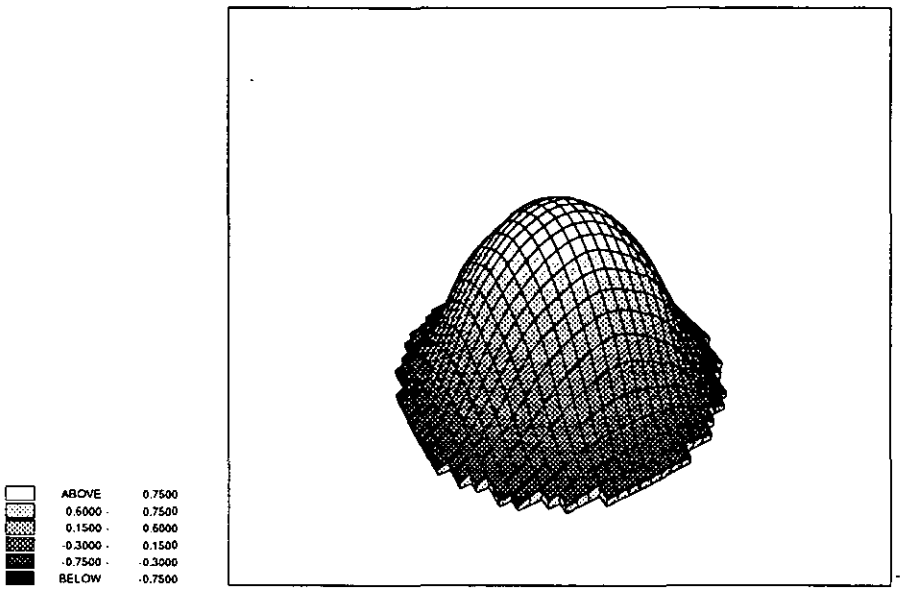

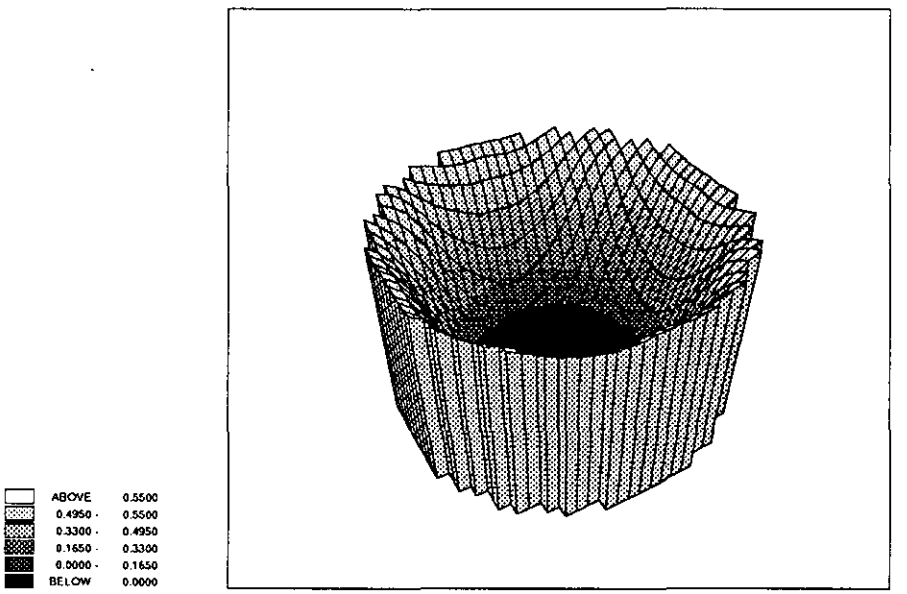

Figure 4.10(b) Mode shape for circular silencer. Mode 2, M=0.0, frequency=500 Hz (upper plot:real part, lower plot:imaginary part)

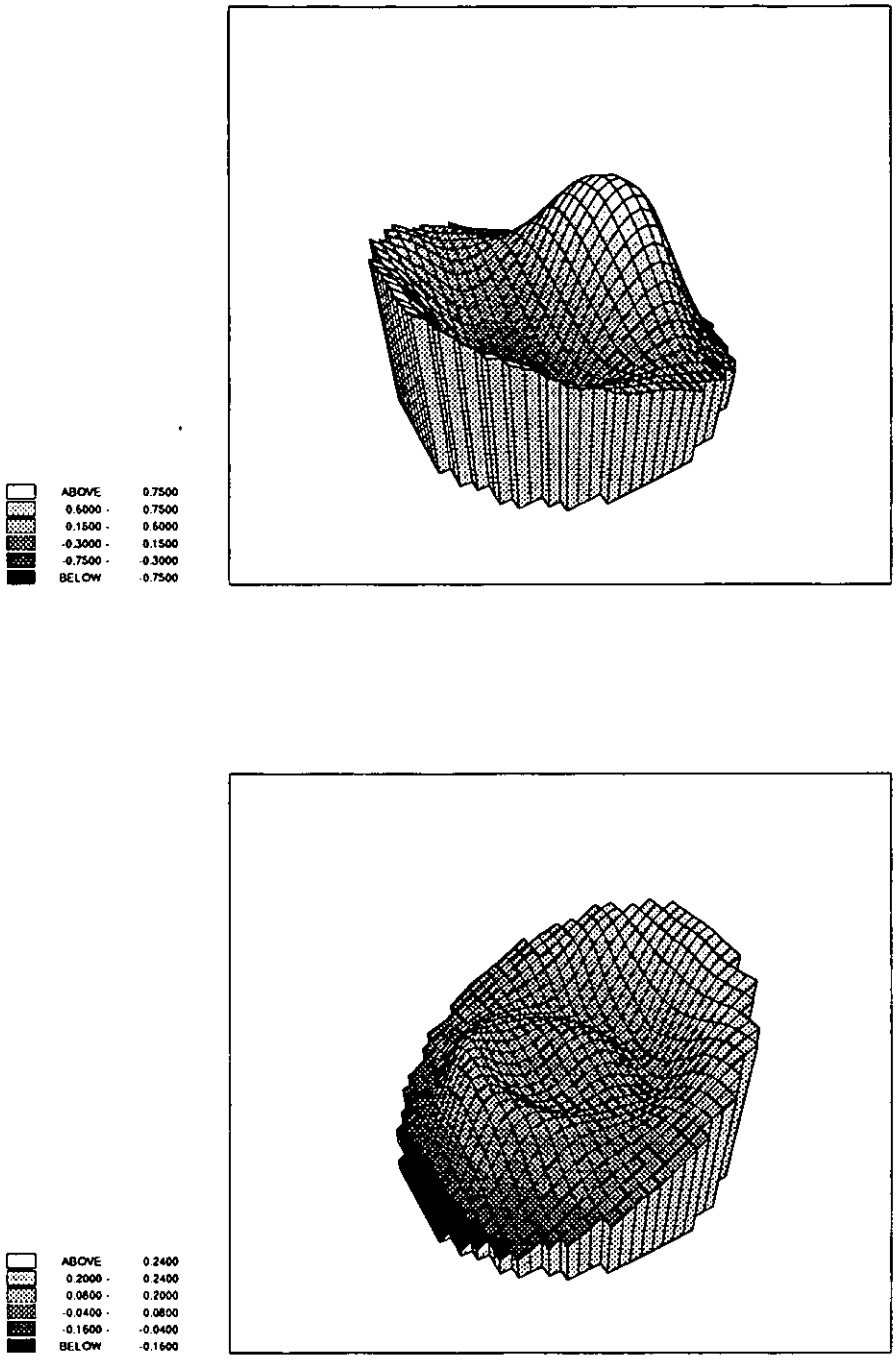

Figure 4.10(c) Mode shape for circular silencer. Mode 3, M=0.0, frequency=500 Hz (upper plot:real part, lower plot:imaginary part)

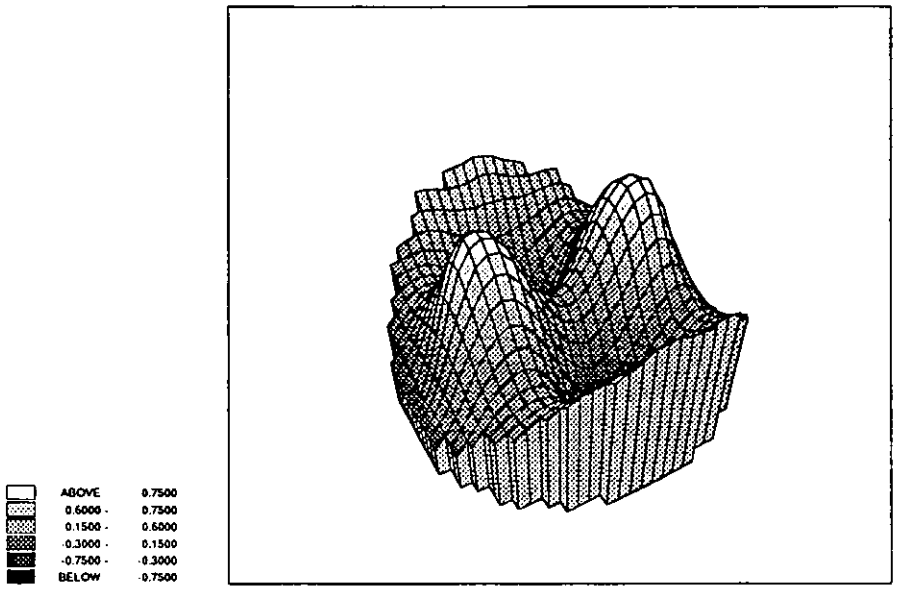

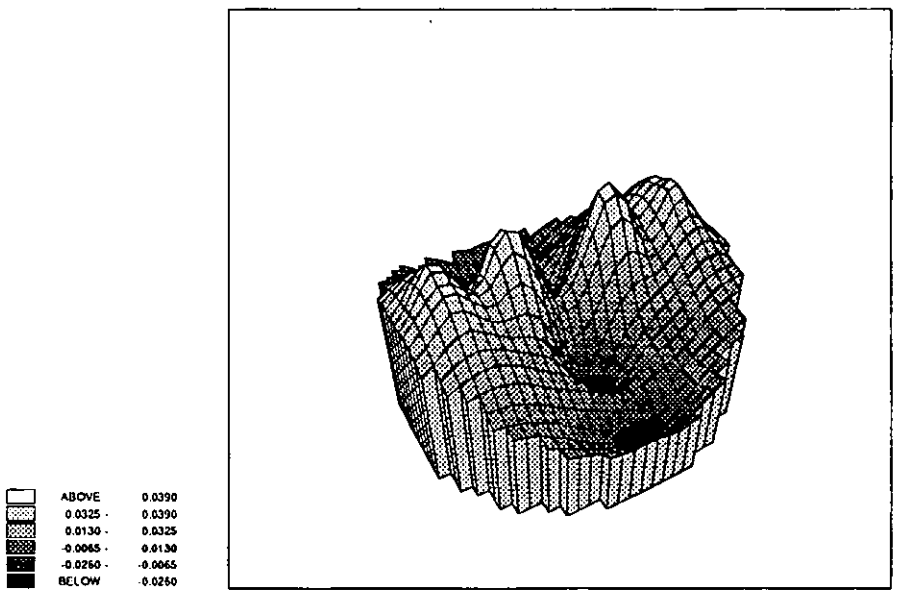

Figure 4.10(d) Mode shape for circular silencer. Mode 4, M=0.0, frequency=500 Hz (upper plot:real part, lower plot:imaginary part)

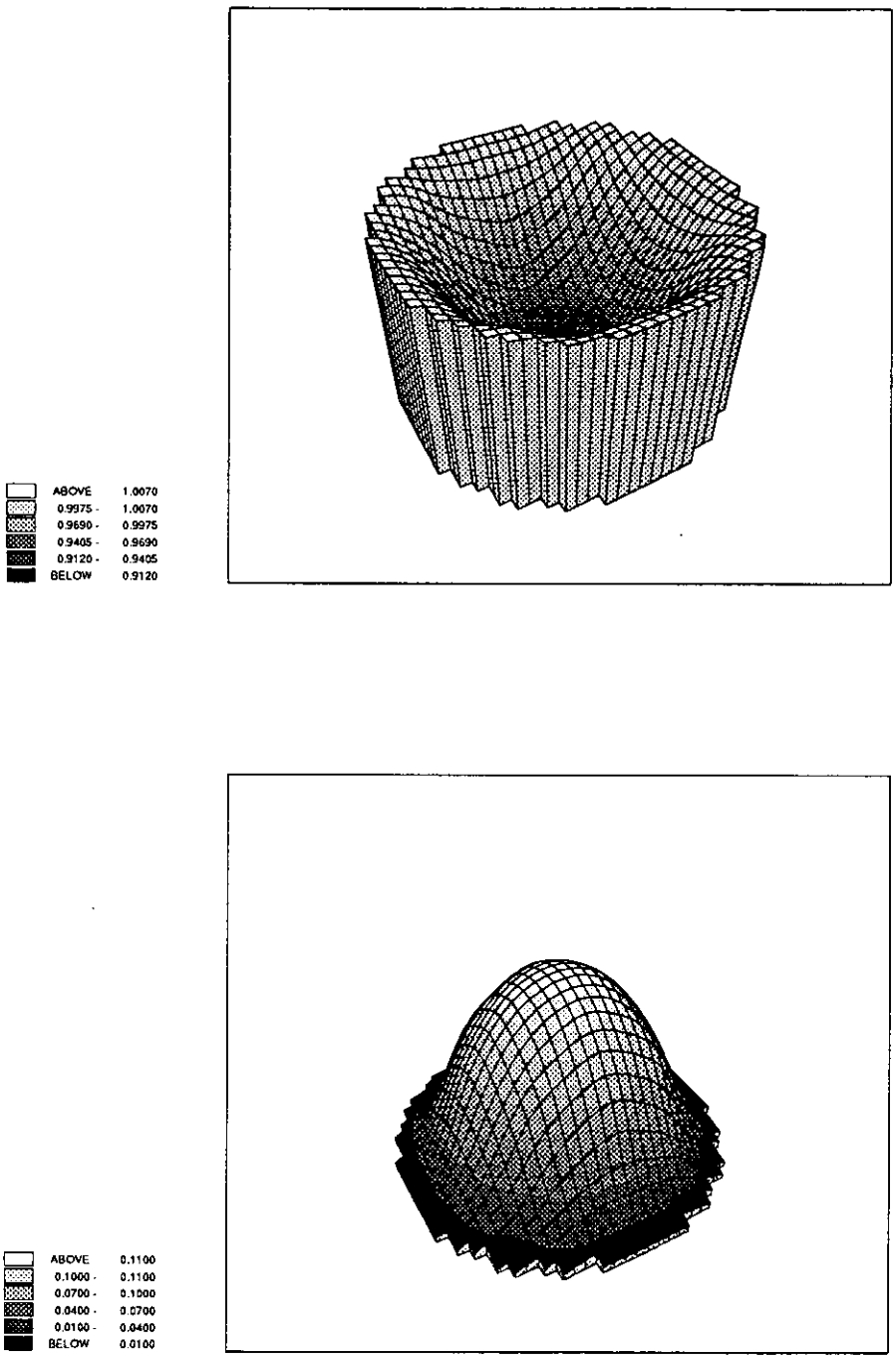

Figure 4.11(a) Mode shape for circular silencer. Mode 1, M=0.0, frequency=2000 Hz (upper plot:real part, lower plot:imaginary part)

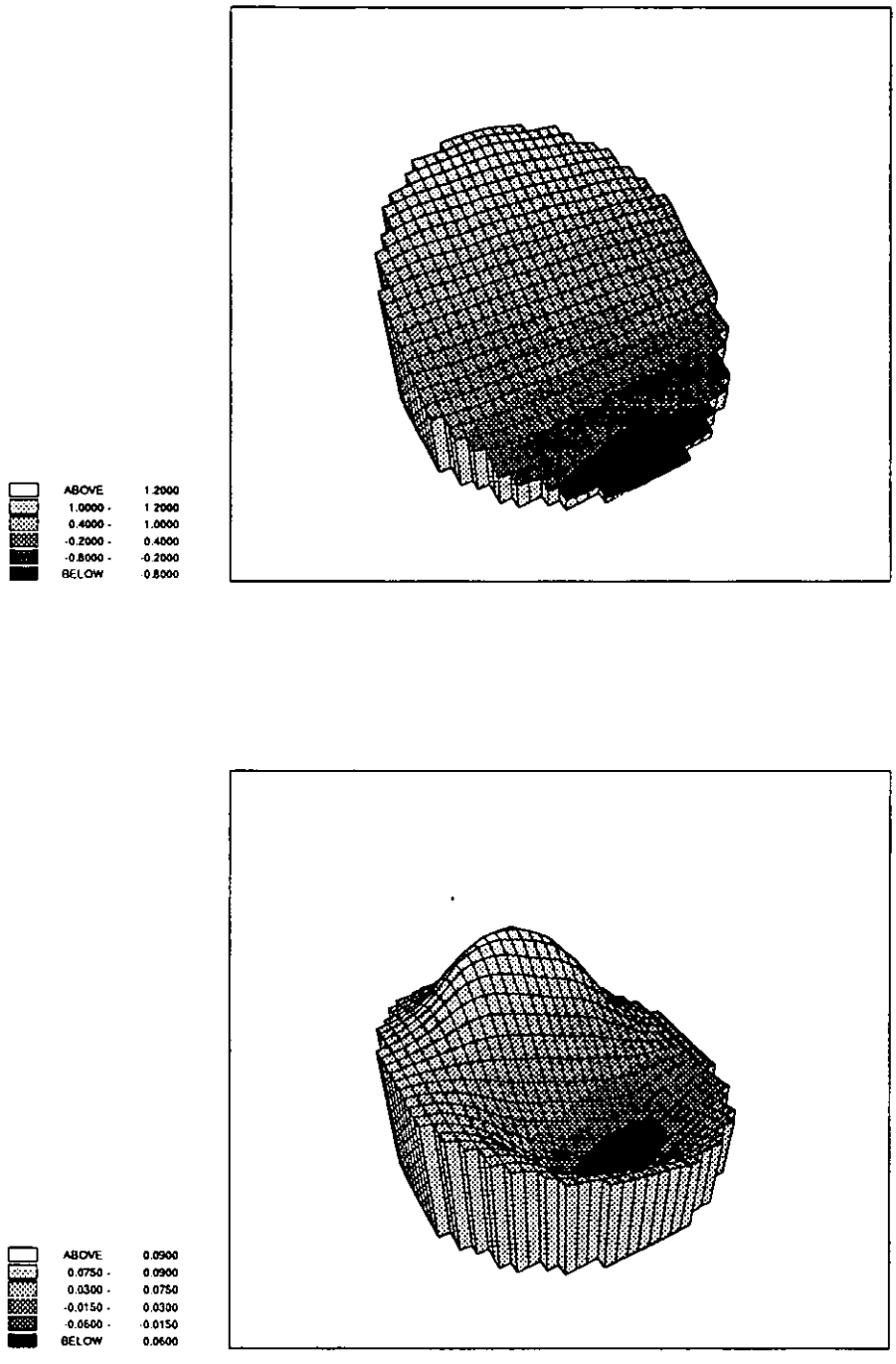

Figure 4.11(b) Mode shape for circular silencer. Mode 2, M=0.0, frequency=2000 Hz (upper plot:real part, lower plot:imaginary part)

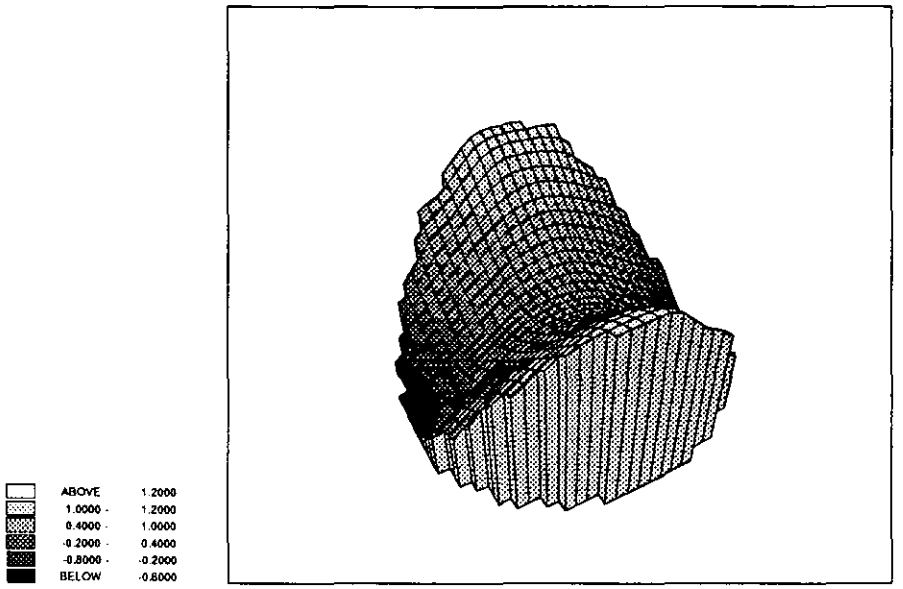

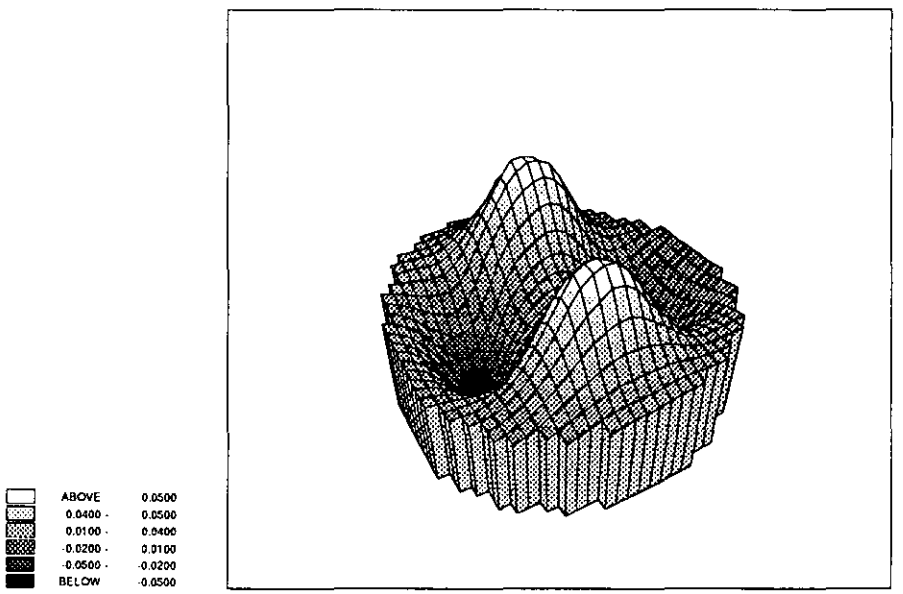

Figure 4.11(c) Mode shape for circular silencer. Mode 3, M=0.0, frequency=2000 Hz (upper plot:real part, lower plot:imaginary part)

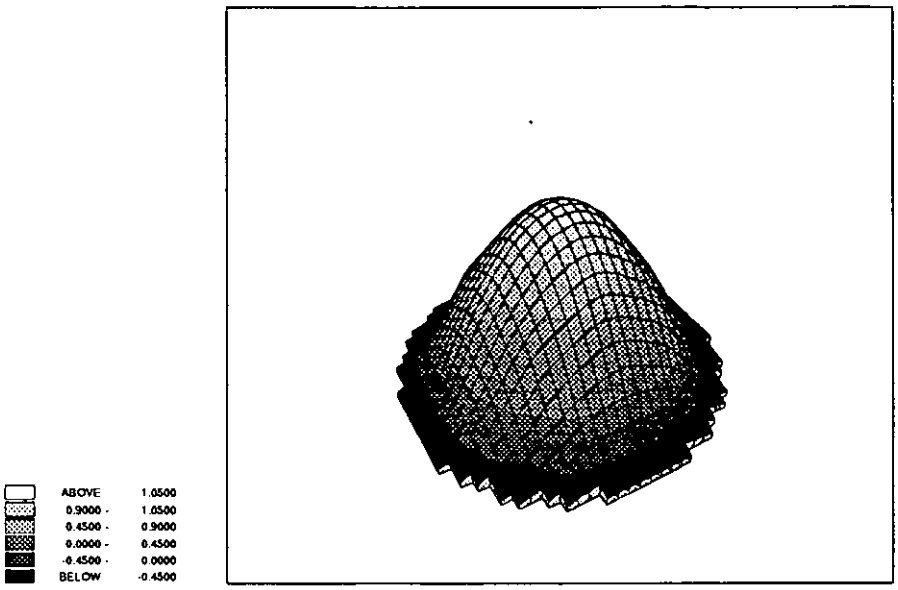

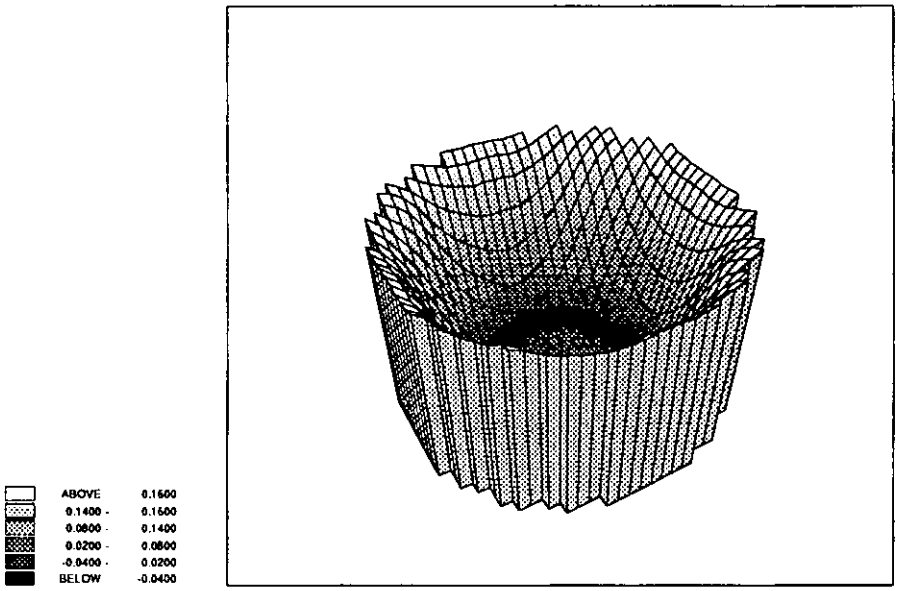

Figure 4.11(d) Mode shape for circular silencer. Mode 4, M=0.0, frequency=2000 Hz (upper plot:real part, lower plot:imaginary part)

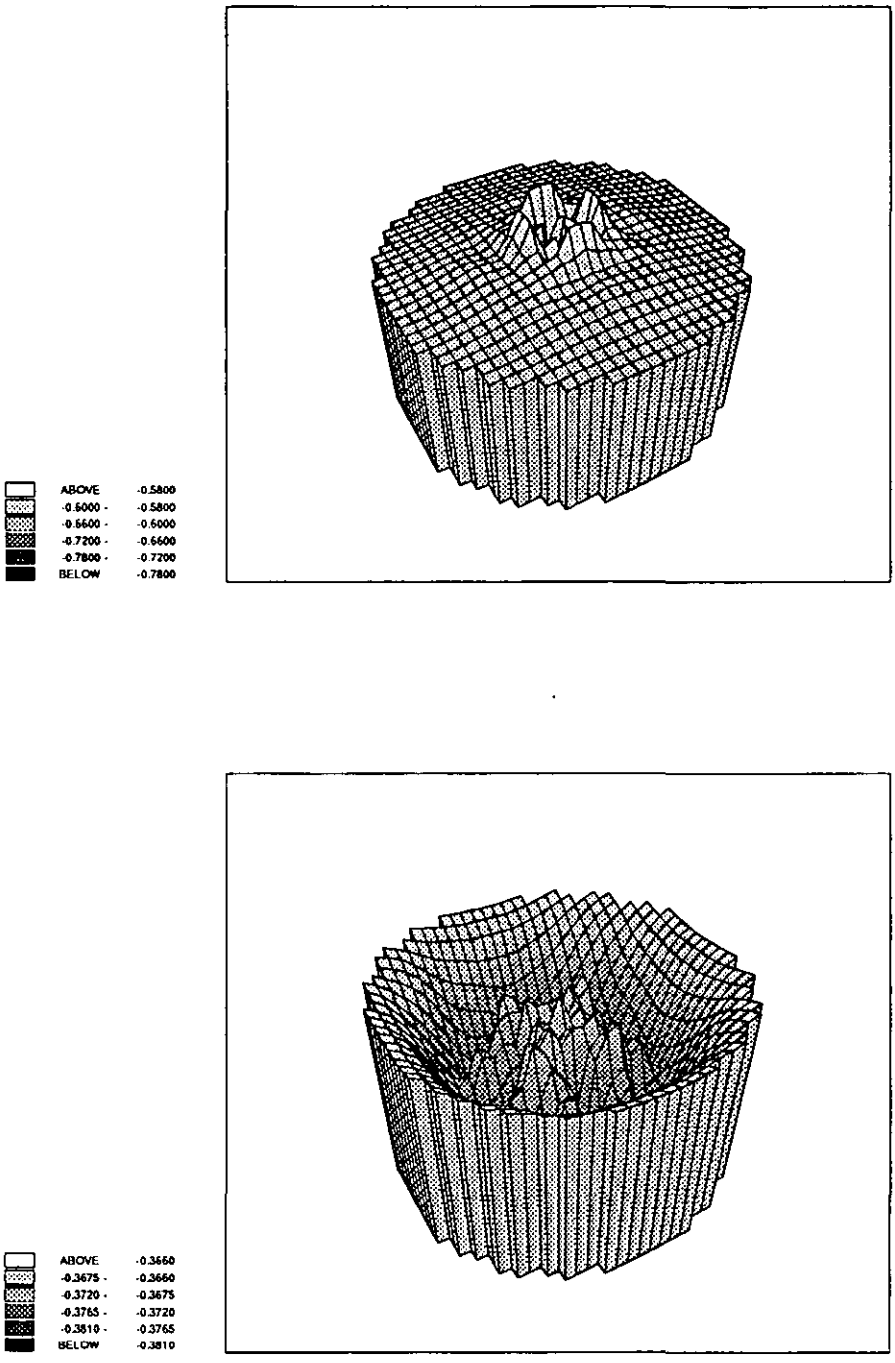

Figure 4.12(a) Mode shape for circular silencer. Mode 1, M=0.197, frequency=500 Hz (upper plot:real part, lower plot:imaginary part)

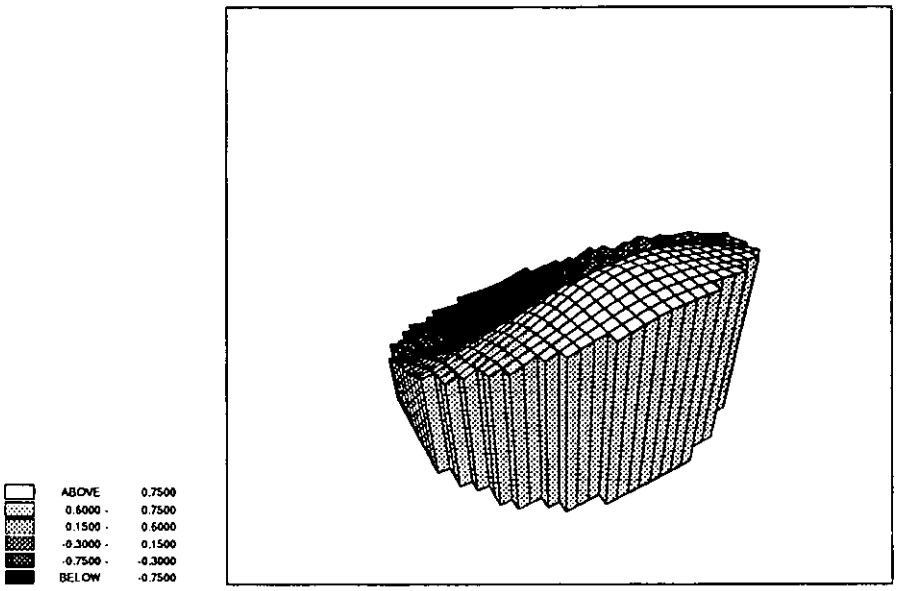

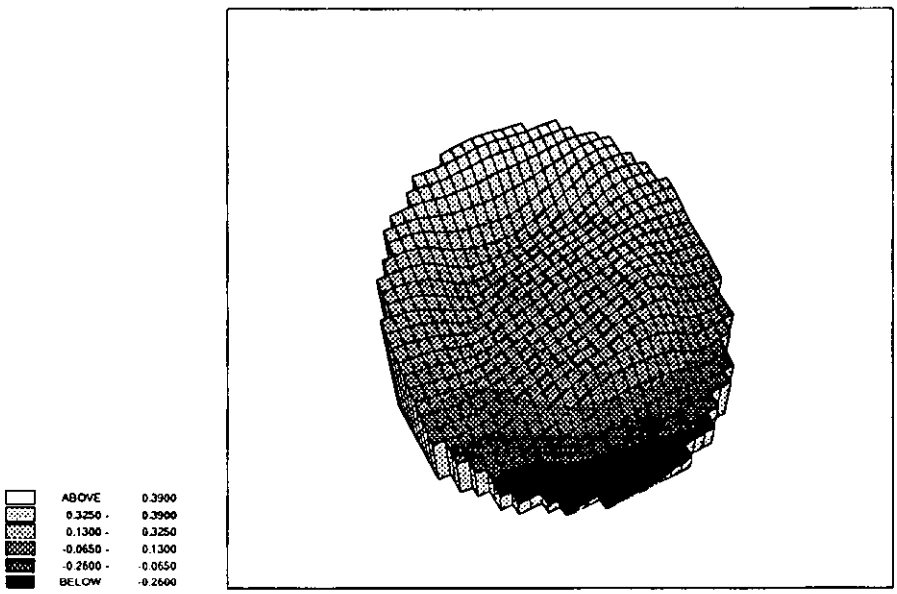

Figure 4.12(b) Mode shape for circular silencer. Mode 2, M=0.197, frequency=500 Hz (upper plot:real part, lower plot:imaginary part)

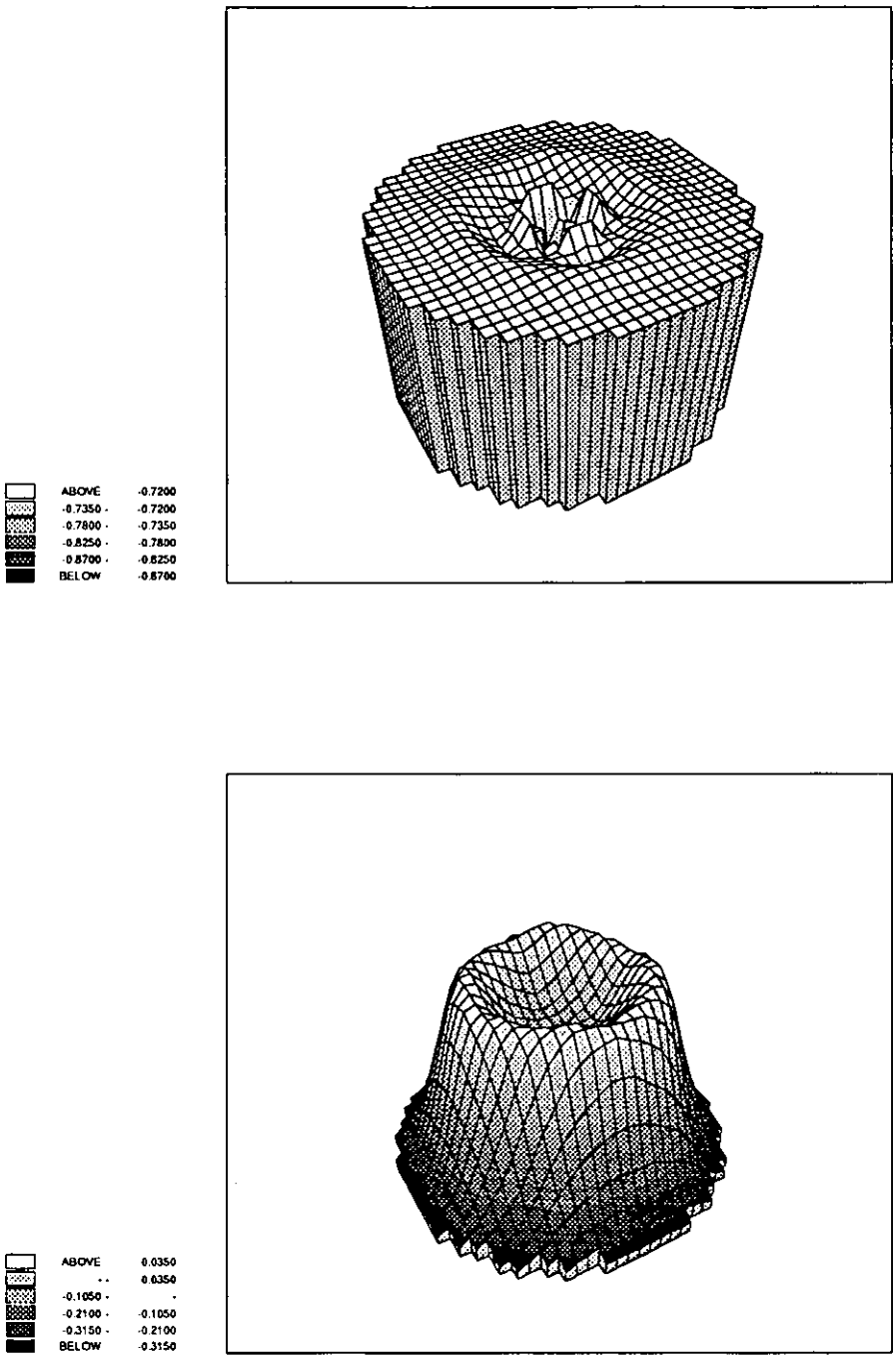

Figure 4.12(c) Mode shape for circular silencer. Mode 3, M=0.197, frequency=500 Hz (upper plot:real part, lower plot:imaginary part)

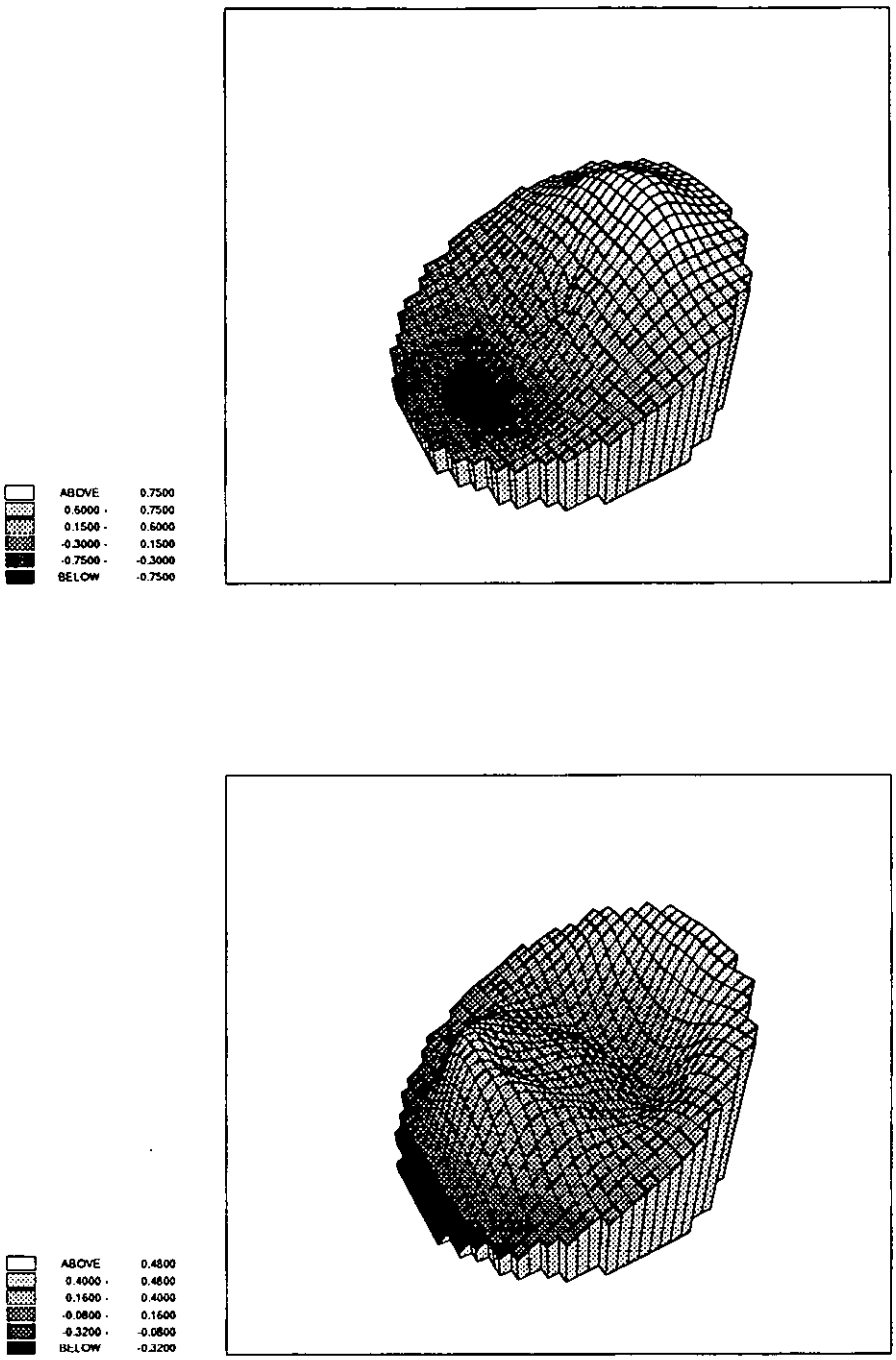

Figure 4.12(d) Mode shape for circular silencer. Mode 4, M=0.197, frequency=500 Hz (upper plot:real part, lower plot:imaginary part)

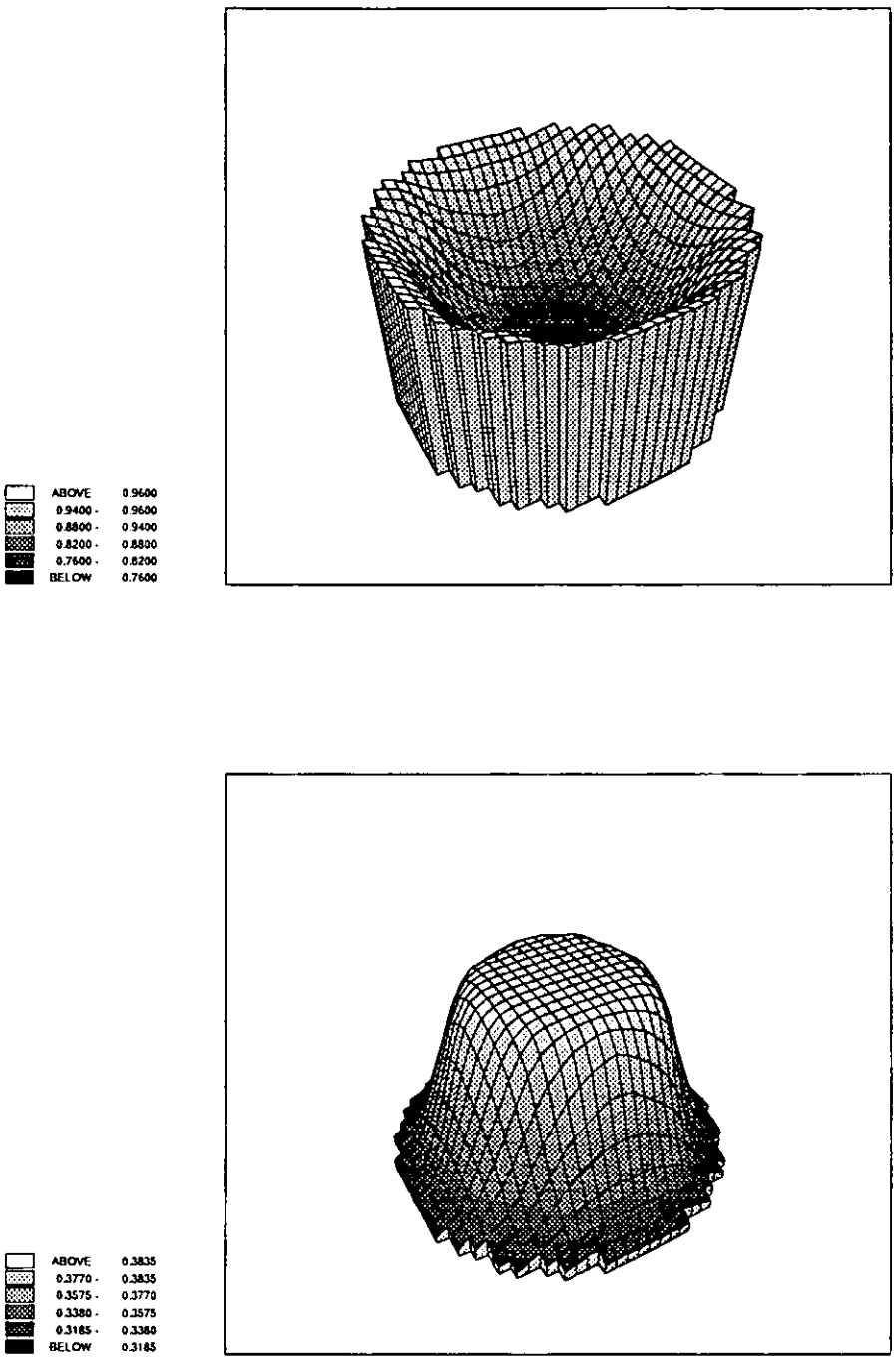

Figure 4.13(a) Mode shape for circular silencer. Mode 1, M=0.197, frequency=2000 Hz (upper plot:real part, lower plot:imaginary part)

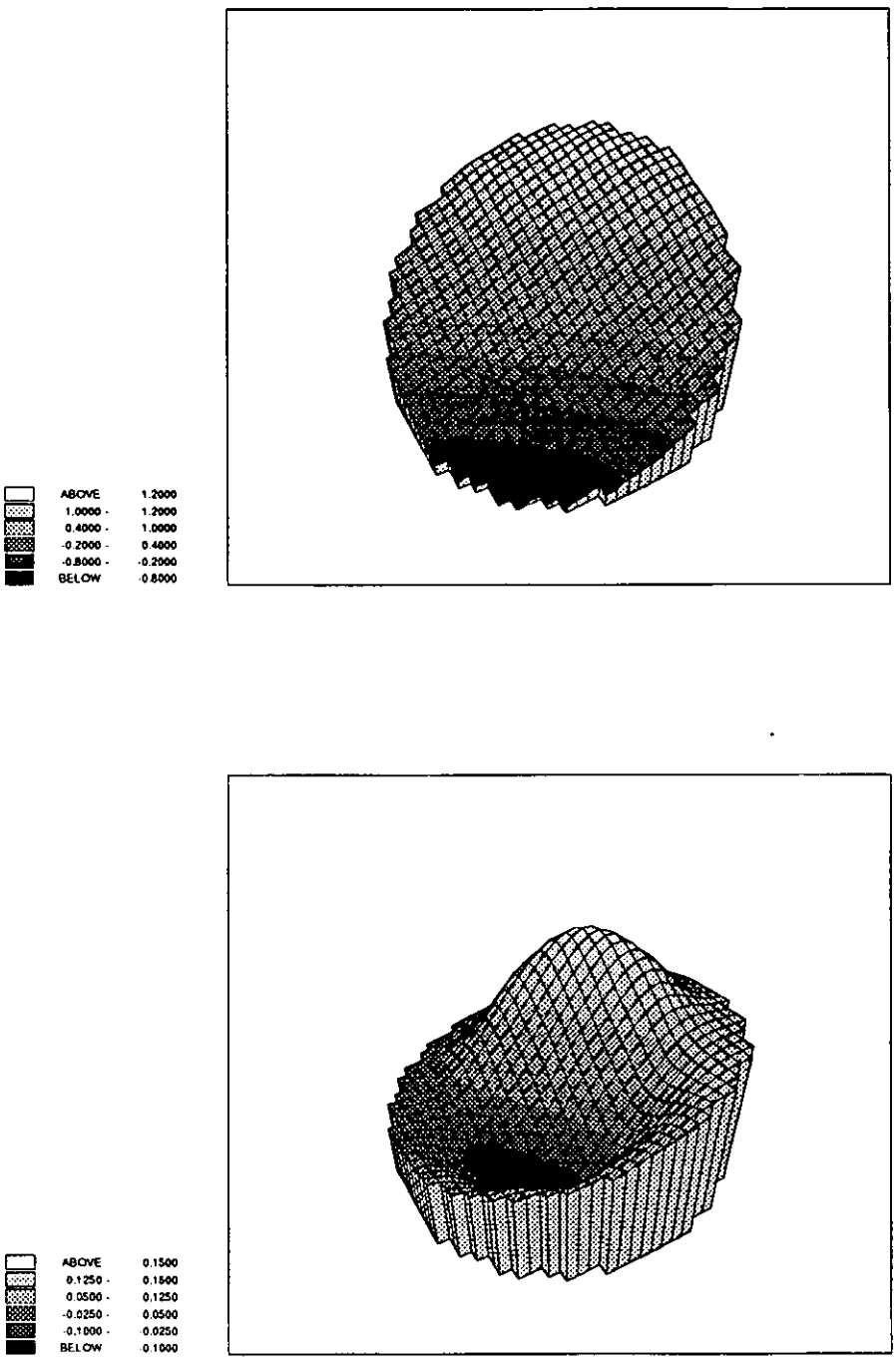

Figure 4.13(b) Mode shape for circular silencer. Mode 2, M=0.197, frequency=2000 Hz (upper plot:real part, lower plot:imaginary part)

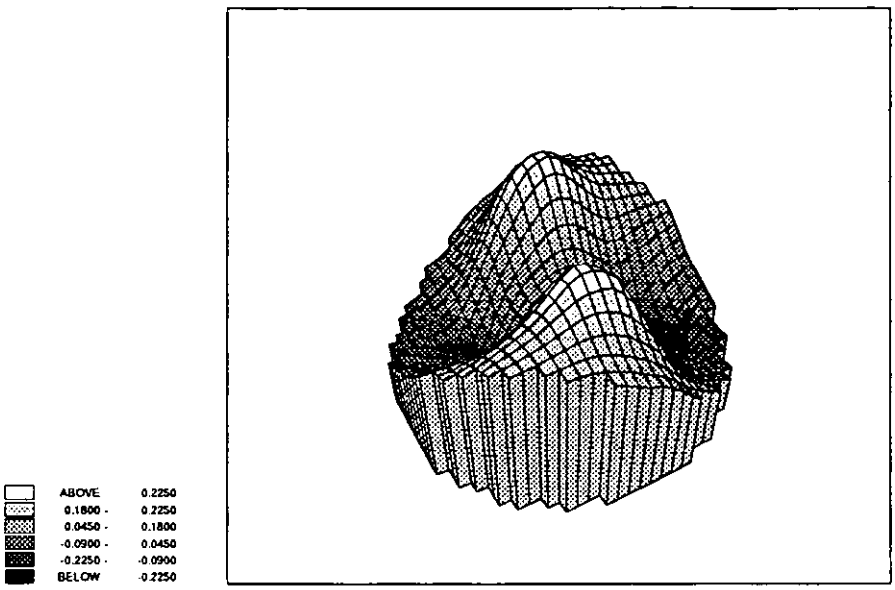

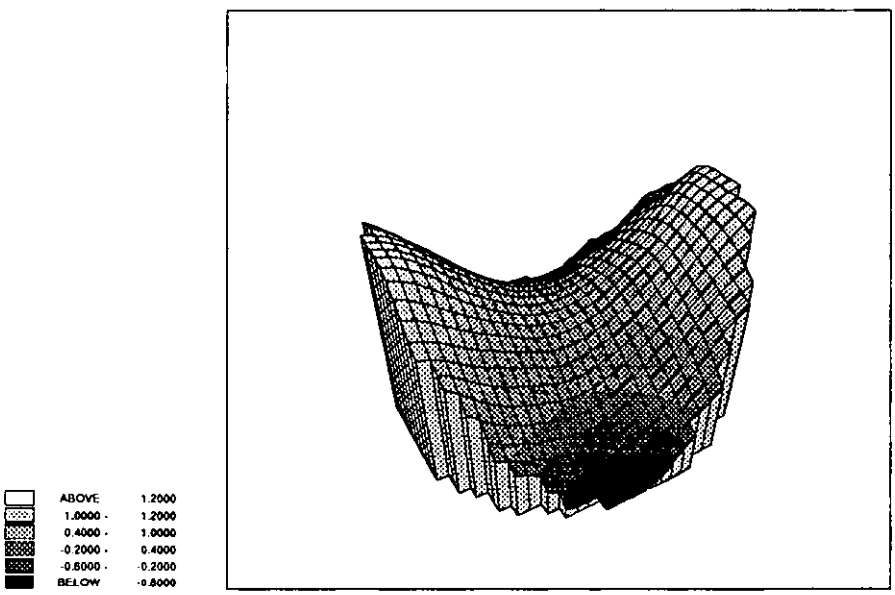

Figure 4.13(c) Mode shape for circular silencer. Mode 3, M=0.197, frequency=2000 Hz (upper plot:real part, lower plot:imaginary part)

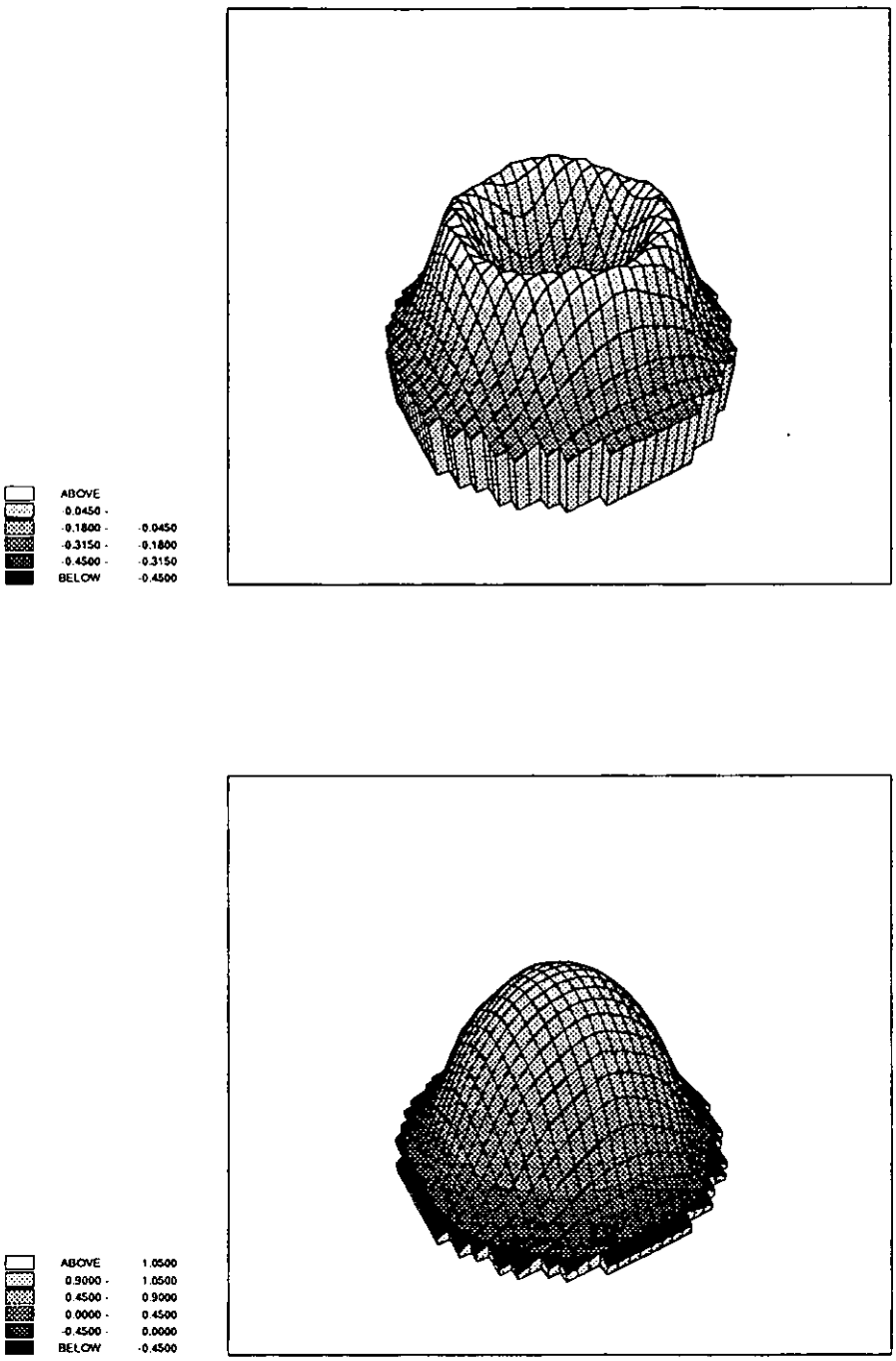

Figure 4.13(d) Mode shape for circular silencer. Mode 4, M=0.197, frequency=2000 Hz (upper plot:real part, lower plot:imaginary part)

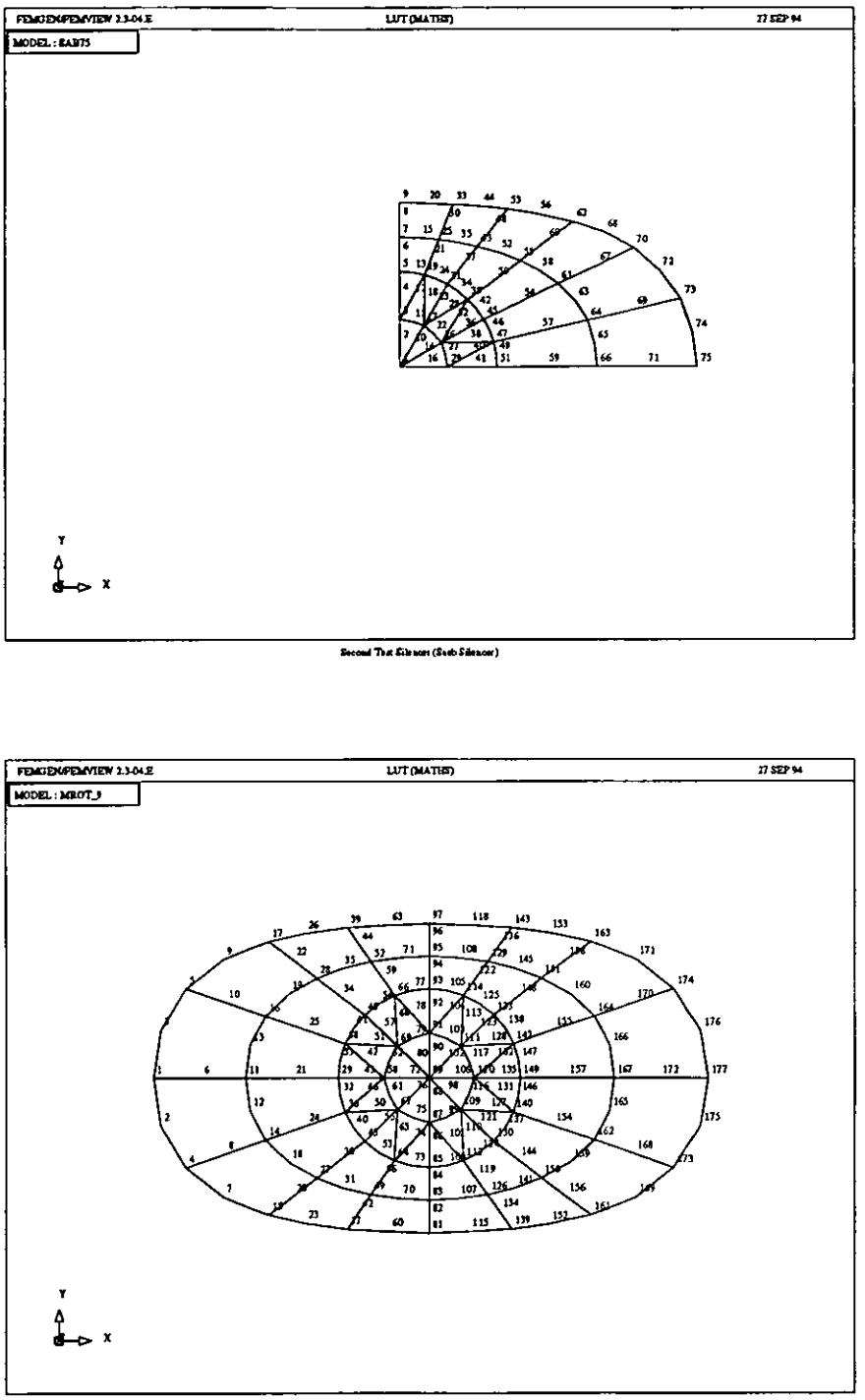

Figure 4.14 Quarter and full mesh model of the SAAB cross-section silencer

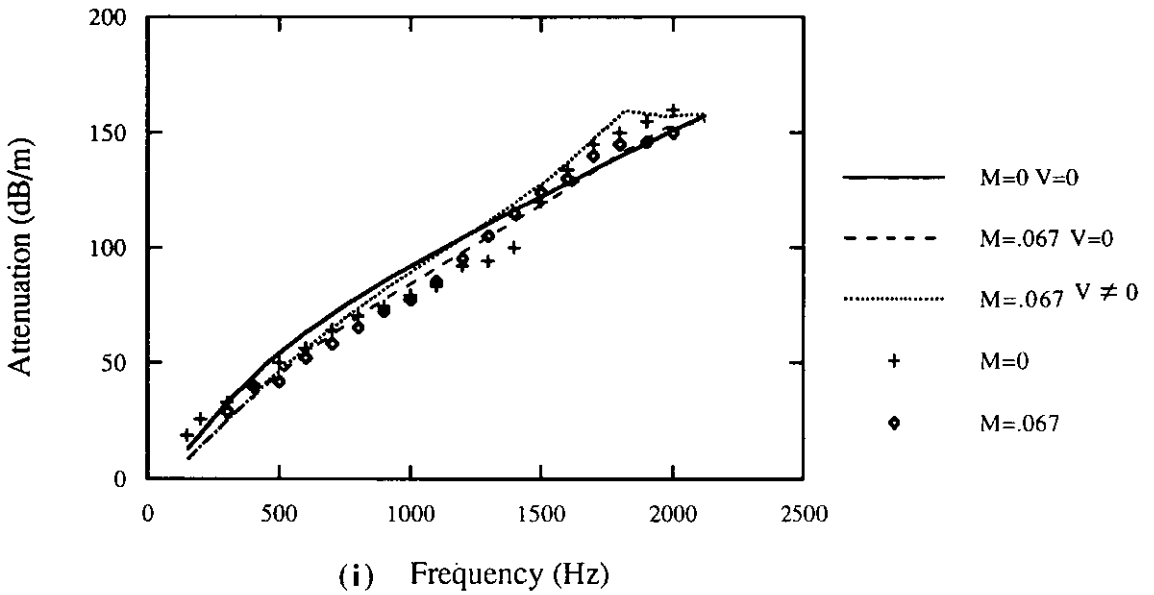

(i) Frequency (Hz)

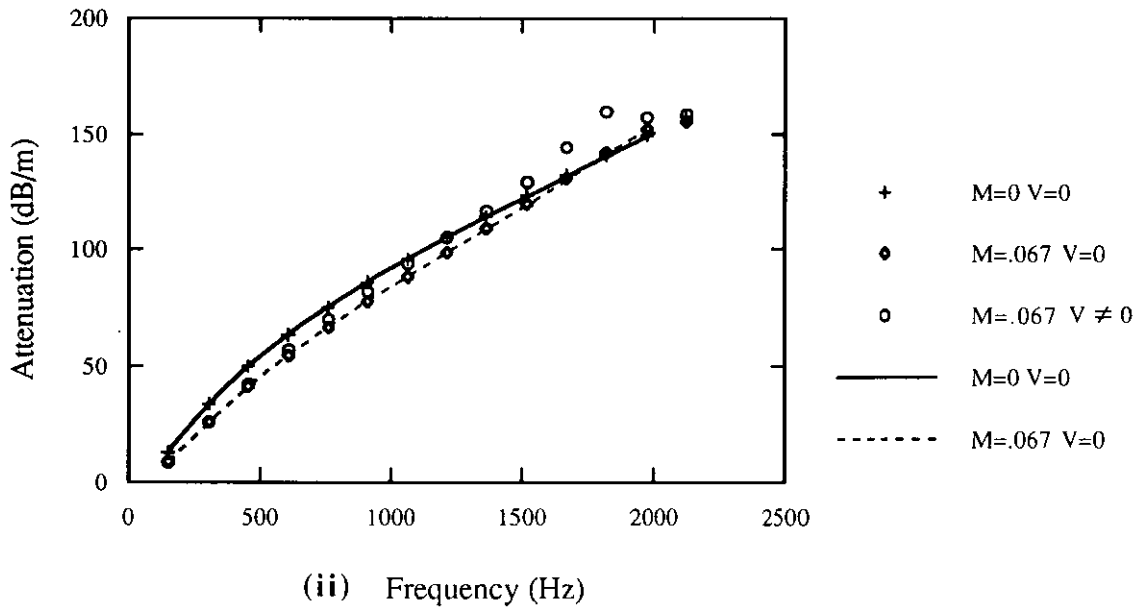

(ii) Frequency (Hz)

Figure 4.15(a). Axial attenuation rate for SAAB silencer. **(i)** Comparison of FE(curves) results with experimental results(symbols) of Cummings [70] **(ii)** Comparision of FE (symbols) with R.R solution (curves) of Cummings [70].

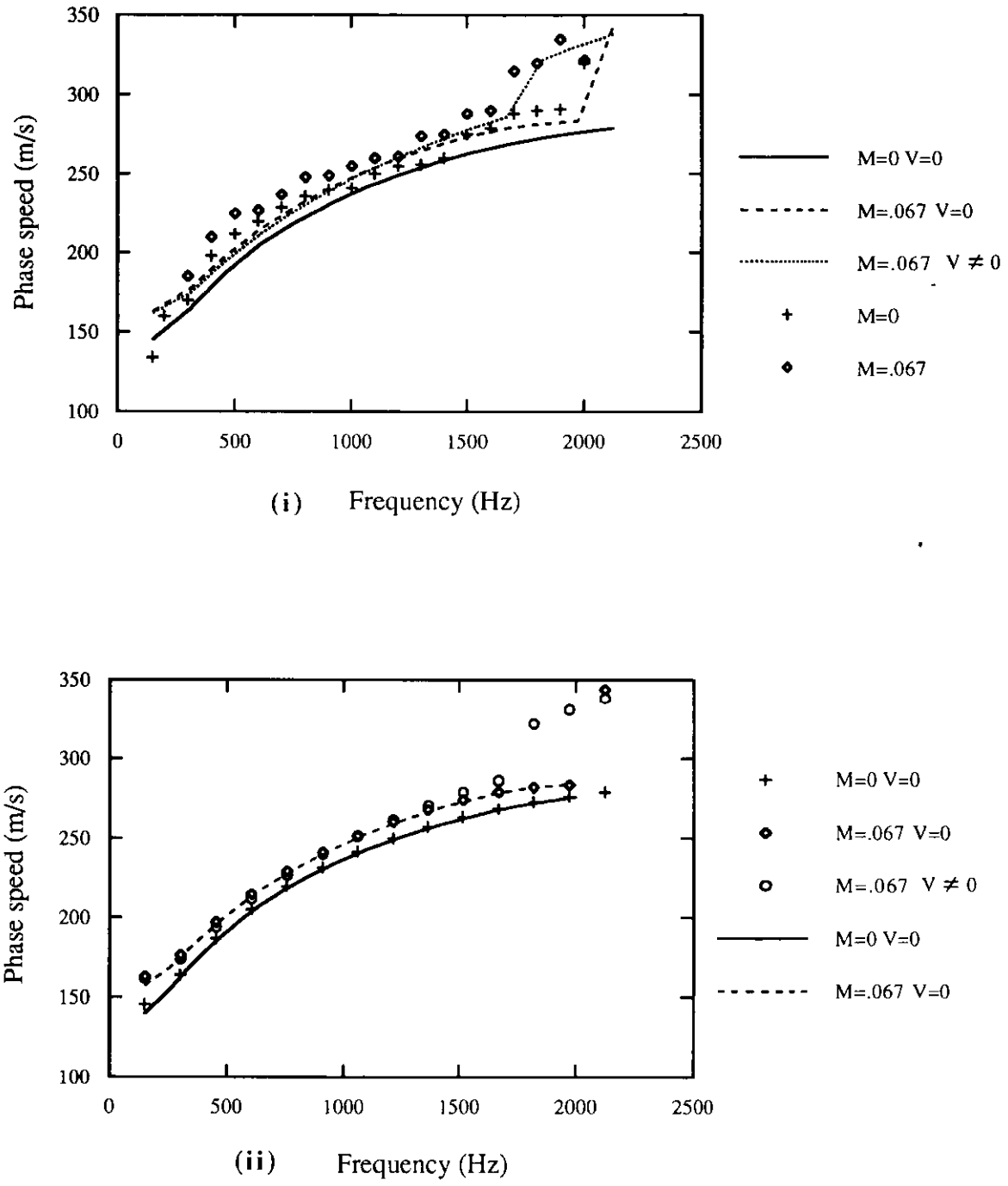

Figure 4.15(b).Phase speed for SAAB silencer. (i) Comparison of FE(curves) results with experimental results(symbols) of Cummings [70] (ii) Comparison of FE (symbols) with R.R solution (curves) of Cummings [70].

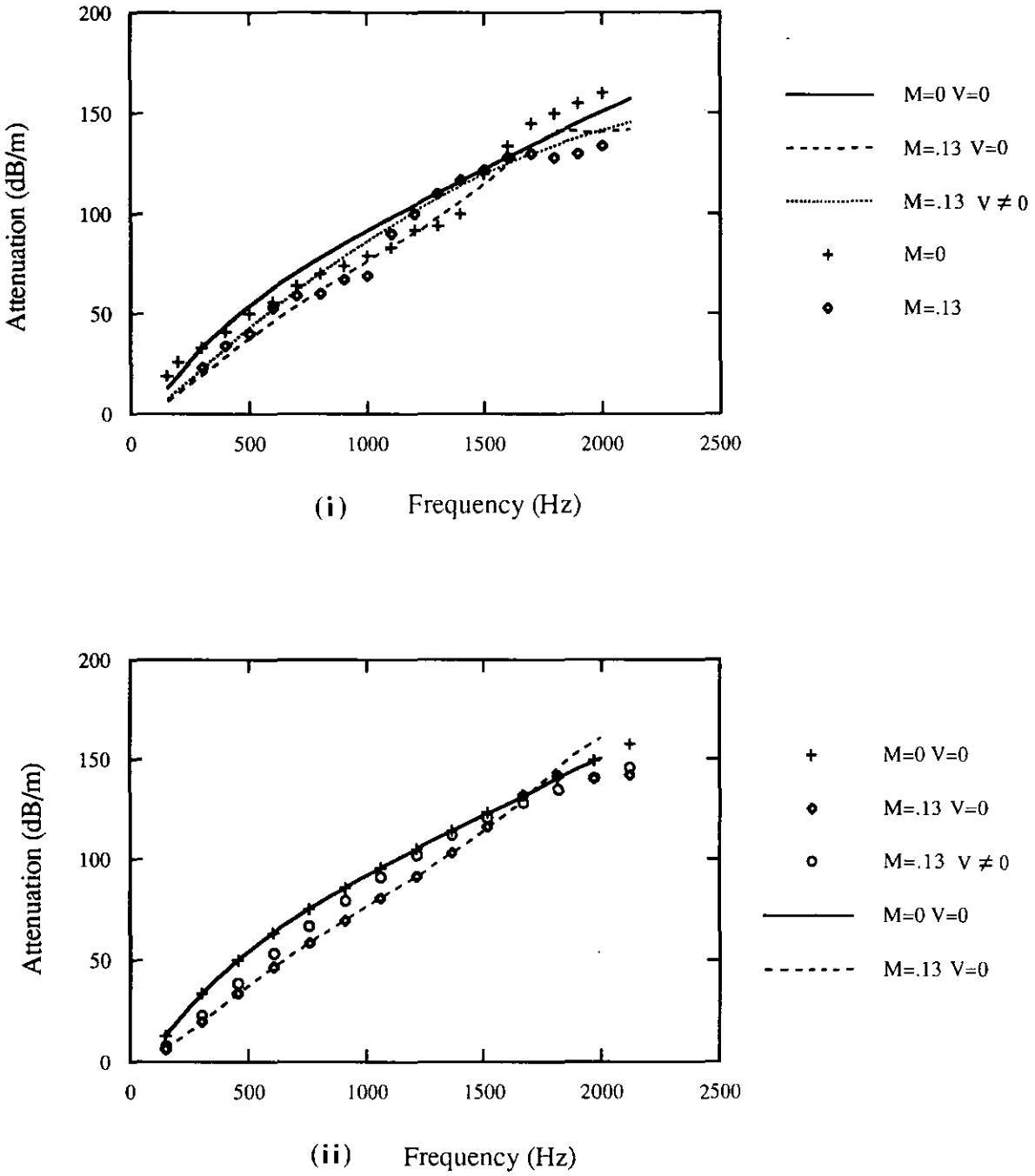

Figure 4.16(a). Axial attenuation rate for SAAB silencer. **(i)** Comparison of FE(curves) results with experimental results (symbols) of Cummings [70] **(ii)** Comparison of FE (symbols) with R.R solution (curves) of Cummings [70].

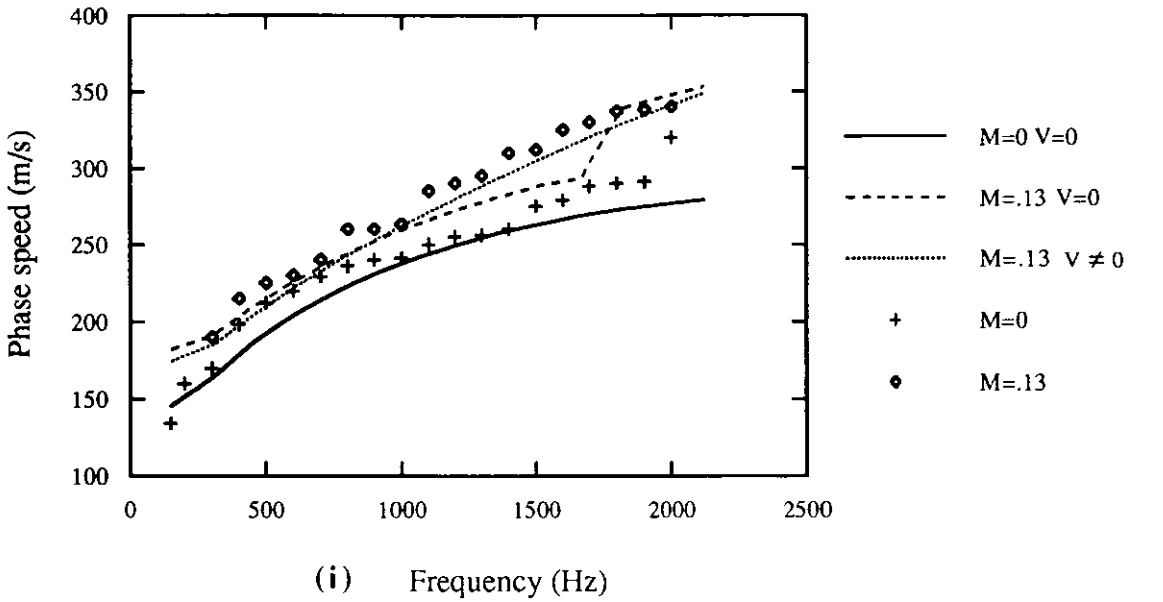

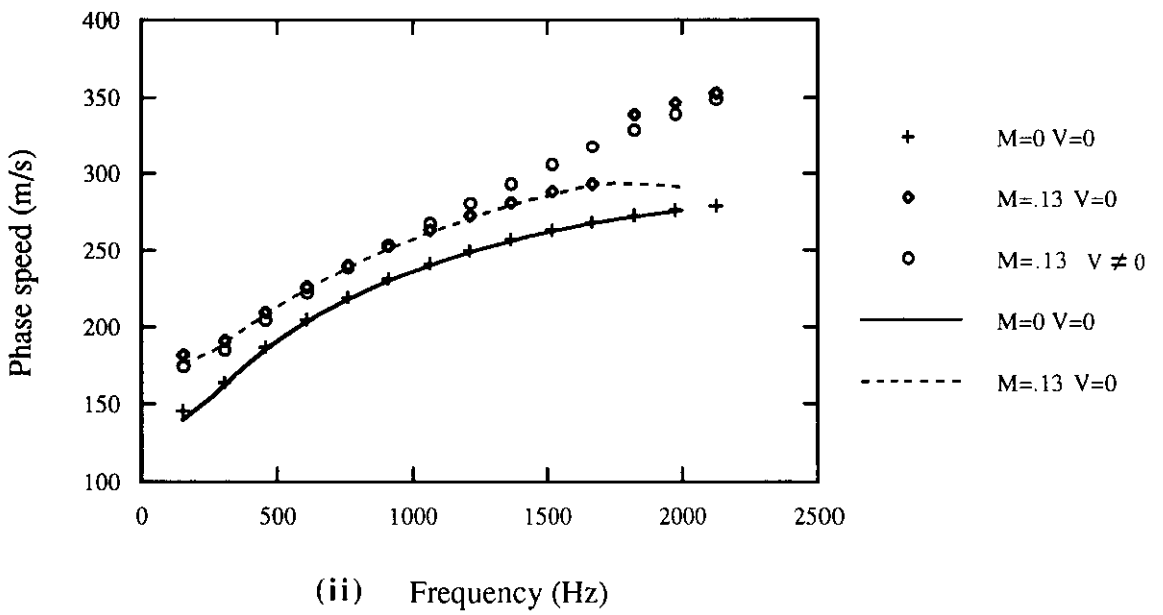

Figure 4.16(b). Phase speed for SAAB silencer. **(i)** Comparison of FE(curves) results with experimental results (symbols) of Cummings [70]. **(ii)** Comparison of FE (symbols) with R.R solution (curves) of Cummings [70].

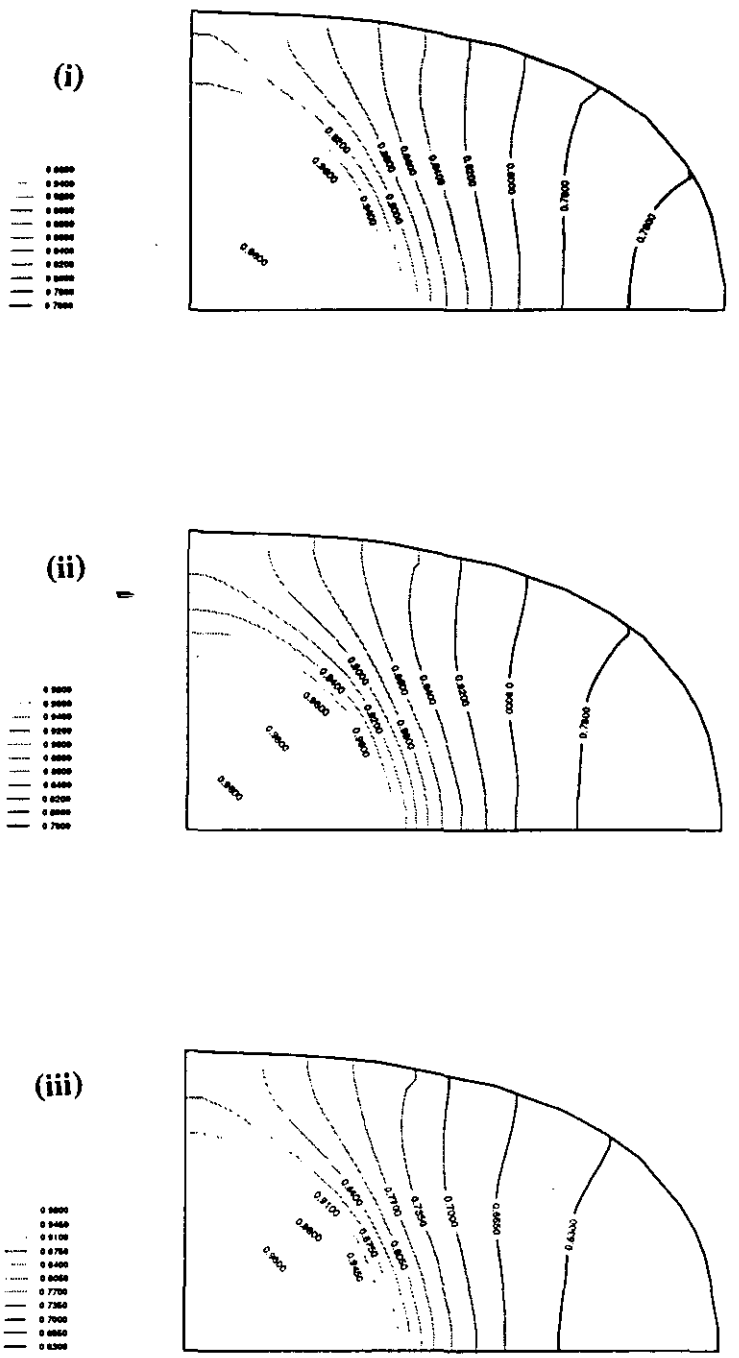

Figure 4.17. Sound pressure amplitude for SAAB silencer least-attenuated mode, frequency =500 Hz (i) M=0.0 (ii) M=0.13 without induced flow (iii) M= 0.13 with induced flow

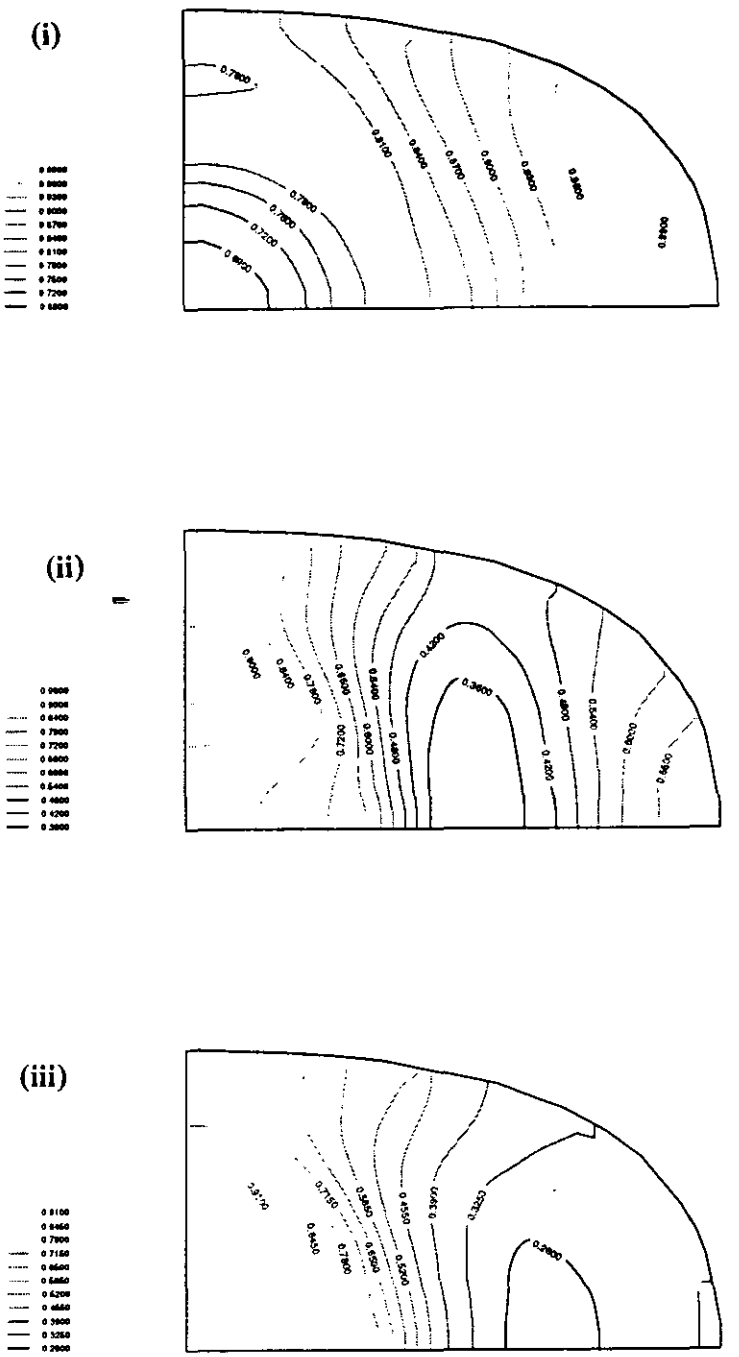

Figure 4.18. Sound pressure amplitude for SAAB silencer least-attenuated mode, frequency =2000 Hz **(i)** M=0.0 **(ii)** M=0.13 without induced flow **(iii)** M= 0.13 with induced flow

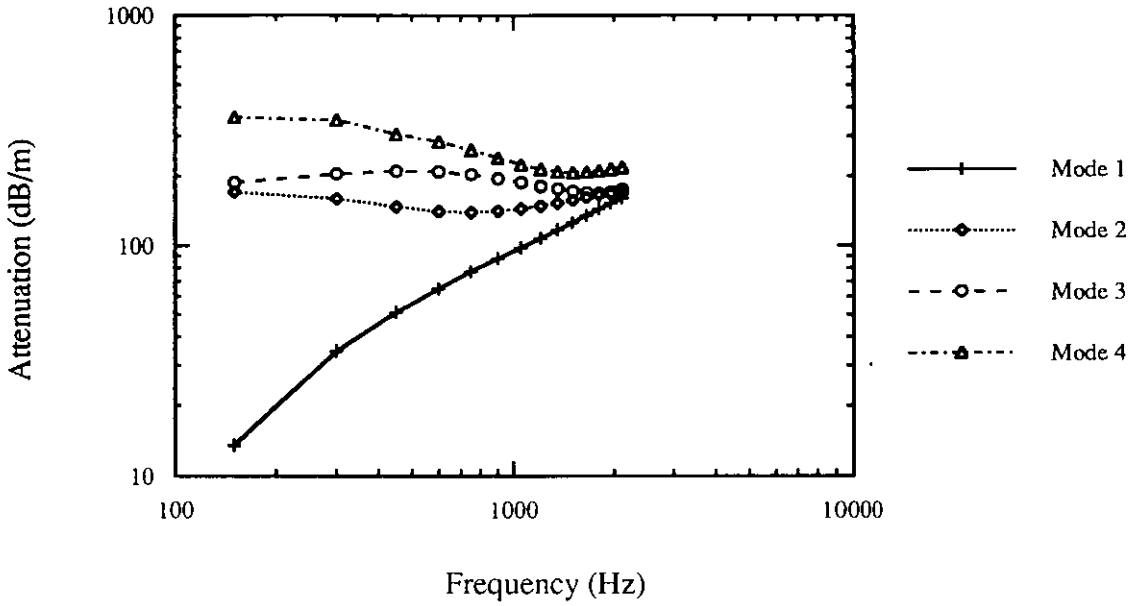

Figure 4.19. Axial attenuation rate for the SAAB test silencer for the four least-attenuated modes.

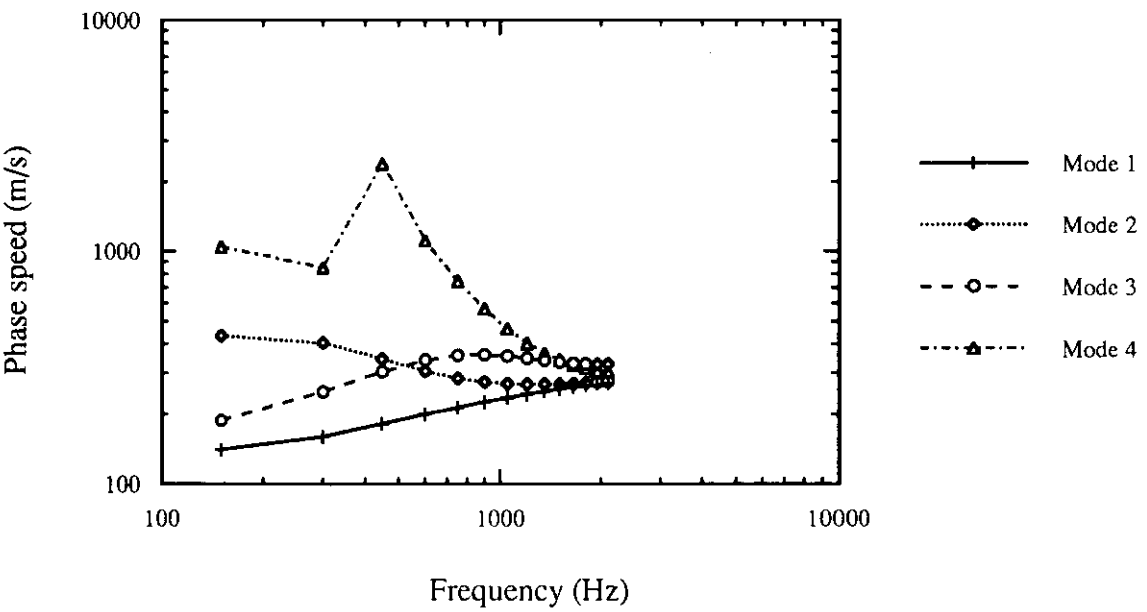

Figure 4.20. Phase speed for the SAAB test silencer for the four least-attenuated modes.

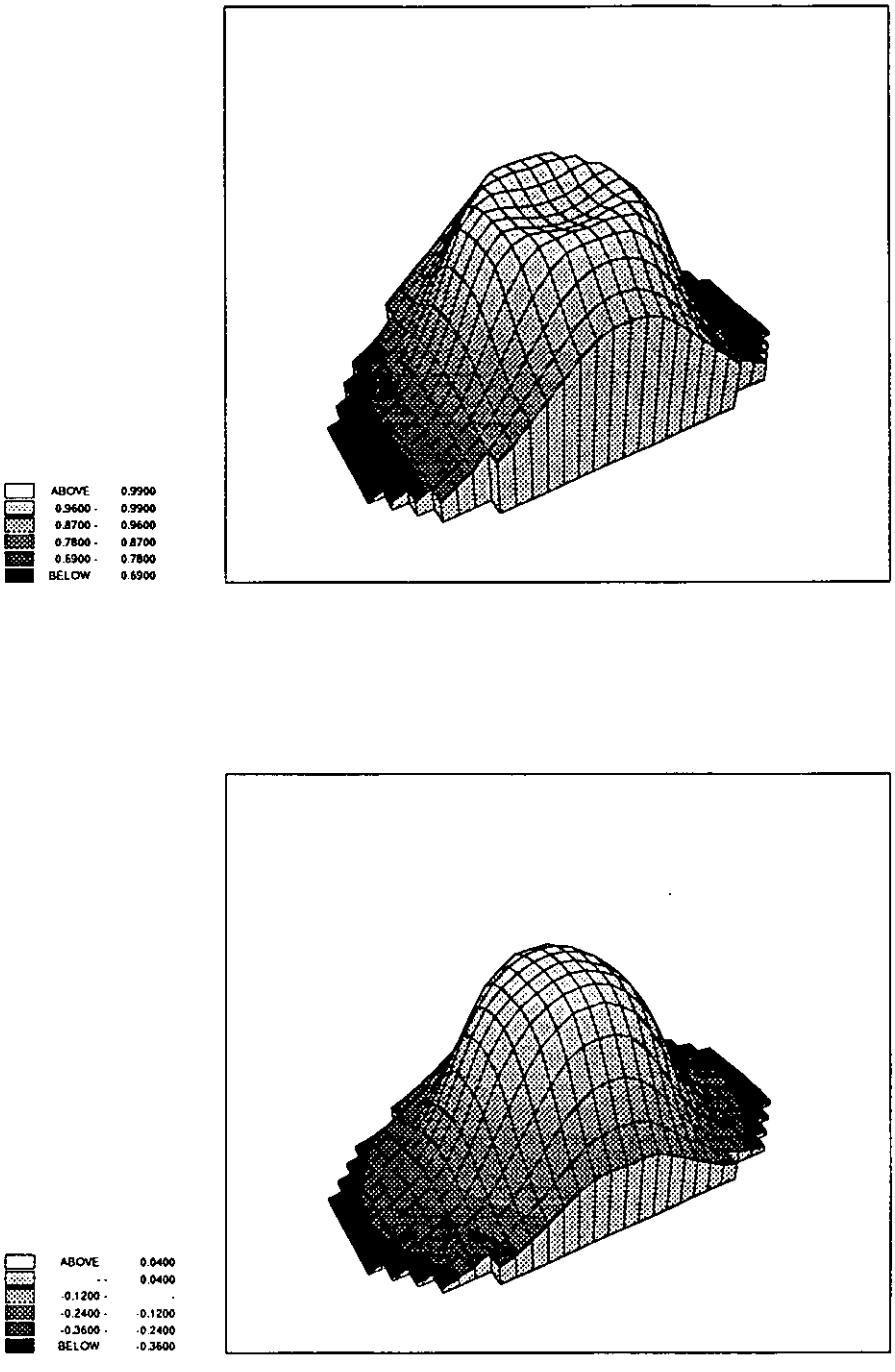

Figure 4.21(a) Mode shape for SAAB silencer. Mode 1, M=0.0, frequency=500 Hz (upper plot:real part, lower plot:imaginary part)

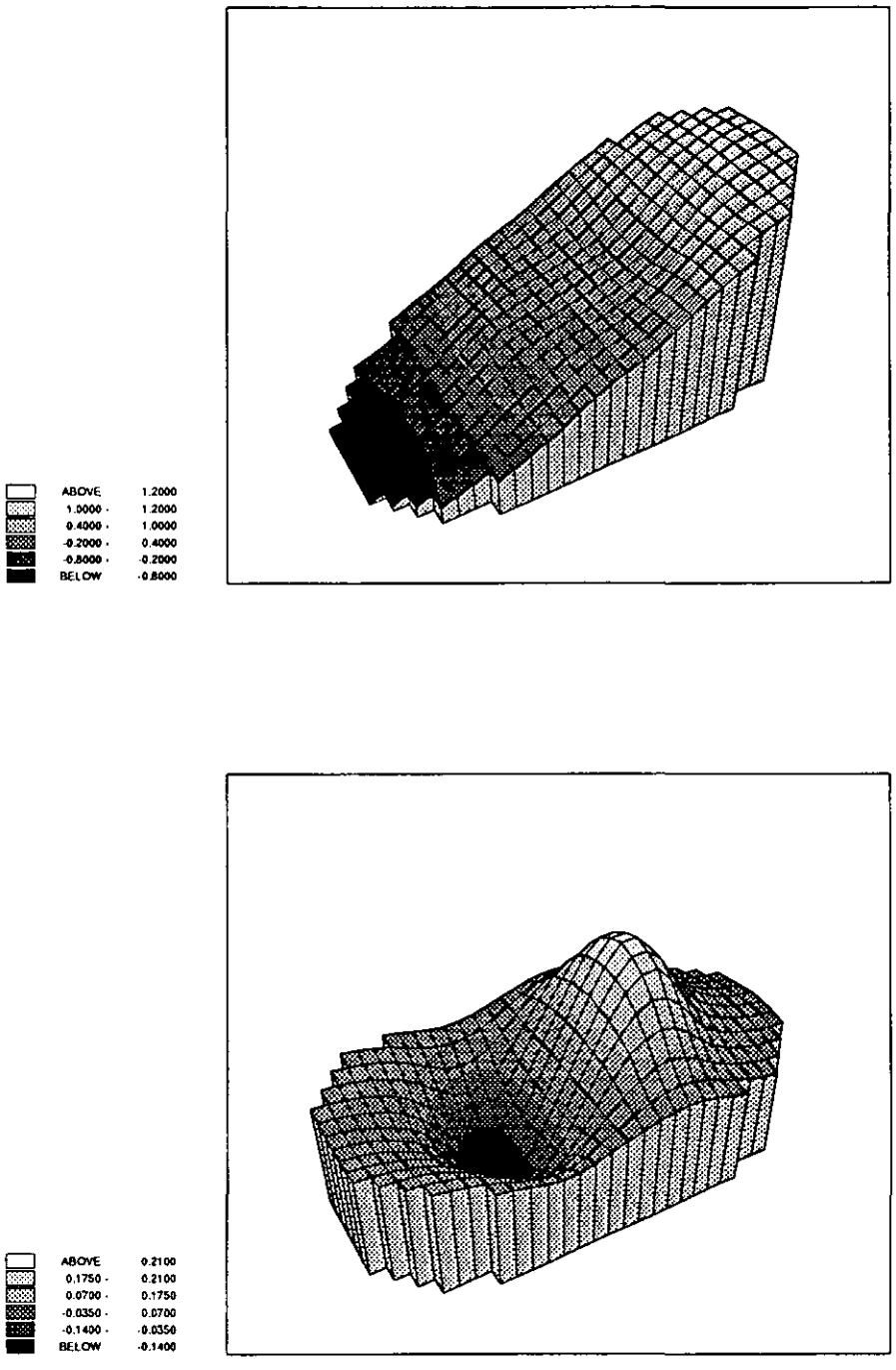

Figure 4.21(b) Mode shape for SAAB silencer. Mode 2, M=0.0, frequency=500 Hz (upper plot:real part, lower plot:imaginary part)

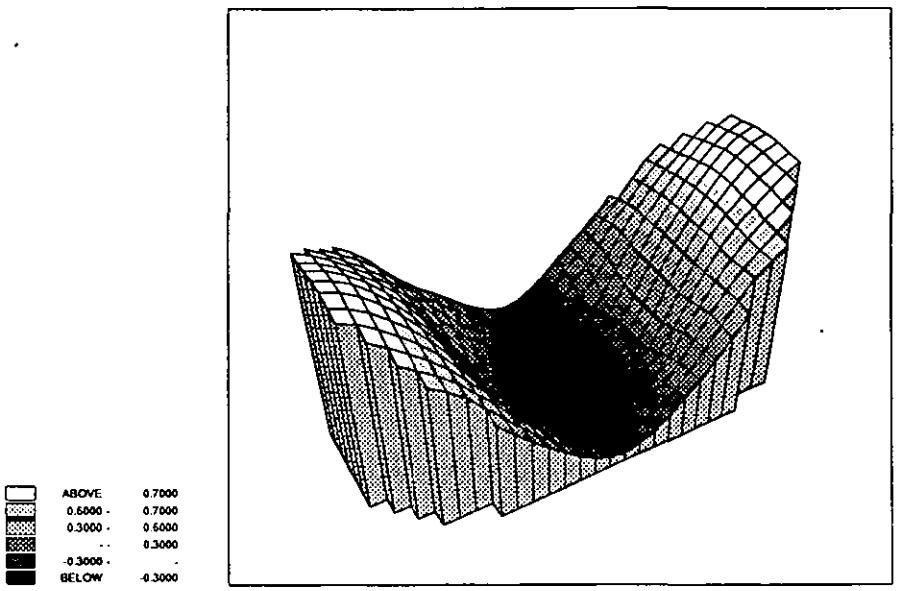

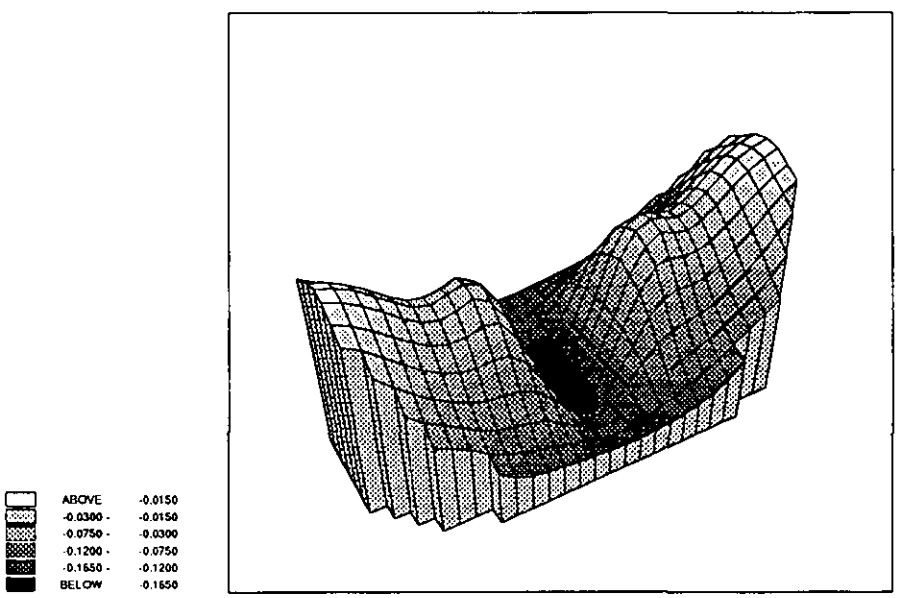

Figure 4.21(c) Mode shape for SAAB silencer. Mode 3, M=0.0, frequency=500 Hz (upper plot:real part, lower plot:imaginary part)

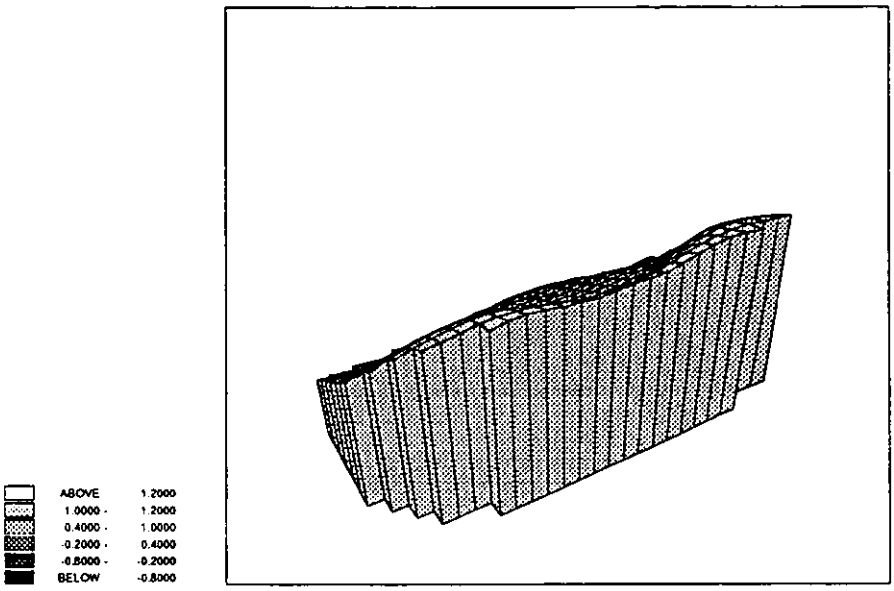

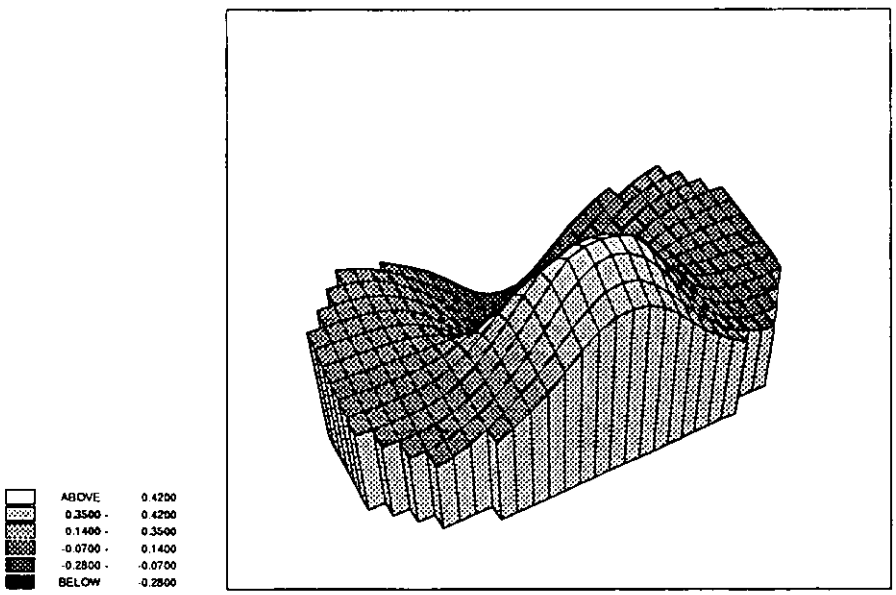

Figure 4.21(d) Mode shape for SAAB silencer. Mode 4, M=0.0, frequency=500 Hz (upper plot:real part, lower plot:imaginary part)

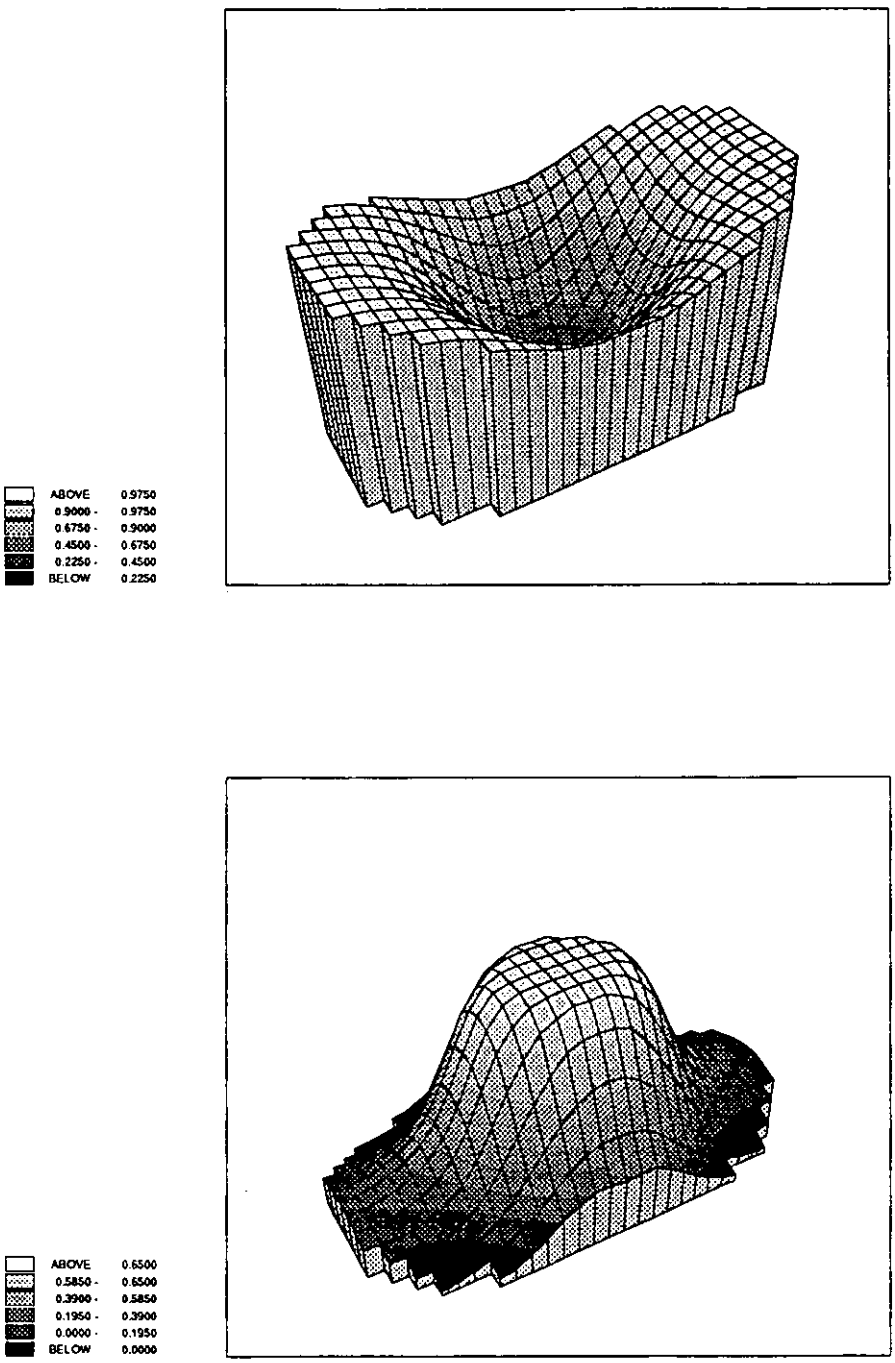

Figure 4.22(a) Mode shape for SAAB silencer. Mode 1, M=0.0, frequency=2000 Hz (upper plot:real part, lower plot:imaginary part)

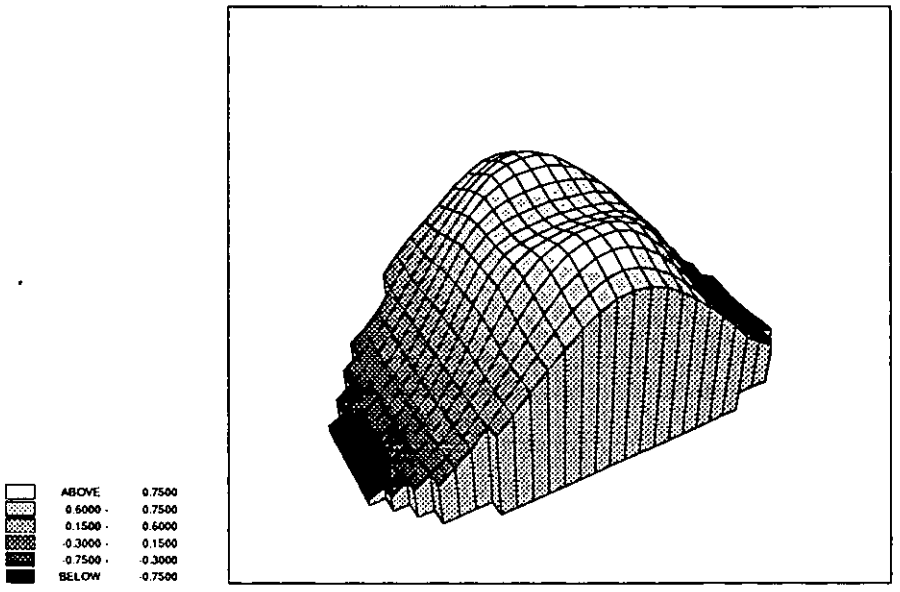

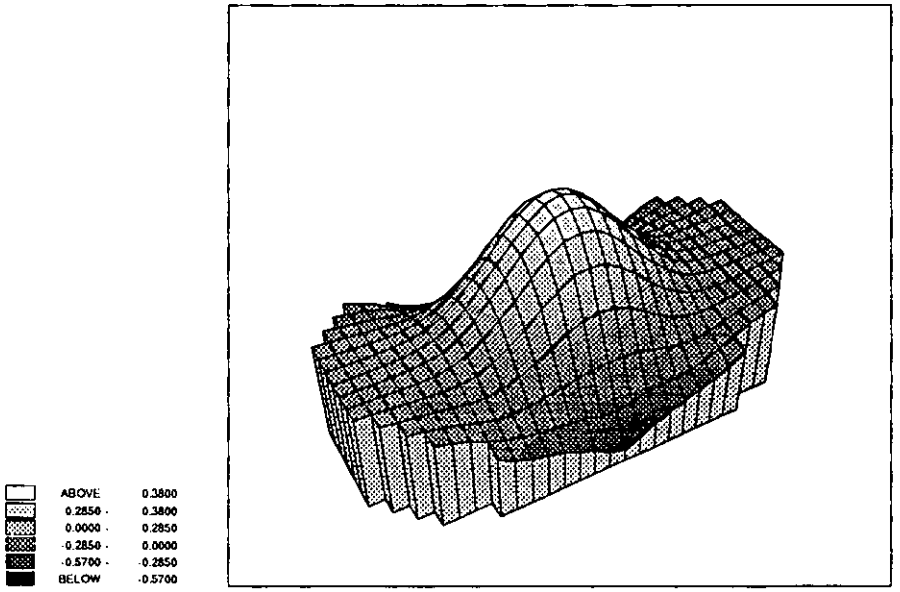

Figure 4.22(b) Mode shape for SAAB silencer. Mode 2, M=0.0, frequency=2000 Hz (upper plot:real part, lower plot:imaginary part)

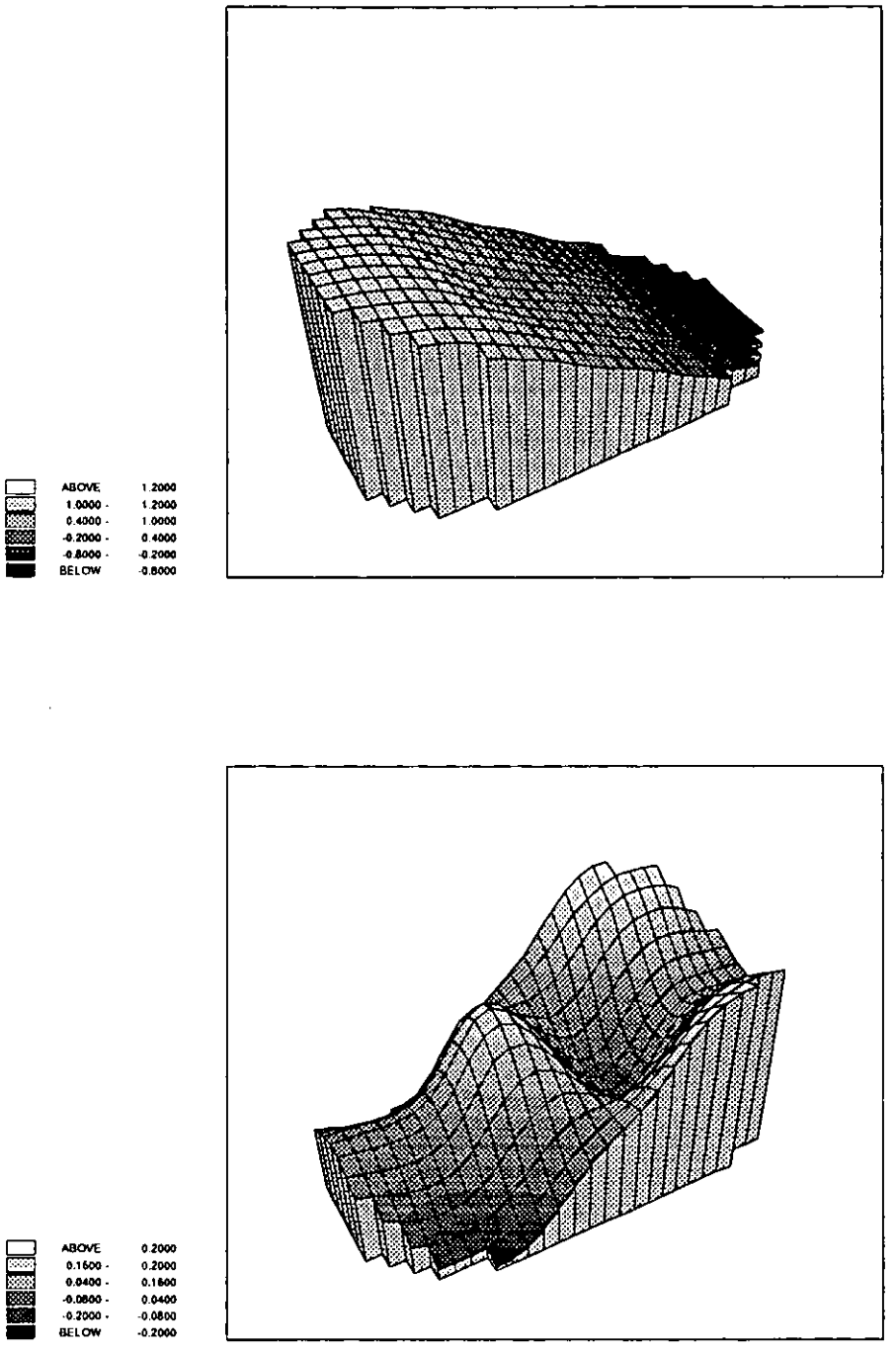

Figure 4.22(c) Mode shape for SAAB silencer. Mode 3, M=0.0, frequency=2000 Hz (upper plot:real part, lower plot:imaginary part)

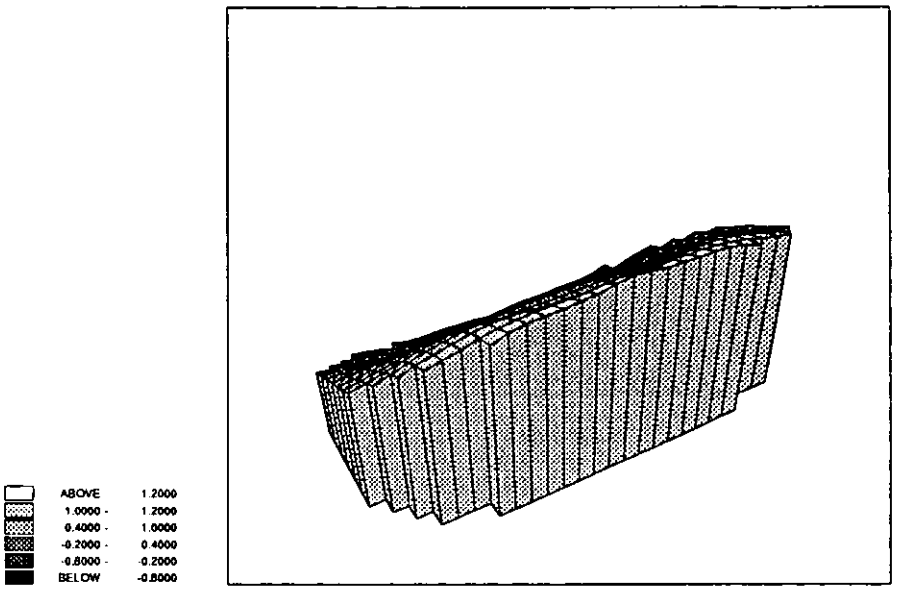

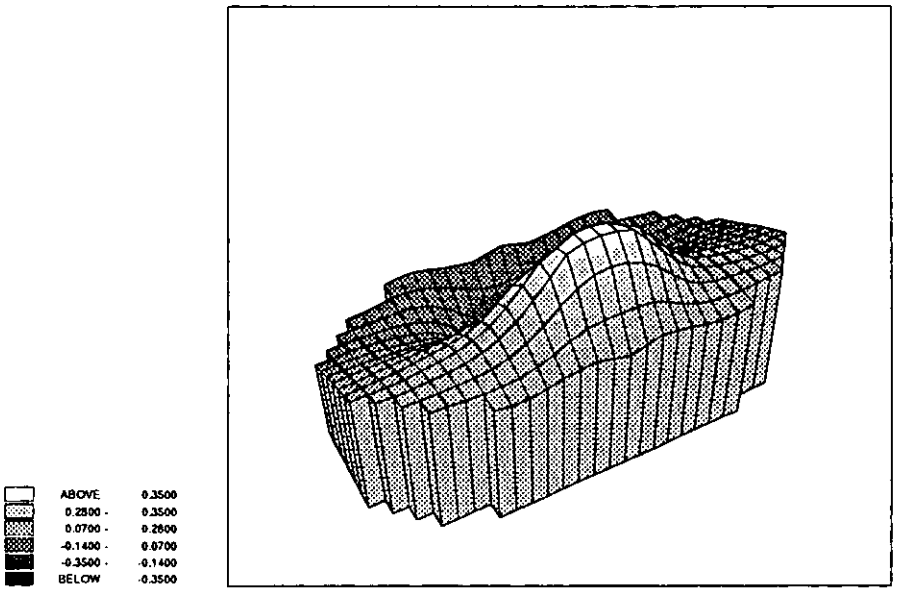

Figure 4.22(d) Mode shape for SAAB silencer. Mode 4, M=0.0, frequency=2000 Hz (upper plot:real part, lower plot:imaginary part)

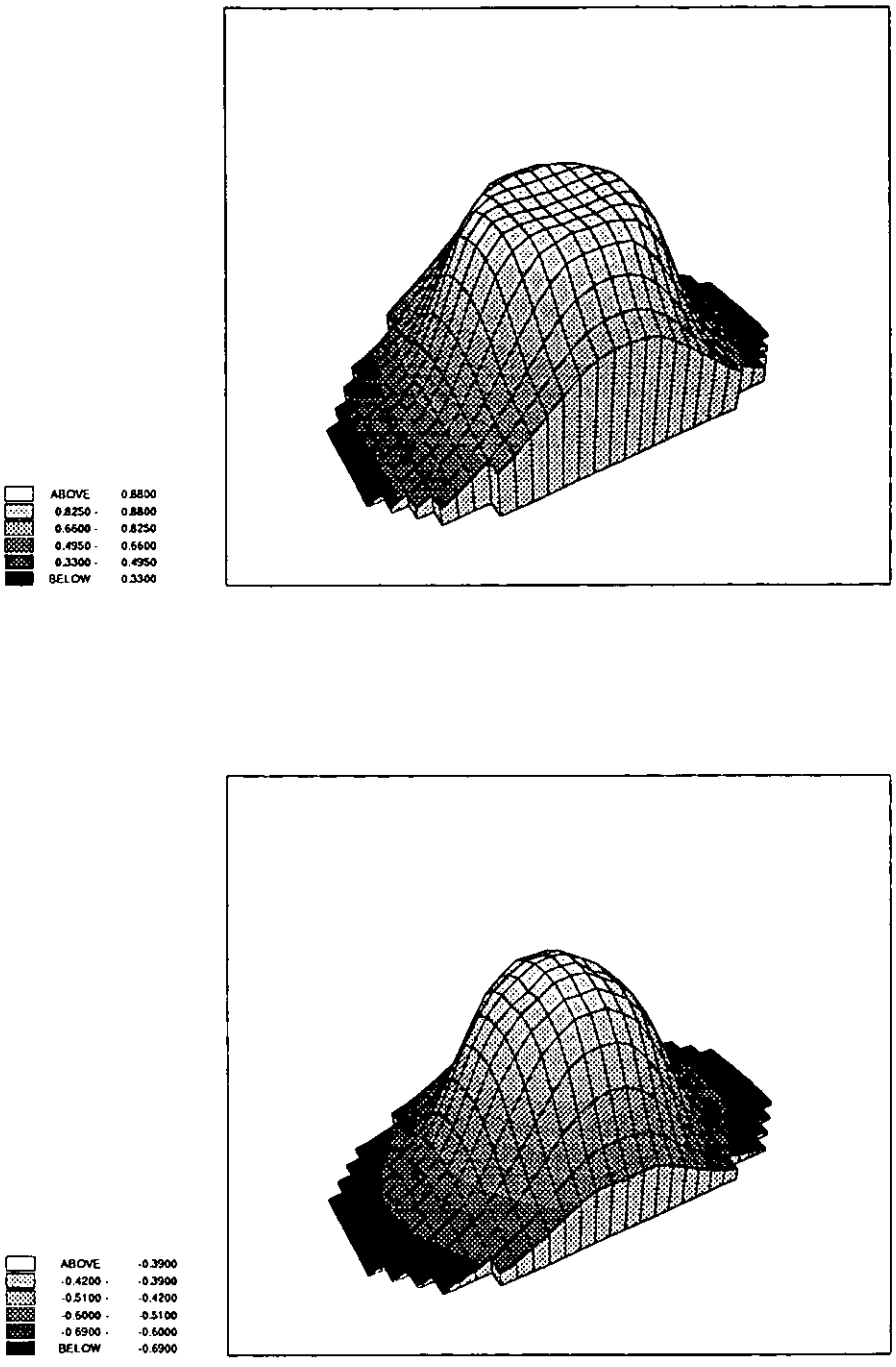

Figure 4.23(a) Mode shape for SAAB silencer. Mode 1, M=0.13, frequency=500 Hz (upper plot:real part, lower plot:imaginary part)

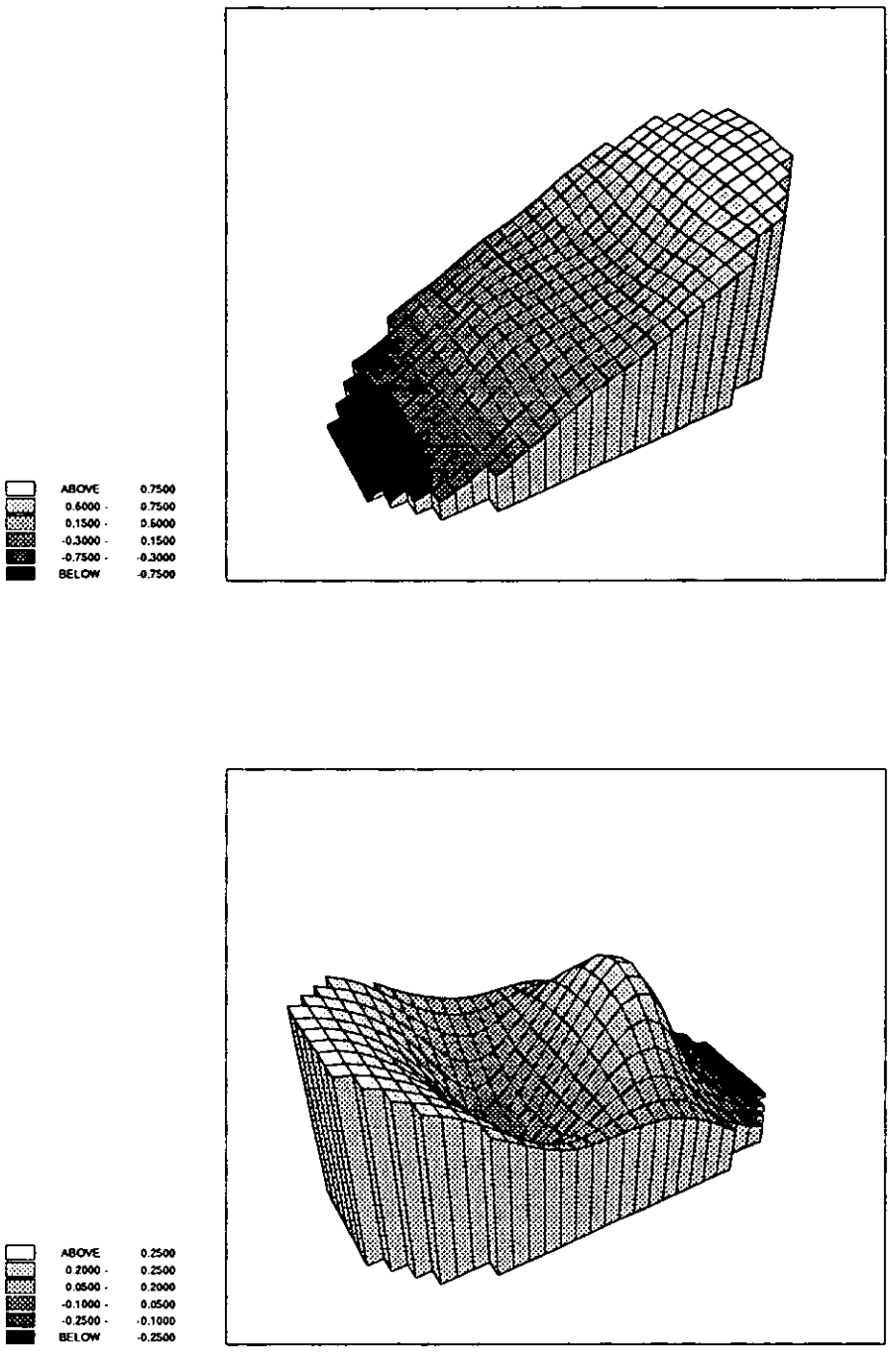

Figure 4.23(b) Mode shape for SAAB silencer. Mode 2, M=0.13, frequency=500 Hz (upper plot:real part, lower plot:imaginary part)

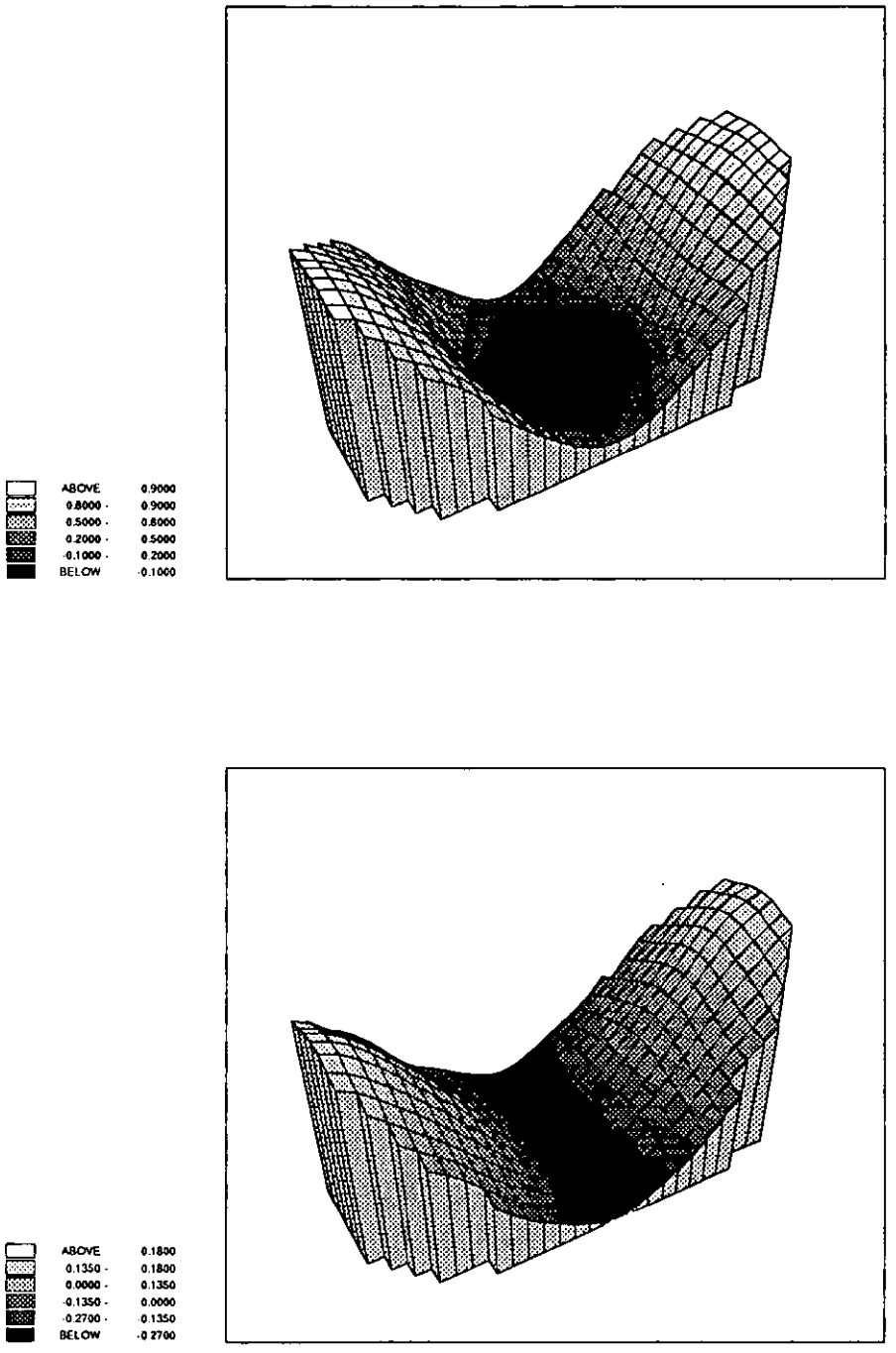

Figure 4.23(c) Mode shape for SAAB silencer. Mode 3, M=0.13, frequency=500 Hz (upper plot:real part, lower plot:imaginary part)

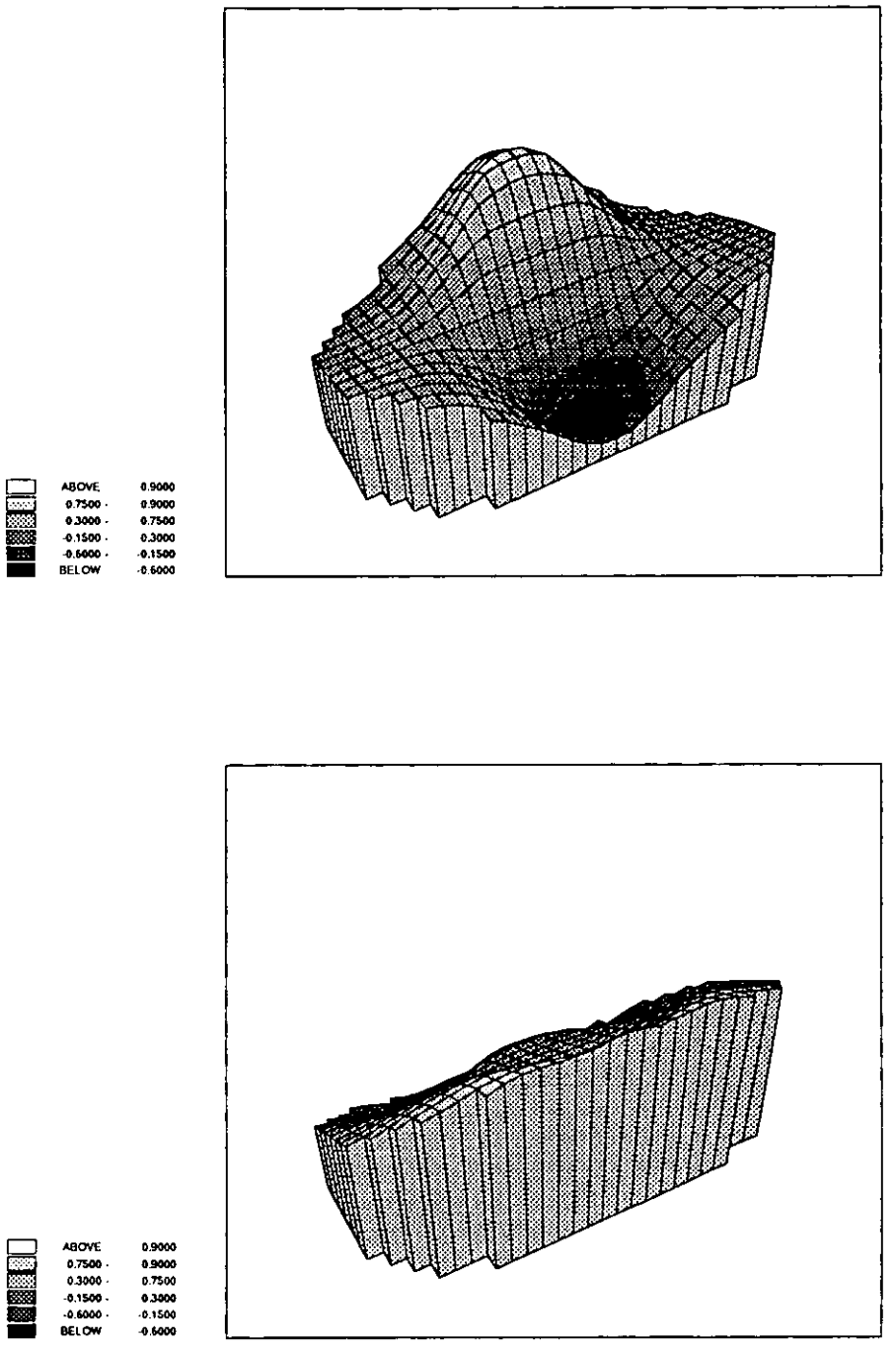

Figure 4.23(d) Mode shape for SAAB silencer. Mode 4, M=0.13, frequency=500 Hz (upper plot:real part, lower plot:imaginary part)

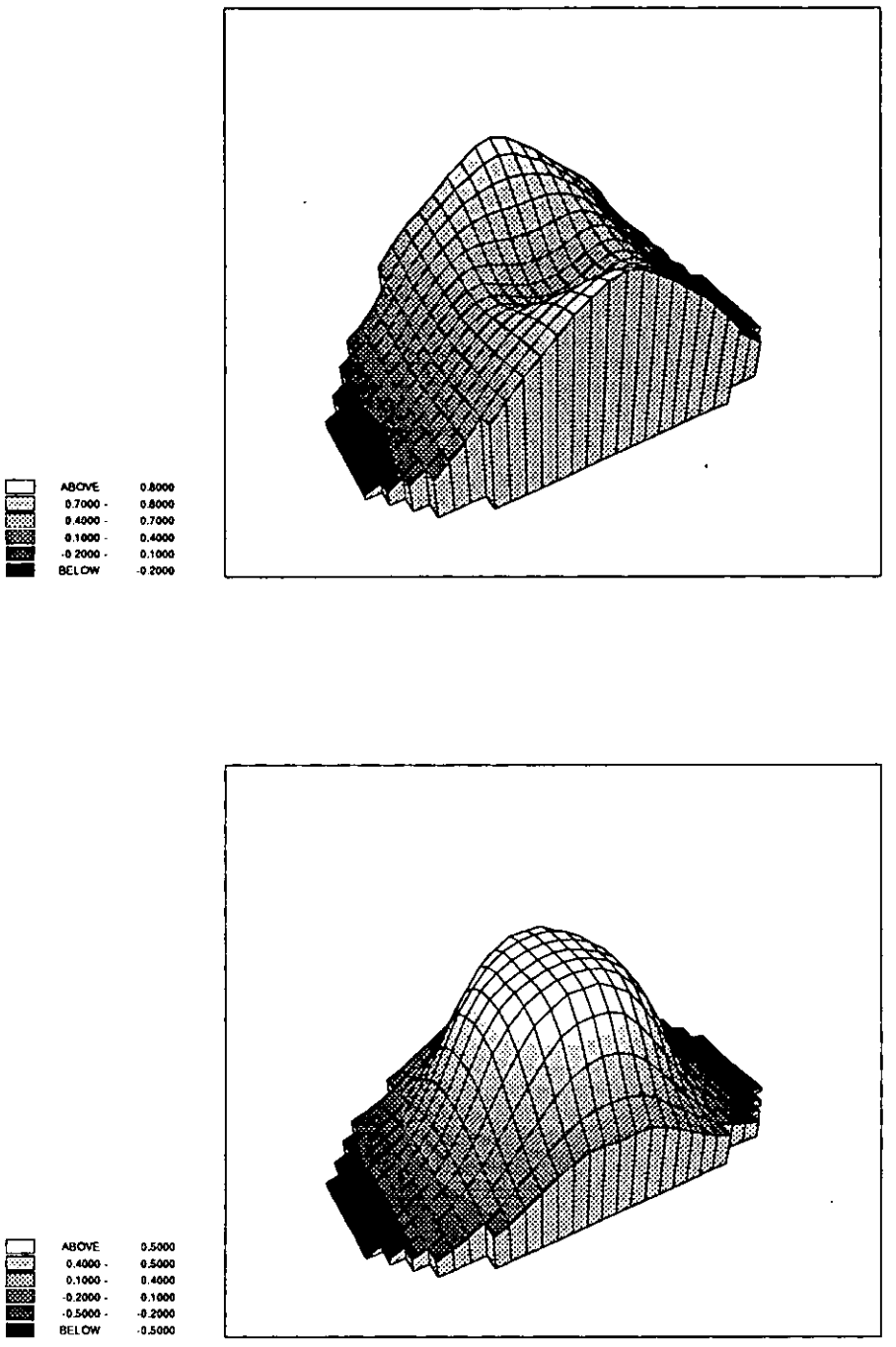

Figure 4.24(a) Mode shape for SAAB silencer. Mode 1, M=0.13, frequency=2000 Hz (upper plot:real part, lower plot:imaginary part)

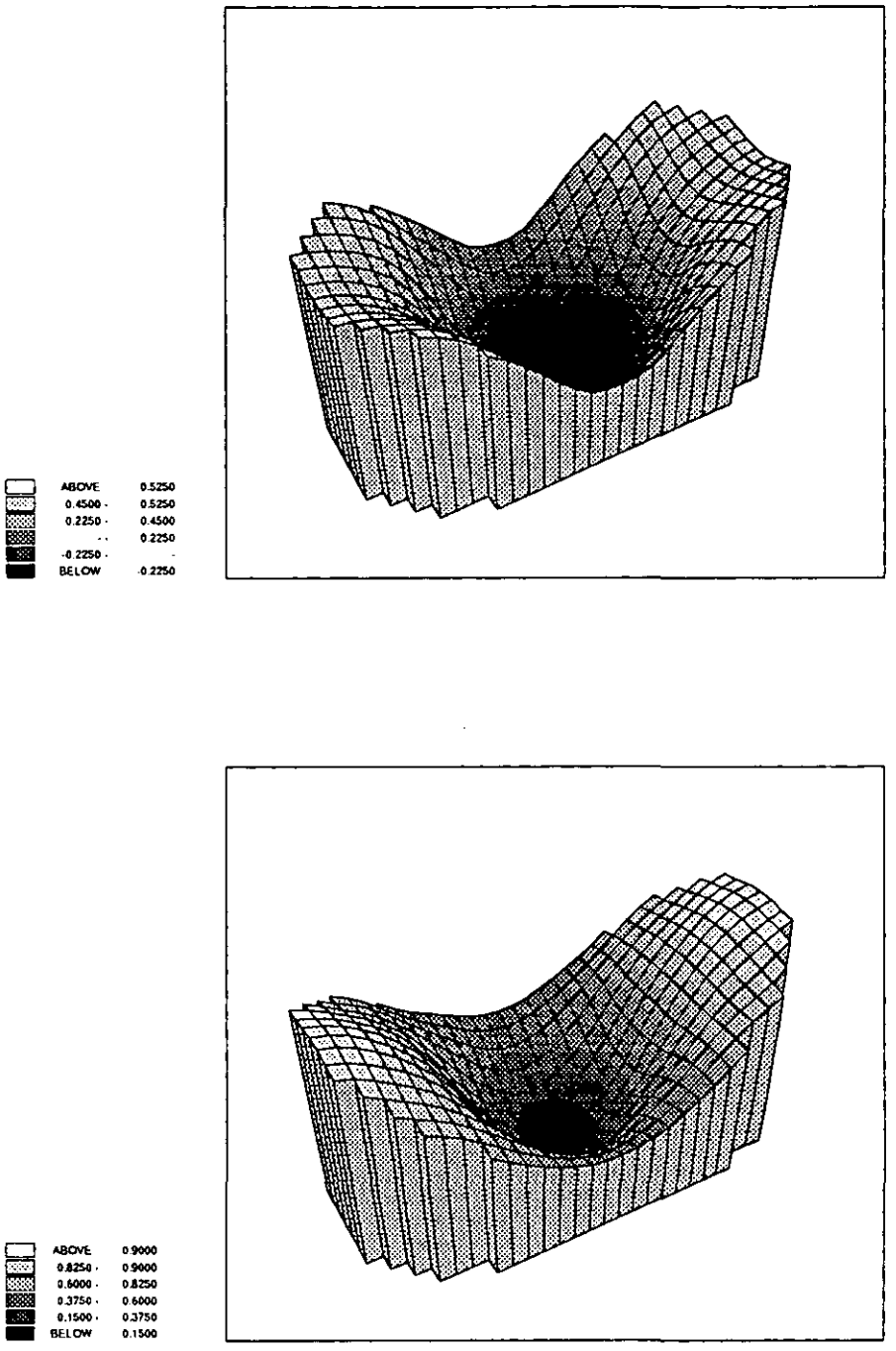

Figure 4.24(b) Mode shape for SAAB silencer. Mode 2, M=0.13, frequency=2000 Hz (upper plot:real part, lower plot:imaginary part)

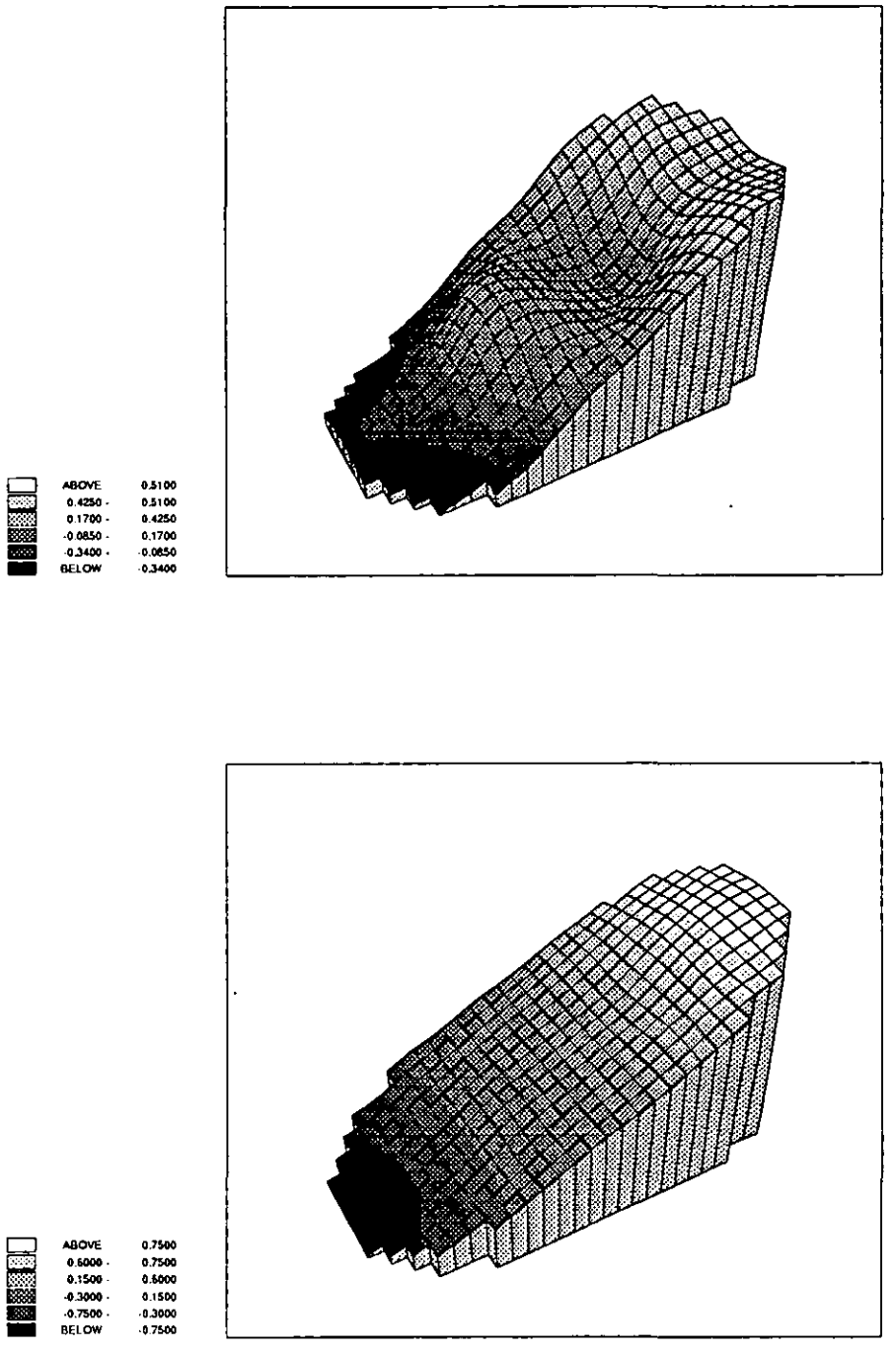

Figure 4.24(c) Mode shape for SAAB silencer. Mode 3, M=0.13, frequency=2000 Hz (upper plot:real part, lower plot:imaginary part)

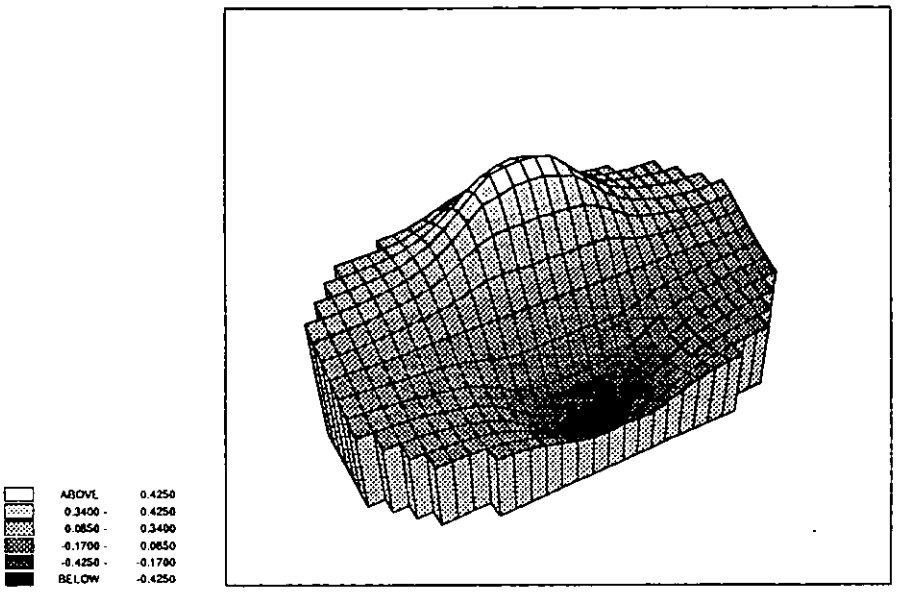

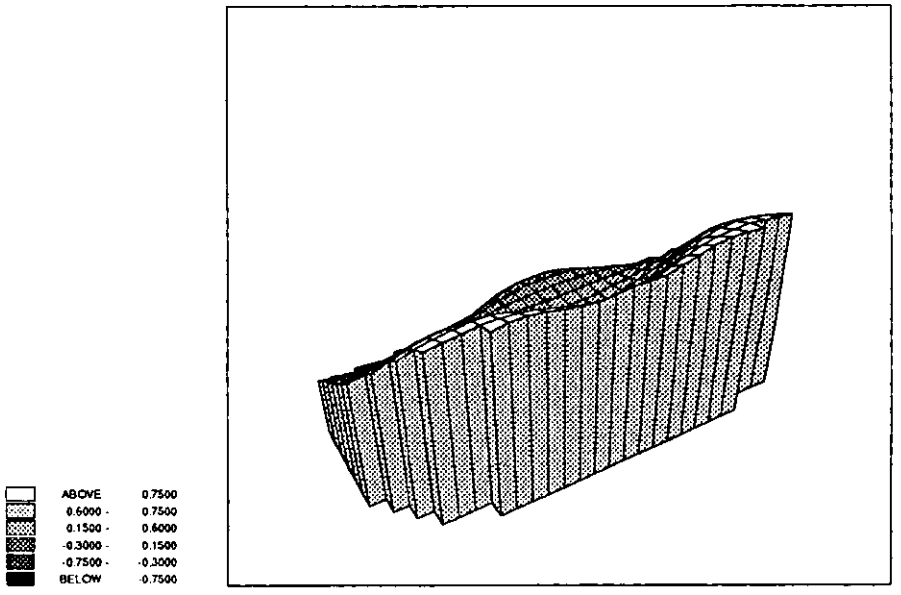

Figure 4.24(d) Mode shape for SAAB silencer. Mode 4, M=0.13, frequency=2000 Hz (upper plot:real part, lower plot:imaginary part)

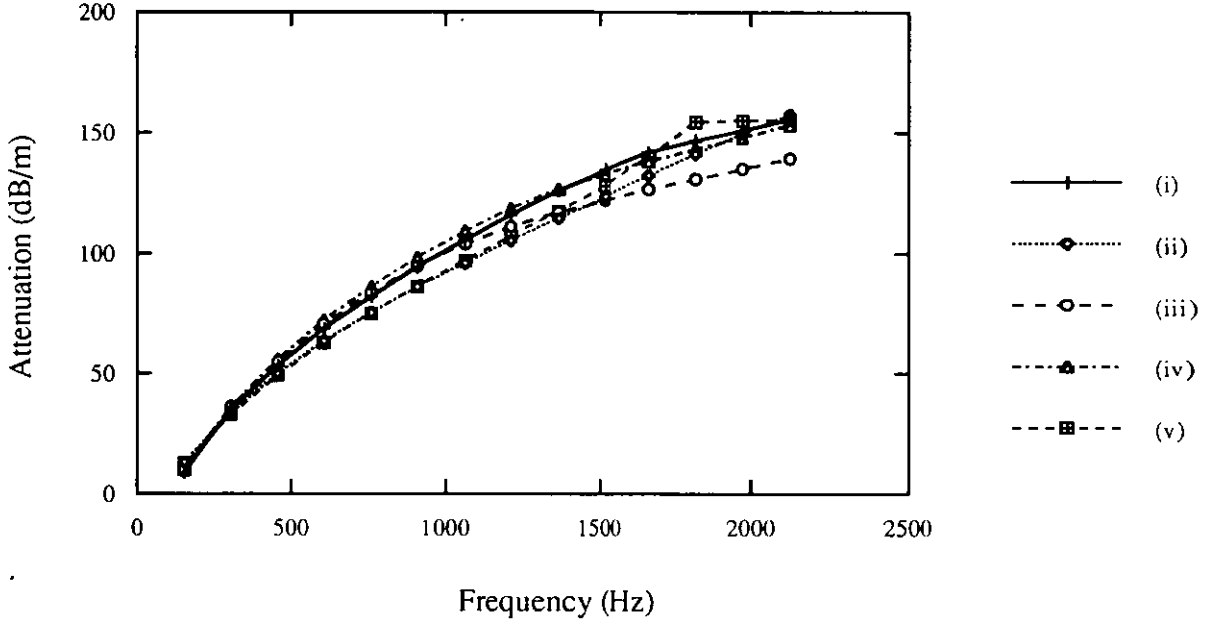

Figure 4.25(a) SAAB silencer, mean flow Mach number M=0.0
(i) No material variation.
(ii) Circumferential variation, highest density on the minor axis to lowest density on the major axis.
(iii) Circumferential variation in opposite sense.
(iv) Radial variation, highest density at outer radius to lowest density at inner radius.
(v) Radial variation in opposite sense.

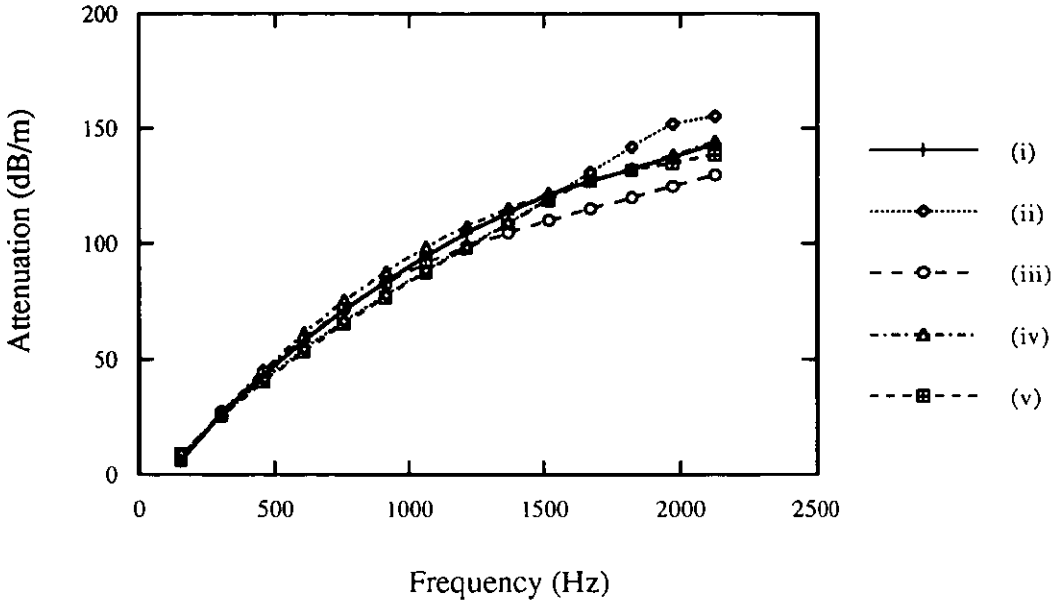

Figure 4.25(b) Material variation as in Figure 4.25(a).
Mean flow Mach number M=0.067 without induced flow in the absorbent.

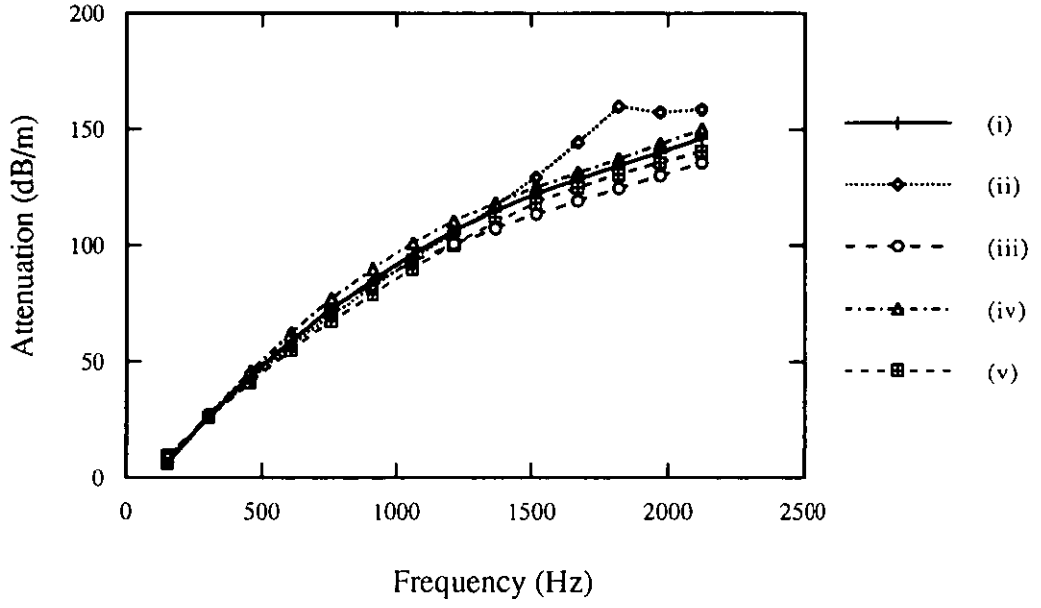

Figure 4.25(c) Material variation as in Figure 4.25(a).
Mean flow Mach number M=0.067 with induced flow in the absorbent.

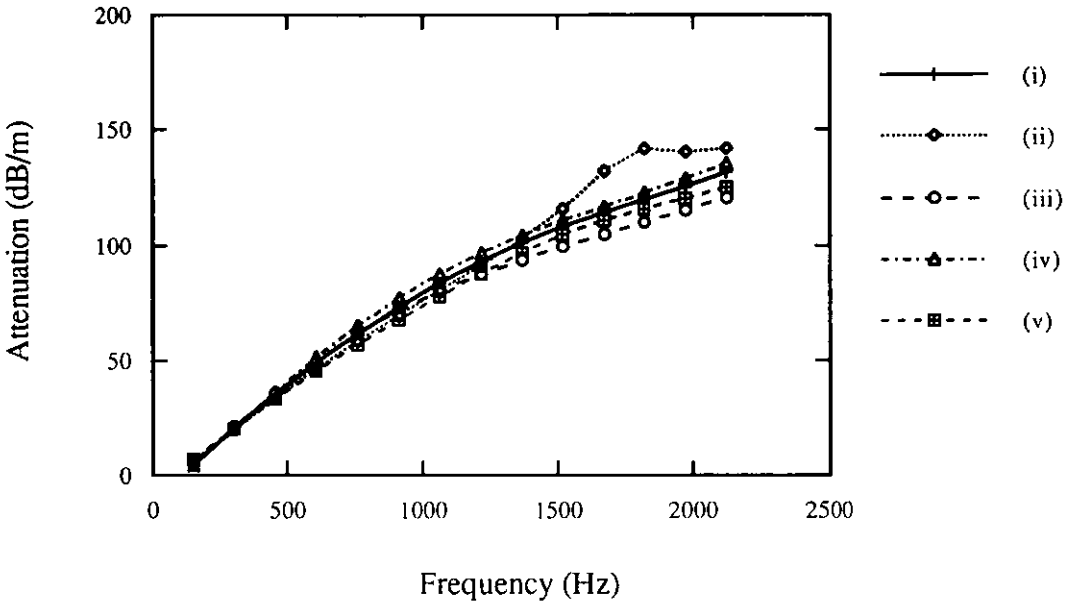

Figure 4.25(d) Material variation as in Figure 4.25(a).
Mean flow Mach number M=0.13 without induced flow in the absorbent.

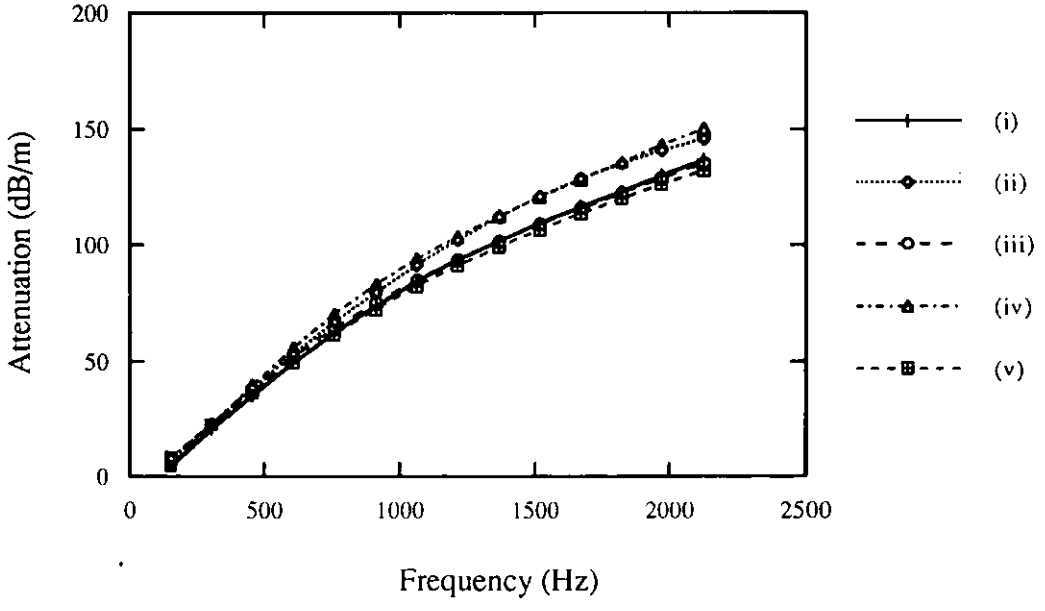

Figure 4.25(e) Material variation as in Figure 4.25(a).
Mean flow Mach number M=0.13 with induced flow in the absorbent.

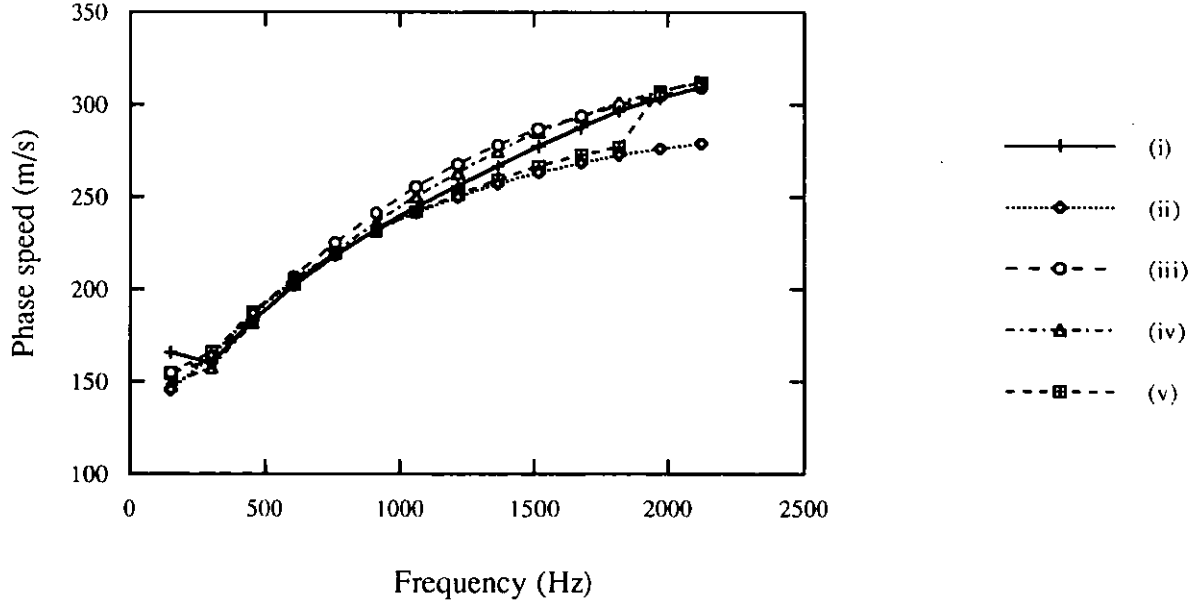

Figure 4.26(a) SAAB silencer, material variation as in Figure 4.25(a). Mean flow Mach number M=0.0.

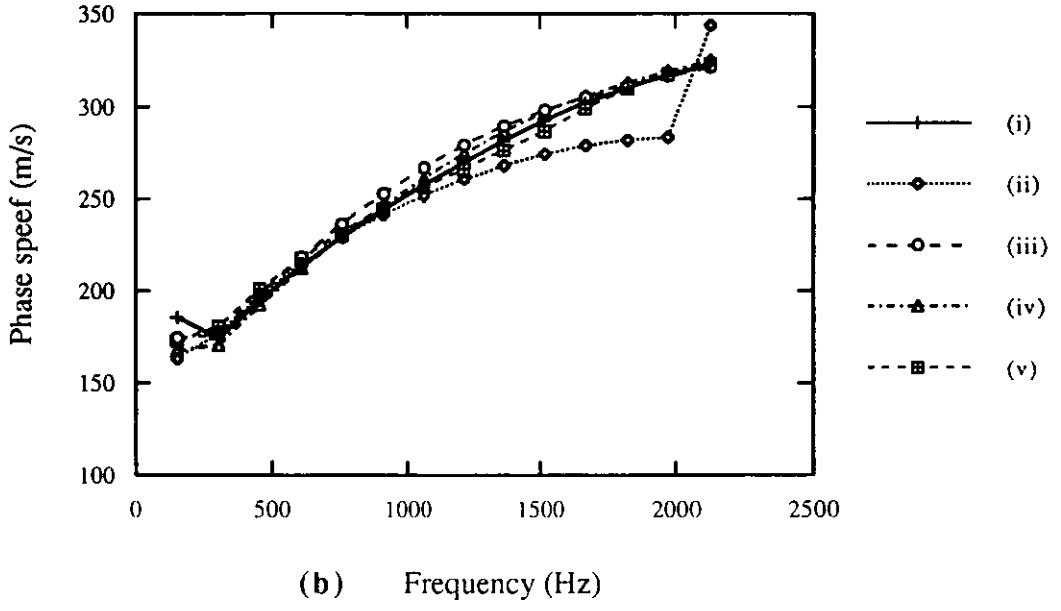

(b) Frequency (Hz)

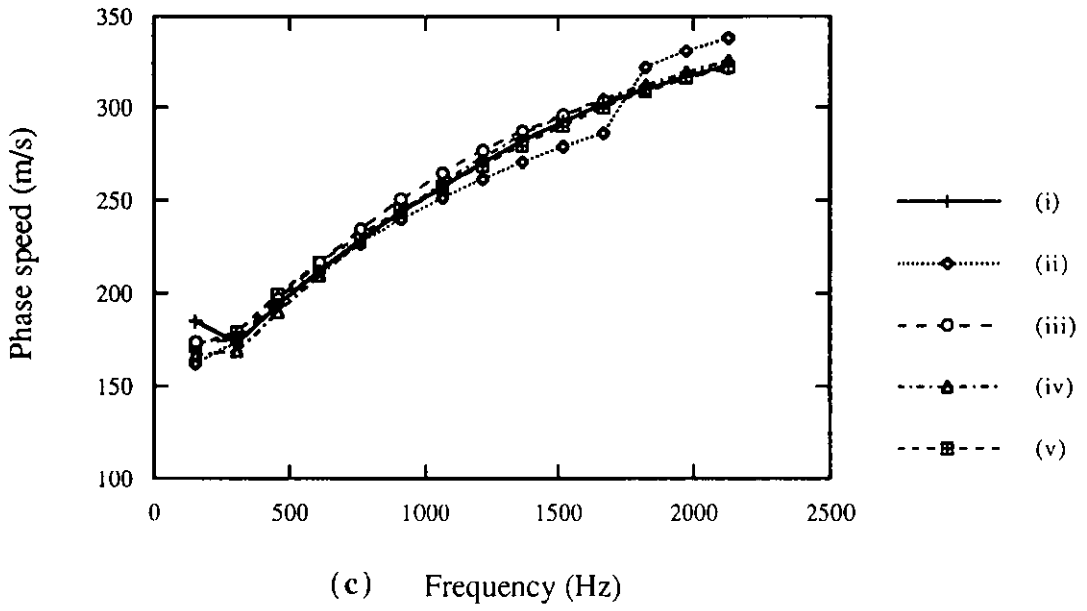

(c) Frequency (Hz)

Figure 4.26 SAAB silencer with material variation as in Figure 4.25.(a) Mean flow Mach number 0.067. **(b)** Without induced steady flow. **(c)** With induced steady flow.

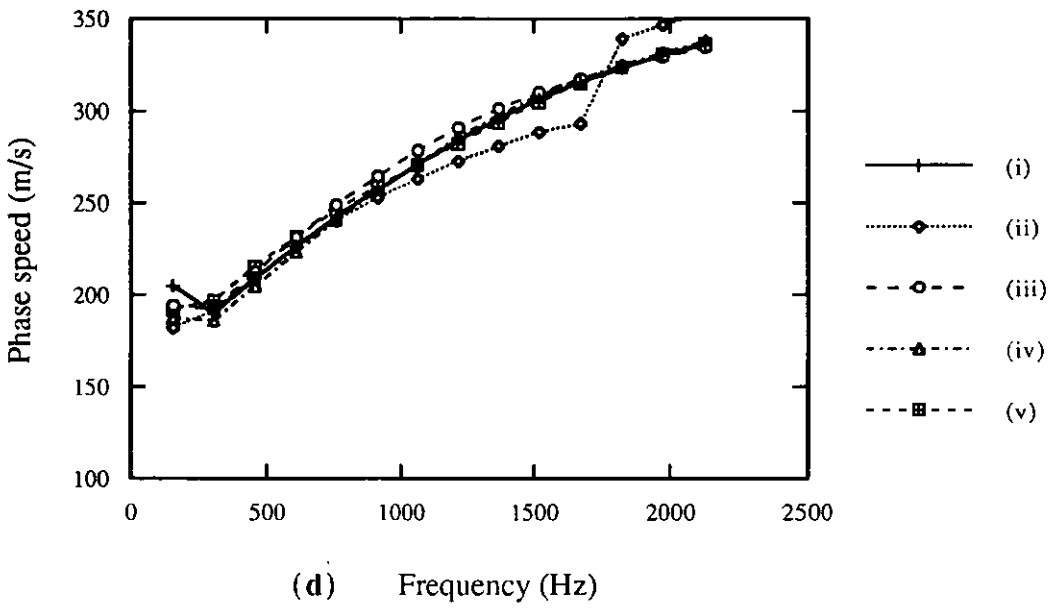

(d) Frequency (Hz)

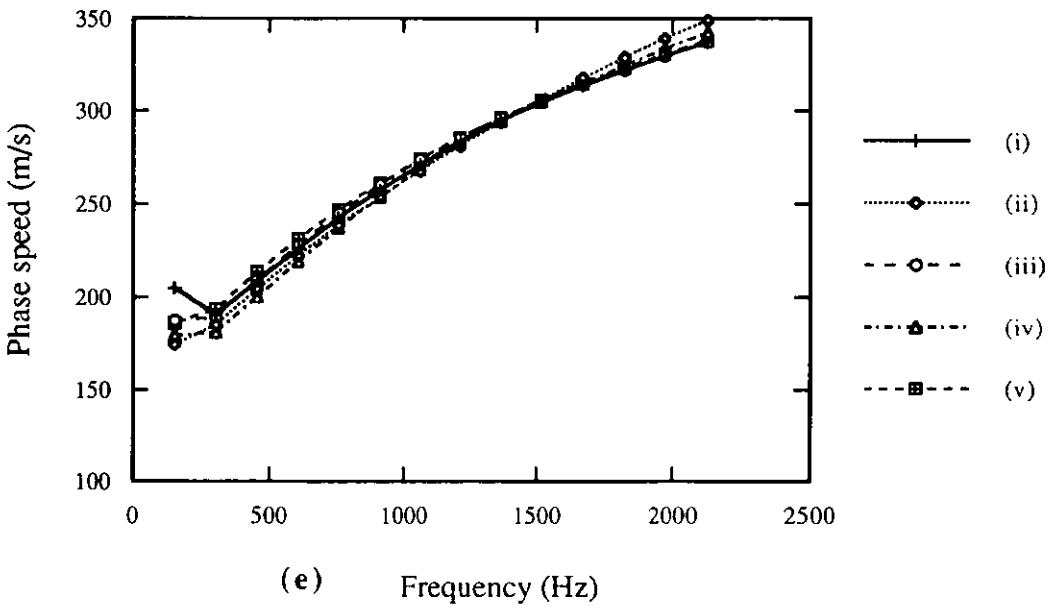

(e) Frequency (Hz)

Figure 4.26 SAAB silencer with material variation as in Figure 4.25.(a) Mean flow Mach number 0.13. **(d)** Without induced steady flow. **(e)**With induced steady flow.

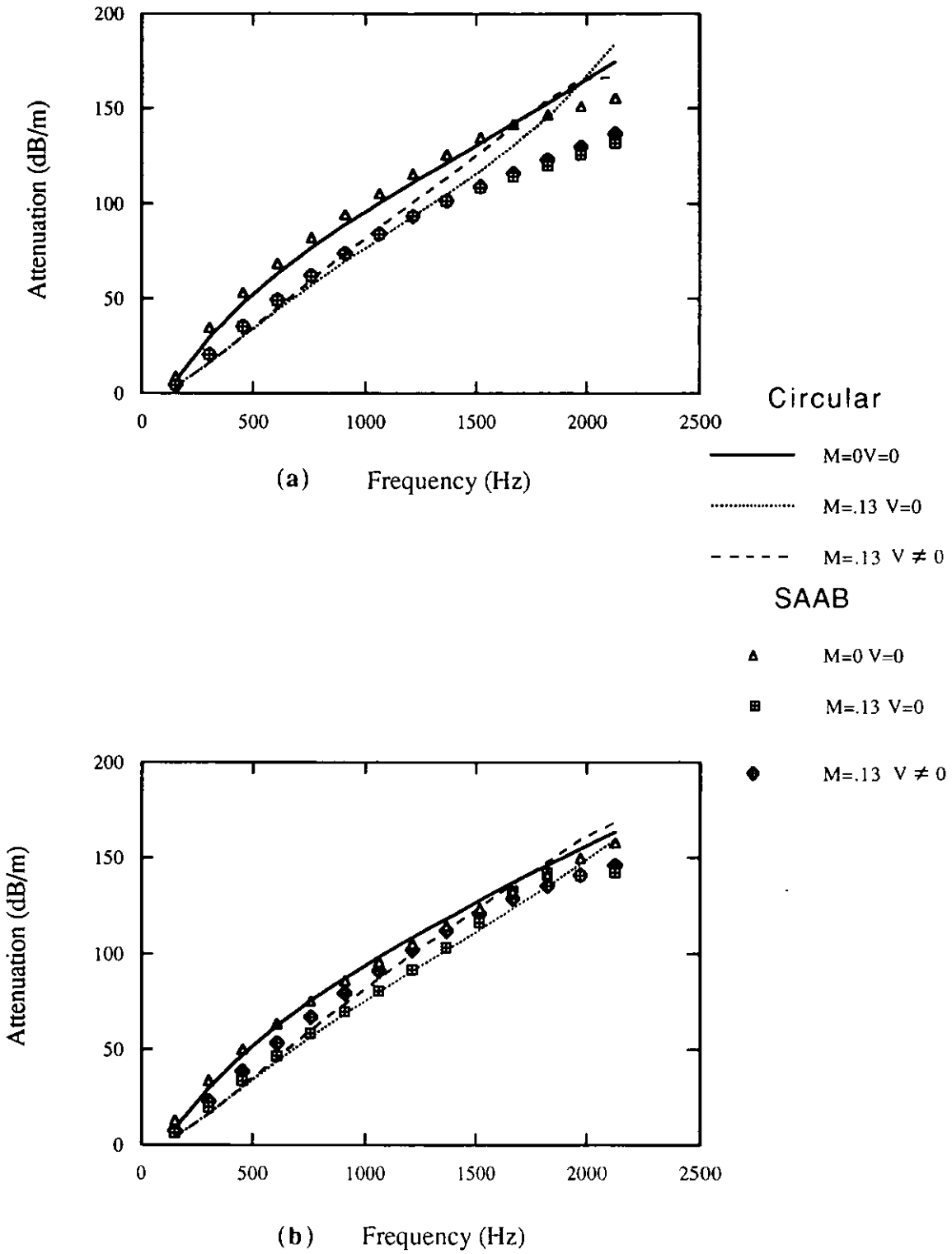

Figure 4.27 Comparison of attenuation rate between equal area circular and SAAB silencer. (**a**) No material variation. (**b**) Variation along circumferential direction from maximum density at minor axis to minimum at major axis.

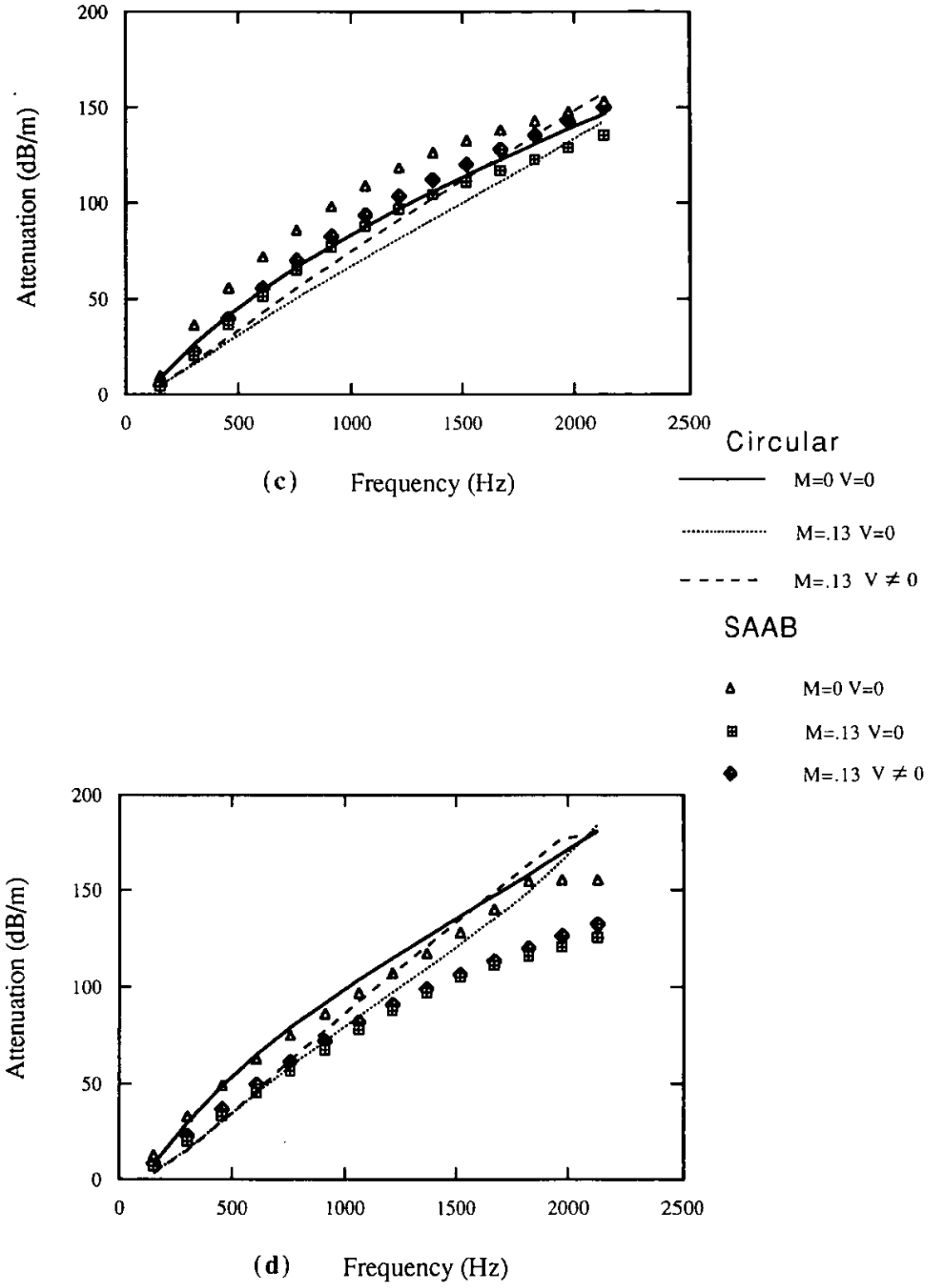

Figure 4.27 Comparison of attenuation rate between equal area circular and SAAB silencer. (**c**) Radial variation of material density from maximum densiy at the outer boundary to least dense at the inner boundary. (**d**) Opposite radial variation.

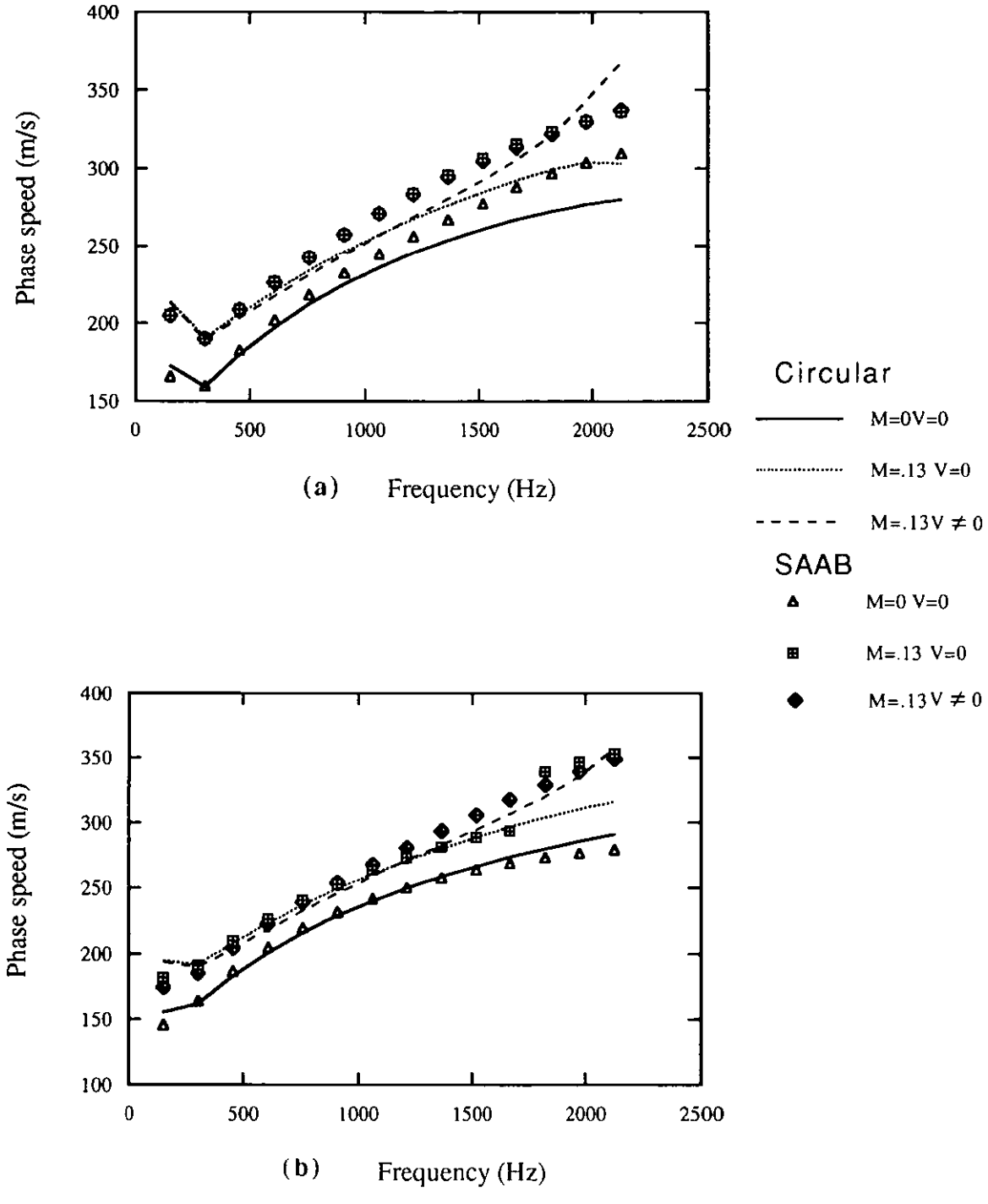

Figure 4.28 Comparison of phase speed between equal area circular and SAAB silencer. (a) No material variation. (b) Variation along circumferential direction from maximum density at minor axis to minimum at major axis.

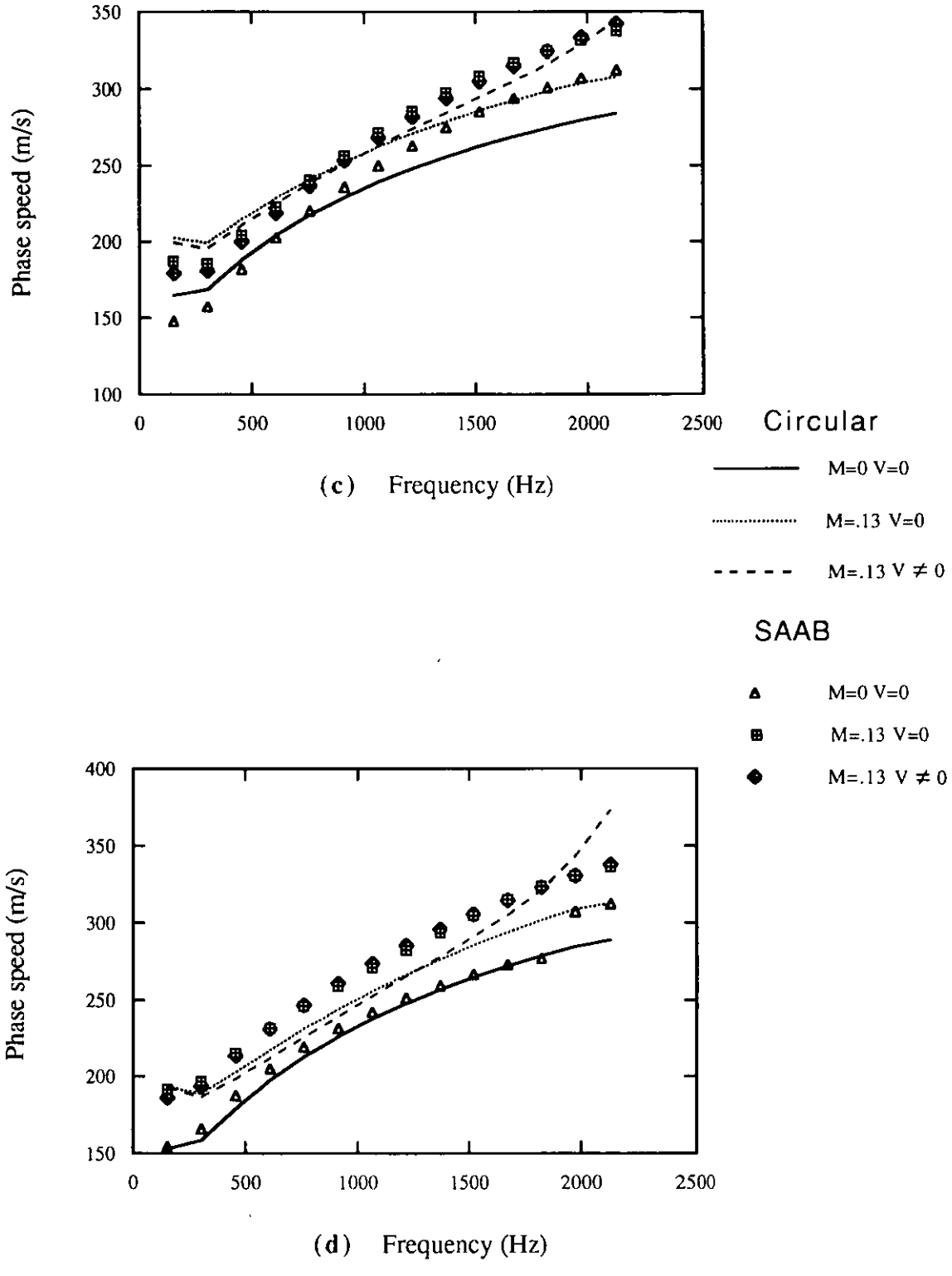

Figure 4.28 Comparison of phase speed between equal area circular and SAAB silencer. (**c**) Radial variation of material density from maximum density at the outer boundary to least dense at the inner boundary. (**d**) Opposite radial variation.

CHAPTER 5

CONVECTED ACOUSTIC WAVE MOTION IN FINITE LENGTH ABSORPTION SILENCER

5.1 Introduction

In this chapter a general finite element formulation for the analysis of the sound field in a finite length flow duct with a surrounding volume filled with porous or fibrous absorbent material is given. The detailed, nonlinear, steady flow field which is induced in the absorbent by the high speed mean flow in the central duct is evaluated. The induced steady flow field causes the acoustic field in the absorbent to be inhomogeneous, anisotropic and nonlinear, even if the material is isotropic and homogeneous. Material anisotropy and inhomogeneity are also included in the formulation, which is therefore applicable to the most complex of dissipative silencers. Rapidly convergent solution schemes for the nonlinear analyses are given and the merits of two different matching schemes between the acoustic fields of the flow duct and the absorption silencer are compared. Results are given which indicate the accuracy of the formulation and the necessity or otherwise to accurately model the induced steady flow field in the absorbent material.

Dissipative silencers within vehicle exhaust systems or heating and ventilation systems are characterised by a central flow duct region, which conveys a pulsating gas flow of

high mean speed, surrounded by an absorptive region which is packed with porous or fibrous material. The flow duct is generally of uniform cross-section, being a direct continuation of the exhaust pipe or ventilation duct prior to the dissipative silencer section. In contrast the absorptive region may have a very complex shape, particularly so for 'clam' type exhaust silencers. The method of manufacture of dissipative silencers can cause significant variation in the packing density of the porous or fibrous material, which in turn causes significant inhomogeneity of the acoustic properties throughout the dissipative unit. This is particularly true for silencer units which are packed with absorptive material prior to having their cases pressed into their final form. In addition, the absorptive material may have significant acoustic anisotropy. This effect would be most noticeable for a dissipative silencer packed with fibrous material and manufactured in a manner which causes the fibres to be aligned in a particular direction, such as when glass wool is 'spun' into a dissipative unit. Cummings and Chang [17] have shown that the mean gas flow in the open pipe region induces a steady flow field within the absorbent which, though small in magnitude, has a significant effect upon the acoustic performance of the silencer. One effect of the steady flow in the absorbent is to cause acoustic anisotropy and inhomogeneity, even if the dissipative material itself is isotropic and homogeneous.

Thus, in order to analyse the acoustic effectiveness of dissipative silencers of the types currently being manufactured, it is necessary for the analysis to include all of the above effects. Furthermore such an analysis scheme could be used not just to predict the acoustic effectiveness of a given design of silencer, but to explore the potential benefits or otherwise of varying the packing density of the absorptive material, or structuring the 'lay' of fibrous material, or designing the shape of the silencer volume with respect to the form of the induced flow field. The requirement to couple together the acoustic fields of a flow duct region and a dissipative region of arbitrary shape, and within the

latter to model material and flow-induced inhomogeneity and anisotropy, leads inevitably to the use of numerical analysis. In particular finite element analysis is ideally suited to the problem.

The present chapter extends previous finite element formulations for finite length silencers to include the effects of mean flow within both the central flow duct and the surrounding absorptive material. Cummings and Chang [17] included these effects in their modal solution of the problem, but they had to assume that the induced steady flow within the absorbent was uniform and axial. Furthermore their method of solution is only applicable to silencers of uniform and simple cross-sectional geometry whose absorbent material is homogeneous. The present analysis begins with a finite element formulation for the nonlinear analysis of the three-dimensional, induced steady flow field within the absorbent. The acoustic properties of the absorbent material are shown to be dependent upon the steady and acoustic flow velocities, in this general case, and thus the analysis of the acoustic field within the absorbent is also found to be nonlinear. Finite element formulations of the acoustic fields within the flow duct and the absorbent region are given, together with two possible methods of coupling together these formulations at their common boundary. The relative merits of these two techniques are compared. Iterative schemes with rapid convergence properties are given for the nonlinear solutions of both the steady flow and acoustic fields within the absorbent. The finite element formulations are for the most general case of arbitrary three-dimensional geometry and non-homogeneous, anisotropic absorbent material. Results are given for axisymmetric absorption silencers packed with homogeneous, isotropic material, to enable comparison with the experimental and modal analysis results of Cummings and Chang [17], and to investigate the practical importance of detailed modelling of the induced steady flow field within the absorbent. Modelling of flow-induced acoustic inhomogeneity and anisotropy is included in these results.

Comparisons are made between the results of the full nonlinear modelling scheme and a simplified analysis in which nonlinear effects in both the steady flow and acoustic equations are ignored. Preliminary results of this type have been presented earlier [90].

5.2 Analysis

5.2.1 Geometry and governing equations

The analysis considers convected acoustic wave motion through a duct and a surrounding silencer volume which is packed with porous material, see Figure 5.1. The duct, region R_1, is taken to be of arbitrary but constant cross-section and to have its axis in the x_1-direction of an orthogonal coordinate system $\mathbf{x} \equiv (x_1,\ x_2,\ x_3)$. The steady convective flow is assumed to have uniform axial velocity U within the duct and to be of low Mach number M, such that the steady flow may be regarded as incompressible. The absorption silencer, region R_2, is a volume of arbitrary shape which is packed with porous material which may be inhomogeneous and anisotropic. The axial pressure gradient of the steady flow in the duct induces a steady flow field within the porous material of region R_2 which can have significant acoustic effect [17,18]. The magnitude of the velocities of the induced flow are very small, typically $\mathrm{O}[10^{-3}U]$, such that the cross-flow between regions R_1 and R_2 does not seriously compromise the assumption of uniform flow in region R_1.

The outer walls of regions R_1 and R_2 are assumed to be rigid and impervious, hence of infinite impedance, and are denoted by Γ_{W1} and Γ_{W2} respectively, or collectively by $\Gamma_W (= \Gamma_{W1} + \Gamma_{W2})$. The duct is taken to extend sufficiently far upstream and downstream of the silencer volume such that plane-wave conditions may be implemented on the inflow and outflow boundaries of region R_1, which are denoted by Γ_I and Γ_O respectively. The frequency of analysis is thus restricted to be below the

cut-on frequency of higher-order modes in the central duct. Regions R_1 and R_2 share a common boundary Γ_c within the silencer volume. In many practical situations a perforated screen separates these two regions, the purposes of which are to keep the porous material in place and to guide the mean flow, in order to keep the back-pressure to a minimum. Generally the porosity of such a screen is so large that its acoustic effect is negligible and its effect is ignored in the following analysis.

5.2.2 Acoustic equations in the airway

For uniform steady flow in the airway, the linearised acoustic wave and momentum equations (3.30) and (3.29) become

$$\nabla^2 p_1' = \frac{1}{\bar{c}^2}\left\{\frac{\partial}{\partial t} + U\frac{\partial}{\partial x_1}\right\}^2 p_1' \tag{5 1}$$

and

$$\rho_0\left\{\frac{\partial}{\partial t} + U\frac{\partial}{\partial x_1}\right\}\phi_1' = -p_1' \tag{5.2}$$

where ρ_0 is the density, p_1' is the acoustic pressure and ϕ_1' is the acoustic velocity potential, such that

$$\boldsymbol{q}_1' = \nabla\phi_1' \tag{5.3}$$

where $\boldsymbol{q}_1'$ is the velocity. For harmonic time variation $e^{i\omega t}$ the equations (5.1) and (5.2) become

$$\nabla^2 p_1' + \left(k - iM\frac{\partial}{\partial x_1}\right)^2 p_1' = 0 \tag{5.4}$$

and

$$\rho_o\left(\mathrm{i}\omega + U\frac{\partial}{\partial x_1}\right)q_1' = -\nabla p_1', \tag{5.5}$$

where $k = \omega / \bar{c}$ is the wavenumber.

5.2.3 Steady flow equations in the absorbent region

The steady flow through the anisotropic porous material in region R_2 is governed by the Ergun or Forchheimer equation (3.42)

$$\nabla\, \bar{p}_2 = -[\bar{\Sigma}]\bar{q}_2 \tag{5.6}$$

where $[\bar{\Sigma}]$ is a diagonal matrix whose jth element is $\left(\sigma_{vj} + \sigma_{ij} \mid \bar{q}_2 \mid\right)$ and σ_{vj}, σ_{ij} are the viscous and inertial flow resistive coefficients respectively, in direction x_j. The continuity equation (3.41)

$$\nabla\cdot\bar{q}_2 = 0 \tag{5.7}$$

together with equation (5.6) implies (equation (3.53))

$$\nabla\cdot[\bar{\Sigma}]^{-1}\nabla\, \bar{p}_2 = 0. \tag{5.8}$$

Since the elements of $[\bar{\Sigma}]$ are dependent upon $\mid \bar{q}_2 \mid$, equations (5.6) and (5.8) must be solved iteratively. A rapidly convergent technique has been found to be as follows:

(i) assume $\mid \bar{q}_2 \mid = 0$ and evaluate $[\bar{\Sigma}]$

(ii) evaluate $\bar{p}_2$ from equation (5.8)

(iii) evaluate $\bar{q}_2$ from equation (5.6), using $[\bar{\Sigma}]$ from (i)

(iv) update $\mid \bar{q}_2 \mid$ and re-evaluate $[\bar{\Sigma}]$

(v) re-evaluate $\bar{q}_2$ from equation (5.6) and repeat step (iv)

(vi) repeat from step (ii)

Step (ii) demands the implementation of boundary conditions, as follows. The normal component of velocity and hence pressure gradient is zero on the hard-wall boundary of region R_2, namely Γ_{w_2}. The axial steady flow pressure gradient $\partial\bar{p}_2 / \partial x_1$ on the common boundary Γ_c is the same as the axial pressure gradient throughout region R_1, $\partial\bar{p}_1 / \partial x_1$, and is assumed to be known from experiment.

The iterative procedure can be simplified for isotropic absorbent material, since in this case equation (5.6) can be used to form a quadratic equation in $|\bar{q}_2|$ with solution

$$|\bar{q}_2| = \left[-\sigma_v + \left(\sigma_v^2 + 4\sigma_i \, |\nabla \bar{p}_2|\right)^{1/2}\right] / 2\sigma_i . \tag{5.9}$$

The preferred iterative technique is then as follows:

(i) assume $|\bar{q}_2| = 0$ and evaluate $[\bar{\Sigma}]$

(ii) evaluate $\bar{p}_2$ from equation (5.8)

(iii) evaluate $\bar{q}_2$ from equation (5.9)

(iv) update $|\bar{q}_2|$ and re-evaluate $[\bar{\Sigma}]$

(v) repeat from step (ii)

5.2.4 Acoustic equations in the absorbent region

For harmonic time variation $e^{i\omega t}$ the linearised wave and momentum equations (3.62) and (3.61) in the absorbent region are (assuming that the convective fluid acceleration is negligible [18])

$$\rho_0 \omega^2 \Omega \chi \, p_2' + \nabla \cdot [R] \nabla p_2' = 0 \tag{5.10}$$

and

$$i\omega\rho_0 q_2' = -[R]\nabla p_2' \tag{5.11}$$

where Ω is the volume porosity, χ is the compressibility and $[R]$ is a diagonal matrix whose jth element is ρ_0 / ρ_{aj}. ρ_{aj} is the effective, complex, mean fluid density in the pores of the material for motion in direction j, equation (3.58), namely

$$\rho_{aj} = \left(\rho_0 m_j / \Omega\right)\left(1 - i\Omega\sigma_{aj}' / \omega\rho_0 m_j\right), \tag{5.12}$$

where m_j is the structure factor and σ_{aj}' is the flow resistivity.

The flow resistivity and hence effective density are dependent upon the steady flow through the porous material. The flow resistivity can be written as equation (3.47)

$$\sigma_{aj}' = \sigma_{0j} + \sigma_{ij}\left[\left|\bar{q}_2\right| + (\bar{q}_2 . q_2')\bar{q}_{2_j} / \ q_{2_j}'\left|\bar{q}_2\right|\right], \tag{5.13}$$

where $\sigma_{0j}(\omega)$ is the complex acoustic flow resistivity in direction j and, as $\omega \to 0$, $\sigma_{0j}(\omega) \to \sigma_{vj}$. If the steady flow in the absorbent is uni-directional in direction l, then equation (5.13) simplifies considerably (see equation 3.69) to

$$\sigma_{al}' = \sigma_{0l} + 2\sigma_{il}\left|\bar{q}_2\right| \ , \quad \sigma_{aj}' = \sigma_{0j} + \sigma_{ij}\left|\bar{q}_2\right| \ , \quad j \neq l. \tag{5.14}$$

In this situation, the acoustic properties are known *a priori* and the acoustic problem is then linear. In the more general case it is seen, from equation (5.13), that the acoustic properties depend upon the acoustic velocity field in addition to the steady flow velocity field and hence the acoustic problem is non-linear. A rapidly convergent iterative scheme for this problem is as follows:

(i) Assume $q_2' = 0$ in equation (5.13) and find all acoustic properties.

(ii) Evaluate the acoustic pressure field from equations (5.4) and (5.10), together with boundary conditions.

(iii) Find q_2' from equation (5.11).

(iv) Re-evaluate the σ_{aj}' from equation (5.13) and hence all acoustic properties.

(v) Re-evaluate q_2' from equation (5.11) with the new acoustic properties.

(vi) Repeat step (iv)

(vii) Repeat from step (ii).

Delany and Bazley [57] formulae are used to define the zero flow acoustic properties of the porous materials. From equations (3.58) and (3.70-71), the general properties are given by

$$\rho_{aj} / \rho_0 = z_j \gamma_j, \quad c_0^2 \Omega \chi \rho_{aj} = \gamma_j^2, \tag{5.15, 5.16},$$

$$z_j^2 - z_{0j}^2 = (-\mathrm{i} z_{oj} / \rho_0 \omega \gamma_{oj})(\sigma_{aj}' - \sigma_{oj}), \tag{5.17}$$

and

$$\gamma_j^2 - \gamma_{0j}^2 = (-\mathrm{i} \gamma_{oj} / \rho_0 \omega z_{oj})(\sigma_{aj}' - \sigma_{oj}), \tag{5.18}$$

where the expression for $(\sigma_{aj}' - \sigma_{0j})$ follows from equation (5.13).

5.2.4 Boundary conditions

The component of acoustic velocity normal to the hard walls of boundary Γ_w is zero, which in turn implies from equations (5.5) and (5.11) that

$$\nabla p' \cdot \boldsymbol{n} = 0 \quad \text{on} \quad \Gamma_w \tag{5.19}$$

for both regions R_1 and R_2, where $\boldsymbol{n}$ is a unit normal vector to the boundary. On the common boundary Γ_c, there is continuity of pressure and the normal component of displacement, thus

$$p_1' = p_2' \quad \text{and} \quad \underline{\xi}_1' \cdot \boldsymbol{n}_c = \underline{\xi}_2' \cdot \boldsymbol{n}_c \text{ on } \Gamma_c \tag{5.20, 5.21}$$

where $\underline{\xi}'$ is the particle displacement vector and $\boldsymbol{n}_c$ is a unit normal vector to Γ_c. Since convective acceleration terms are negligible in region R_2

$$\mathrm{D}\underline{\xi}_1' / \mathrm{D}t = \boldsymbol{q}_1' \quad \text{and} \quad \partial \underline{\xi}_2' / \partial t = \boldsymbol{q}_2'. \tag{5.22a,b}$$

Assuming harmonic time variation $e^{i\omega t}$, use of the momentum equations (5.5) and (5.11) together with equations (5.22) enables one to re-write the continuity of displacement boundary condition (5.21) in terms of normal pressure gradients,

$$[1 - \mathrm{i}M / k\,\partial / \partial x_1]^2 [R] \nabla p_2' \cdot \boldsymbol{n}_c = \nabla p_1' \cdot \boldsymbol{n}_c. \tag{5.23}$$

It is assumed that sufficient length of inlet and outlet duct is modelled such that plane-wave conditions apply on the inlet and outlet flow boundaries Γ_I and Γ_O of region R_1. In particular, the four-pole parameters and hence transmission loss of the overall system can be evaluated from two separate solutions of the entire problem with different inflow and outflow boundary conditions, namely [32]

$$\partial p_1' / \partial x_1 = \text{constant on } \Gamma_I \quad , \quad p_1' = 0 \text{ on } \Gamma_O \tag{5.24a,b}$$

and

$$p_1' = \text{constant on} \quad \Gamma_I \quad , \quad \boldsymbol{q}_1' = 0 \;\Rightarrow\; \partial p_1' / \partial x_1 = \mathrm{i}kMp_1' \quad \text{on} \quad \Gamma_O \tag{5.25a,b}$$

5.3 Finite Element Formulation

The first task is to determine the pressure and hence velocity field of the steady flow in the absorbent, region R_2. The steady flow velocity field is required in order to determine the acoustic properties of the absorbent material, for use in the coupled acoustic analysis of regions R_1 and R_2. The weak Galerkin method of formulation is used throughout.

5.3.1 Steady flow in the porous material

Let $\psi_J(x_1, x_2, x_3)$ be a global basis function associated with node J of a finite element mesh. The basis functions are chosen to be the element-based shape function over any element containing node J and to be zero everywhere else, such that for a mesh of N_2 nodes, the approximation to the steady flow pressure $\bar{p}_2$ is of the form of the trial solution

$$\bar{p}_2 = \sum_{J=1}^{N_2} \psi_J \bar{p}_{2J} \tag{5.26}$$

where $\bar{p}_{2J}$ is the value of $\bar{p}_2$ at the Jth node.

The Galerkin formulation uses weighting functions $\psi_I(x_1, x_2, x_3)$ to form weighted residual statements of equation (5.8) of the form

$$\int_{R_2} \psi_I(\nabla\cdot[\bar{\Sigma}]^{-1}\nabla\bar{p}_2)\,dV = 0 \quad , \quad I = 1 \text{ to } N_2 \tag{5.27}$$

where dV is a volume element in (x_1, x_2, x_3) space.

The 'weak' Galerkin formulation follows from application of Green's theorem to equation (5.27) to give, with substitution from equation (5.26),

$$\left\{ \int_{R_2} \left(\nabla \psi_I \cdot [\bar{\Sigma}]^{-1} \nabla \psi_J \right) \, dV \right\} \{ \bar{p}_2 \} = \int_{\Gamma_2} \psi_I [\bar{\Sigma}]^{-1} \nabla \bar{p}_2 \cdot \boldsymbol{n}_2 \, d\Gamma , \tag{5.28}$$

where $\{ \bar{p}_2 \}$ is the vector of nodal values $\bar{p}_{2J}$ and Γ_2 is the entire bounding surface of region R_2. The boundary integral is zero over Γ_{w2}, due to the hard-walled boundary condition, and is redundant over Γ_c, where $\bar{p}_2$ is known to within a constant from the given axial pressure gradient. Hence equation (5.28) can be solved for the unknown nodal values $\bar{p}_2$. However, it should be remembered that the equation is non-linear, since the terms of $[\bar{\Sigma}]$ are flow-dependent. The iterative scheme for solution is outlined in Section 5.2.2. The velocity field can be found from the finite element solution of the pressure field, at any stage of the iteration, from a combination of equations (5.6) and (5.26), namely

$$\bar{q}_2 = -\sum_{J=1}^{N_2} [\bar{\Sigma}]^{-1} \nabla \psi_J \, \bar{p}_{2J} \tag{5.29}$$

5.3.2 Acoustic field in the duct

Let there be N_1 nodes within the finite element mesh of region R_1, such that the approximation to the acoustic pressure is given by the trial solution

$$p_1' \approx \sum_{J=1}^{N_1} \psi_J p_{1J}' \tag{5.30}$$

where $\psi_J(x_1, x_2, x_3)$ are the global basis functions and p_{1J}' is the value of p_1' at the Jth node. The Galerkin formulation of equation (5.4) is then

$$\int_{R_1} \psi_I \left(\nabla\cdot[M]\nabla p_1' + k^2 p_1' - 2\mathrm{i}Mk\,\partial p_1'/\partial x_1\right)dV = 0 \quad , \quad I = 1 \text{ to } N_1 \tag{5.31}$$

where $[M]$ is the diagonal matrix, $\begin{bmatrix} 1-M^2 & 0 & 0 \\ 0 & 1 & 0 \\ 0 & 0 & 1 \end{bmatrix}$.

The weak Galerkin formulation follows from the application of Green's theorem to equation (5.31) which gives, following substitution from equation (5.30),

$$\left\{\int_{R_1} \left(\nabla\psi_I\cdot[M]\nabla\psi_J + 2\mathrm{i}Mk\partial\psi_J/\partial x_1 - k^2\psi_I\psi_J\right)\,dV\right\}\{p_1'\} = \int_{\Gamma_1} \psi_I[M]\nabla p_1'\cdot\boldsymbol{n}_1\;d\Gamma, \tag{5.32}$$

where $\boldsymbol{p}_1'$ is the vector of nodal p_{1J}' values and $\boldsymbol{n}_1$ is the unit outward normal to Γ_1, the boundary of region R_1.

5.3.3 Acoustic field in the absorbent

The approximation to the acoustic pressure in region R_2 is given by the trial solution

$$p_2' \approx \sum_{J=1}^{N_2} \psi_J\, p_{2J}'. \tag{5.33}$$

The Galerkin formulation of equation (5.10) is then

$$\int_{R_2} \psi_I\left(\nabla\cdot[R]\nabla p_2' + \rho_0\omega^2\Omega\chi\, p_2'\right)\,dV = 0 \quad , \quad I = 1 \text{ to } N_2 \tag{5.34}$$

and Green's theorem gives the 'weak' formulation

$$\int_{R_2} \left(\nabla \psi_I \cdot [R] \nabla p_2' - \rho_0 \omega^2 \Omega \chi \psi_I p_2'\right) dV = \int_{\Gamma_2} \psi_I [R] \nabla p_2' \cdot \boldsymbol{n}_2 \; d\Gamma . \tag{5.35}$$

Substitution from equations (5.16) and (5.33) yields

$$\left\{ \int_{R_2} \left(\nabla \psi_I \cdot [G] \nabla \psi_J - k^2 \psi_I \psi_J\right) dV \right\} \{p_2'\} = \int_{\Gamma_2} \psi_I [G] \nabla p_2' \cdot \boldsymbol{n}_2 \, d\Gamma , \tag{5.36}$$

where $[G]$ is a diagonal matrix whose jth element is $1/\gamma_j^2$ and p_2' is the vector of nodal p_{2J}' values.

5.4 Solution of System

5.4.1 Matching of the acoustic fields

The finite element meshes of regions R_1 and R_2 share a common set of, say, N_c nodes along the common boundary Γ_c. The hard-wall boundary condition of equation (5.20) implies that the surface integral contribution to equation (5.36) is zero except over Γ_c, since $\Gamma_2 = \Gamma_{w2} + \Gamma_c$. Similarly the surface integral of equation (5.32) has zero contribution from Γ_{w1}, but finite contributions from Γ_I, Γ_0 and Γ_c. The two sets of inflow and outflow boundary conditions on Γ_I and Γ_0 given in equations (5.24) and (5.25) are, variously, Dirichlet, Neumann and Cauchy conditions which are implemented within the finite element technique in the standard fashion. Thus equations (5.32) and (5.36) may be written in matrix form as:

$$\left[\begin{array}{c|c} K_{11} & K_{1c} \\ \hline K_{c1} & K_{cc}^1 \end{array}\right] \left\{\begin{array}{c} p_1 \\ \hline p_c \end{array}\right\} = \left\{\begin{array}{c} f_1 \\ \hline f_c^1 \end{array}\right\} \quad , \quad \left[\begin{array}{c|c} K_{cc}^2 & K_{c2} \\ \hline K_{2c} & K_{22} \end{array}\right] \left\{\begin{array}{c} p_c \\ \hline p_2 \end{array}\right\} = \left\{\begin{array}{c} f_c^2 \\ \hline \mathbf{0} \end{array}\right\} \tag{5.37a,b}$$

where $[K_{11}]$ is of order $(N_1 - N_c)\times(N_1 - N_c)$, $[K_{22}]$ is of order $(N_2 - N_c)\times(N_2 - N_c)$, $[K^1_{cc}]$ and $[K^2_{cc}]$ are of order $(N_c \times N_c)$, *et cetera*. p_1, p_2 are the vectors of p'_{1J}, p'_{2J} values which do not lie on Γ_c, and p_c is the vector of p' values on Γ_c. f_1 is a forcing vector whose elements are known from the appropriate inflow and outflow boundary conditions, as discussed above, while

$$f^1_{c_i} = \int_{\Gamma_e} \psi_l [M] \nabla p'_1 \cdot \boldsymbol{n}_1 \, d\Gamma \quad , \qquad f^2_{c_i} = \int_{\Gamma_e} \psi_l [G] \nabla p'_2 \cdot \boldsymbol{n}_2 \, d\Gamma . \tag{5.38a,b}$$

Implementation of the displacement boundary condition of equations (5.23), with $\boldsymbol{n}_c = \boldsymbol{n}_1 = -\boldsymbol{n}_2$, leads to

$$f^1_{c_i} = \int_{\Gamma_e} \psi_l \left(1 - \mathrm{i}(M/k)\partial/\partial x_1\right)^2 \left[(\rho_0/\rho_{an})(\partial p'_2/\partial x_n)\right] d\Gamma , \tag{5.39}$$

$$f^2_{c_i} = -\int_{\Gamma_e} \left(\psi_l / \gamma_n^2\right)(\partial p'_2/\partial x_n) \; d\Gamma , \tag{5.40}$$

where $x_n = \boldsymbol{x} \cdot \boldsymbol{n}_1$ and only the unitary elements of $[M]$ were of relevance since x_n is perpendicular to x_1. The order of differentiation in equation (5.39) can be reduced by integration to give

$$f^1_{c_i} = \int_{\Gamma_e} \left[\psi_l - \left(2\mathrm{i}(M/k)\psi_l - (M/k)^2 \partial\psi_l/\partial x_1\right) \partial/\partial x_1\right] \left[(\rho_0/\rho_{an})(\partial p'_2/\partial x_n)\right] d\Gamma - (M/k)^2 \int_{S_e} \psi_l (\rho_0/\rho_{an})(\partial p'_2/\partial x_n) \; dS \tag{5.41}$$

where $dS\,dx_1 = d\Gamma$ and S_c is the pair of circuits which mark the ends of boundary Γ_c at inlet and outlet to the silencer volume, see Figure 5.1. There are two basic techniques which may be used to couple together equations (5.37a,b), as follows.

5.4.2 Gradient elimination

Let the variation of $\partial p_2' / \partial x_n$ over Γ_c be approximated by the use of N_c global basis functions $\psi(x_1,\ x_2,\ x_3)$ for nodes which lie on Γ_c, such that

$$\partial p_2' / \partial x_n \approx \sum_{m=1}^{N_c} y_m \left(\partial p_2' / \partial x_n\right)_m \tag{5.42}$$

where $\left(\partial p_2' / \partial x_n\right)_m$ is the value of $\left(\partial p_2' / \partial x_n\right)$ at the mth node. Equations (5.41) and (5.40) can then be written in the matrix form

$$\left\{f_c^1\right\} = [F_1] \left\{\frac{\partial p_2}{\partial x_n}\right\} \quad , \quad \left\{f_c^2\right\} = [F_2] \left\{\frac{\partial p_2}{\partial x_n}\right\} \tag{5.43a,b}$$

where $\left\{\partial p_2 / \partial x_n\right\}$ is the vector of N_c nodal values of $(\partial p_2 / \partial x_n)$. $[F_1]$ and $[F_2]$ are square matrices of order N_c whose $(l,m)^{\text{th}}$ elements are given by

$$(F_1)_{l,m} = \int_{\Gamma_c} \left[\psi_l - (2\mathrm{i}(M/k)\psi_l - (M/k)^2 \partial\psi_l / \partial x_1)\ \partial / \partial x_1\right] \left[\psi_m\ (\rho_0 / \rho_{an})\right]\ \mathrm{d}\Gamma$$
$$- \ (M/k)^2 \int_{S_c} \psi_l \psi_m (\rho_0 / \rho_{an})\ dS \tag{5.44a}$$

$$(F_2)_{l,m} = -\int_{\Gamma_c} \psi_l \psi_m / \gamma_n^2\ d\Gamma. \tag{5.44b}$$

The vectors f_c^1 and f_c^2 in equation (5.37) can now be replaced by use of equation (5.43) and the common vector $\{\partial p_2 / \partial x_n\}$ can then be eliminated from equations (5.37a) and (5.37b) to give

$$\left[\begin{array}{c|c|c} [K_{11}] & [K_{1c}] & 0 \\ \hline [F_1]^{-1}[K_{c1}] & [F_1]^{-1}[K_{cc}^1]-[F_2]^{-1}[K_{cc}^2] & -[F_2]^{-1}[K_{c2}] \\ \hline 0 & -[K_{2c}] & -[K_{22}] \end{array}\right] \left\{\begin{array}{c} p_1 \\ \hline p_c \\ \hline p_2 \end{array}\right\} = \left\{\begin{array}{c} f_1 \\ \hline \mathbf{0} \\ \hline \mathbf{0} \end{array}\right\}. \tag{5.45}$$

5.4.3 Gradient evaluation

It is simpler to substitute directly into equations (5.41) and (5.40) the trial solution form of p_2' given in equation (5.33), such that

$$\left\{f_c^1\right\} = \left[\tilde{F}_{1c} \mid \tilde{F}_{12}\right] \left\{\begin{array}{c} p_c \\ \hline p_2 \end{array}\right\} \quad , \quad \left\{f_c^2\right\} = \left[\tilde{F}_{2c} \mid \tilde{F}_{22}\right] \left\{\begin{array}{c} p_c \\ \hline p_2 \end{array}\right\} \tag{5.46a,b}$$

where $[\tilde{F}_1]$ and $[\tilde{F}_2]$ are $(N_c \times N_2)$ matrices whose $(l,J)^{\text{th}}$ elements are given by

$$(\tilde{F}_1)_{l,J} = \int_{\Gamma_c} \left[\psi_l - (2\mathrm{i}(M/k)\psi_l - (M/k)^2 \partial\psi_l / \partial x_1)\ \partial / \partial x_1\right] [\partial\psi_J / \partial x_n$$

$$(\rho_0 / \rho_{an})]\ d\Gamma - (M/k)^2 \int_{S_c} \psi_l (\partial\psi_J / \partial x_n)(\rho_0 / \rho_{an})\ dS, \tag{5.47a}$$

$$(\tilde{F}_2)_{l,J} = -\int_{\Gamma_c} \psi_l (\partial\psi_J / \partial x_n) / \gamma_n^2\ d\Gamma. \tag{5.47b}$$

Equations (5.37) and (5.46) can then be combined to give

$$\left[\begin{array}{c|c|c} K_{11} & K_{1c} & 0 \\ \hline K_{c1} & K_{cc}^{1} - \tilde{F}_{1c} + K_{cc}^{2} - \tilde{F}_{2c} & K_{c2} - \tilde{F}_{12} - \tilde{F}_{22} \\ \hline 0 & K_{2c} & K_{22} \end{array}\right] \left\{\begin{array}{c} p_1 \\ \hline p_c \\ \hline p_2 \end{array}\right\} = \left\{\begin{array}{c} f_1 \\ \hline 0 \\ \hline 0 \end{array}\right\}. \qquad (5.48)$$

This approach has the advantage, with reference to the gradient elimination approach of equation (4.45), that matrix inversions are not required. The benefit in terms of computing cost is substantial for large systems of equations. The drawback with this gradient evaluation approach is that second-order derivatives occur in the boundary integral of equation (4.47a). This in turn requires the use of C^1 continuous elements to guarantee inter-element compatibility in all circumstances.

5.5 Overall Acoustic Performance

The whole system of equations was solved for the two sets of inlet and outlet boundary conditions given in equations (5.24) and (5.25). The overall acoustic performances of the silencers were then found in terms of the four-pole parameters, equation (3.76), from which the transmission loss or insertion loss follow by using equations (3.77) and (3.78).

5.6 Results

The results shown all refer to the transmission loss of axisymmetric silencers, the absorptive region of which is filled with the homogeneous, isotropic foam considered by Cummings and Chang [17], who gave the relevant acoustic properties. The flow duct geometry and flow Mach numbers have also been restricted to the values used by

Cummings and Chang [17], such that their measured values of axial pressure gradient could be used in the determination of the induced velocity field. The finite element results have all been obtained by the use of eight-noded, quadrilateral, isoparametric elements. Mesh refinement was used to establish convergence and the necessary inlet and outlet duct lengths such that the assumption of plane-wave inlet and boundary conditions was valid.

The first test case was exactly the same silencer as considered by Cummings and Chang [17], shown in Figure 5.2(a), such that comparison can be made against their results. The finite element results shown refer to a mesh of 152 elements as shown in Figure 5.2(b). The computed velocity vectors of the induced flow within the absorbent, Region 2, are shown in Figure 5.2(c), where the location of the computed velocity is at the tail of the plotted vector. It is seen that the velocity is almost uniform throughout the whole of the absorbent region, with non-uniform and non-axial flow being confined to very short entry and exit lengths.

Finite element results have been obtained upon the assumption of zero induced flow in the absorbent, uniform axial induced flow in the absorbent, and calculated variable induced flow in the absorbent. The first two of these cases relate directly to the results of Cummings and Chang [17]. The finite element results are compared with the mode-matching results of Cummings and Chang [17] in Figures 5.3(a) and 5.3(b), and with the fundamental mode solutions of Peat [46] in Figures 5.3(c) and 5.3(d). Figures 5.3(a) and 5.3(c) refer to a mean flow Mach number of 0.163, while Figures 5.3(b) and 5.3(d) refer to a mean flow Mach number of 0.196, as considered by Cummings and Chang [17]. The corresponding speed of uniform axial induced flow in the absorbent for the two Mach numbers was 0.44 [m/s] and 0.6 [m/s] respectively. It is seen that the mean flow in the airway reduces or increases the transmission loss of the

silencer, according to whether it is in the same sense or opposite sense to that of the initial acoustic propagation. In contrast, the effect of the small induced flow in the absorbent is always to increase, by a significant amount, the transmission loss of the silencer. These effects have been well-documented by Cummings and Chang [17, 18] and the results here serve merely to validate the finite element analysis. In this regard, it is seen from Figures 5.3(a) and 5.3(c) that agreement between the finite element and mode-matching results is generally good, with the worst discrepancies at low frequencies, which is somewhat surprising. In contrast, the agreement between the finite element and the fundamental mode solutions, seen in Figures 5.3(b) and 5.3(d), is good at low frequencies but not at high frequencies. This is to be expected, since the fundamental mode solutions cannot be expected to be accurate at high frequencies, but are accurate at low frequencies. Thus it would appear that the finite element analysis itself remains accurate at low frequencies, as one would expect, and that an alternative explanation is required for the differences seen in Figures 5.3(a) and 5.3(b). The finite element and the fundamental mode solutions were both evaluated using precisely the same expressions for wave propagation in the absorbent material, whereas only the underlying material properties and Delaney and Bazley coefficients were known to be the same between the finite element and the mode-matching solutions. This offers one possible explanation for the differences in transmission loss, particularly at very low frequencies where the Delaney and Bazley formulae are not accurate.

The finite element results for transmission loss which were obtained upon the basis of the computed induced flow field in the absorbent, as shown in Figure 5.2(c), do not differ from those calculated with an assumed uniform axial flow by any observable degree. The differences are less than 0.1% and hence the 'induced flow' results shown in Figures 5.3(a) to 5.3(d) refer equally to either case. This result is not of any great surprise, given the uniformity of the induced flow field in Figure 5.2(c) and the close

correlation between experimental and analytical results [17], where the latter were obtained with an assumption of uniform axial induced flow. Clearly the assumption of uniform axial induced flow in a long, thin dissipative silencer of uniform cross-section with homogeneous absorbent material is valid, with regard to calculation of transmission loss. The induced flow field would be less uniform if at least one of the following criterion were met: the diameter to length ratio of the silencer were increased; the cross-section were non-uniform; the absorbent material were non-homogeneous. All of these situations commonly arise within dissipative silencers, for which the geometry of the silencer in Figure 5.2(a) would be an extreme case. In order to gain some insight into the necessity or otherwise for detailed calculation of the induced flow field, a uniform, homogeneous absorption silencer of large diameter to length ratio, at the opposite extreme of practical interest, was considered.

The dimensions of this second silencer unit are shown in Figure 5.4(a), the finite element mesh used for computation is given in Figure 5.4(b), and the computed flow field within the absorbent is shown in Figure 5.4(c). The latter clearly indicates that the flow field is now far from uniform and axial, as one would expect. Finite element results of the transmission loss of the silencer for a mean flow within the airway of M = 0.163 are given in Figures 5.5(a) and 5.5(b), for flow in the same sense and the opposite sense respectively to that of initial acoustic propagation. In each figure, results are given for three cases, namely zero flow in the absorbent, uniform axial flow in the absorbent, and the computed flow field in the absorbent. It is seen that there is now an observable difference between the results obtained assuming uniform flow and those which follow from the use of the computed flow field, although this difference is much smaller than that between the results for uniform induced flow and zero induced flow. Similar results are presented in Figures 5.6(a) and 5.6(b) for a steady flow Mach number within the airway of M = 0.196 and the same comments apply. In these

figures, and similarly in Figures 5.8 to 5.11, finite element results have only been calculated at the discrete frequencies indicated by the symbols on the plots, and linear interpolation has been used between these values to give the plotted lines.

It is clearly a drawback of the current approach that a measured value for the steady flow axial pressure gradient in the flow duct is required in order to evaluate the induced steady flow in the absorbent. It would be possible to use an empirical estimate of this pressure gradient, but the resulting value could not be expected to be as accurate as that given by direct measurement. In this regard, an investigation has been made into the sensitivity of the results for transmission loss to changes in the axial pressure gradient, for the silencer of Figure 5.2 at the highest flow Mach number of 0.196. The results showed that changes of ±12.5% in the magnitude of the axial pressure gradient gave changes in transmission loss of ±1.2% at 1 kHz, rising to ±1.9% at 2 kHz. Furthermore changes of ±25% in the magnitude of the axial pressure gradient gave changes in transmission loss of ±2.3% at 1 kHz, rising to ±3.7% at 2 kHz. The error when decreasing the axial pressure gradient was always slightly greater than when increasing the axial pressure gradient. In summary, it is seen that the transmission loss is not very sensitive to the value of axial pressure gradient and that the use of an empirical estimate for the latter is in order.

The normalised radial pressure distribution at the axial mid-point of the silencer, at frequencies of 1000 Hz and 1890 Hz, are shown in Figures 5.7(a) and 5.7(b) for the silencers of Figures 5.2(a) and 5.4(a) respectively. The pressure distribution across the cross-section is near to being uniform for the long, thin silencer of Figure 5.2(a) and indicates that the acoustic energy propagates in the lowest order mode. In contrast, there is marked radial variation, indicating significant energy propagation in higher-order modes, for the short, fat silencer of Figure 5.4(a). In both cases there is a change

in the magnitude, but not of underlying shape, of the radial pressure distribution with frequency. In particular, there is no evidence of energy propagation in a newly cut-on mode between the results at low and high frequencies, either side of the peak in transmission loss.

Figures 5.5 and 5.6 indicate that the frequency of the peak in transmission loss is not affected by induced flow in the absorbent. Figure 5.8 shows the transmission loss of the short silencer of Figure 5.4(a) for various mean flow Mach numbers in the flow duct, assuming zero induced flow in the absorbent. One interesting feature of Figure 5.8 is that the magnitude of the peak transmission loss is increased for mean flow in the same direction as the initial sound propagation and reduced when the mean flow is in the opposite sense. This is the opposite of the effect of steady flow throughout the rest of the frequency spectrum. Cummings [15] reported a cross-over of greatest attenuation of rectangular splitter silencers from the sound against flow situation at low frequencies to the sound with flow case at high frequencies and attributed this to the relative dominance of the convective effect of the mean flow in contrast to the refractive effect into the absorbent. A similar effect can be observed in the case of the attenuation of a square duct lined on all four sides [20]. However, the cross-over effect of flow on the resonance peak for a circular silencer of finite length, shown in Figure 5.8, is far more marked in magnitude and restricted in frequency than anything seen in these earlier results for attenuation. Figures 5.9, 5.10 and 5.11 show further transmission loss results with varying steady flow for three cases in which the geometry of the silencer of Figure 5.4(a) is perturbed in different ways. Figure 5.9 corresponds simply to a doubling of the length of the silencer. The frequency of the peak of transmission loss is unaltered but the peak is less pronounced and there is no cross-over effect due to changing the direction of the steady flow. Figures 5.10 and 5.11 refer to situations where only the radial dimension of the absorbent region of the silencer of Figure 5.4(a)

has been altered, by reductions of 25% and 50% respectively. The frequency of the peak transmission loss increases as the radius is reduced and the peak becomes progressively less noticeable as the length/diameter ratio of the silencer is increased. In particular, the cross-over effect due to a change in direction of the steady becomes less evident as this ratio is increased.

Two techniques for coupling the finite element analyses of the acoustic fields in Regions R_1 and R_2 were given in Sections 5.4.2 and 5.4.3. The results corresponding to Figures 5.3, 5.5 and 5.6 were obtained by both techniques and found to be almost identical. Eight-noded, quadrilateral, isoparametric elements, as used for all of the results for this paper, only possess C^0 continuity. As noted earlier, since the surface integral of equation (5.47a) involves second-order derivatives of the shape function, C^1 continuous elements are required to guarantee inter-element compatibility in the general case. However in all the grids used to generate the results for Figures 5.3, 5.5 and 5.6, the element boundaries were aligned to both the axial and its normal (radial) directions. Thus continuity of the normal derivative at an inter-element boundary is guaranteed, since the normal pressure variation is uniquely defined by the three shared nodes on the element boundary. Thus the second derivative term in the integral equation experiences only a finite discontinuity at the inter-element boundary, which requires only C^0 continuity. In order to give a more demanding test for the gradient evaluation approach, the mesh of Figure 5.2(b) was altered such that the element boundaries in the absorbent region, and hence the ends of the silencer box in Figure 5.2(a), were inclined at an angle of 40° clockwise from the vertical. The result was to give a maximum discrepancy of transmission loss of 4% between the gradient elimination results and the gradient evaluation results. It would imply, therefore, that while the eight-noded C^0 elements are not compatible for the gradient evaluation method, they are complete and non-conforming, since inter-element compatibility has

occurred. Further studies of inter-element compatibility in the gradient evaluation technique are required for cases in which the elements along the common interface boundary are not aligned with the axial direction, but this would imply a non-uniform flow duct and is outside the scope of the current chapter. Since the gradient evaluation technique is by far the most computationally efficient of the two techniques, it was adopted for all subsequent analyses, which also have all element boundaries aligned to the axial and radial directions.

For further detailed information regarding the effects of non-homogeneous absorbent material packing, of similar variation to that encountered in the SAAB silencer of Chapter 4, material density variation was taken into account in the finite length silencer of Figure 5.2. Acoustic performance was found in terms of transmission loss, using the maximum to minimum density variation along the axial direction, from both the inlet and outlet ends and along the radial direction, in both senses. Figure 5.12 shows the comparison between each variation, namely: (i) no material variation, average density; (ii) variation along length from highest density at the inlet end to the lowest density at the outlet end; (iii) variation along length with highest density at outlet end and lowest at inlet end; (iv) radial variation form highest density at the inner radius to lowest at the outer radius (v) radial variation from highest density at the outer to lowest at the inner radius. Separate plots are shown for the cases of zero mean flow and mean flow of Mach number M=0.163 both with and without induced flow in the absorbent. In the case of zero mean flow, maximum to minimum variation from inlet to outlet axially and inner to outer radially, both give significantly better transmission loss at low frequencies than uniform packing, but at high frequencies uniform packing is best. In the case of mean flow of Mach number M=.163, variation of absorbent material from minimum to maximum density from inlet to outlet axially and inner to outer radially gives increasingly higher transmission loss, as compared with uniform packing, as the

frequency increases. The opposite variations, which were best of all in the no-flow case, are significantly worse than the uniform packing case. The presence of induced flow in the absorbent slightly exaggerates all the mean flow effects. It should be noted that, while the slight difference in overall mass of absorbent could be thought to explain the observed differences for radial variation, there is no such discrepancy for axial variation.

A major drawback of the method outlined above is the large computational effort required. This problem is compounded by the non-linearity of the problem, resulting in iterative solutions. It was decided to investigate the errors which are incurred by employing simplified governing equations of linear form. Thus an "average" induced velocity was used to factor the inertial flow resistivity, see equation (3.53), such that the steady induced flow field could be determined from the linear equation (3.54). Similarly the solution of the acoustic equation was made linear by neglecting the acoustic terms in determining the acoustic flow resistivity from equation (5.13). Effectively this implies using only the first iteration from the full nonlinear analysis with, of course, non-exact solution of the steady flow velocity field. Clearly this "linearised" solution represents a compromise between the complete nonlinear solution above and the solution obtained on the basis of a uniform flow field. Results have been obtained to compare all these of three solutions for the silencers of Figure 5.2 and 5.4 with steady flow Mach number of 0.13. These results are shown in Tables 5.1 and 5.2 and Figures 5.13 and 5.14.

It has been noted earlier that, in the case of the long thin silencer of Figure 5.2 for which the flow field is virtually uniform and axial, there is very little difference between the results of the full nonlinear analysis and those obtained assuming uniform flow. It is seen in Table 5.1 and Figure 5.13 that the results from the "linear" analysis are worse

than those obtained assuming uniform flow. The reason for this is that the neglect of acoustic effect on the axial flow resistivity has, in essence, removed the factor 2 in equation (5.14a). In the case of the short, wide silencer of Figure 5.4, for which the flow field is markedly non-uniform, the "linear" results are generally slightly closer to the nonlinear results than those assuming uniform axial flow, but not consistently so. In summary, bearing in mind that these two silencers are extreme cases, if one is to use a simplified form of modelling then one may as well as choose the simplest case of an assumed uniform flow. However, since the fully nonlinear analysis has always been found to be rapidly convergent, and since the time spent on analysis is only one contribution to the overall cost of a finite element solution scheme, one may as well conduct the full nonlinear analysis if embarking upon a finite element solution.

5.7 Conclusions

Finite element formulations have been developed for two related nonlinear problems concerned with convected acoustic wave motion in dissipative silencers of general geometry and non-homogeneous, anisotropic absorbent material. The first refers to the solution of the induced flow field within the absorbent material, given the axial pressure gradient of the steady flow in the central flow duct region. The second formulation is for the coupled acoustic wave motion between the convected acoustic waves in both the flow duct and absorbent regions. The induced flow in the absorbent causes acoustic inhomogeneity and anisotropy even if the material itself is homogeneous and isotropic. Rapidly convergent iterative schemes for both nonlinear analyses have been given. Two or three iterations only have been found necessary for convergence to practical limits of accuracy.

The finite element formulations have been validated with reference to a simple axisymmetric silencer of high length to diameter ratio, for which experimental and analytical results were available [17]. The latter results assumed uniform, axial induced flow in the absorbent. The calculated induced flow field was non-uniform and non-axial only in small regions at the inflow and outflow planes of the silencer. No difference was found between finite element results of transmission loss with assumed uniform axial flow or with the computed flow field. In a second test case, namely an axisymmetric silencer of much lower length to diameter ratio, the computed induced flow field for the silencer was markedly non-uniform and non-axial. In this case there were observable, but very small, differences between the transmission loss results with the computed non-uniform induced flow field and with an assumed uniform, axial induced flow. Thus, even for short, wide silencers of this type, little error results from ignoring non-uniformity in the induced flow field. Flow non-uniformity could equally well be caused by a silencer of non-uniform cross-section or inhomogeneous absorbent material and, particularly for extreme cases of the latter, it is possible that detailed calculation of the induced field, and its convective effect upon wave propagation in the absorbent, may be necessary.

The matching condition of the two acoustic fields can be implemented by a simple and efficient gradient evaluation technique using standard C^0 elements, even though such elements are non-conforming in this case.

Variation in the density of the absorbent material can cause significantly beneficial effects in terms of transmission loss as compared with using the same total amount of absorbent packed uniformly. The form of variation required is different with and without mean flow.

TABLE 5.1

FREQUENCY (Hz)	**TRANSMISSION LOSS (dB)**		
	Uniform flow	*Linear flow*	*Non linear flow*
273	5.0	5.2	5.0
546	8.5	8.2	8.5
819	10.9	10.3	10.9
1093	13.4	12.6	13.4
1366	15.3	14.3	15.3
1639	17.2	16.0	17.2
1913	18.9	17.6	18.9
2186	20.6	19.1	20.6
2459	22.5	20.9	22.5
2733	24.5	22.7	24.4

TABLE 5.2

FREQUENCY (Hz)	**TRANSMISSION LOSS (dB)**		
	Uniform flow	*Linear flow*	*Non linear flow*
270	15.8	16.2	15.9
541	19.4	19.1	19.0
811	22.9	21.3	21.7
1082	29.8	28.4	28.9
1352	42.2	47.4	41.4
1623	26.8	26.3	26.3
1893	21.7	20.9	21.2
2164	20.1	19.2	19.6
2435	20.2	19.1	19.6
2705	21.6	20.4	21.0

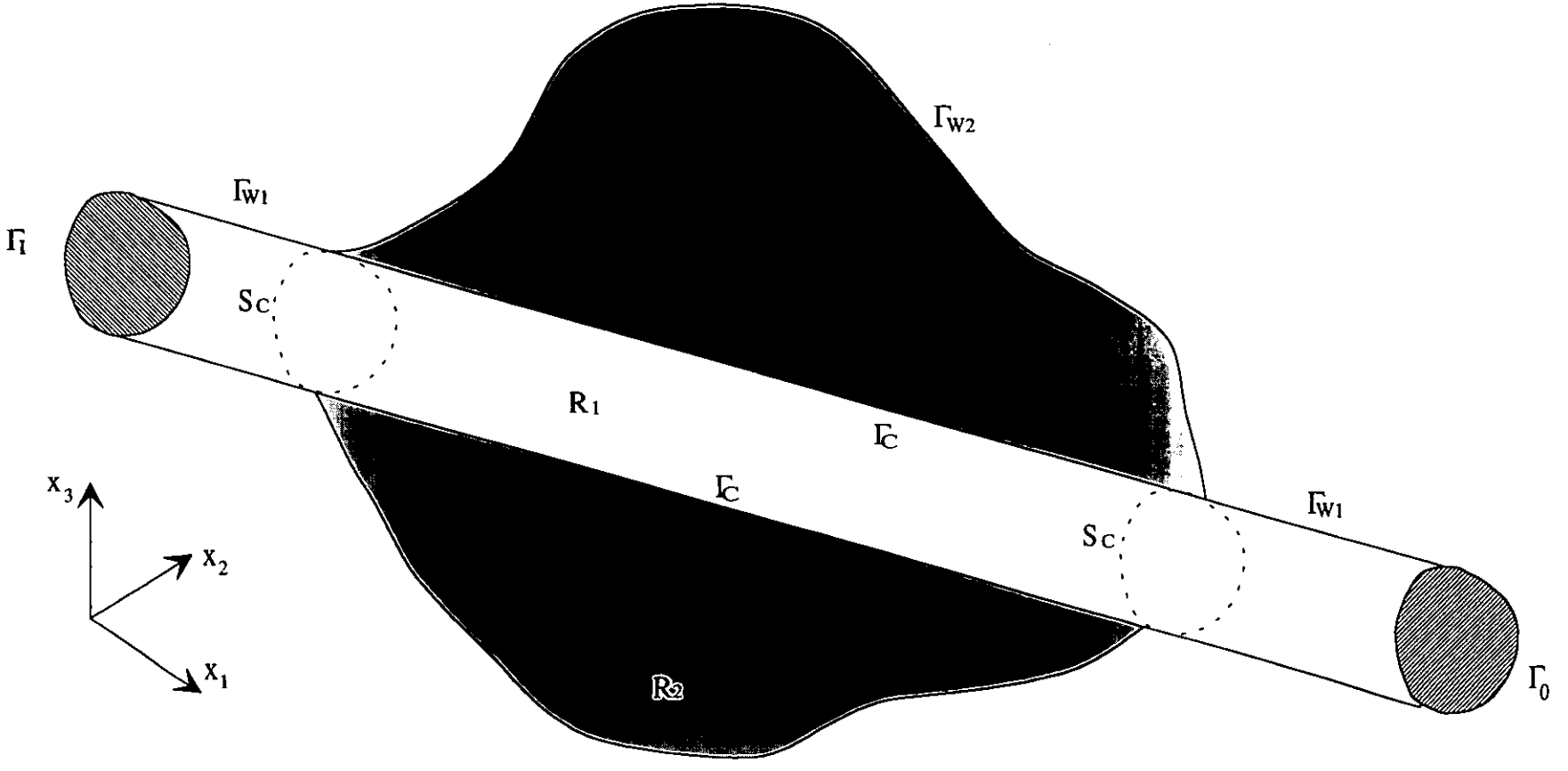

Figure 5.1 Geometry and coordinate system

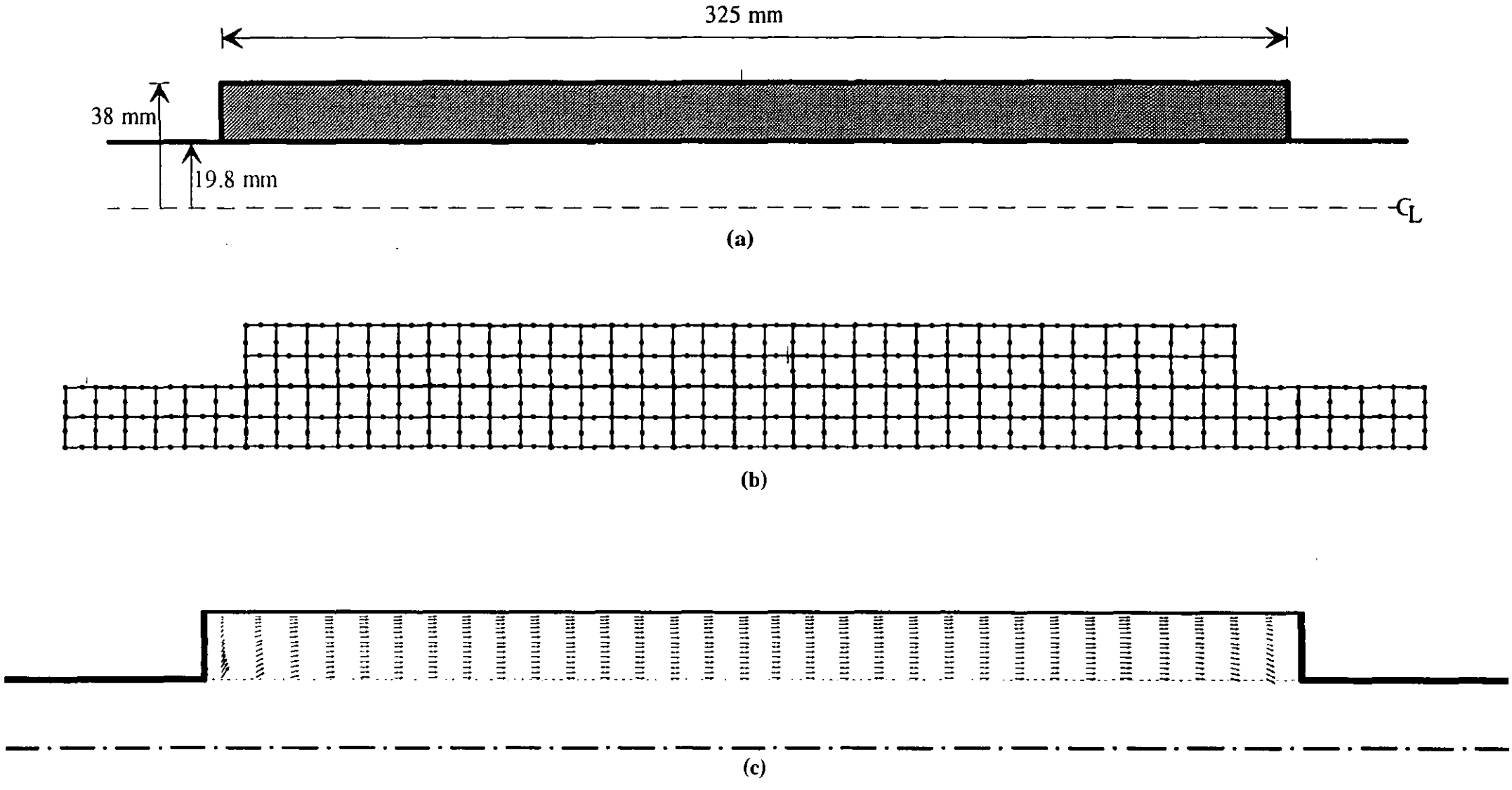

Figure 5.2 First Test Silencer. (a) Geometry (b) Finite element mesh (c) Induced steady flow velocities.

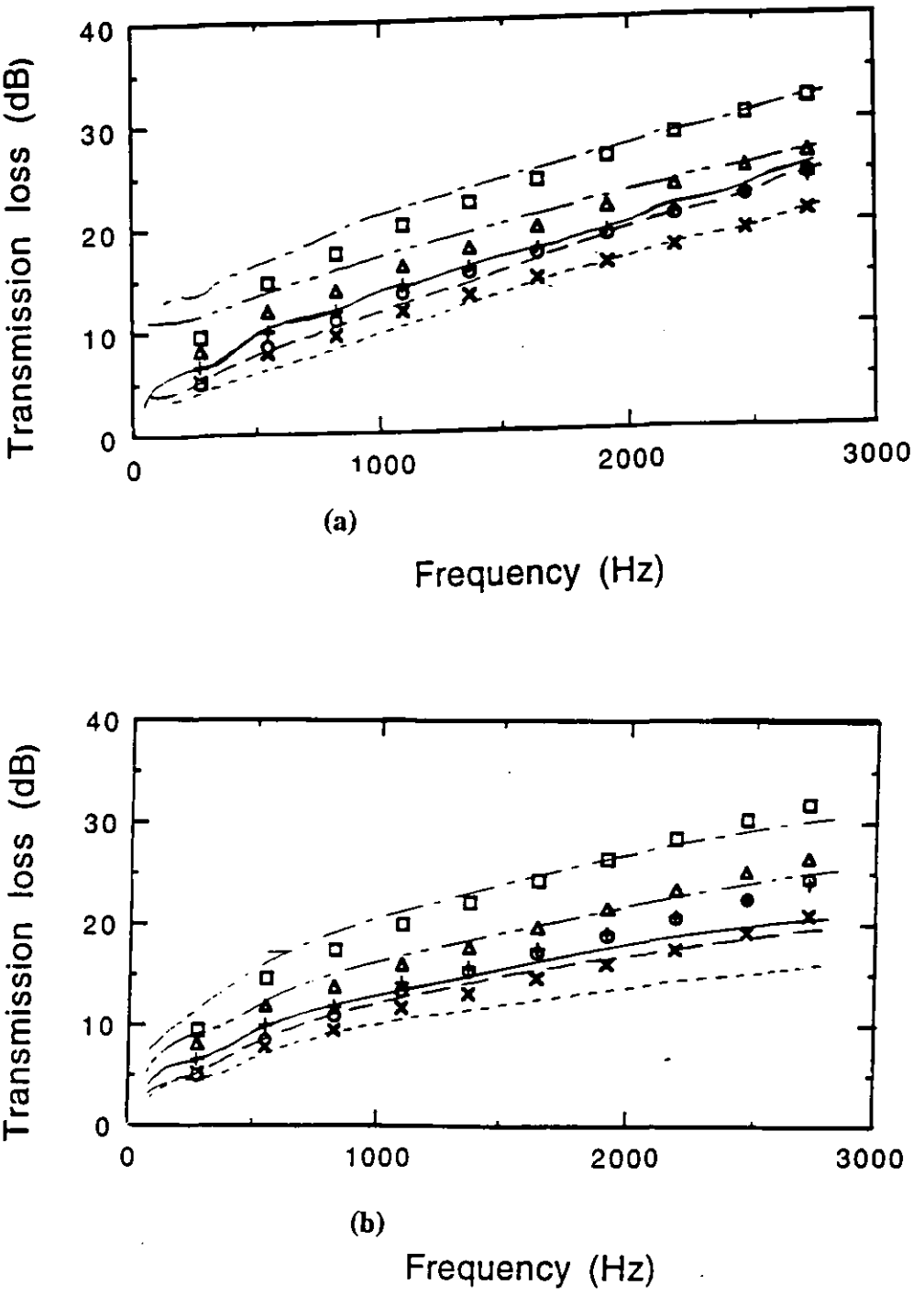

Figure 5.3 Transmission loss of the first test silencer. (a) Comparison of FE results with the mode-matching results of Cummings and Chang [17] (b) Comparison of FE results with the fundamental mode solution of Peat [46].

|M| = 0.163 ;

Without induced flow: x, _ _ _ _ FE, Modal for M +ve.

Without induced flow: Δ, ___ _ _ FE, Modal for M -ve.

With induced flow: o ___ FE, Modal for M +ve.

With induced flow: □, ___ _ FE, Modal for M -ve.

\+ . _____ , FE, Modal for M = 0

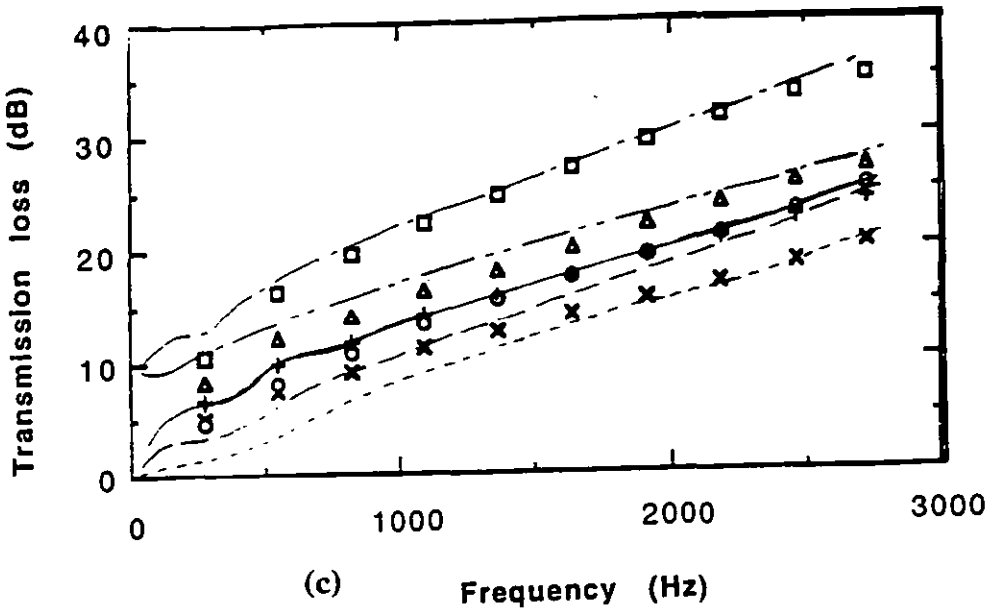

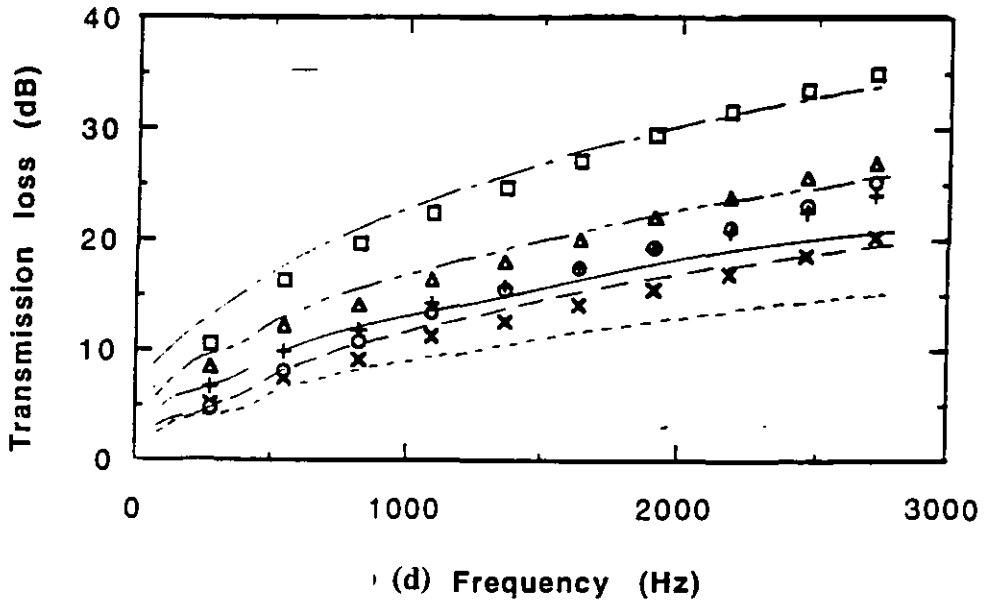

Figure 5.3 Transmission loss of the first test silencer. (c) Comparison of FE results with the mode-matching results of Cummings and Chang [17] (d) Comparison of FE results with the fundamental mode solution of Peat [46].

|M| = 0.196 ;

Without induced flow: x, _ _ _ _ FE, Modal for M +ve.

Without induced flow: Δ, _ _ _ _ FE, Modal for M -ve.

With induced flow: o , _ _ _ FE, Modal for M +ve.

With induced flow: □, _ _ _ FE, Modal for M -ve.

+ , _____ , FE, Modal for M = 0

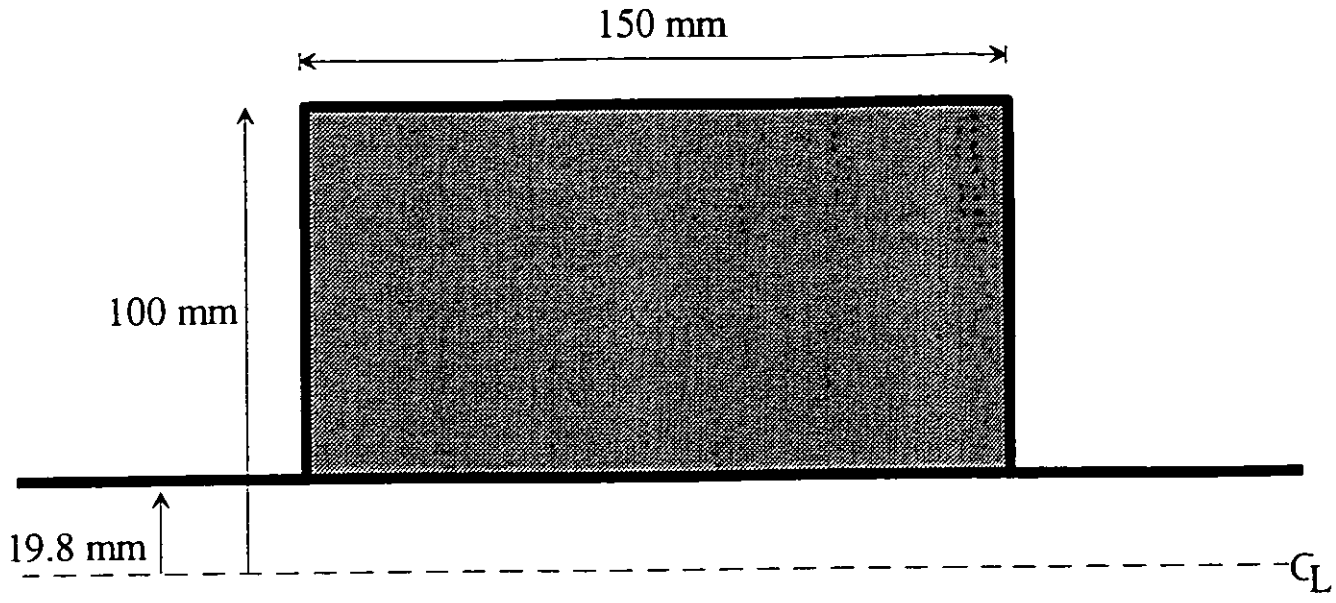

(a)

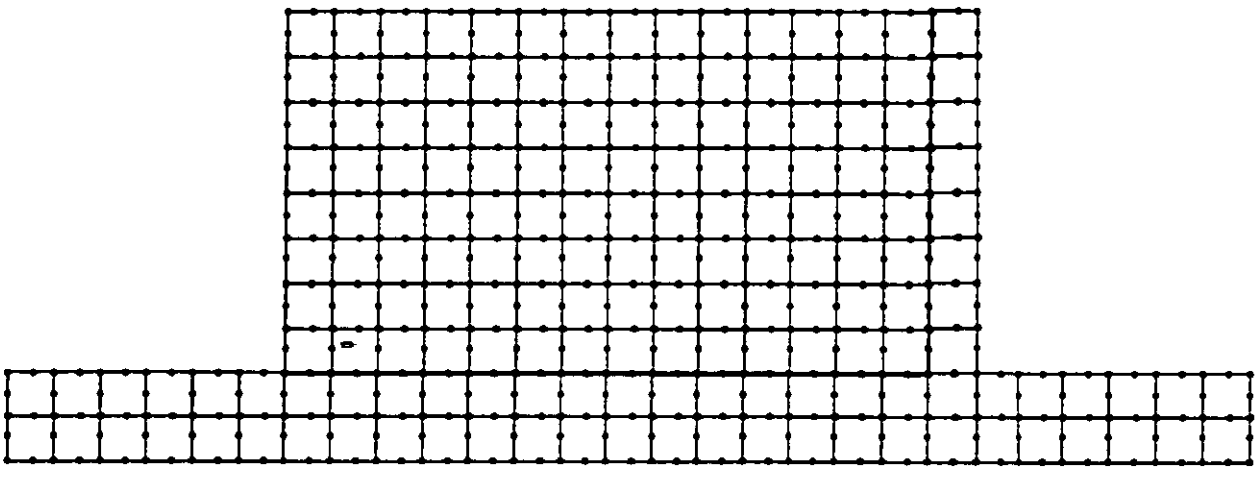

(b)

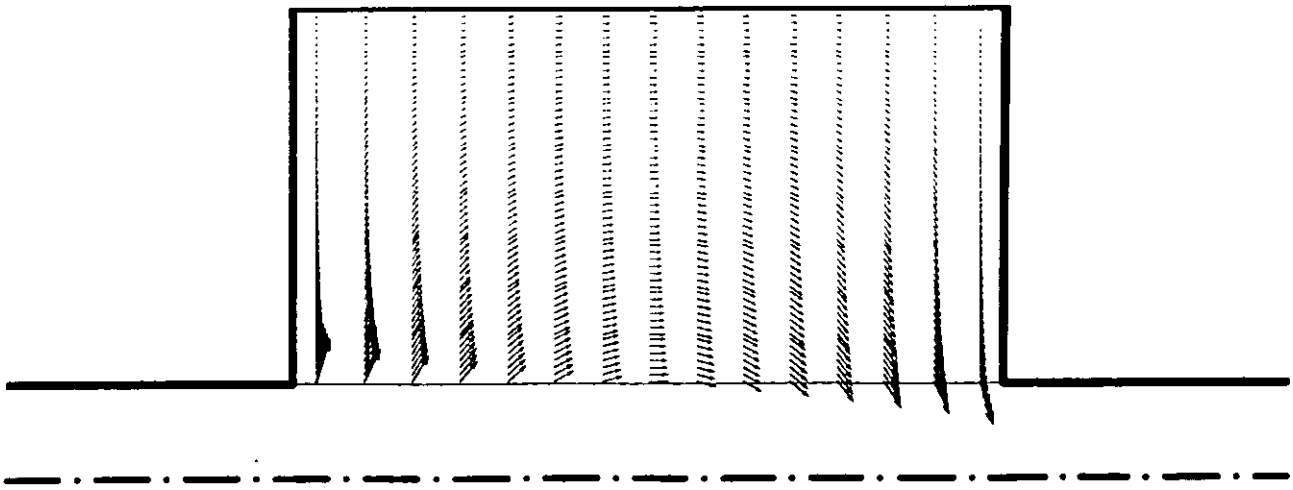

(c)

Figure 5.4 Second Test Silencer. (a) Geometry (b) Finite element mesh (c) Induced steady flow velocities.

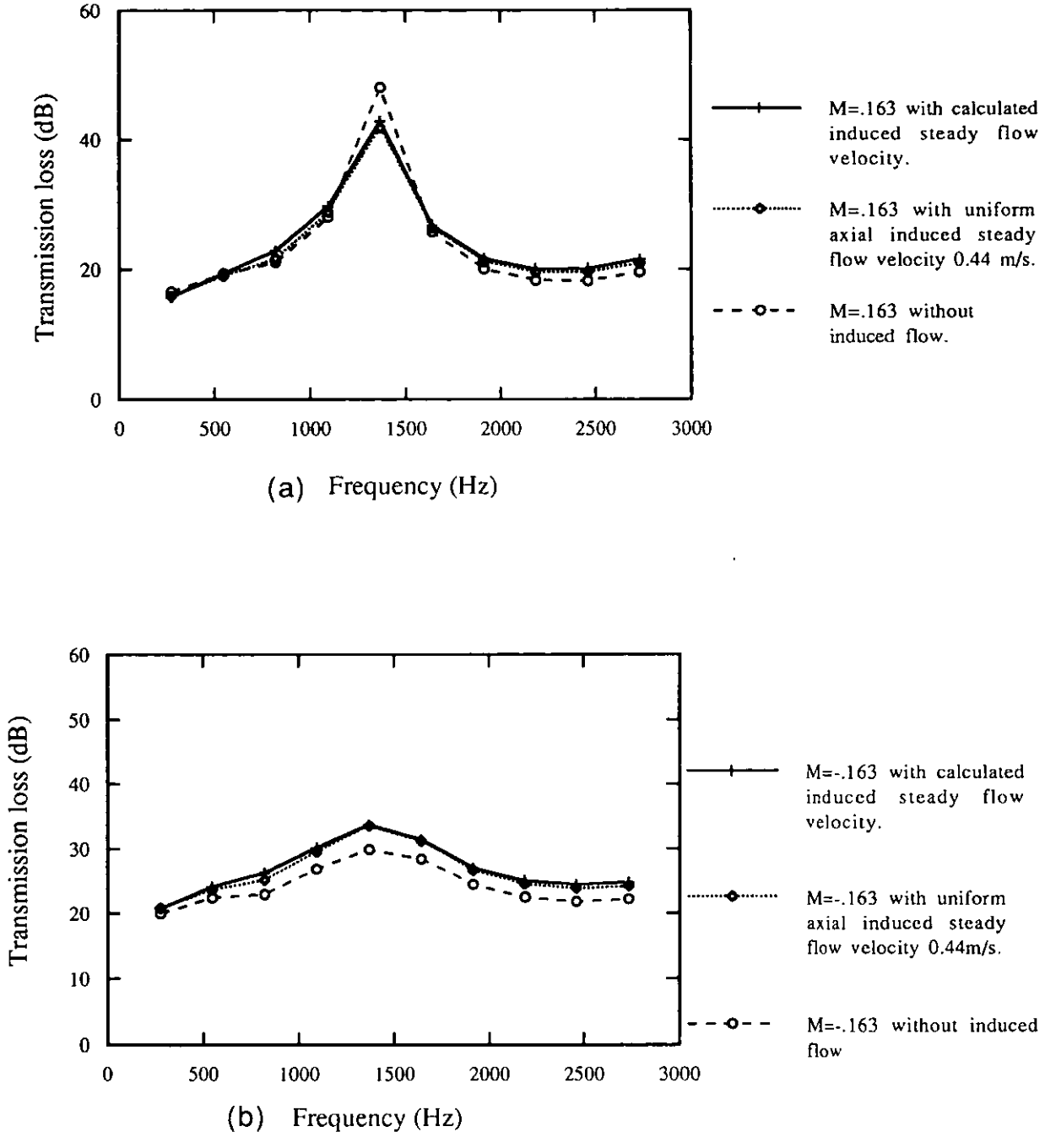

Figure 5.5. Transmission loss of the second test silencer.

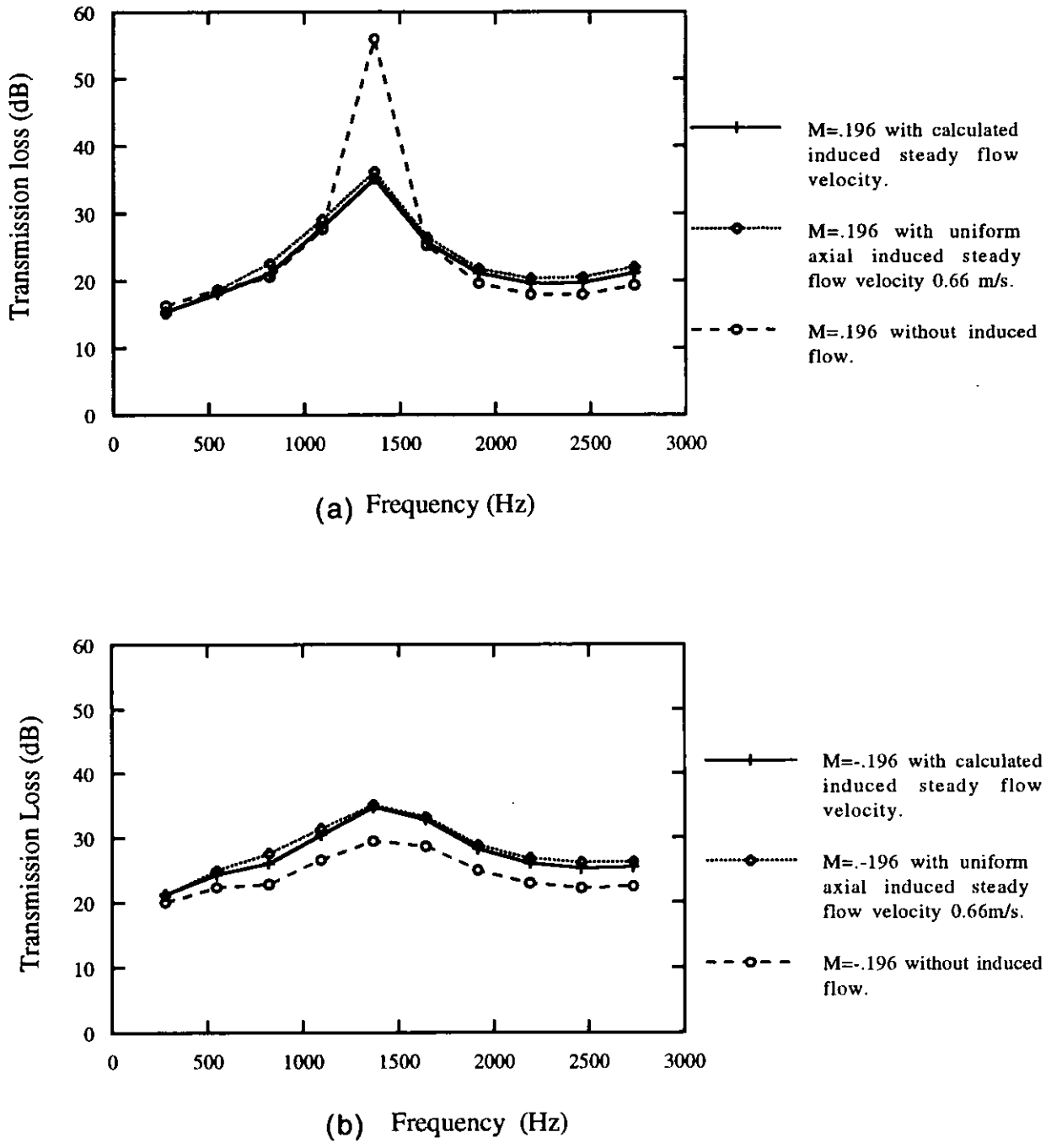

Figure 5.6. Transmission loss of second test silencer.

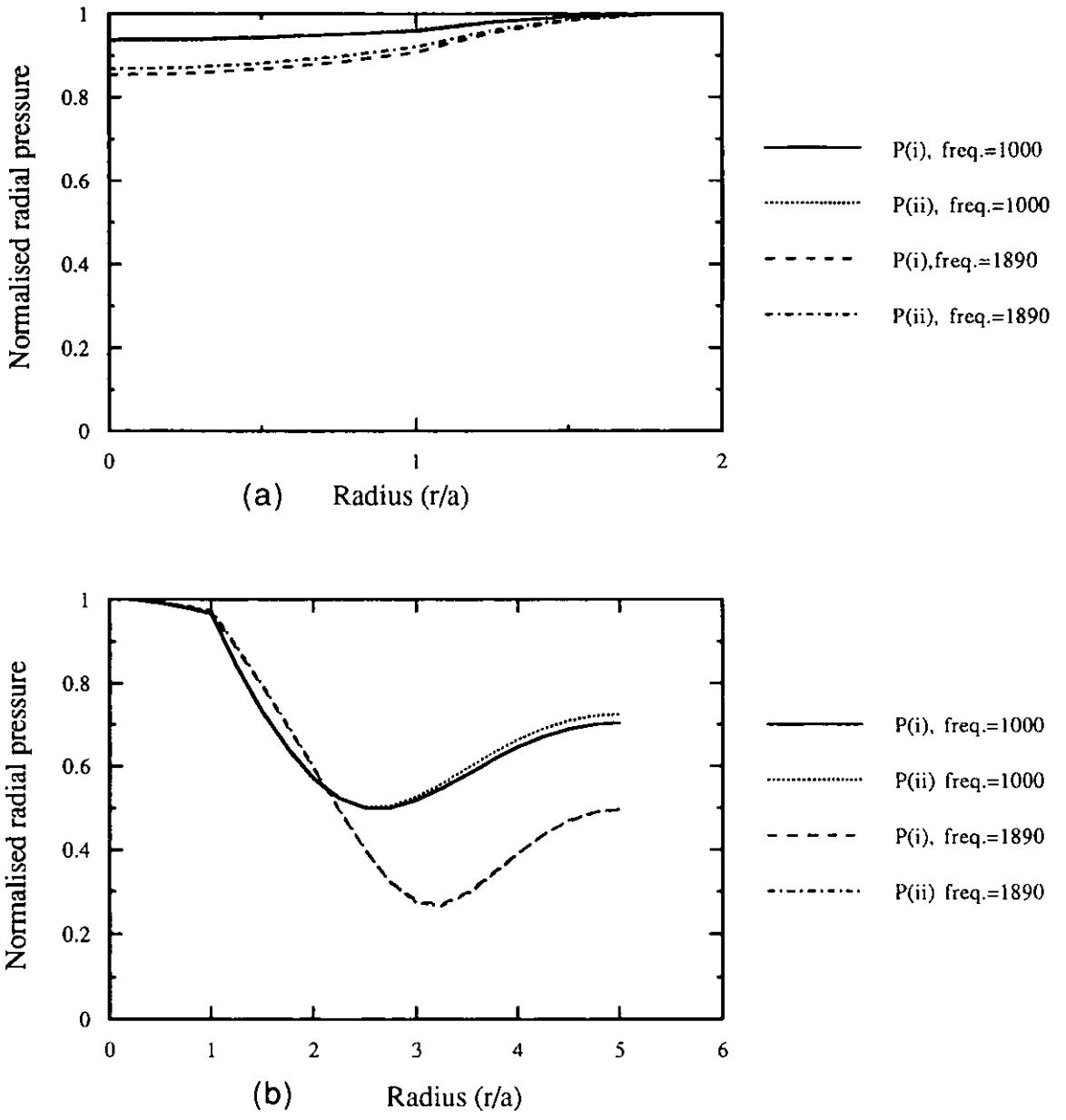

Figure 5.7. Radial pressure distribution at axial mid-point of the silencer for M=0.163 with calculated, induced steady flow velocity field.(**a**) First test silencer. (**b**) Second test silencer. P(i) & P(ii) refer to the two sets of inflow and out flow boundary conditions.

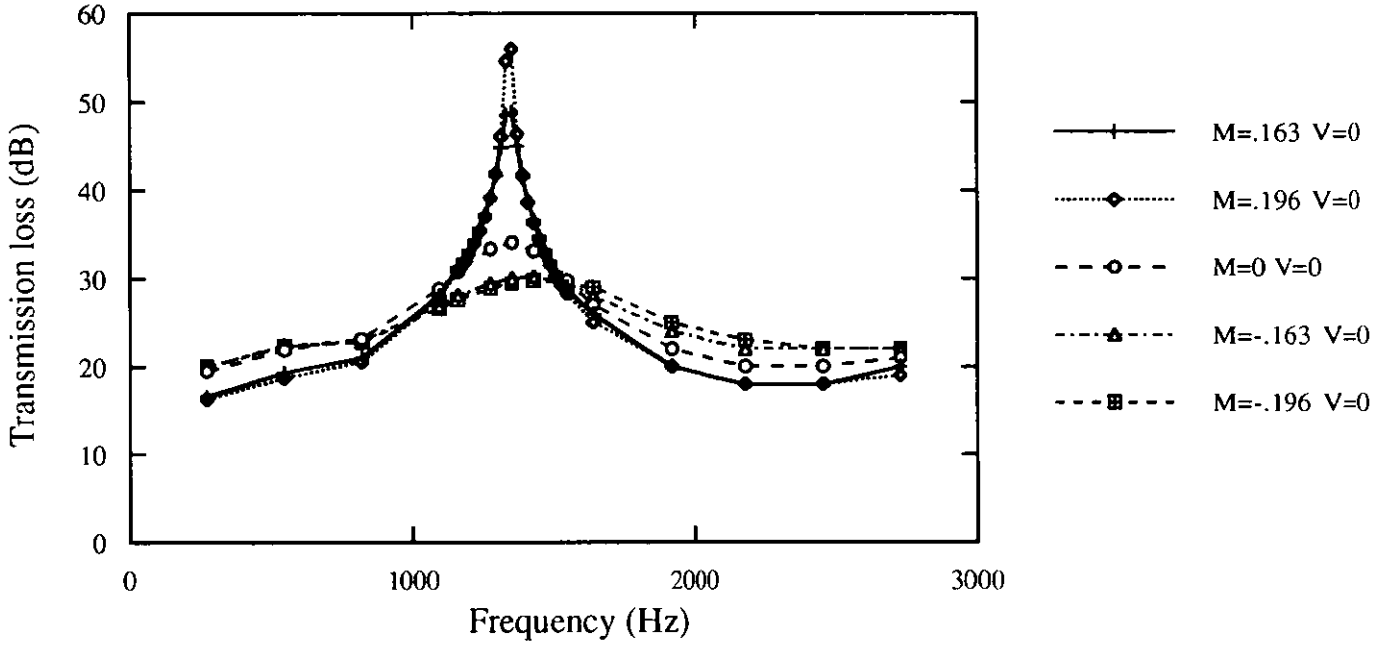

Figure 5.8. Transmission loss of second test silencer without induced steady flow.

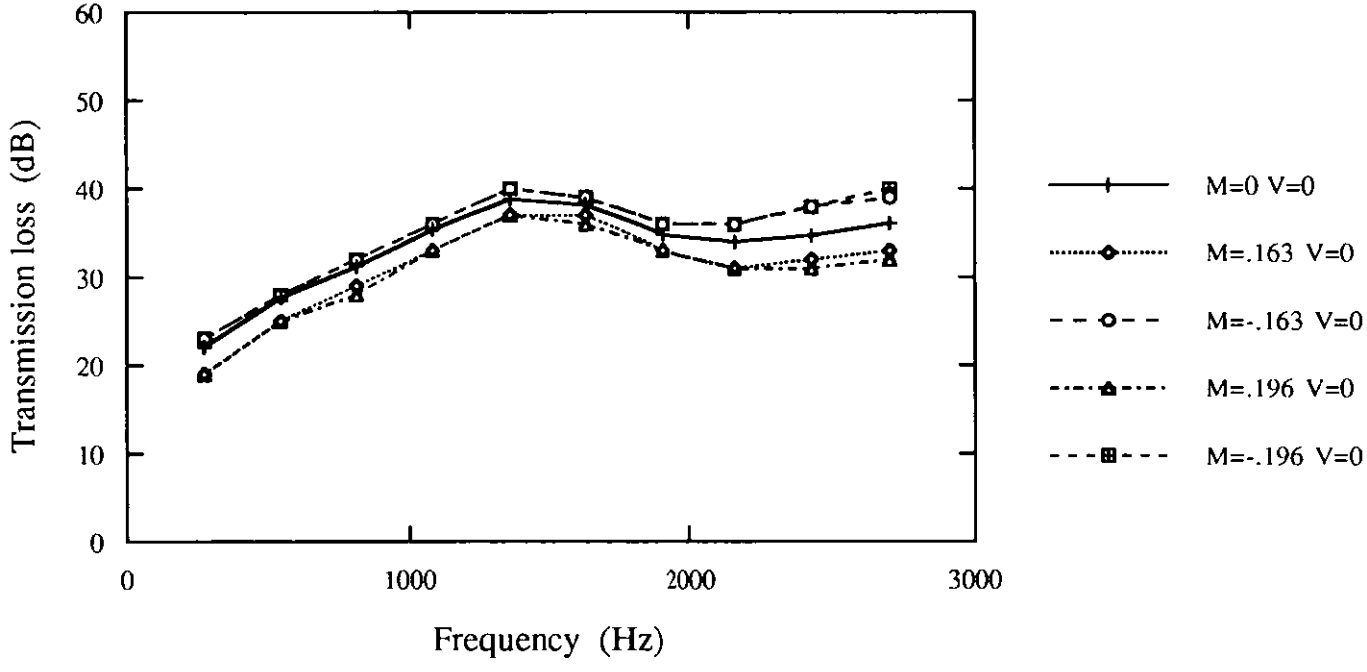

Figure 5.9. Transmission loss of the second test silencer extended to a length of 300mm. without induced steady flow.

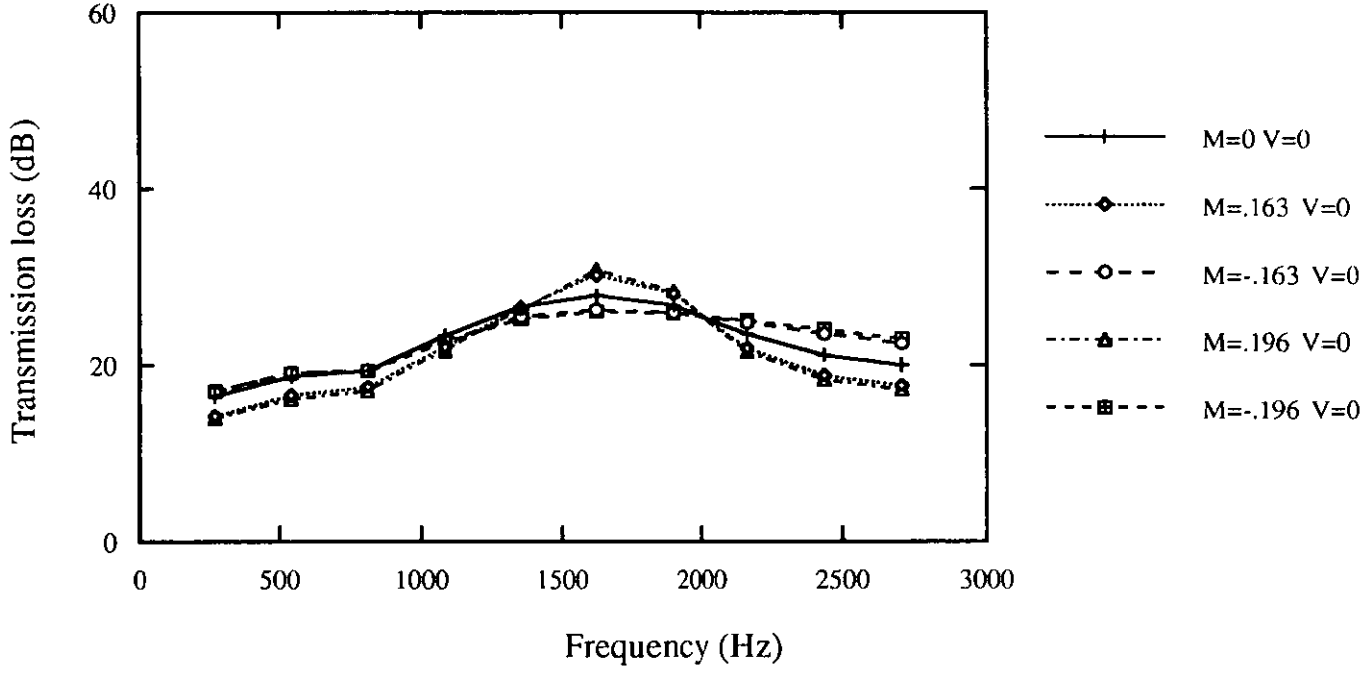

Figure 5.10. Transmission loss of the second test silencer with the outer radius reduced to 80mm, without induced steady flow.

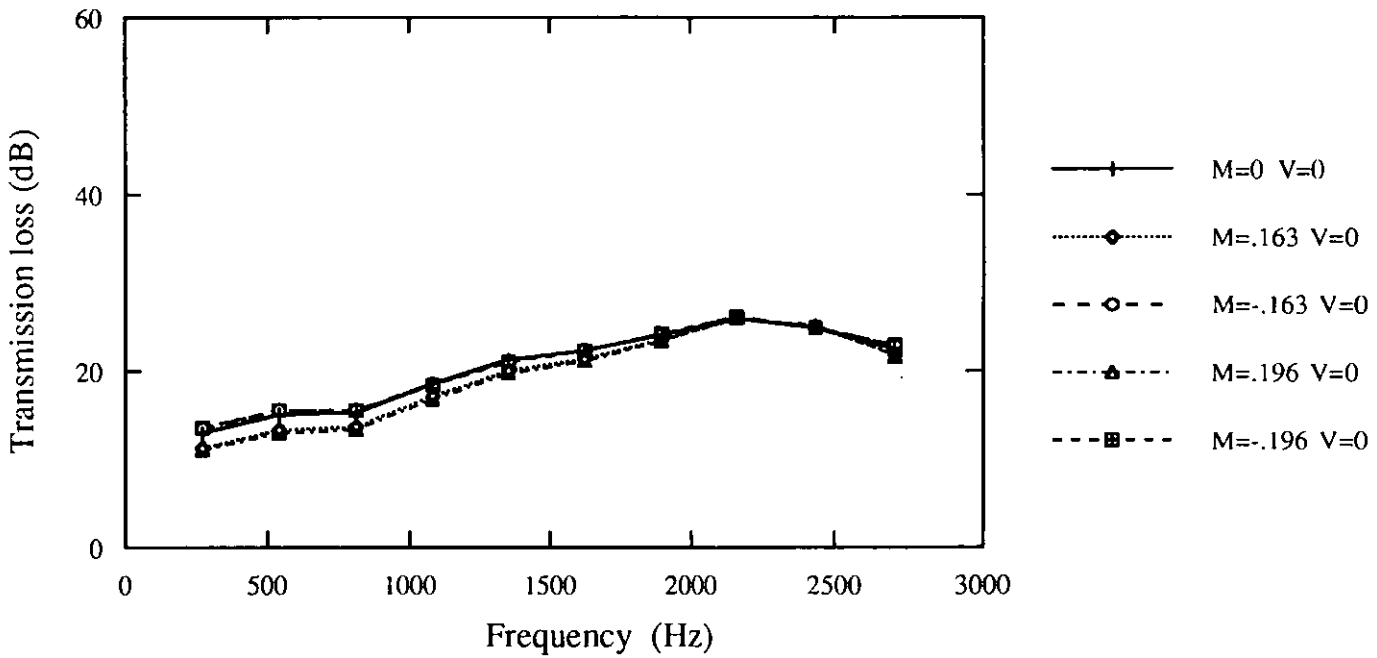

Figure 5.11. Transmission loss of the second test silencer with the outer radius reduced to 60mm, without induced steady flow.

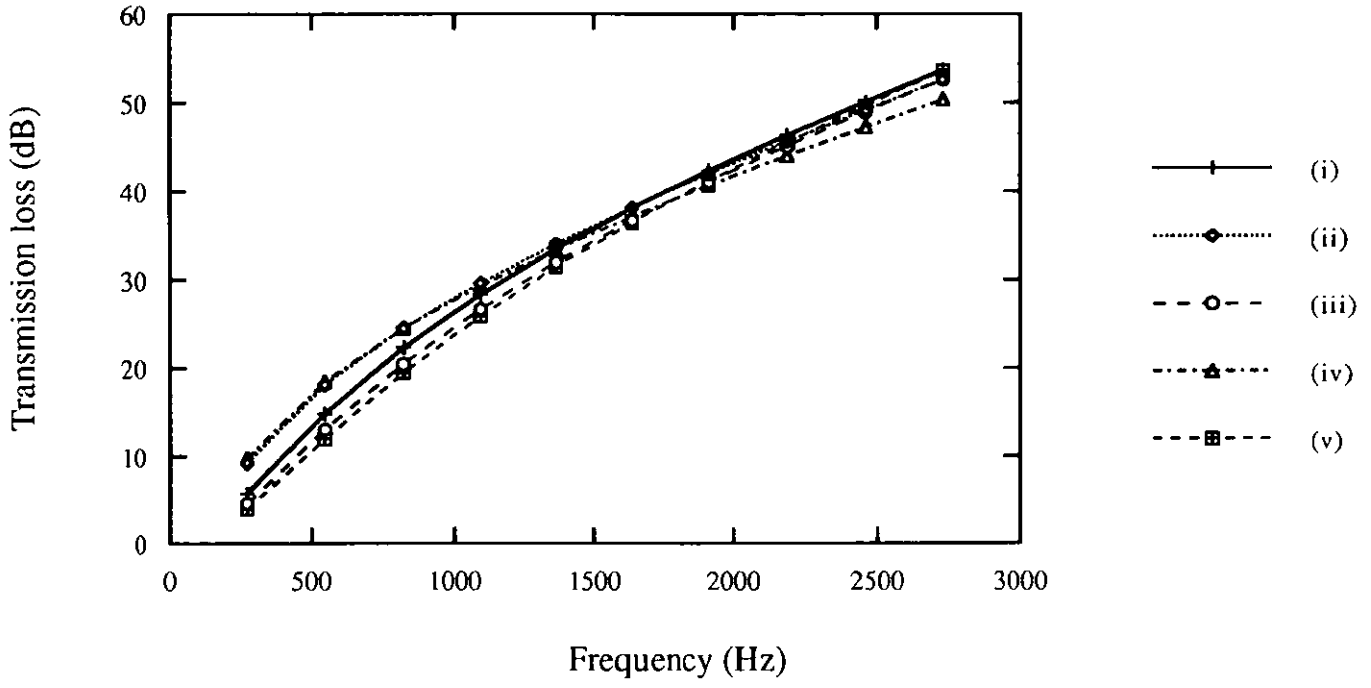

Figure 5.12(a). Transmission loss in the first test silencer, mean flow Mach number M=0.0, (i) No material variation. (ii) Variation along length, from highest density at the inlet end to the lowest density at the outlet end. (iii) Variation along length in opposite sense. (iv) Radial variation from highest density at the inner radius to the lowest density at the outer radius. (v) Radial variaton in opposite sense.

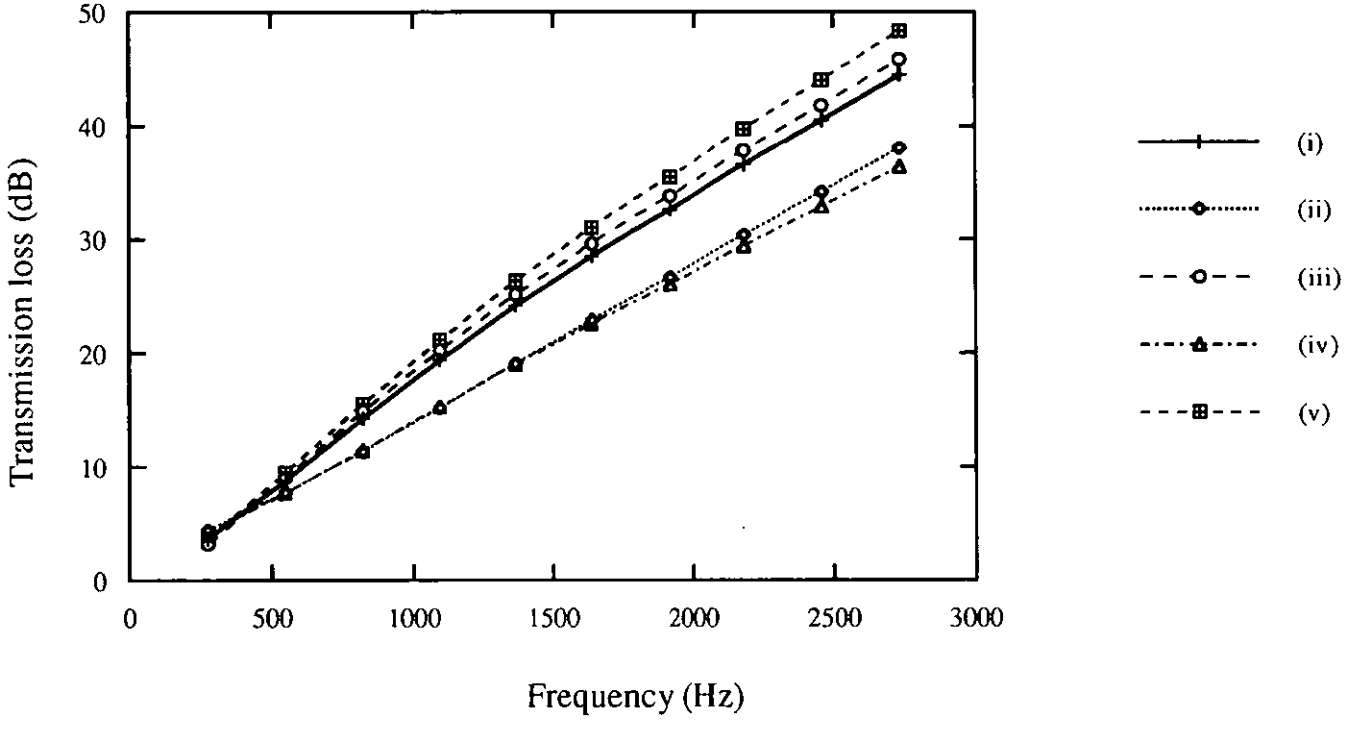

Figure 5.12(b). Transmission loss in the first test silencer, mean flow Mach number M=0.163 Without induced steady flow, (i) No material variation. (ii) Variation along length, from highest density at the inlet end to the lowest density at the outlet end. (iii) Variation along length in opposite sense. (iv) Radial variation from highest density at the inner radius to the lowest density at the outer radius. (v) Radial variaton in opposite sense.

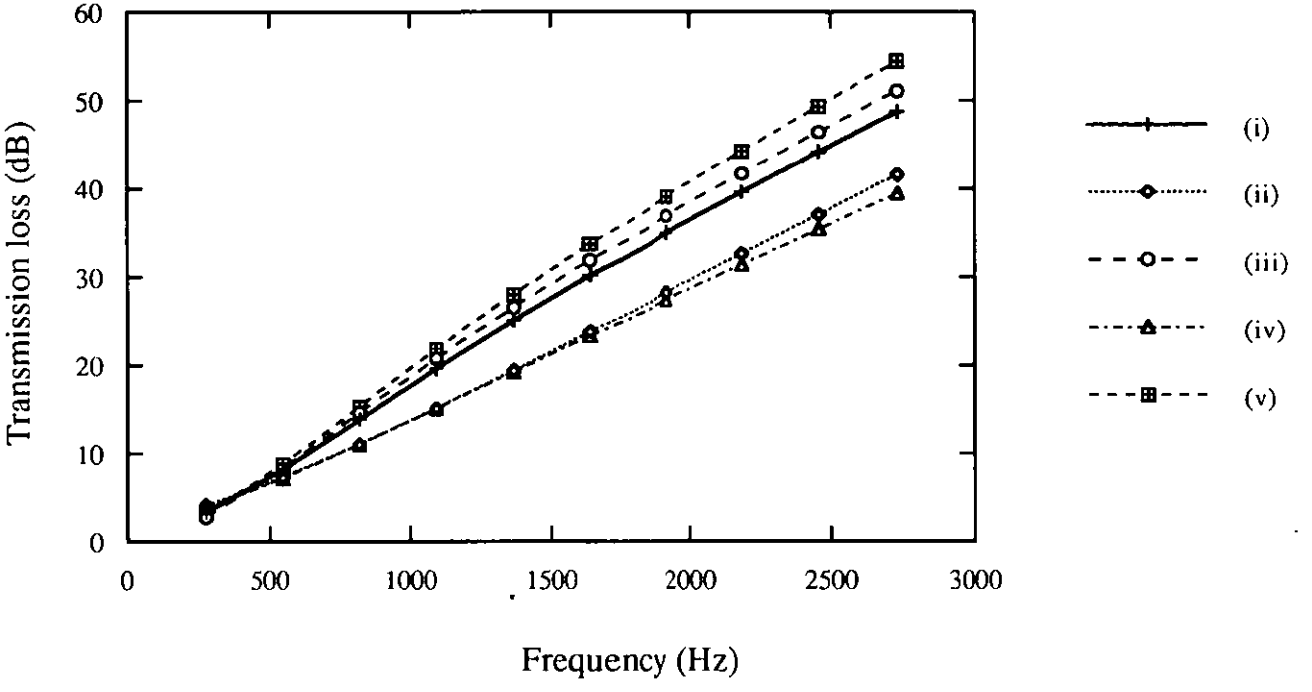

Figure 5.12(c). Transmission loss in the first test silencer, mean flow Mach number M=0.163 with induced steady flow (i) No material variation. (ii) Variation along length, from highest density at the inlet end to the lowest density at the outlet end. (iii) Variation along length in opposite sense. (iv) Radial variation from highest density at the inner radius to the lowest density at the outer radius. (v) Radial variaton in opposite sense.

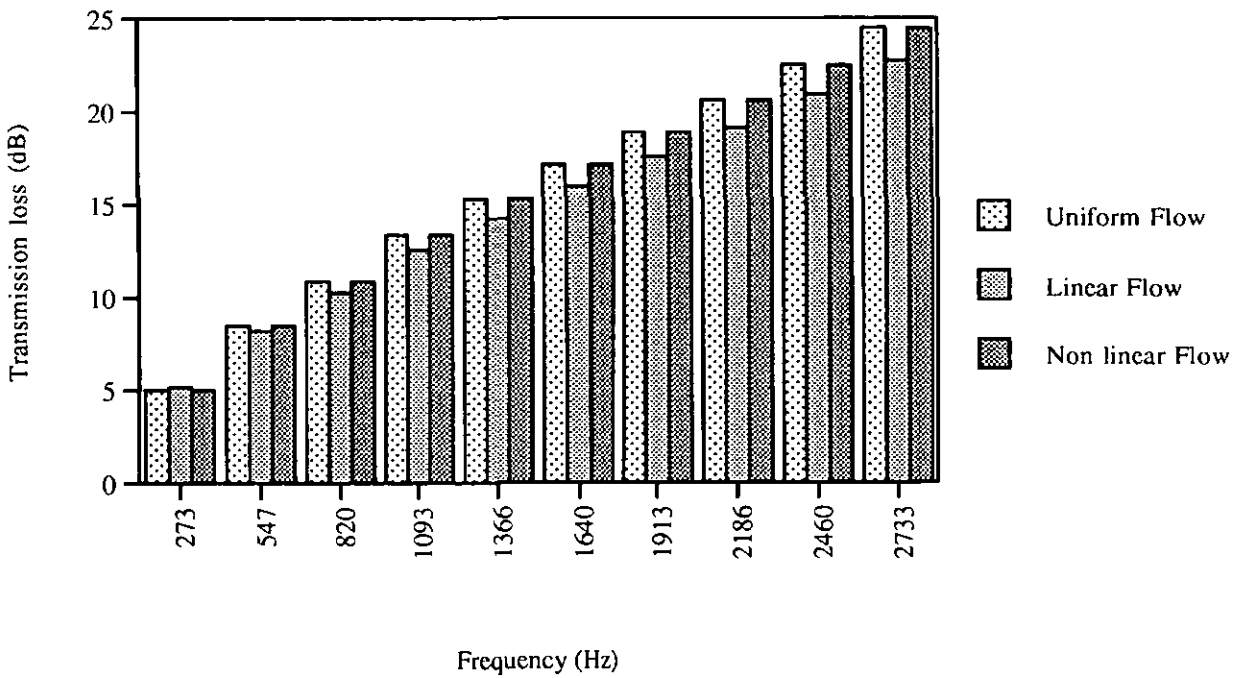

Figure 5.13. Comparison of results between uniform, linear and nonuniform induced steady flow in the first test silencer, mean flow Mach number M=.163

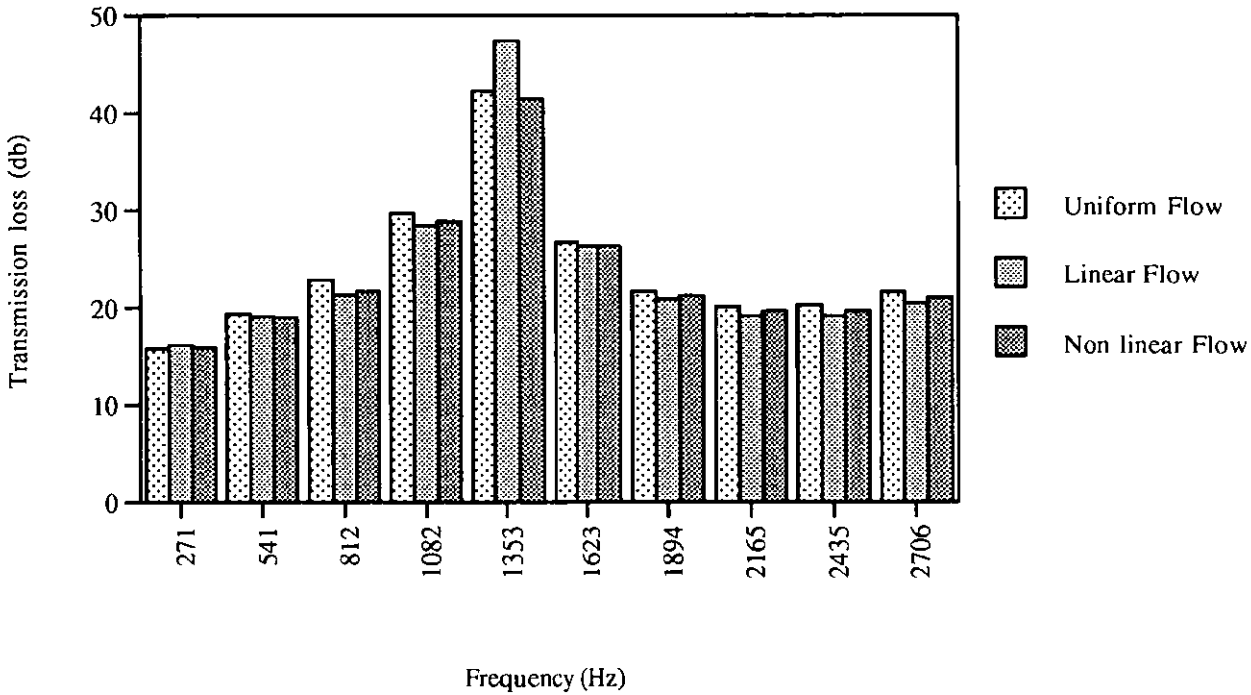

Figure 5.14. Comparison of results between uniform, linear and nonuniform induced steady flow in the second test silencer, mean flow Mach number M=.163

CHAPTER 6

ANALYSIS OF ABSORPTION SILENCERS WITH A NON-UNIFORM FLOW DUCT

6.1 Introduction

This chapter extends the finite element formulation given in Chapter 5 to consider non-uniform flow in the central duct, caused either by non-uniformity in cross-section of the flow duct or by regions of absorbent material placed within the flow duct. Both non-uniform steady flow of low Mach number in the central duct and the nonlinear steady flow field which is induced in the absorbent are evaluated. In subsequent acoustic analysis, the effects of these steady flow fields on the convection of acoustic waves and the properties of the absorbent material are included.

The non-uniform flow formulation is first applied to the case of non-uniform dissipative silencers of arbitrary cross-section with non-uniform mean flow in the central duct, and then the boundary conditions are modified to consider the case of "anechoic" terminations of flow ducts.

6.2 Analysis

In this analysis, the formulation used in chapter 5 is modified to consider a duct R_1 of arbitrary, non-uniform cross-section and of finite length, see Figure 6.1. Thus the steady convective flow within the duct is non-uniform, with velocity $U(x_1, x_2, x_3)$ say, and is assumed to be of low Mach number M, such that the steady flow may be regarded as incompressible. Region R_2 is a volume of arbitrary shape which is packed with porous material, which may be inhomogeneous and anisotropic. The outer walls of regions R_1 and R_2, the boundary $\Gamma_W = \Gamma_{W1} + \Gamma_{W2}$, are assumed to be rigid and impervious. Upstream and downstream of the absorbent region, it is assumed that only plane-wave components are present in the flow duct on the inflow and outflow boundaries of region R_1, Γ_I and Γ_O respectively. Regions R_1 and R_2 share a common boundary Γ_c, as in Chapter 5.

6.2.1 Governing equations in the flow duct

For non-uniform steady flow of low Mach number in the flow duct, the equation of the steady flow and the acoustic wave and momentum equations follow from equations (3.31), (3.35) and (3.34) respectively, namely

$$\nabla^2 \overline{\phi} = 0, \tag{6.1}$$

$$\nabla^2 p_1' = \frac{1}{c_0^2}\left\{\frac{\partial^2 p_1'}{\partial t^2} + 2\nabla\overline{\phi}\cdot\nabla\frac{\partial p_1'}{\partial t}\right\} \tag{6.2}$$

and

$$\rho_0\left\{\frac{\partial}{\partial t} + \nabla\overline{\phi}\cdot\nabla\right\}\phi_1' = -p_1', \tag{6.3}$$

where ρ_0 is the density of the mean flow, p_1' is the acoustic pressure, $\overline{\phi}$ is the steady flow velocity potential and ϕ_1' is the acoustic velocity potential, such that

$$U(x_1, x_2, x_3) = \nabla\overline{\phi} \quad \text{and} \quad q_1' = \nabla\phi_1', \tag{6.4 a,b}$$

where q_1' is the acoustic velocity. For harmonic time variation $e^{i\omega t}$, the acoustic equations (6.2) and (6.3) become

$$\nabla^2 p_1' + 2ik\nabla\tilde{\phi}M \cdot \nabla p_1' + k^2 p_1' = 0 \tag{6.5}$$

and

$$\rho_o c_0 \left(ik + M\nabla\tilde{\phi}\cdot\nabla\right) q_1' = -\nabla p_1', \tag{6.6}$$

where $k = \omega / c_0$ is the wavenumber and $\tilde{\phi}$ is a dimensionless velocity potential, such that $M\nabla\tilde{\phi} = U / c_0$, where M is the Mach number and c_0 is the speed of sound.

6.2.2 Governing equations in the absorbent

Conditions in the absorbent region are exactly the same as for the formulation in Chapter 5, thus the governing equations are identical. From equation (5.8) the steady flow equation is

$$\nabla\cdot[\overline{\Sigma}]^{-1}\nabla\overline{p}_2 = 0 \tag{6.7}$$

where $[\overline{\Sigma}]$ is a diagonal matrix whose jth element is $\left(\sigma_{vj} + \sigma_{ij} \mid \overline{q}_2 \mid\right)$ and σ_{vj}, σ_{ij} are the viscous and inertial flow resistive coefficients respectively, in direction x_j.

The acoustic wave and momentum equations follow from equations (5.10) and (5.11), namely

$$\rho_0 \omega^2 \Omega \chi p_2' + \nabla \cdot [R] \nabla p_2' = 0 \tag{6.8}$$

and

$$i\omega \rho_0 q_2' = -[R] \nabla p_2' \tag{6.9}$$

where Ω is the volume porosity, χ is the compressibility and $[R]$ is a diagonal matrix whose jth element is ρ_0 / ρ_{aj}. ρ_{aj} is the effective, complex, mean fluid density in the pores of the material for motion in direction j. Expressions for relevant acoustical properties are given in equations (5.12) to (5.18)

6.2.3 Boundary conditions

The first task is to determine the steady flow field in the non-uniform duct. A set of boundary conditions are imposed at the input and output ends. Thus for mean flow the boundary conditions are:-

$$\frac{\partial \tilde{\phi}}{\partial n} = 0 \tag{6.10}$$

along the duct wall and centreline, n being the outward normal to the surface, such that component of velocity normal to a hard wall boundary is zero,

$$\frac{\partial \tilde{\phi}}{\partial n} = \text{constant} \tag{6.11}$$

along the outlet plane, i.e. axial velocity is uniform at outflow and

$$\tilde{\phi} = \text{constant} \tag{6.12}$$

at the inlet plane boundary, such that the inflow velocity is axial.

For the complete acoustic solutions, two different sets of boundary conditions are implemented for the two different areas of applications, namely complete absorption silencers and "anechoic" terminations of flow ducts. In both cases the component of acoustic velocity normal to the hard walls of boundary Γ_w is zero, which in turn implies from equations (6.6) and (6.9) that

$$\nabla p' \cdot \boldsymbol{n} = 0 \quad \text{on} \quad \Gamma_w \tag{6.13}$$

for both regions R_1 and R_2, where $\boldsymbol{n}$ is a unit normal vector to the boundary. Similarly on the common boundary Γ_c, in both applications, there is continuity of pressure and the normal component of displacement, thus

$$p_1' = p_2' \quad \text{and} \quad \underline{\xi}_1' \cdot \boldsymbol{n}_c = \underline{\xi}_2' \cdot \boldsymbol{n}_c \text{ on } \Gamma_c, \tag{6.14 a,b}$$

where $\underline{\xi}'$ is the particle displacement vector and $\boldsymbol{n}_c$ is a unit normal vector to Γ_c. Since convective acceleration terms are negligible in region R_2, the continuity of displacement boundary condition (6.14) can be re-written in terms of normal pressure gradients

$$[1 - \mathrm{i}(M/k)\nabla\tilde{\phi} \cdot \nabla]^2 [R] \nabla p_2' \cdot \boldsymbol{n}_c = \nabla p_1' \cdot \boldsymbol{n}_c \tag{6.15}$$

Case 1

This case involves the solution of any general noise reduction measure for non-uniform absorption silencer systems. Hence boundary conditions are imposed on the inlet and outlet flow boundaries Γ_I and Γ_0 of flow duct R_1, such that the four-pole parameters

can be evaluated. This involves two separate solutions of the entire problem with different inflow and outflow boundary conditions, which follow from equations (5.24) and (5.25) of Chapter 5, namely

$$\nabla p_1' = \text{constant on } \Gamma_I \quad , \quad p_1' = 0 \text{ on } \Gamma_O \tag{6.16a,b}$$

and

$$p_1' = \text{constant on} \quad \Gamma_I \quad , \quad q_1' = 0 \;\Rightarrow\; \nabla p_1' = (ikM\nabla\tilde{\phi})p_1' \quad \text{on} \quad \Gamma_O. \tag{6.17a,b}$$

Case 2

This case involves the analysis of the effectiveness of so-called "anechoic" terminations of flow ducts. Thus a set of boundary conditions are imposed to determine the reflection coefficient at the inlet plane of the termination. It is assumed that, at the outlet plane of the termination, sound radiates into free space and that there is a known radiation impedance at this boundary. Furthermore, it is assumed that only the plane-wave component is present at the inflow boundary and that the flow is uniform and axial on both inflow and outflow boundaries. Thus

$$p_1' = \text{const. on} \quad \Gamma_I \qquad \partial p_1' / \partial x_1 = (ikM\,\partial\tilde{\phi} / \partial x + ik / Z)p_1' \quad \text{on} \quad \Gamma_O \tag{6.18a,b}$$

where the radiation impedance, Z, in the presence of mean flow from the open end of an unflanged pipe of circular cross-section is given by

$$Z = Z_0 - M(1 + k^2(0.6133r_0)^2), \tag{6.19}$$

see Munjal [1], where Z_0 is the value of the radiation impedance in the zero flow case and is given in tabular form in Morse and Ingard [37]. For radiation from pipes of

non-circular cross-section, the radiation impedance was assumed to be that from a circular pipe of equivalent cross-sectional area.

6.3 Finite Element Formulation

The only new formulation required here is that for steady flow in a non-uniform duct. The other formulations follow almost straight from Chapter 5.

6.3.1 Steady flow in non-uniform duct

Let $\psi_J(x_1,\ x_2,\ x_3)$ be the a global basis function associated with node J of a finite element mesh. Suppose there are N_1 global nodes within the flow duct region R_1, such that the approximation to the steady flow velocity potential $\tilde{\phi}$ is given by the trial solution

$$\tilde{\phi} \approx \sum_{J=1}^{N_1} \psi_J \tilde{\phi}_J, \tag{6.20}$$

where $\tilde{\phi}_J$ is the value of $\tilde{\phi}$ at the Jth node. The Galerkin formulation uses weighting functions $\psi_I(x_1,\ x_2,\ x_3)$ to form weighted residual statements of equation (6.1), namely

$$\int_{R_1} \psi_I \left(\nabla\cdot\nabla\tilde{\phi}\right) dV = 0 \ , \ I = 1 \text{ to } N_1. \tag{6.21}$$

The 'weak' Galerkin formulation follows from application of Green's theorem to equation (6.21) to give,

$$\left\{\int_{R_1} (\nabla \psi_I \cdot \nabla \psi_J)\, dV\right\}\{\underline{\tilde{\phi}}\} = \int_{\Gamma_1} \psi_I \nabla \tilde{\phi} \cdot \boldsymbol{n}_1\, d\Gamma, \tag{6.22}$$

where $\{\underline{\tilde{\phi}}\}$ is the vector of nodal values $\tilde{\phi}_J$ and Γ_1 is the entire bounding surface of region R_1. The boundary integral is zero over Γ_{w1}, due to the hard-wall boundary condition, and at the inlet boundary Γ_I, $\tilde{\phi}$ is set constant whereas at the outlet boundary Γ_0, the normal derivative of $\tilde{\phi}$ is set constant and equal to 1, such that M is the actual flow Mach number in this plane. Thus equation (6.22) can be solved for the unknown nodal values $\tilde{\phi}$, where the boundary conditions are implemented in the manner outlined in Chapter 2.

6.3.2 Steady flow in the porous material

The 'weak' Galerkin formulation for steady flow in porous region follows from Chapter 5 equations (5.28) and (5.29) to give the steady flow velocity field, namely

$$\left\{\int_{R_2} \left(\nabla \psi_I \cdot [\overline{\Sigma}]^{-1} \nabla \psi_J\right)\, dV\right\}\{\overline{p}_2\} = \int_{\Gamma_2} \psi_I [\overline{\Sigma}]^{-1} \nabla \overline{p}_2 \cdot \boldsymbol{n}_2\, d\Gamma, \tag{6.23}$$

$$\overline{q}_2 = -\sum_{J=1}^{N_2} [\overline{\Sigma}]^{-1} \nabla \psi_J \overline{p}_{2J} \tag{6.24}$$

where $\{\overline{p}_2\}$ is the vector of nodal values $\overline{p}_{2J}$ and Γ_2 is the entire bounding surface of region R_2. It should be remembered that the equation is non-linear, since the terms of $[\overline{\Sigma}]$ are flow-dependent. The iterative scheme for solution is outlined in Section 5.2.2 of Chapter 5.

6.3.3 Acoustic field in the flow duct

Taking the same assumptions of trial functions as in Chapter 5 the final Galerkin form of acoustic field equation in flow duct equation (6.4) can be written as

$$\left\{\int_{R_1}\left(\nabla\psi_I\cdot\nabla\psi_J+2\mathrm{i}Mk\nabla\tilde{\phi}\cdot\nabla\psi_J-k^2\psi_I\psi_J\right)\,dV\right\}\{p_1'\}$$
$$=\int_{\Gamma_1}\psi_I\nabla p_1'\cdot\boldsymbol{n}_1\;d\Gamma, \qquad (6.25)$$

where $\tilde{\phi}$ is the velocity potential obtained from the solution of the steady flow equation (6.22). There are two differences from the corresponding equation of Chapter 5, where the mean flow was uniform. The first-order term in the Mach number now has the term $\nabla\tilde{\phi}$ which varies throughout the flow field and the second-order term in the Mach number is absent. The reason for this is that terms of $0[M^2]$ had to be negligible for the mean flow to be regarded as incompressible, see Chapter 3, hence it would be inconsistent to retain terms of $0[M^2]$ in the acoustic equation.

6.3.4 Acoustic field in the absorbent

The Galerkin formulation of the acoustic equation in region R_2 follows from Chapter 5, equation (5.36), namely

$$\left\{\int_{R_2}\left(\nabla\psi_I\cdot[G]\nabla\psi_J-k^2\psi_I\psi_J\right)\,dV\right\}\{p_2'\}=\int_{\Gamma_2}\psi_I[G]\nabla p_2'\cdot\boldsymbol{n}_2\,d\Gamma, \qquad (6.26)$$

where $[G]$ is a diagonal matrix whose jth element is $1/\gamma_j^2$ and $\boldsymbol{p}_2'$ is the vector of nodal p_{2J}' values.

For coupling the two acoustic equations, the gradient evaluation technique which was outlined in Chapter 5 has been used.

6.4 Results

The computational scheme for the finite element formulation described above was initially tested for an absorption silencer, the first test silencer of Chapter 5 shown in Figure 5.2, with the same uniform mesh as given there. The formulation was then applied to analyse a similar test silencer of non-uniform cross-section, obtained by modifying the shape, see Figure 6.2, such that the outflow diameter is increased by about 200%. This resulted is an expansion angle of 5^0, around the limit before which flow separation would occur making the potential solution of the mean flow invalid. The results were obtained in terms of transmission loss with a flow Mach number at the outlet end of M=.163. They are compared with the results from the uniform duct case in Figure 6.3. There is an increase in the transmission loss for the non-uniform expansion nozzle case as compared with the uniform duct case, both with and without mean flow. The difference is greater without steady flow. It should be noted that the mass of absorbent material in the silencer is greater for the expansion nozzle case than for the uniform duct. Furthermore, in the case of the uniform duct results with mean flow, the transmission loss is greater than for the identical case in Chapter 5, Figure 5.3, due to neglect of the higher order terms of flow Mach number in the present theoretical model.

Analysis has been carried out for the two "anechoic" termination models shown in Figures 6.4 and 6.5. Both models are axisymmetric, the simplest case for application of the above formulation to three-dimensional ducts. The flow duct of the first is non-uniform due to the insertion of an absorbent core, whereas in the second case there is slight expansion of the actual flow duct. This second test case is exactly as prescribed in ISO 7235 [95] except for the omission of a perforated screen (the effects of such

screens are assumed to be negligible), whereas the first test case is an approximation to an ISO standard termination.

Results have been obtained in terms of the pressure reflection coefficient at the inlet to the termination and are shown in Figures 6.6 to 6.9. Two types of absorption material, E. Glass (Lancaster Glass Fibre) and polyether foam, with different densities were used in determining the pressure reflection coefficient. Figure 6.6 shows the reflection coefficient for the first test case anechoic termination with polyether foam as the porous material. The material properties are given in Table 4.1. Figure 6.7 shows results for the same termination but with E. Glass as the porous material. It was assumed that the E. Glass had uniform density and the values of flow resistivity used were the average of the extremes given in Table 6.1. For both materials, results in terms of pressure reflection coefficient have been computed for flow Mach numbers of M=0, M=0.163 and M=0.196. In these results resonances of the termination section are clearly observed both with and without mean flow. Even between the resonances, the terminations are far from being "anechoic", the best result being for polyether foam absorbent at frequencies approaching 1 kHz.

The reflection coefficients obtained from the second test case, with no flow and with both flow Mach numbers, are shown in Figures 6.8 and 6.9. For the results of Figure 6.8 the absorbent material was taken to be polyether foam of uniform density, see Table 4.1, whereas for the results of Figure 6.9, E. Glass of two different densities was used, exactly as specified in the ISO standard [95] and as given in Table 6.1. In both figures, the reflection coefficient seems to be reasonably low at frequencies from 100 Hz to 800 Hz, both with flow and without flow. Indeed the presence of mean flow makes for very little difference. It is clear from the figures of both test cases that the geometry of the termination strongly affects the pressure reflection coefficient, whereas

the choice of the porous material has marginal effects. The performance of the second type of anechoic termination is much better than that of the first type.

6.5 Conclusion

A theoretical model for the analysis of acoustic wave motion in a non-uniform flow duct and adjacent bulk-reacting absorbent material has been presented. The finite element formulation and computational scheme used in chapter 5 have been modified for this non-uniform flow formulation. Two different applications have been given, firstly results in terms of four-pole parameters and overall transmission loss for complete absorption silencers, and secondly computation of the pressure reflection coefficient for "anechoic" terminations of flow ducts. Effects of differing flow Mach number and type of absorbent material packing have been studied. Although only a few test cases have been examined, so only a limited amount of acoustic design information has been obtained, the method can easily be applied to the study of different combinations of materials and different termination or silencer geometries.

Table 6.1

Delany-Bazley coefficients for E glass absorbent material*

Delany-Bazley coefficient	Porous material
	E Glass
c_1	0.2202
c_2	-0.5827
c_3	0.2010
c_4	-0.5829
c_5	0.0954
c_6	-0.6687
c_7	0.1689
c_8	-0.5707

Flow resistivity coefficients

Porous material	Flow resistivity σ_v, σ_i
E.Glass	max 5948,4170
	min 1717,1140

* Data kindly provided by Dr. A. Cummings and R. Kirby, Department of Engineering Design and Manufacture, University of Hull.

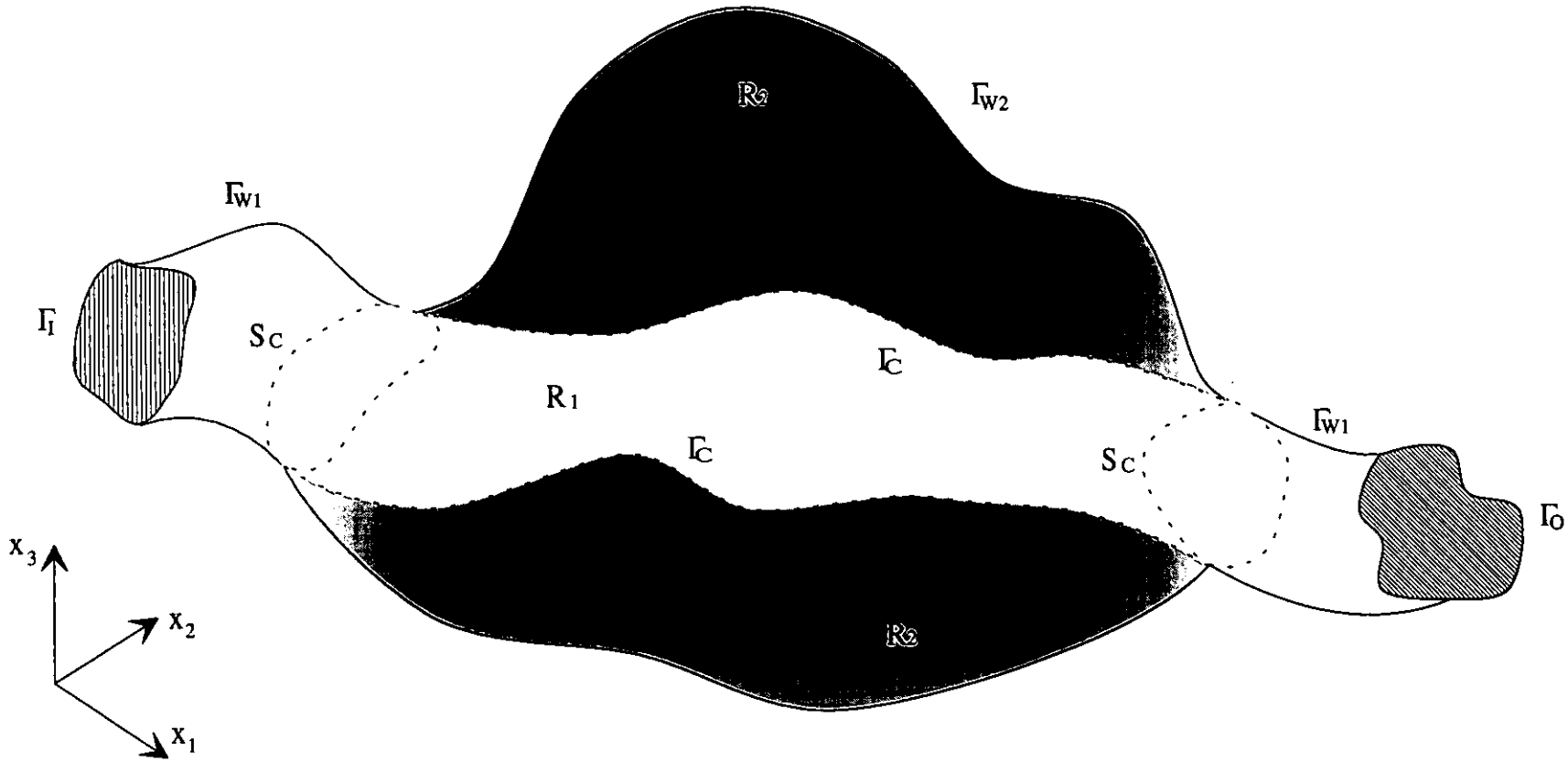

Figure 6.1 Geometry and coordinate system

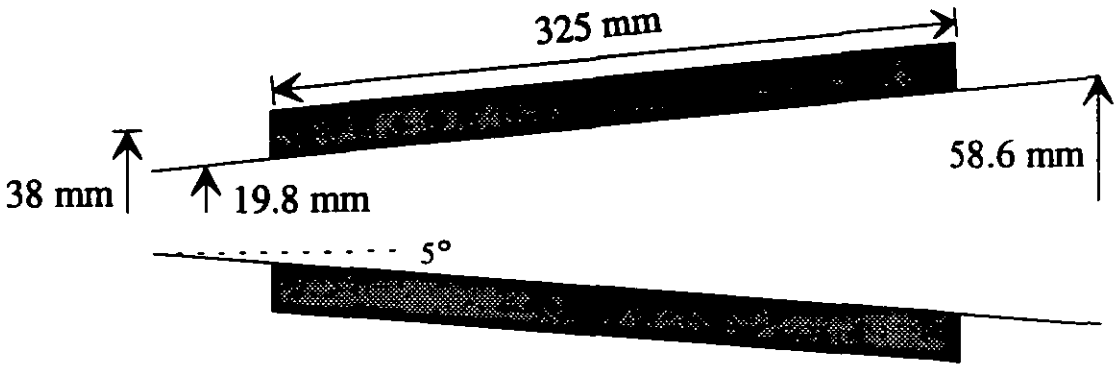

(a)

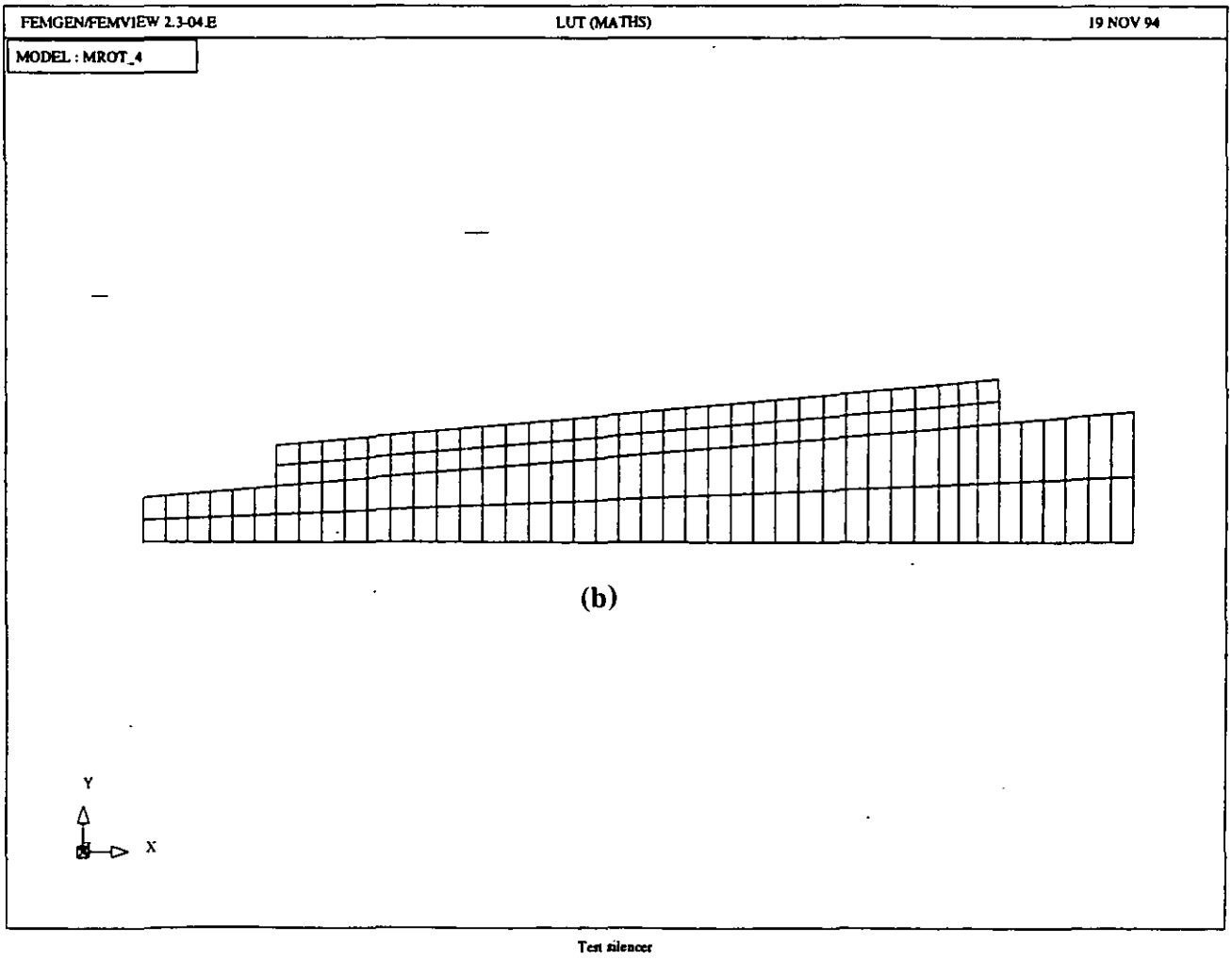

(b)

Figure 6.2 Variation of the test silencer of Figure 5.2 to a non-uniform duct. **(a)** Geometry **(b)** Finite element mesh

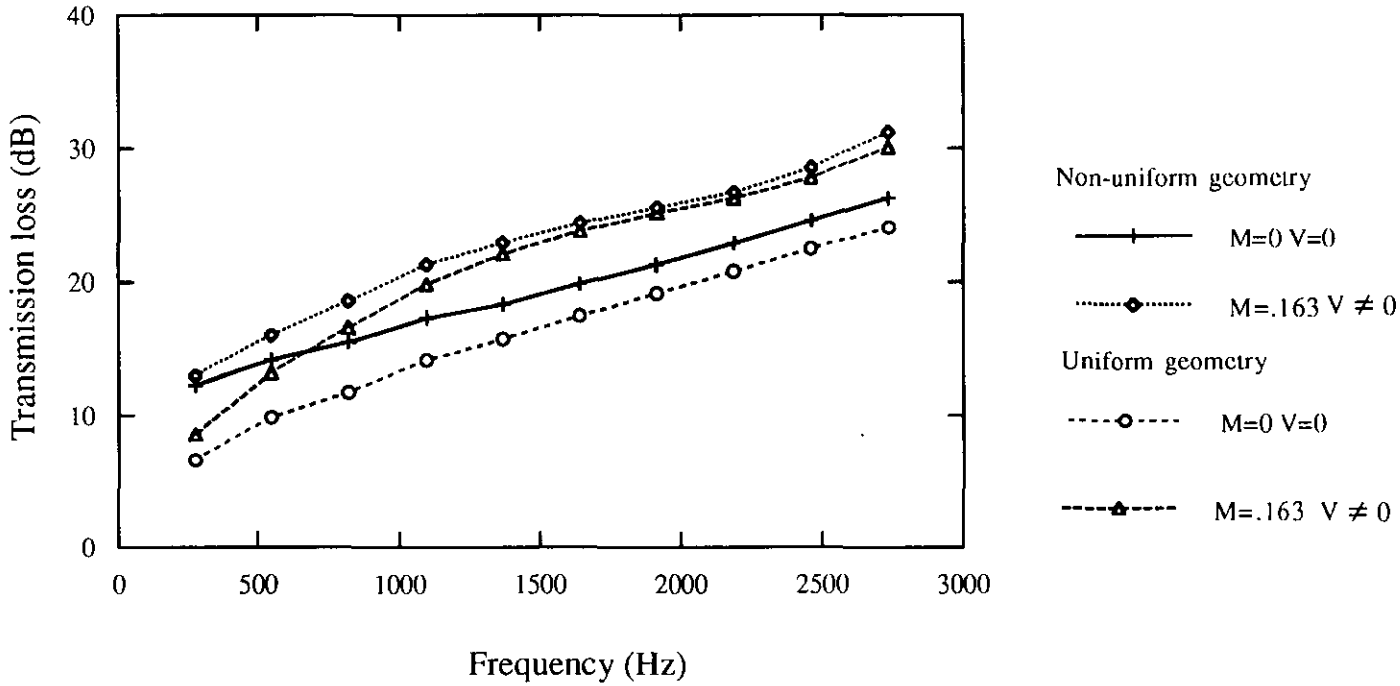

Figure 6.3 Comparison of transmission loss between uniform and non-uniform ducts.

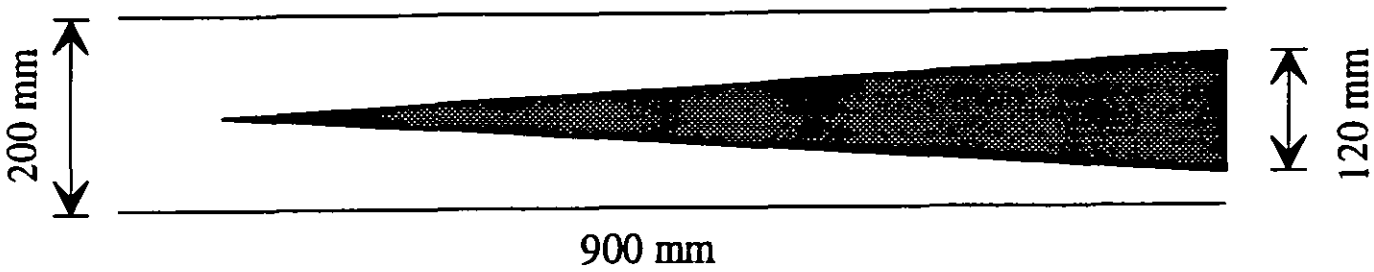

(a)

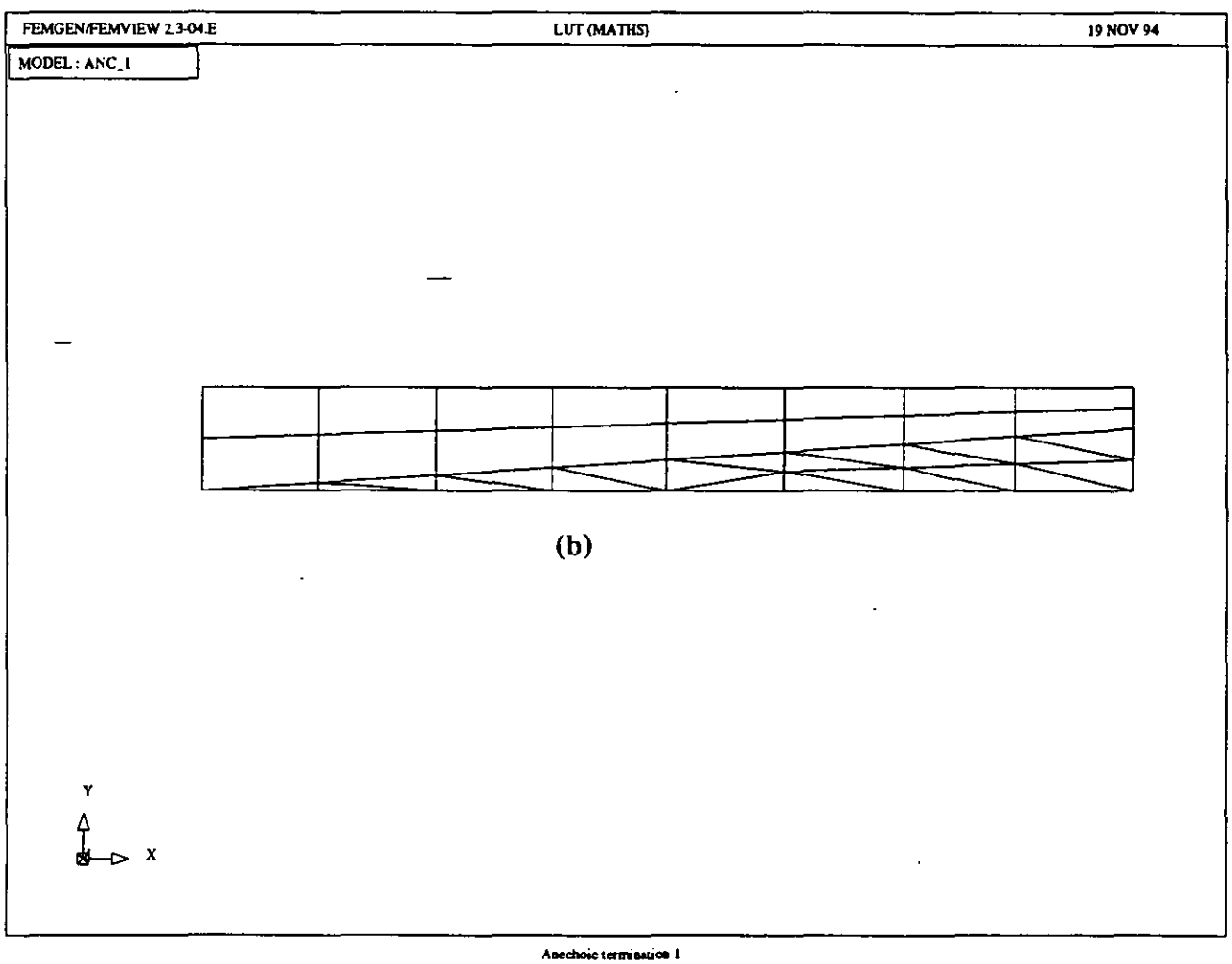

(b)

Figure 6.4 Anechoic termination of flow duct, test case 1. **(a)** Geometry **(b)** Finite element mesh

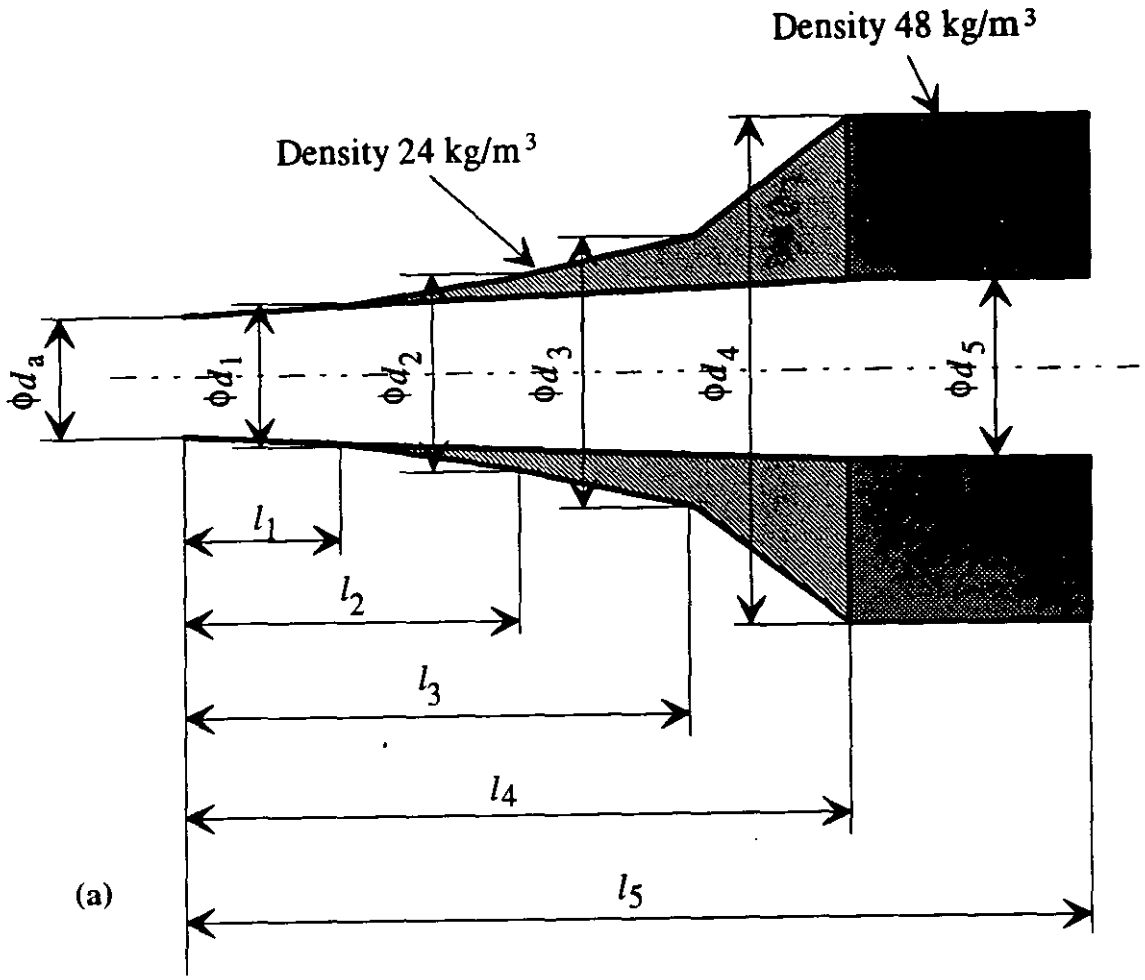

Duct internal diameter, d_a = 460 mm			
d_1	1,15 d_a	l_1	1,44 d_a
d_2	1,64 d_a	l_2	2,89 d_a
d_3	2,25 d_a	l_3	3,89 d_a
d_4	3,44 d_a	l_4	5,11 d_a
d_5	1,67 d_a	l_5	6,44 d_a

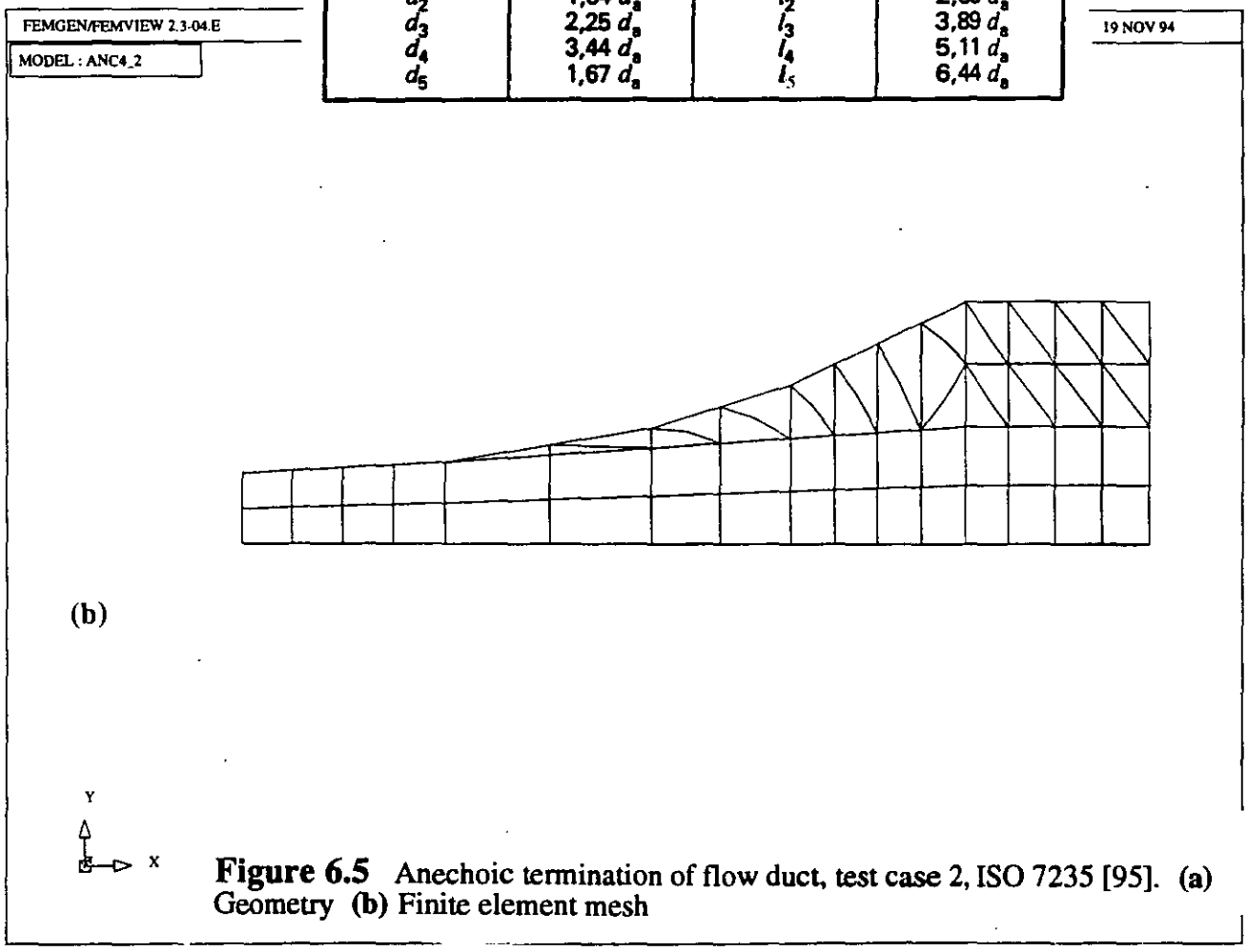

Figure 6.5 Anechoic termination of flow duct, test case 2, ISO 7235 [95]. **(a)** Geometry **(b)** Finite element mesh

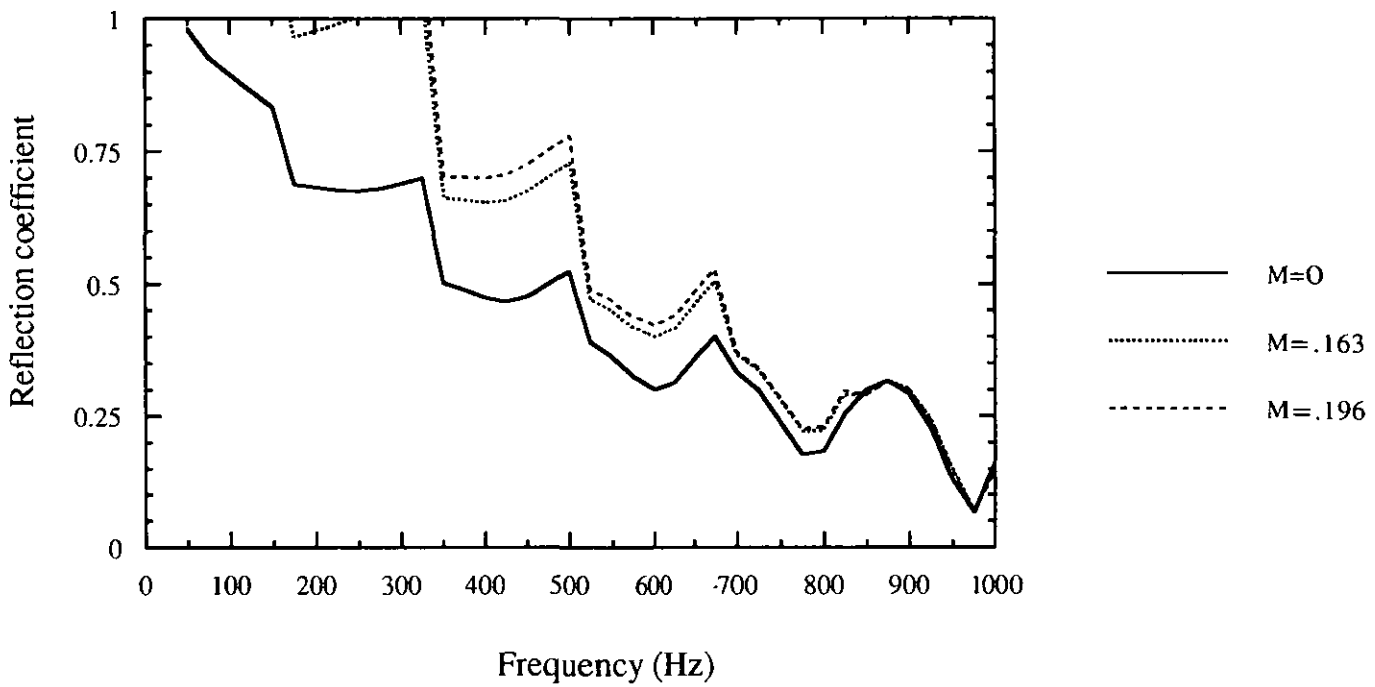

Figure 6.6 Pressure reflection coefficient vs. frequency of first test case anechoic termination with polyether foam absorbent material.

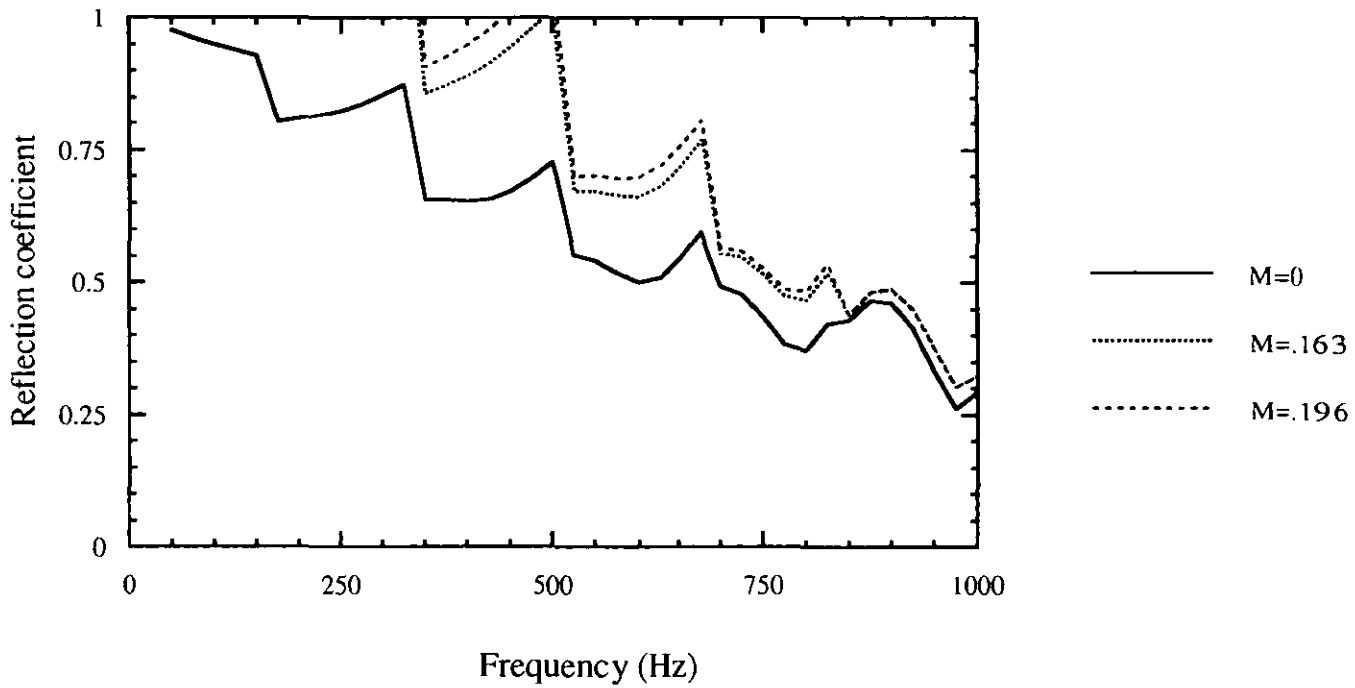

Figure 6.7 Pressure reflection coefficient vs. frequency of first test case anechoic termination with E. glass absorbent material.

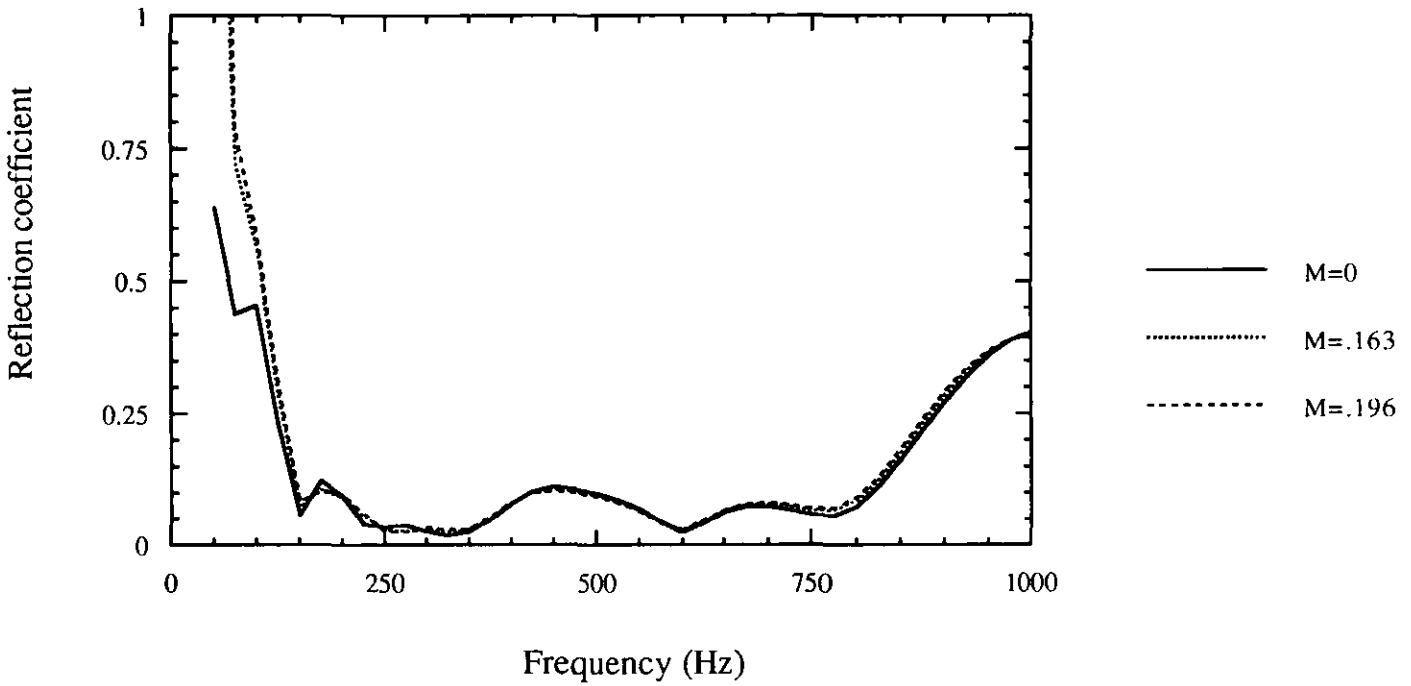

Figure 6.8 Pressure reflection coefficient vs. frequency of second test case anechoic termination with polyether foam absorbent material.

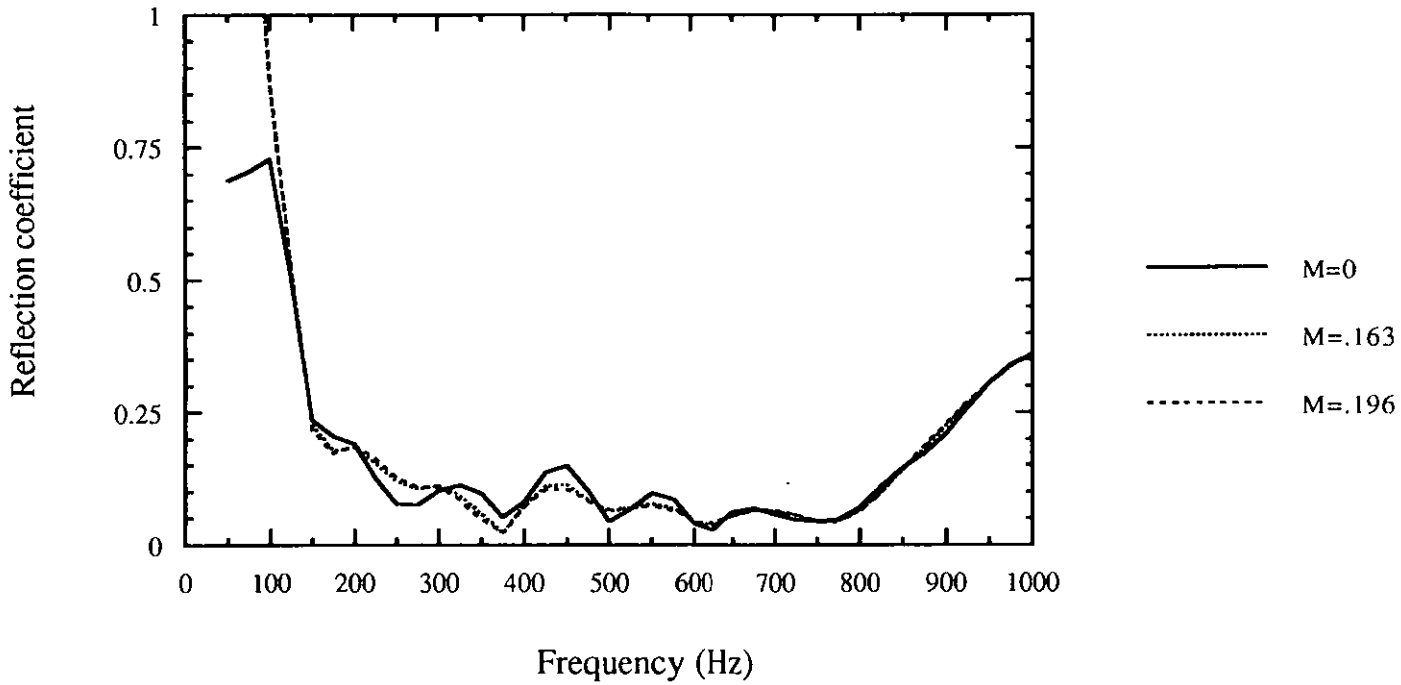

Figure 6.9 Pressure reflection coefficient vs. frequency of second test case anechoic termination with E. glass absorbent material.

CHAPTER 7

CONCLUSIONS AND SUGGESTIONS FOR FURTHER WORK

7.1 Discussion

Acoustic wave motion in complex absorption silencers with mean flow has been studied. Computational techniques using the Galerkin finite element method were developed for determination of the acoustic performance of such systems, both by forced response and eigenvalue analysis. The finite element proved to be an ideal choice to perform such analysis and to predict accurate results which are of use in the design of such complex silencers. Acoustic design information was obtained in terms of sound attenuation and phase speed from the eigenvalue analysis model and this compared well with some established results by Cummings and Chang [18] for simple silencers. Detailed investigations were then carried out to obtain design information regarding the effects upon performance of silencer shape, the density variation of absorbent material and inclusion of induced mean flow in the absorbent. The model incorporated both uniform flow of gas in the open central passage and non-uniform induced flow in the absorbent.

In the forced response model, a comprehensive finite element scheme has been developed for convected acoustic wave motion in finite length dissipative silencers of

general geometry with non-homogeneous, anisotropic absorbent material. Formulations for the coupled acoustic wave motion between the convected acoustic waves in both the flow duct and absorbent regions were presented. Results have been validated against experimental and analytical results [17] of axisymmetric silencers. The four-pole parameters of the transfer matrix were determined and from these various noise reduction properties, such as transmission loss, can be computed for different test silencers. Nonlinear analysis of the three-dimensional, induced, steady flow in the absorbent was carried out and the velocity field was determined on the basis of a known pressure gradient at the common boundary. Rapidly convergent iterative schemes for the nonlinear analyses of both the steady flow and acoustic fields have been given. The matching conditions of the two acoustic fields were implemented by two different techniques and it was found that a simple and efficient gradient evaluation technique, using standard C^0 elements, was suitable. It was found that a circular cross-section silencer with uniform packing was not always the best. Careful choice of shape and variation of the packing density, within a fixed total mass of absorbent, could produce slight benefits. Conversely the wrong choice of geometry and density variation of absorbent made matters significantly worse. It was also found that non-uniform steady flow in the central duct can have important effects upon the transmission loss.

7.2 Future Work

There are several directions in which the results of this thesis can be usefully pursued and extended. Thus far, for simplicity, the geometry of complete absorption silencers has been restricted to those which are axisymetric in nature. The given formulations are for general three-dimensional silencers, hence it would be simple to extend the

applications to consider fully three-dimensional, non-axisymmetric silencers. However, such analyses would be very time consuming and costly, both in terms of direct computational cost and user input in creating the corresponding meshes. In order to avoid these problems, an alternative approach to the modelling of fully three-dimensional silencers would be to use the eigenvalue model on the cross-section of a given silencer, to determine the dominant modes of wave propagation along an infinite length of duct, and then to use boundary conditions at the inlet and outlet of the finite silencer to determine the relative amplitude and phase of the various modes, in order to achieve a complete model of the silencer. This approach has the advantage that only two-dimensional finite element modelling is necessary. One disadvantage, however, is that both the flow duct and the absorbent section must be of uniform cross-section along the entire length of the silencer. Thus the method would not be applicable to the most general of three-dimensional silencers.

Throughout this thesis it has been assumed that the effects of a perforated screen, which may be used to separate the flow duct from the absorbent packing of the silencer, are negligible. Typically the porosity of such perforates is 25% or more, for which this is a valid assumption. However, it would be possible to include these effects, subject to the availability of data for the impedance of the perforate, by an alteration of the matching boundary conditions between the two regions. For perforates of low porosity, such as often occurs with louvred screens, such analysis would be necessary for accurate prediction of overall effectiveness.

Another area which needs further attention concerns the modelling of absorption silencers with varying density of the absorbent packing. In the analysis given in this thesis, the density was varied linearly between the same two extremes, which meant that the total mass of absorbent material varied slightly when the variation was made

along the radial or circumferential directions. It would be useful to use a non-linear variation chosen to maintain a constant total mass, but there is then the problem that there are infinitely many ways of achieving this goal.

A further area for development follows from the modelling of the induced steady flow velocity field in the absorbent, where the pressure gradient along the common boundary is a required boundary condition. In this thesis, the pressure gradient has been assumed to be known and in actual examples measured values have been used. It would be possible to determine this pressure gradient from a viscous flow analysis of the flow in the open duct, with appropriate conditions at the common boundary. In practice, detailed modelling of induced flow field proved to be of little benefit, hence modelling of the pressure gradient may not be considered to be worth the effort. Furthermore, if a perforated plate separates the absorbent from the flow duct, the pressure gradient and induced flow would both be reduced

Another problem remaining is that of the correct radiation impedance for analysing a general "anechoic" termination of a non-uniform flow duct. In this work, the radiation impedance was assumed to be that for radiation from a circular pipe of the same overall cross-sectional area as that of the actual outlet of the termination. It would be possible to calculate the precise radiation impedance for any given non-circular cross-section, including cases for which sound does not radiate into a free-field, such as occurs in the some of the ISO standard terminations [95] where there is a reflecting disk offset a small axial distance from the outlet of the termination.

Throughout the work of this thesis it has been assumed that the wall of the ducts and silencers are rigid. Further work could include the modelling of non-rigid walls and the

consequent effects upon the sound attenuation of silencers and shell noise/breakout noise from the vibrating surfaces.

It has been mentioned earlier that the theoretical models in this thesis consider only linearised acoustic wave motion, which is valid for general silencer analysis. However if analysis is required for high amplitude sound levels such that non-linear terms must be retained in the governing wave equations, then it is necessary to use a time-domain rather than a frequency domain analysis. It would be possible to use similar finite element formulations for the spatial variation to those used in this thesis, together with a finite difference formulation to step through the time variation. In essence, a separate finite element solution is required for each step and the time steps have to be very small to guarantee convergence. Thus the computing resources required are an order of magnitude greater than for frequency domain analysis.

REFERENCES

1. M. L. Munjal 1987 *Acoustics of Ducts and Mufflers:* with application to exhaust and ventilation system design. (J.Wiley, New York .)
2. A. Cummings 1990 *Proc. Inter-noise 90* pp. 17-38. Prediction method for the performance of flow duct silencers.
3. A. H. Nayfeh, J. E. Kaiser and D. P. Telionis 1975 *AIAA Journal,* **13** (2) pp. 130-153. Acoustics of aircraft engine-duct systems.
4. J. W. S. Rayleigh 1878 *The theory of sound,* (Dover publication inc. 1945. re-issue in two volumes New York)
5. L. J. Sivian 1937 *Journal of Acoustical Society of America,* **9** (2) pp. 135-140. Sound propagation in ducts lined with absorbing materials.
6. P. M. Morse 1939 *Journal of Acoustical Society of America,* **11** (2) pp. 205-211. Transmission of sound inside pipes.
7. H. J. Sabine 1940 *Journal of Acoustical Society of America,* **12** (1) pp. 53-57. The absorption of noise in ventilating ducts.
8. R. A. Scott 1946 *Proceedings of the Physical Society,* **58** pp. 358-368. The propagation of sound between walls of porous material.
9. D. H. Tack and R. F. Lambert 1965 *Journal of Acoustical Society of America*, **38** (4) pp. 655-666. Influence of shear flow on sound attenuation in a lined duct.
10. A. Bokor 1969 *Journal of Sound and Vibration,* **10** (3) pp. 390-403. Attenuation of sound in lined ducts.
11. A. Bokor 1971 *Journal of Sound and Vibration,*. **14** (3) pp. 367-373. A comparison of some acoustic duct lining materials according to Scott's theory.

12. C. Wassilieff 1987 *Journal of Sound and Vibration,* **114** (2) pp. 239-251. Experimental verification of duct attenuation models with bulk reacting linings.

13. U. J. Kurze and I. L. Vér 1972 *Journal of Sound and Vibration,* **24** (2) pp. 177-187. Sound attenuation in ducts lined with non-isotropic material.

14. A. H. Nayfeh, J. Sun and D. P. Telionis 1974 *A. I. A. A. Journal,* **12** (6) pp. 838-843. Effect of bulk-reacting liners on wave propagation in ducts.

15. A. Cummings 1976 *Journal of Sound and Vibration,* **49** (1) pp. 9-35. Sound attenuation in ducts lined on two opposite walls with porous material, with some application to splitters.

16. W. Frommhold and F. P. Mechel 1990 *Journal of Sound and Vibration,*. **141** (1) pp. 103-125. Simplified methods to calculate the attenuation of silencers.

17. A. Cummings and I. -J. Chang 1988 *Journal of Sound and Vibration,* **127** (1) pp. 1-17. Sound attenuation of a finite length dissipative flow duct silencer with internal mean flow in the absorbent.

18. A. Cummings and I. -J. Chang 1987 *Acustica,* **64** (4) pp. 169-178. Internal mean flow effects on the characteristics of bulk-reacting liners in circular ducts.

19. S. W. Rienstra 1985 *Journal of Acoustical Society of America,* **77** (5) pp. 1681-85. Contribution to the theory of sound propagation in ducts with bulk -reacting lining.

20. R. J. Astley and A. Cummings 1987 *Journal of Sound and Vibration,* **116** (2) pp. 239-263. A finite element scheme for attenuation in ducts lined with porous material: comparison with experiment.

21. R. J. Astley 1987 *Journal of Sound and Vibration,* **117** (1) pp. 191-197. A comparative note on the effects of local versus bulk reaction models for air moving ducts lined on all sides.

22. R. J. Astley 1990 *Proc. Inter-Noise 90,* pp. 575-578. Acoustical modes in lined ducts with flexible walls: A variational approach.

23. B. J. Tester 1973 *Journal of Sound and Vibration,* **28** (2) pp. 151-203. The propagation and attenuation of sound in lined ducts containing uniform or "plug" flow.

24. R. J. Astley and W. Eversman 1979 *Journal of Sound and Vibration,* **65** (1) pp. 61-74. A finite element formulation of the eigenvalue problem in lined ducts with flow.

25. W. Eversman 1970 *Journal of Acoustical Society of America,* **48** (2) pp. 425-428. The effect of Mach number on the tuning of an acoustic lining in a flow duct.

26. C. -I. J Young and M. J. Crocker 1975 *Journal of Acoustical Society of America,* **57** (1) pp. 144-48. Prediction of transmission loss in mufflers by the finite element method .

27. A. Craggs 1976 *Journal of Sound and Vibration,* **48** (3) pp. 377-392. A finite element method for damped acoustic systems: An application to evaluate the performance of reactive mufflers.

28. A. Craggs 1977 *Journal of Sound and Vibration,* **54** (2) pp. 285-296. A finite element method for modelling dissipative mufflers with a locally reactive lining.

29. K. J. Baumeister 1981 *Journal of Engineering for Industry,* **103** (3) pp. 270-81. Numerical techniques in linear duct acoustics-A status report.

30. P. J. Filippi 1983. *Theoretical Acoustics and Numerical Techniques,* pp. 51-103. Finite element technique for acoustics. (Springer-Verlag, Wien Austria.).

31. D. F. Ross 1980 *Journal of Sound and Vibration,* **69** (4) pp. 509-518. A finite element analysis of parallel-coupled acoustic systems using subsystems.

32. K. S. Peat 1982 *Journal of Sound and Vibration,* **84** (3) pp. 389-395 Evaluation of four-pole parameters for ducts with flow by the finite element method.

33. J. F. Unruh and W Eversman 1972 *Journal of Sound and Vibration,* **23** (2) pp. 187-197. The utility of the Galerkin method for the acoustic transmission in an attenuating duct.

34. A. Kapur and P. Mungur 1976 *Progress in Astronauticss and Aeronautics,* **44** pp. 363-370. Duct acoustic and acoustic finite element method

35. P. E. Doak 1973 *Journal of Sound and Vibration,* **28** (3) pp. 527-561. Fundamentals of aerodynamic sound theory and flow duct acoustics

36. O. C. Zienkiewicz 1977 *The Finite Element Method in engineering science,* (Mc Graw -Hill Book Co. London).

37. P. M. Morse and U. K. Ingard 1968 *Theoretical acoustics,* New York, McGraw -Hill Book Company (CH-6).

38. M. A. McCormick 1975 *Journal of Sound and Vibration,* **39** (1) pp. 35-41. The attenuation of sound in lined rectangular ducts containing uniform flow.

39. R. K. Sigman, R. K. Majjigi and B. T. Zinn 1978 *A. I. A. A. Journal,* **16** (11) pp. 1139-1145. Determination of turbofan inlet acoustics using finite elements.

40. A. Craggs 1981 *Proceedings of American Society of Mechanical Engg New York*, pp. 1-9. Application of acoustic and absorptive finite element.

41. S. F. Ling, L. F. Hanilton and J. J. Allen. 1982 *Journal of Mechanical Design, Transaction of the A.S.M.E,* pp. 1-7. A two-dimensional isoparametric Galerkin finite element for acoustic-flow problems.

42. A. Craggs 1979 *Journal of Sound and Vibration,* **66** (4) pp. 605-613. Coupling of finite element acoustic absorption models.

43. A. Craggs 1986 *Journal of Sound and Vibration,* **108** (2) pp. 327-337. A finite element model for acoustically lined small rooms.

44. P. S. Christiansen and S. Krenk 1988 *Journal of Sound and Vibration,* **122** (1) pp. 107-118. A recursive finite element technique for acoustic field in pipes with absorption.

45. H. S. Hobbeling 1989 *Acustica,* **67** pp. 275-283. Calculation of complex absorption- and reflection- silencers using a finite element method.

46. D. A. Bies, C. H. Hansen and C. E. Bridges 1991 *Journal of Sound and Vibration,* **146** (1) pp. 47-80. Sound attenuation in rectangular and circular cross-section ducts with flow and bulk-reacting liner.

47. A. Craggs 1989 *Journal of Sound and Vibration,* **132** (2) pp. 393-402. The application of the transfer matrix and matrix condensation methods with finite elements to duct acoustics.

48. K. S. Peat 1991 *Journal of Sound and Vibration,* **146** (2) pp. 353-360. A transfer matrix for an absorption silencer element.

49. A. Craggs 1987 *Finite element news,* **6** pp. 14-17. Comparison of finite element solutions with those from the simple theory of duct acoustics.

50. M. J. Alghatam. 1985 *Loughborough University Ph.D. Thesis,* Solar ventilation and air conditioning system investigation using the finite element method.

51. A. A. Syed 1980 *Loughborough University Ph.D. Thesis,* On the prediction of sound attenuation in acoustically lined circular ducts.

52. A.S.H.R.A.E 1980 *Handbook and product directory*, systems chapter 35.

53. SERC 1991 Science and Engg. Research Council Nag Finite element library Manual Release 3.0 Rutherford Appleton Laboratory.

54. K. S. Peat 1990 *Proc. of Inter-Noise 90*, **1** pp. 579-582. A numerical decoupling analysis of absorption silencer elements.

55. E. R. Rademaker 1990 *The American Society of Mechanical Engineer Annual Meeting, Dallas*, Texas, pp. 1-9. Experimental validation of lined-duct acoustics model including flow.

56. S. Shimode 1982-83 *Acustica,* **52** pp. 98-105. Acoustical properties of porous material and dissipative silencers with several gas media.

57. M. E. Delany and E. N. Bazley 1970 *Applied Acoustics,* **3** pp. 105-116. Acoustical properties of fibrous absorbent materials.

58. E. A. Leskov, G. I. Osipov and E. J. Yudin 1970 *Applied Acoustics,* **3** pp. 47-56. Experimental investigation of splitter duct silencers.

59. P. G. Smith and R. A. Greenkorn 1972 *Journal of Acoustical Society of America,* **52** (1) pp. 247-253. Theory of acoustical wave propagation in porous media.

60 A. Cummings and I. -J. Chang 1987 *Journal of Sound and Vibration,* **114** (3) pp. 565-581. Acoustic propagation in porous media with internal mean flow.

61. V. Easwaran and M. L. Munjal 1993 *Journal of Sound and Vibration,* **160** (2) pp. 333-350. Finite element analysis of wedges used in anechoic chambers.

62. A. Cummings and N. Sormaz 1993 *Journal of Sound and Vibration,* **168** (2) pp. 209-227. Acoustic attenuation in dissipative splitter silencers containing mean fluid flow.

63. R. J. Astley, A. Cummings and N. Sormaz 1991 *Journal of Sound and Vibration,* **150** (1) pp. 119-138. A finite element scheme for acoustic propagation in flexible-walled ducts with bulk-reacting liners, and comparison with experiment.

64. F. P. Mechel 1991 *Acustica,* **73** pp. 223-239. Modal solutions in rectangular ducts lined with locally reacting absorbers.

65. T. Morel, J. Morel and D. A. Blaster 1992 *SAE paper 910072,* pp. 35-51. Fluid dynamic and acoustic modelling of concentric-tube resonators/silencers.

66. B. Brouard, J. -F. Allard and H. Bruneau 1993 *Noise Control Engineering Journal,* **41** (1) pp. 289-297. Acoustical impedance and absorption coefficient of porous layers covered by a facing perforated by parallel slits.

67. Y. Miki 1990 *Journal of Acoust. Soc. Japan.*(E), **11** (1) pp. 19-25. Acoustical properties of porous materials modifications of Delany-Bazley models.

68. R. Ramakrishnan and W. Watson 1991 *Noise Control Engineering Journal,* **36** (3) pp. 107-120. Design curves for circular and annular duct silencers.

69. R. Ramakrishnan and W. Watson 1992 *Applied Acoustics,* **35** pp. 1-24. Design curves for rectangular splitter silencers.

70. A. Cummings 1992 *Proceedings of Second International Congress on Recent Development in Air-and Structure-borne Sound and Vibration,* pp. 689-696. Sound absorbing ducts.

71. R. Woodcock and M. Hodgson 1992 *Journal of Sound and Vibration,* **153** (1) pp. 186-191. Acoustic methods for determining the effective flow resistivity of fibrous materials.

72. I. -J. Chang and A. Cummings 1988 *Journal of Sound and Vibration,* **122** (2) pp. 243-259. A time domain solution for the attenuation at high amplitudes, of perforated tube silencers and comparison with experiment.

73. Y. Kagawa, T. Yamabuchi and A. Mori 1977 *Journal of Sound and Vibration,*. **53** (3) pp. 357-374. Finite element simulation of an axisymmetric acoustic transmission system with a sound absorbing wall.

74. E. Meyer, F. Mechel and G. Kurtze 1958 *Journal of acoustical Society of America,* **30** (3) pp. 165-174. Experiments on the influence of flow on sound attenuation in absorbing ducts.

75. K. U. Ingard 1959 *Journal of acoustical Society of America,* **31** (7) pp. 1035-1036. Influence of fluid motion past a plane boundary on sound reflection, absorption and transmission.

76. A. Cummings and R. J. Astley 1993 *Proc. of the Institute of Acoustics,* **15** (3) pp. 739-746. The effects of flanking transmission on sound attenuation in lined ducts.

77. Y. Kagawa, T. Yamabuchi and T. Yoshikawa 1980 *Journal of Sound and Vibration,* **69** (2) pp. 207-228. Finite element approach to acoustic transmission-radiation system and application to horn and silencer design.

78. C. I. J. Young and M. J. Crocker 1976 *Journal of acoustical Society of America,* **60** (5) pp. 1111-1118. Acoustical analysis, testing and design of flow reversing muffler chambers.

79. C. -N. Wang, C. -C. Tse and Y. -N. Chen 1993 *Applied Acoustic,* **40** pp. 91-106. Analysis of three dimensional muffler with boundary element method.

80. A. J. King 1958 *Journal of acoustical Society of America,* **30** (6) pp. 505-507. Attenuation of sound in lined air ducts.

81. S. -H. Ko 1971 *Journal of acoustical Society of America,* **50** (5) pp. 1418-1432. Sound attenuation in lined rectangular ducts with flow and its application to the reduction of aircraft engine noise.

82. S. -H. Ko 1972 *Journal of Sound and Vibration,* **22** (2) pp. 193-210. Sound attenuation in acoustically lined circular ducts in the presence of uniform flow and shear flow.

83. S. -H. Ko 1973 *Journal of acoustical Society of America,* **54** (6) pp. 1592-1606. Theoretical prediction of sound attenuation in acoustically lined annular ducts in the presence of uniform flow and shear flow.

84. S. -H. Ko 1975 *Journal of Sound and Vibration,* **39** (4) pp. 471-487. Theoretical analysis of sound attenuation in acoustically lined flow ducts separated by porous splitters (rectangular, annular and circular ducts).

85. B. Nilsson and O. Brander 1980 *J. Inst. Maths. Applics,* **26** pp. 269-298. The propagation of sound in cylindrical ducts with mean flow and-bulk-reacting lining- I. Modes in an infinite duct.

86. B. Nilsson and O. Brander 1980 *J. Inst. Maths. Applics,* **26** pp. 381-410. The propagation of sound in cylindrical ducts with mean flow and-bulk-reacting lining- II. Bifurcated ducts.

87. B. Nilsson and O. Brander 1980 *IMA Journal of Applied Mathematics,* **27** pp. 105-131. The propagation of sound in cylindrical ducts with mean flow and-bulk-reacting lining- III. Step discontinuities.

88. B. Nilsson and O. Brander 1980 *IMA Journal of Applied Mathematics,* **27** pp. 263-289. The propagation of sound in cylindrical ducts with mean flow and-bulk-reacting lining- III. Several interacting discontinuities.

89. C. A Brebbia 1982 *Finite Element Systems: A Handbook.* (New York: Springer-Verlag, Inc.)

90. K. L. Rathi and K. S. Peat 1993 *Proc. Inter-Noise 93, Leuven, Belgium,* pp. 1581-1584. Finite element analysis of absorption silencers.

91. J. Zhenlin, M. Qiang and Z. Zhihua 1994 *Journal of Sound and Vibration,* **173** (1) pp. 57-71. Application of the boundary element method to predicting acoustic performance of expansion chamber mufflers with mean flow.

92. C. Zwikker and C. W Kosten 1949 *Sound Absorbing Materials* (Elsevier, Amsterdam,)

93. P. C. Carman 1956 *Flow of Gases Through Porous Media* (London: Butterworths Scientific Publications.)

94. K. Attenborough 1983 *Journal of acoustical Society of America,* **73**(3) pp. 785-799. Acoustical characteristics of rigid fibrous absorbents and granular materials.

95. ISO 7235:1991(E) 1991 *Acoustics.- Measurement procedures for ducted silencers.*. pp 19-27. Anechoic terminations (Annex D).